MATHEMATICAL MODELING FOR DOWEL LOAD TRANSFER SYSTEMS

By

Hua Guo

A DISSERTATION

Submitted to
Michigan State University
in partial fulfillment of the requirements
for the degree of

DOCTOR OF PHILOSOPHY

Department of Civil and Environmental Engineering

1992

ABSTRACT

MATHEMATICAL MODELING FOR DOWEL LOAD TRANSFER SYSTEM

By

HUA GUO

It has been discovered and proven that the dowel bar stiffness matrix used by some finite element computer programs, for simulating the mechanism of dowel bars without looseness, fails to meet some of the basic requirements of the finite element method. An alternative component model, consisting of two finitely long bending beams embedded in concrete and connected by a shear-bending beam, has been developed. The model has been proven to be theoretically correct. The model can be installed into a finite element program to predict the responses of the load transfer system, including distributions of bending moment, shear force and the bearing stress of each dowel without using the assumption of effective length. A detailed comparison between experimental and analytical results verified the component model can reasonably predict the responses of a dowel bar load transfer system.

Hundreds of numerical calculations were conducted using the developed component model to test the accuracy of existing design procedures. It has been found that the maximum bearing stress of concrete, under the critical dowel, can not be accurately predicted by the "effective length" assumption which is currently used in engineering analysis. Errors in computed values of maximum bearing stress can affect the prediction of joint faults in pavement performance models. Three tables listing maximum bearing stresses of concrete, for the critical corner loading cases, have been given for dowel design in this dissertation.

A nonlinear elastic structural model has also been developed to simulate the dowel bar looseness mechanism. The model can be used to predict various pavement responses, including stresses, displacement distributions and load transfer capability at different stages of pavement service life. Numerical analyses based upon the new structural model were conducted to investigate the effects of dowel bar looseness on critical pavement responses. Parameters included amount of dowel looseness, configuration and location of traffic loads, shoulder edge support effects, and dowel bar dimensions. Many findings of the study are relevant to current rigid pavement design and rehabilitation procedures.

DEDICATION

To my mother, my wife and all friends, who encouraged and supported me throughout my Ph.D program.

ACKNOWLEDGEMENTS

The successful completion of the research described herein required the input and assistance of many individuals. The author gratefully acknowledges:

Mr. James A. Sherwood of the Federal Highway Administration, who was the major advisor of the author during the period of the Fellowship Program sponsored by the FHWA.

Mr. Roger M. Larson of the Federal Highway Administration, who was the first advisor of the author during the period of the Fellowship Program.

Mr. William J. Kenis of the Federal Highway Administration, who provided advice and suggestions in various phases of the conduct of the study.

Mr. Michael R. Smith of the Federal Highway Administration, who shared his experience in scientific paper organization.

Mr.Thomas J. Pasko,Jr. of the Federal Highway Administration, who carefully reviewed the draft of the thesis and provided many significant suggestions.

Mr. Byron N. Lord of the Federal Highway Administration, who encouraged the author to seek the truth without hesitation.

Mr. Hisao Tomita of Federal Aviation Administration, who reviewed a part of the thesis and provided valuable advise to improve Chapter 9.

Dr. Robert Wen, Dr. Gilbert Baladi, Dr. Thomas Wolff, Dr. David Yen of the Michigan State University, who provided technical guidance in the conduct of this research effort.

Mr. Jamel Hammouda of the Computer Communication and Graphics Company, who numerically verified some findings presented in this dissertation.

Mr. Shawn Truelove, Mrs. Linda Phillipich and Mrs. Nina McMillan of the Michigan State University, Miss. Marcia Simon, Ms. Elke Lower and Mrs. Jeanie LaBudie of the Federal Highway Administration, who provided valuable and patient assistance to the author during his Ph.D program.

Special thanks are offered to Dr. Mark B. Snyder for his helpful advice, strong support, and sincere encouragement throughout the course of this research, and for his patience and confidence in the production of this thesis.

TABLE OF CONTENTS

LIST OF FIGURES

LIST OF TABLES

CHAPTER ONE
INTRODUCTION

1 Major Steps of Engineering Analysis

Since high speed digital computers have become more available, the Finite Element Method (FEM) has become one of the most powerful tools which are being employed to solve a wide range of complex boundary value problems in engineering. (Zienkiewicz[1977] and Bathe[1982]) Many computer programs for jointed concrete pavement analysis based on FEM have been developed in the past decade. (Huang[1973], Tabatabaie[1979], Chou[1981], Ioannides[1984], Majidzadeh[1984], Tayabji[1986], Hoit[1988] and Nashizawa[1989])

The major steps of the analysis can be summarized as follow:

(1) Physical Model. Based on some assumptions, pavement systems are simplified into a physical theoretical model. Using the FEM, the pavement system can be simplified as an assemblage of finite number of plates, bars and elastic springs interconnected at structural nodes as shown in Fig. 1-1 and Fig. 1-2. During this simplification procedure, the effects of many secondary parameters have been ignored. For example, the variation of the slab thickness, the non-uniform distribution of properties of concrete and the permanent deformation features of the soil. One engineering system can be simplified into several physical models, more or less complicated, depending on the needs of engineers and current level of computation techniques.

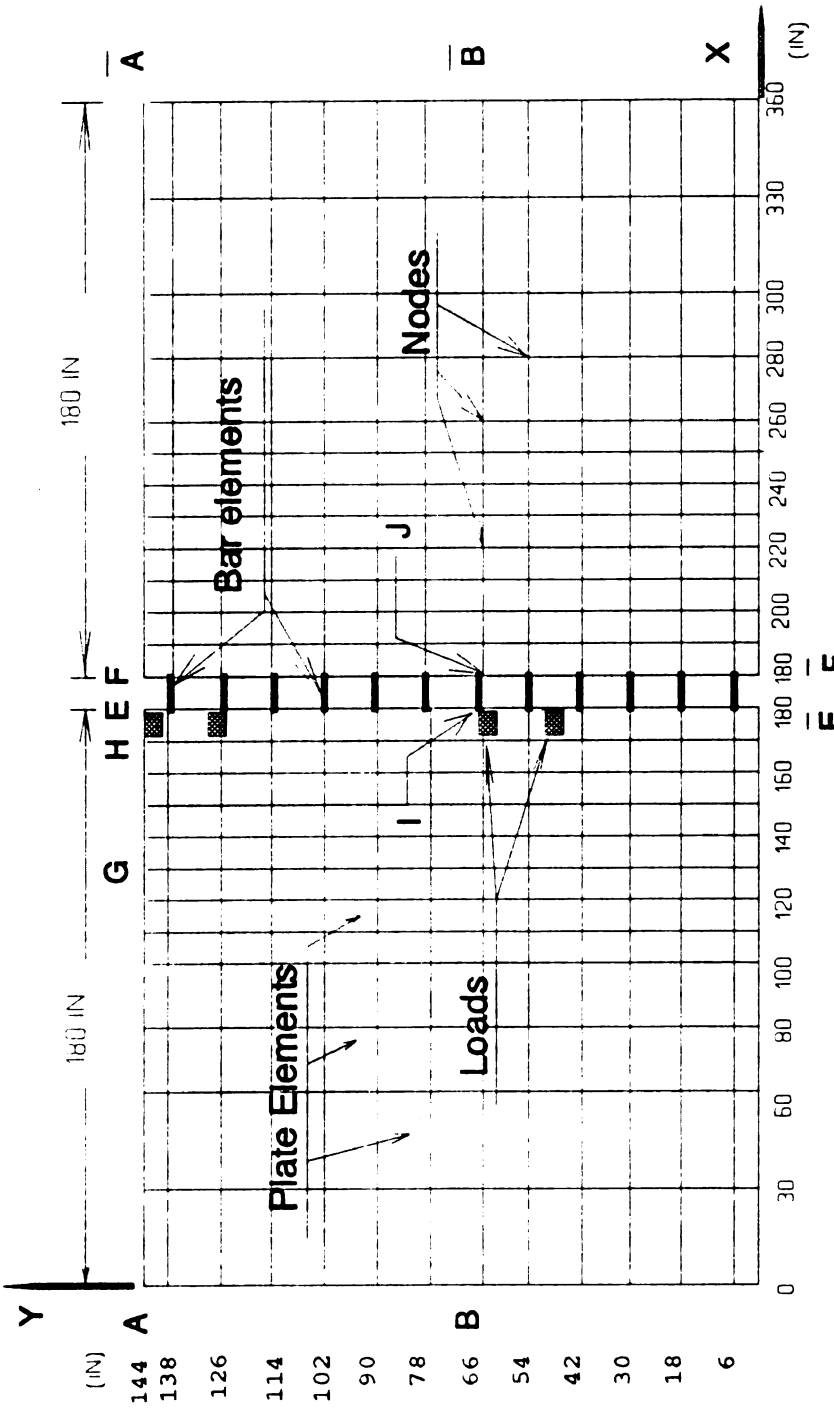

Fig. 1-1 Physical Model of a PCC Pavement

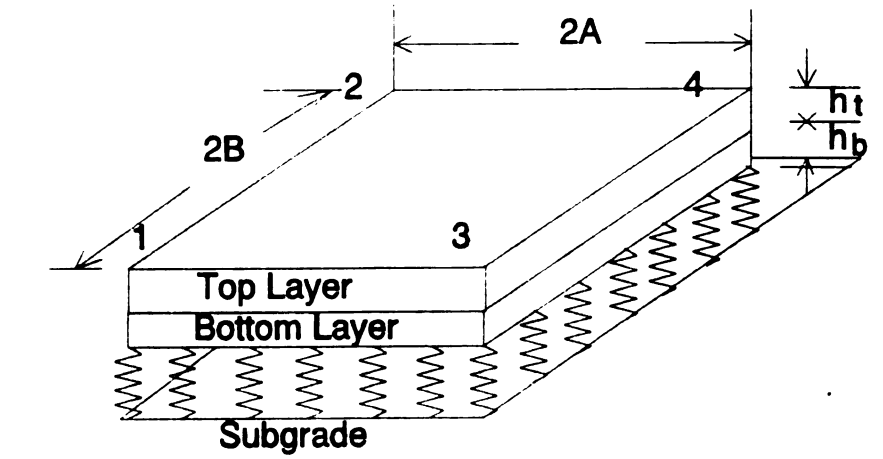

(a) Plate Element

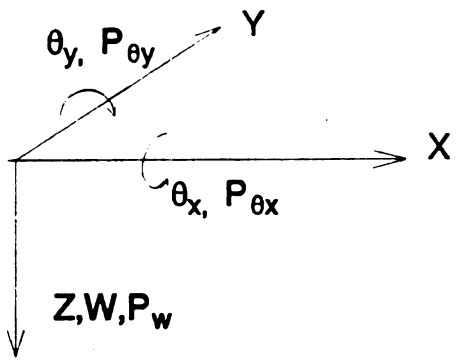

(b) The Coordinate System

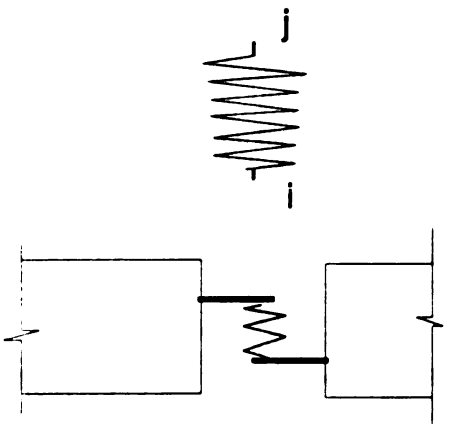

(c) Spring Element

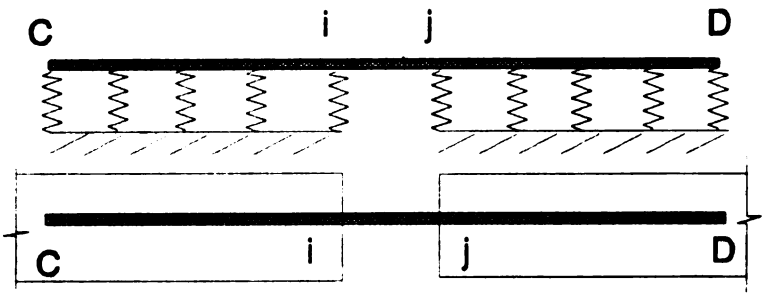

(d) Bar Element

Fig. 1-2 Element Models in FEM Program

(2) Mathematical Model. Based on more assumptions, the physical theoretical model is simplified into a mathematical model which can be described by a group of differential or algebraic equations. During this simplification procedure, several important parameters are selected to simulate the original system's behavior under a certain environment. For example, the nodal displacements are taken as basic parameters based on stiffness method of the FEM. When traffic is the only type of loads to be considered, the traditional Winkler equation can be used to simulate the behavior of the base and subgrade, so that the corresponding equations can be derived. However, if temperature gradient is considered for the responses of the pavement, the subgrade must at least be modeled by "extensionless springs", and another type of equations should be employed. One physical model may also be simulated by several different mathematical models (or different types of mathematical equations) which mainly depends on the working environment of the pavement, the level of precision required by engineers and the mathematical tools currently available.

(3) Engineering practice. The results produced in step two will be checked with the data collected in laboratory and field tests to verify the accuracy and validity of the simplifications made in previous two steps. The discrepancy between the calculated results using the mathematical model and the data from laboratory or field usually leads to modification of the physical and/or mathematical models or calibration of the model's input. Engineering practice is the most important criterion to evaluate the related analytical models. Only those models which are theoretically correct and practically verified can be confidently employed

in engineering practice.

The emphasis in this research was on the second step: mathematical modeling of dowel bar load transfer system for the PCC pavement analysis. Attention was paid to evaluate the correctness in theory for existing mathematical models of dowelled joints, and to verify the proposed models by theory and by available laboratory and field data.

2 Joint Functions and Related Deteriorations

Joints are widely used in portland cement concrete pavement design and rehabilitation. The major functions of joints are:

- To provide enough space and freedom for movement of pavement slabs due to volume change of the concrete due to the change in temperature and moisture content
- To effectively transfer traffic loads from one to the adjacent slab
- To control the width and location of cracking
- To temporarily stop construction

Concrete pavement joints may be designed as contraction, expansion, construction, or longitudinal joints according to their functions. However, the joints are usually the weakest portion of PCC pavements, and the earliest deteriorations are often discovered near the joints. These include faulting, pumping, water bleeding and seal damage. Many types of distresses of PCC pavement, such as transverse cracking, corner break,

longitudinal cracking, blowup, lane and/or shoulder drop off, D cracking, and lane and shoulder separation etc., are directly or indirectly caused by the deterioration of the joints. These distresses caused by lack of attention to such structural weakness often occupy most of the time of the maintenance engineers.

The most common load transfer device is the smooth steel dowel bar. The objectives of past research on load transfer include investigating the effects of dowel systems on the behavior of pavement structures, cost effective design and rehabilitation procedures for dowel load transfer systems. Many projects have been supported by the Federal, State and local agencies to survey the joint related deteriorations of the PCC pavement, to discover and verify the sources of the distress, and to develop new techniques to improve the joint capabilities. (Hveem[1949], Darter[1984], Van Ness[1987] and Smith[1990])

3 Research on Dowel Bar Load Transfer Systems

Experimental Studies

The earliest large scale field tests of dowel bar performance were conducted by Teller[1936], in Arlington, VA. Laboratory study to investigate the behavior of a loaded single dowel embedded in concrete was performed by Friberg[1938]. The first experiment of dowel load transfer across a full-scale concrete pavement slab joint, with the dowel instrumented to observe their behavior, including the distributions of

deflection, bending moment and shear force along the dowel bars, was conducted by Keeton[1956][1957]. Shortly after, another significant laboratory research project was conducted by Teller[1958]. He studied the effects of several variables which influence the structural performance of the dowel bars used in the joints of concrete pavement. The parameters include diameter and embedded length of the dowel bars, width of the joint opening, thickness of the slabs, initial and developed dowel bar looseness caused by repetitive loading. The project was evaluated by Friberg[1958] as a research which "Fills a gap in joint design which has existed for many years." Ciolko[1979] performed lab tests to determine the relative ability of dowel bars and starlugs and verified many of Teller's findings. Snyder[1989] conducted a laboratory study which involved repetitive shear loads to dowels anchored in hole drilled in concrete specimens and investigated the relationship between dowel deflection, looseness(the gap or void between dowel and the concrete hole), number of the repeated loads and geometrical and mechanical properties of the dowels. A review on the significant experimental projects in the past decades can be found in Snyder's Ph.D thesis[1989].

Analytical Studies

As early as 1920s, Westergaard[1928] started to analyze the dowel bar behavior based on Timoshenko theory[1925]. Then, Bradbury[1932] and Friberg[1940] performed more analysis and developed their formulae for design. All these investigations were based on the model of an infinitely long elastic beam embedded in an elastic medium. The deflection, bending

moment, shear force and the critical bearing stress of the concrete can be calculated if the shear force transmitted across the dowel is known. Based on experimental results and Westergaard's work, Friberg[1940] proposed a procedure to estimate the maximum force using the assumptions that load transfer efficiency is known, the distribution of shear forces along the joint is linear, the maximum transmitted force is located at the loading point and the force of dowel with distance 1.8 (l) from the loading point is zero, where l is radius of relative stiffness of the pavement system. Kushing[1940] proposed an analytical procedure to approximately estimate the forces to be transmitted by each dowel bar.

A potential for a real breakthrough in analytical procedure for doweled joints was created in the late 70's with the introduction of the finite element method into pavement engineering. The earliest finite element program for PCC pavement analysis (Huang[1983]) employed the concept of load transfer efficiency to calculate the responses of slab, so that the behavior of individual dowel bars could not be predicted. Tabatabaie[1979], Chou[1981], Ioannides[1984], Tayabji[1986], Hoit[1988] and Nashizawa[1989] developed computer programs which are capable of simulating the mechanism of individual dowel bars. Among the above programs, COMBO (Hoit[1988]) requires linear and torsional spring coefficients to be determined by users as input data for dowel bars, all the others require direct input of the physical dowel properties such as dimensions, spacing and mechanical properties. The finite element models make it possible to directly predict the responses of dowel bars using the analytical model employed by the program without further assumptions. The review and comparison of

different programs can be found in Heinrichs[1988] and Smith[1990].

After looseness was observed and measured by Teller[1958], Majizadeh[1984] suggested input of a smaller bar diameter to the finite element analysis to consider the looseness effects. This method considers the reduction of stiffness of dowelled joint as a whole, but can not simulate the mechanism of individual dowel looseness.

Field Survey

During the past decades, many projects supported by Federal, State and local government agencies collected field data, including detailed design, construction, maintenance, traffic, environmental and pavement distresses, verified the available analysis procedures and design methods, investigated the discrepancies between the originally expected and the actual pavement performances, and intended to find the sources which had caused the discrepancies. Darter[1984] developed a concrete pavement evaluation system based on the available data. Recently, Smith[1990] documented the performance of 95 experimental or other in-service rigid concrete pavements and described the evaluation of various design and analysis models and the development of improved prediction models.

4 Descriptions of Existing Problems

Research efforts have resulted in many significant achievements, however, some problems still remain unsolved and new problems are continuously brought up with the application of new techniques. The following problems, closely related to the PCC joint modeling, have been discovered:

- Smith[1990] found differences, between computer programs ILLISLAB (Ioannides[1984]) and JSLAB (Tayabji[1986]), in computed deflections of up to 20 percent due to traffic loads, and differences of up to 100% due to thermal gradients - even though the two finite element models were based on the same assumptions to deal with slabs resting on a Winkler base.

- Guo[1992] discovered that the dowel bar stiffness matrices used by JSLAB and ILLISLAB do not meet some of the basic requirements of the finite element method. The stiffness matrices represent elements that are not in equilibrium (e.g., an assumed rigid body movement vector produces non-zero-element forces).

- Based on Friberg's research (Friberg[1940]), dowels at distances greater than 1.8 (l) from the point of application of the external load were inactive, and 1.8 (l) was defined as "effective length" of the load transfer system. Tabatabaie[1979] and Henrichs[1988] concluded that the effective length should be 1.0 (l) according to their results produced by program ILLISLAB. In dowel bar design, the diameter is dominated by the maximum concrete bearing stress which is in proportional to the effective

length. (if the total of the loads transmitted across the joints are the same.) The difference of assumptions 1.8 (1) and 1.0 (1) would affect the dowel bar design significantly.

- Faulting is one of the most critical distresses affecting the performance of rigid concrete pavements and is directly (Henrichs[1988]) or indirectly (Smith[1990]) determined by the maximum concrete bearing stress under the dowels. The discovered problems in the dowel bar stiffness matrix used in finite element programs would influence the prediction of pavement faulting. It would also affect predictions of other pavement performance measures.

- Many experimental studies show that dowel bar looseness greatly affects the load transfer efficiency which is an important index to determine the quality and capability of the dowel load transfer system. Teller[1958] also found 40,000 load cycles (2% of 2,000,000 total cycles in his tests) produced about 50% of total looseness. That suggest most pavements currently in service are working under a certain looseness. The existence of looseness not only affects the behavior of joint, but also affects the responses of slabs and other pavement performances. So far, however, there exists no mechanistic model to simulate individual dowel bar behavior under looseness.

5 Research Objectives and Scope

Objective

The purpose of this study is to advance the state-of-the-art of the mathematical modeling of dowelled load transfer systems, by:

- Establishing a theoretically correct and practically adjustable dowel bar model for finite element programs, instead of the inappropriate ones employed by current programs

- Developing a new mechanistic model to simulate the looseness mechanism of individual dowel bars and making the looseness simulation level consistent with the dowel bar simulation level in finite element programs for PCC pavement analysis.

- Investigating the impact of the new models on the pavement analysis, design and performance predictions.

Scope

- All analysis and verification in this project was conducted using available computer programs so that the reliability of the program was extremely important for obtaining meaningful results. The first task was

to evaluate the reliability of the selected computer program JSLAB, and correct all discovered errors.

- Accumulated information from existing studies on modeling the dowelled joint was reviewed to verify the discovered problems on dowel bar stiffness matrices currently employed in some widely used finite element programs. Detailed derivation was conducted to reveal the existence of the errors. Numerical examples are given to demonstrate the inaccuracy of the results produced by using the questionable dowel bar stiffness matrix.

- Some available experimental data are used to compare the analytical results produced by the proposed model, including bending moment distribution on the dowel bars.

- A model to simulate the looseness mechanism is proposed and the corresponding numerical iteration procedure was designed to perform the simulation. Numerical examples are given to compare the response of dowelled concrete pavement with and without dowel looseness.

- Analyses were conducted to investigate the impact of the new dowel model to the design of dowelled joints and pavement thickness designs. Both theoretical and numerical sensitivity analyses are conducted to determine the effective length of dowelled joints. The impact of the findings to joint design procedures is also discussed.

- An effort was made in numerical calculation to use the dowel looseness model to quantitatively understand the effects of dowel looseness, including: critical stress and location of the slabs, performance prediction models of the joints, etc.

CHAPTER TWO
BASIC ELEMENTS IN FINITE ELEMENT PROGRAMS

The matrices for basic elements in finite element programs are given in this chapter for evaluating the reliability of JSLAB-86 (Tayabji[1986]). The rectangular plate element in Fig. 1-2(a) which contains a pavement slab, stabilizing base and subgrade, is modeled by top layer and bottom layer plates, and extensionless distributed springs. The bar elements in Fig. 1-2(d) are used to model dowel bars with consideration of dowel - concrete interaction. Aggregate interlock and keyway are represented by spring element in Fig. 1-2(c). These are the physical models of PCC pavements. The mathematical models are given below.

1 Plate Element

The stiffness matrix of a rectangular and bending slab (Zienkiewicz[1977]) is based on classical small displacement theory for thin plate with uniform thickness. At each node of the element in Fig. 1-2(a), there are three displacement components: a vertical deflection W in Z direction, a rotation θ_x about the x-axis and a rotation θ_y about the y-axis in Fig. 2-2(b).

A polynomial in terms of 12 parameters is used to define the displacement function as follow:

$$W(x,y) = a_1 + a_2x + a_3y + a_4x^2 + a_5xy + a_6y^2 + a_7x^3 + a_8x^2y + a_9xy^2 + a_{10}y^3 + a_{11}x^3y + a_{12}xy^3 \quad (2\text{-}1)$$

or:

$$\underset{(1x1)}{W} = \underset{(1x12)}{\phi}\ \underset{(12x1)}{a} \quad (2\text{-}2)$$

where:

$$\phi = [1\ x\ y\ x^2\ xy\ y^2\ x^3\ x^2y\ xy^2\ y^3\ x^3y\ xy^3]$$
$$a = [a_1\ a_2\ a_3\ a_4\ a_5\ a_6\ a_7\ a_8\ a_9\ a_{10}\ a_{11}\ a_{12}]^T \quad (2\text{-}3)$$

At any point within the element:

$$\underset{(3x1)}{\Delta} = \begin{pmatrix} W \\ \theta_x \\ \theta_y \end{pmatrix} = \begin{pmatrix} W \\ -\frac{\partial W}{\partial y} \\ \frac{\partial W}{\partial x} \end{pmatrix} \quad (2\text{-}4)$$

Twelve simultaneous equations for a plate element with 4 nodes can be written in matrix form:

$$V^e = A\,a \quad (2\text{-}5)$$

where:

$$\underset{(12x1)}{V^e} = \begin{pmatrix} \Delta_1 \\ \Delta_2 \\ \Delta_3 \\ \Delta_4 \end{pmatrix} \quad (2\text{-}6)$$

and **A** is a 12x12 matrix in terms of nodal coordinates. Inverting Eq. (2-5) to obtain:

$$a = A^{-1} V^{\bullet} \tag{2-7}$$

Substituting Eq. (2-7) into Eq. (2-2) to obtain:

$$W = \underset{(1x12)}{\phi} \quad \underset{(12x12)}{A^{-1}} \quad \underset{(12x1)}{V^{\bullet}} = \underset{(1x12)}{N} \quad \underset{(12x1)}{V^{\bullet}} \tag{2-8}$$

where N is a 1x12 vector of the shape functions. Their expressions (Zienkiewicz[1977] and Ioannides[1984]) are shown in Appendix A.

A strain vector due to W at a distance z from the mid-plane is:

$$\underset{(3x1)}{\epsilon} = \begin{pmatrix} \epsilon_x \\ \epsilon_y \\ \gamma_{xy} \end{pmatrix} = z \begin{pmatrix} -\dfrac{\partial^2 W}{\partial x^2} \\ -\dfrac{\partial^2 W}{\partial y^2} \\ 2\dfrac{\partial^2 W}{\partial x \partial y} \end{pmatrix} = z \underset{(3x1)}{K_c} = z \underset{(3x12)}{B} \quad \underset{(12x1)}{V^{\bullet}} \tag{2-9}$$

where, K_c is a curvature vector and B is a 3x12 strain matrix:

$$K_c = B V^{\bullet} \tag{2-10}$$

$$B = \begin{pmatrix} -\dfrac{\partial^2 N}{\partial x^2} \\ -\dfrac{\partial^2 N}{\partial y^2} \\ 2\dfrac{\partial^2 N}{\partial x \partial y} \end{pmatrix} \tag{2-11}$$

The stresses including the contribution by temperature gradient can be expressed by strains (Przemienieski[1968]):

$$\underset{(3\times1)}{\sigma} = \begin{pmatrix}\sigma_x\\ \sigma_y\\ \tau_{xy}\end{pmatrix} = \frac{E}{1-\mu^2}\begin{pmatrix}1 & \mu & 0\\ \mu & 1 & 0\\ 0 & 0 & \frac{1-\mu}{2}\end{pmatrix}\begin{pmatrix}\epsilon_x\\ \epsilon_y\\ \gamma_{xy}\end{pmatrix} - \frac{E\alpha T}{1-\mu}\begin{pmatrix}1\\ 1\\ 0\end{pmatrix} \qquad (2\text{-}12)$$

$$= \underset{(3\times3)}{C}\ \underset{(3\times1)}{\epsilon} + \underset{(3\times1)}{\sigma_t}$$

where:

	E	Young's modulus of the slab
	u	Poisson's ratio of the slab
	α	Thermal coefficient
	T	Temperature change

$$\sigma_t = -\frac{E\alpha T}{1-\mu}\begin{pmatrix}1\\ 1\\ 0\end{pmatrix} \qquad (2\text{-}13)$$

$$C = \frac{E}{1-\mu^2}\begin{pmatrix}1 & \mu & 0\\ \mu & 1 & 0\\ 0 & 0 & \frac{1-\mu}{2}\end{pmatrix} \qquad (2\text{-}14)$$

The moments in each layer can be defined as the following:

$$M = \begin{pmatrix}M_x\\ M_y\\ M_{xy}\end{pmatrix} = \int_h z\,\sigma dz \qquad (2\text{-}15)$$

Integrating Eq. (2-15) over the thickness h leads to:

$$M = D\,K_\sigma + M_t = D\,B\,V^\circ + M_t = R\,V^\circ + M_t \qquad (2\text{-}16)$$

where:

$$M_t = -\frac{E\alpha}{1-\mu}\begin{pmatrix}1\\1\\0\end{pmatrix}\int_h Tzdz \qquad (2\text{-}17)$$

If the temperature variation along slab thickness h is assumed linear and the temperature on top and bottom surfaces of the slab are T' and T" respectively, M_t in Eq. (2-17) can be obtained:

$$M_t = \frac{E\alpha h^3}{12(1-\mu)}\ \frac{T'-T''}{h}\begin{pmatrix}1\\1\\0\end{pmatrix} = \frac{E\alpha h^3}{12(1-\mu)}\,g\begin{pmatrix}1\\1\\0\end{pmatrix} \qquad (2\text{-}18)$$

where:

$$g = \frac{T' - T''}{h} \qquad (2\text{-}19)$$

g is defined as temperature gradient in pavement, daytime case (the top surface is warmer than the bottom) is defined as positive.

D in Eq. (2-16) is an Elastic Matrix. Two cases, fully bonded and fully unbonded two layer systems are considered in JSLAB. Their detail derivations are given in Appendix B. The major conclusions are listed as below. For the unbonded case:

$$D = D_{top} + D_{bottom}$$

$$= \sum_{layer} \frac{E h^3}{12(1-\mu^2)}\begin{pmatrix}1 & \mu & 0\\ \mu & 1 & 0\\ 0 & 0 & \frac{1-\mu}{2}\end{pmatrix} \qquad (2\text{-}20)$$

Where the summation includes both of the top and bottom layers.

For the bonded case:

$$\alpha_b = \frac{\frac{1}{2} h_t (h_t + h_b)}{h_t + \frac{E_b}{E_t} h_b} \tag{2-21}$$

$$\alpha_t = \frac{1}{2} (h_t + h_b) - \alpha_b \tag{2-22}$$

$$D = D_{top} + D_{bottom}$$

$$= \sum_{layer} \left(\frac{E(12\alpha^2 h + h^3)}{12(1-\mu^2)} \begin{bmatrix} 1 & \mu & 0 \\ \mu & 1 & 0 \\ 0 & 0 & \frac{1-\mu}{2} \end{bmatrix} \right) \tag{2-23}$$

where α_t and α_b are distances from the mid-plane of the top and bottom layers to the neutral axis of the equivalent cross section respectively. (See Fig. B-2, Appendix B).

The general "stress" matrix (Zienkiewicz[1977]) in Eq. (2-16) can be written as:

$$R = D B \tag{2-24}$$

Eq. (2-24) offers a transfer matrix between nodal displacements and Bending Moments for elements. R and B are given in appendix A. After bending moment M is obtained, bending stress σ can be calculated by following expression:

$$\sigma = \frac{12M}{h^3} z \qquad (2\text{-}25)$$

where z is measured from the plate neutral-plane and its positive direction is given in Fig. 1-2(b).

There are three nodal forces corresponding to the three displacements given in Eq. (2-4):

$$p = \begin{pmatrix} p_w \\ p_{\theta x} \\ p_{\theta y} \end{pmatrix} \qquad (2\text{-}26)$$

The stiffness equations of a plate element in Fig. 1-2(a) are derived by the virtual work principle as shown in Appendix C. The results used in computer program are exhibited as follow.

For each plate element:

$$(S_{top} + S_{bottom} + S_{sub})\, V^e = P_d + P_t = P^e \qquad (2\text{-}27)$$

where:

S_{top}	Stiffness matrix of the top layer
S_{bottom}	Stiffness matrix of the bottom layer
S_{sub}	Stiffness matrix of the subgrade
P_d	Equivalent nodal force vector due to external applied loads
P_t	Equivalent nodal force vector due to temperature gradient
P^e	Total equivalent nodal force vector of the element

Their expressions are given below:

$$
\begin{aligned}
S_{top} &= \iint_{area} B^T D_{top} B \, dxdy \\
S_{bottom} &= \iint_{area} B^T D_{bottom} B \, dxdy \\
S_{sub} &= \iint_{area} k N^T N \, dxdy \\
P_d &= \iint_{area} p(x,y) N^T \, dxdy \\
P_t &= -\iint_{area} B^T M_t \, dxdy
\end{aligned}
\qquad \text{(2-28)}
$$

where $p(x,y)$ is intensity of the applied loads and k is modules of pavement subgrade. All element formulae in above equations are derived and listed in Appendix C. Thus, the stiffness matrix of plate element are:

$$
S^e = S_{top} + S_{bottom} + S_{sub} \qquad \text{(2-29)}
$$

2 Bar Element

The dowel bar system can be modeled by three segments of beams: two bending beams embedded in concrete, Ci_b and j_bD in Fig. 2-1(a), and one shear-bending beam in the joint, i_bj_b in Fig. 2-1(a). Before pavement being loaded, the nodes of slab and dowel bar, i_s and i_b or j_s and j_b, are assumed identical. However, after the pavement being loaded, they are separated as shown in Fig. 2-1(b).

The stiffness matrix of beam i_bj_b can be written as:(Przemieniecki[1968])

$$S_b = \frac{EI}{l^3(1+\phi)} \begin{bmatrix} 12 & 6l & -12 & 6l \\ 6l & (4+\phi)l^2 & -6l & (2-\phi)l^2 \\ -12 & -6l & 12 & -6l \\ 6l & (2-\phi)l^2 & -6l & (4+\phi)l^2 \end{bmatrix} \qquad \textbf{(2-30)}$$

$$= \begin{bmatrix} D1x & D2x & -D1x & D2x \\ D2x & D3x & -D2x & D4x \\ -D1x & -D2x & D1x & -D2x \\ D2x & D4x & -D2x & D3x \end{bmatrix} = \begin{bmatrix} S_{11} & S_{12} \\ S_{21} & S_{22} \end{bmatrix}$$

Where:

E	Elastic Modulus of the bar
I	Moment of inertia of the cross section
l	Length of the bar (or width of the joint)
ϕ	$24(1+u)I/A_s l^2$
A_s	Cross-sectional area effective in shear
u	Poison ratio
D1X	$= 12EI/l^3(1+\phi)$
D2X	$= 6EI/l^2(1+\phi)$
D3X	$= (4+\phi)EI/l(1+\phi)$
D4X	$= (2-\phi)EI/l(1+\phi)$

$$\mathcal{S}_{11} = \begin{bmatrix} D1x & D2x \\ D2x & D3x \end{bmatrix}$$

$$\mathcal{S}_{12} = \begin{bmatrix} -D1x & D2x \\ -D2x & D4x \end{bmatrix}$$

$$\mathcal{S}_{21} = \mathcal{S}_{12}^{T}$$

$$\mathcal{S}_{22} = \begin{bmatrix} D1x & -D2x \\ -D2x & D3x \end{bmatrix}$$

The force and displacement vectors are defined as:

$$P_b = [Q_i \; M_i \; Q_j \; M_j]_b^T \tag{2-31}$$

$$V_b = [w_i \; \theta_i \; w_j \; \theta_j]_b^T \tag{2-32}$$

Where w and θ are vertical and rotational displacements, and Q and M are shear force and bending moment at the bar nodes respectively. Their positive directions are defined in Fig. 2-2.

Most dowel bar models employed in currently available computer programs are based on Eq. 2-30 (Tabatabaie[1979], Majidzadeh[1984], Tayabji[1986] and Nashizawa[1989]). Different authors modified Eq. (2-30) using different assumptions to consider the interaction between dowel bars and concrete. Guo[1992] has found that the dowel bar stiffness matrices employed by some

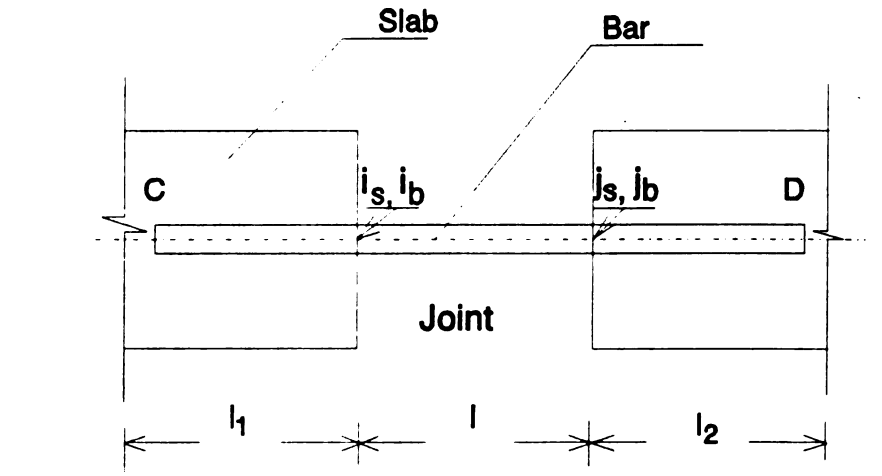

(a) Before Deflection

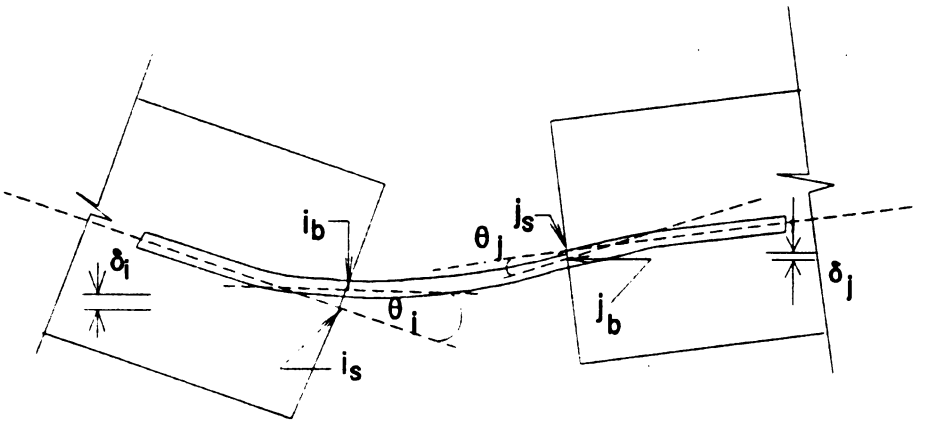

(b) After Deflection

Fig. 2-1 Dowel Bar Before and After Deflection

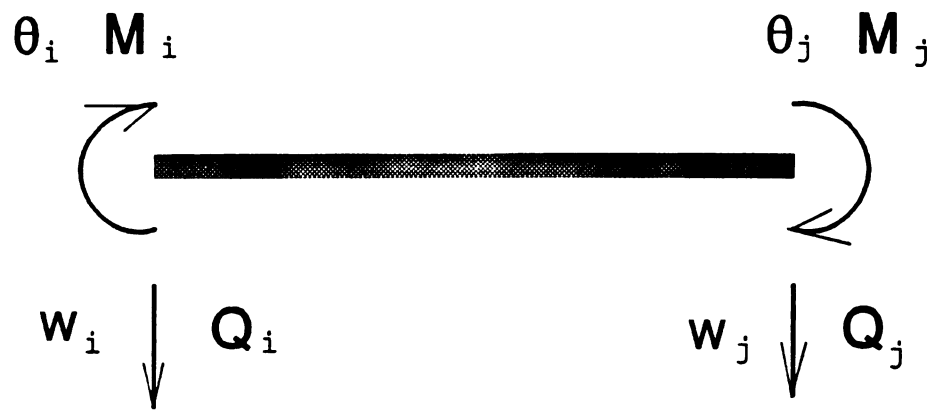

Fig. 2-2 Positive Directions of Bar's Displacements and Forces

computer programs for jointed concrete pavement analysis, including JSLAB-86 and ILLISLAB, failed to satisfy the equilibrium condition which is one of the basic requirements of the FEM. A component dowel bar model has been proposed to simulate the behavior of the dowel bar load transfer system. The detailed discussion is given in Chapter 4.

3 Spring Element

Spring elements are used to model aggregate interlock and the keyway in which only the vertical forces are transferred across the joint. At each node of the spring element shown in Fig. 1-2(c) , only one displacement

unknown, vertical displacement W in z direction, is defined. The nodal force corresponding to the vertical displacement is vertical shear force Q. The stiffness equation is:

$$\begin{Bmatrix} Q_i \\ Q_j \end{Bmatrix} = \begin{bmatrix} SP & -SP \\ -SP & SP \end{bmatrix} \begin{Bmatrix} W_i \\ W_j \end{Bmatrix} = \mathbf{S}_p \mathbf{W} \tag{2-33}$$

The stiffness matrix of a spring element can be written as:

$$\mathbf{S}_p = \begin{bmatrix} SP & -SP \\ -SP & SP \end{bmatrix} \tag{2-34}$$

where SP, which may be defined as the equivalent spring stiffness for aggregate interlock or keyway, can be obtained by laboratory and/or field tests.

CHAPTER THREE
MODIFICATION OF PROGRAM JSLAB-86

1. Need for Modification

Many computer programs are available for analysis of jointed concrete pavements for both design and research purposes. Because these programs were developed independently, it is necessary to evaluate their purported capabilities and assess their accuracies before using them in engineering practice. Recently Smith[1990] and Mueller[1990] presented their evaluation for many programs popularly used in the United States. As stated by Mueller[1990], some widely used programs, such as ILLISLAB (Ioannides[1984]) and JSLAB (Tayabji[1986]), both based on the finite element method and employing the same assumptions, produce results that are significantly different. For example, the differences in predicted maximum displacements can be as great as 20 percent, and the difference in predicted thermal stresses can exceed 100 percent.

It can be expected that all correct computer programs employing the same theory and assumptions should produce reasonably close results. The most efficient means to check the accuracy of a program is to compare its results with those produced by using a precise analytical procedure. A simple analytical procedure is proposed to calculate the response of a beam resting on Winkler elastic base under uniformly distributed and concentrated loads, temperature gradient or both. The major advantage of this model is to provide solutions as precise as desired when a portion of

the beam is separated from the base. Separation cases are commonly encountered when predicting thermal stresses of concrete slabs on elastic base. Timoshenko[1941] and Westergaard's models (Yoder[1975]) are unable to treat the case accurately, since they assume that "extension springs" still exist between the separated portion of the beam and the Winkler base. In fact, there is no interaction between the beam and base when they are separated from each other. An numerical iteration technique is employed by almost all computer programs to approach the final results. However, the correct results will never be received unless the contact condition is appropriately defined and the iteration loops are logically written. A precise and closed form solution, even if only one dimension, would be very helpful to validate these computer programs.

In this chapter, the analytical model is first developed, and detailed derivations are given. Numerical demonstrations are given to prove the accuracy of the analytical results through comparisons between results calculated and those by other theoretical models. (Timoshenko[1941] and Yoder[1975].) More numerical examples are presented to briefly introduce the features of the responses due to combinations of loads and temperature gradient. Then the proposed analytical procedure is employed to detect problems in computer program JSLAB-86. Finally, numerical examples indicate that the modified JSLAB, JSLAB-92, produces responses of single slab under different traffic loading identical to those produced by ILLISLAB. The discussion of dowel bar modeling problems discovered in JSLAB and ILLISLAB is presented in Chapter 4.

2. A Simple Analytical Model

Basic model assumptions include:

(1) The material behavior of beams is linear elastic

(2) The intensity of base reaction is proportional to the deflection at any section which is in contact with the base

(3) The intensity of the base reaction is zero at any section which is separated from the base

(4) The temperature variation is linear along the thickness of the beam

(5) The beam, loads and temperature gradient are symmetrical to y axis (see Fig. 3-1).

Although the beam and base are both assumed elastic, the responses of the system (beam plus base) under loads and temperature gradient are nonlinear since the contact length between beam and base always varies with the temperature gradient and loads. The major difference between the defined problem and the solved problems in many classical textbook, such as "Strength of Materials" by Timoshenko[1941], is the added third assumption. The classical theory assumes the intensity of the interaction forces between the beam and base are always proportional to the section deflection, whether they are in contact or separated from each other. The classical theory is accurate enough to predict the responses of slender beams on elastic bases due to loads, since the weight of the beam usually causes contact between the beam and base when additional loads are added. However, the third assumption must be added to deal with the responses, in

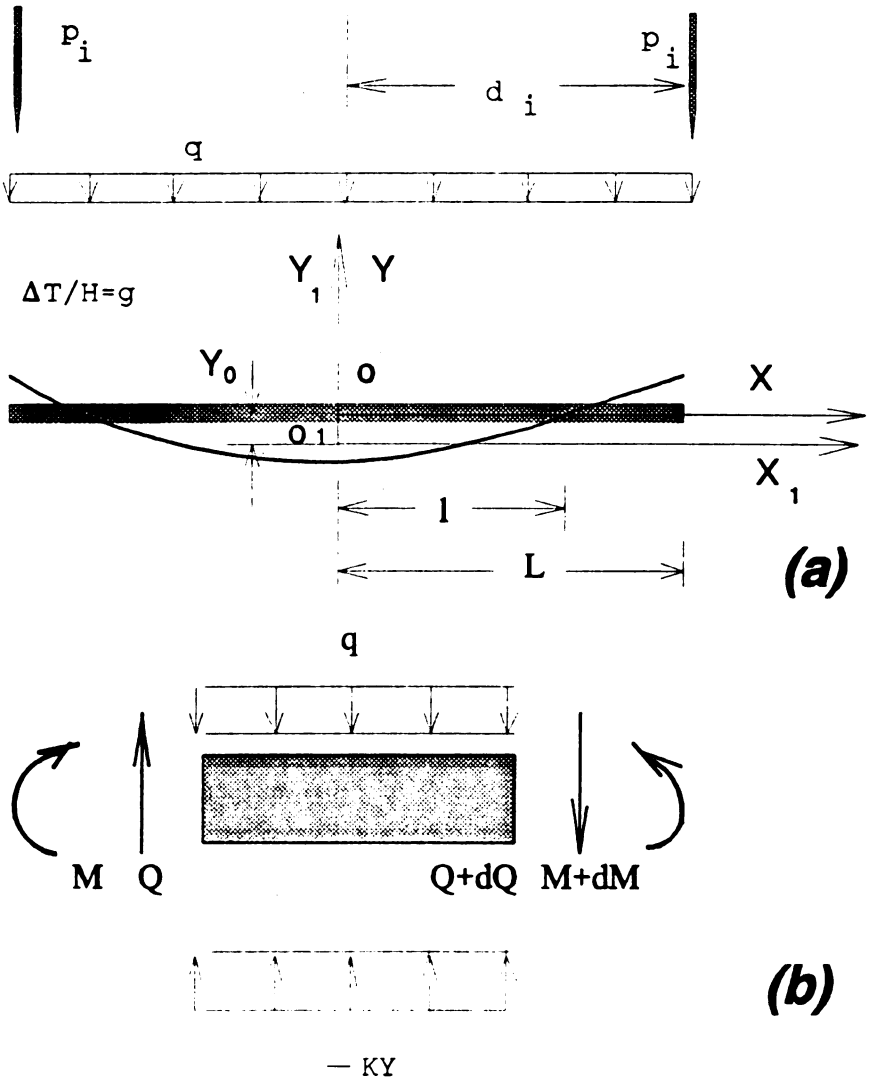

All notations presented are positive

Fig. 3-1 A Beam on Extensionless Elastic Base

case the beam and base become significantly separated.

Basic equations

The coordinate system and assumed positive notations are presented in Fig. 3-1 where coordinate XOY is defined at the center horizontal line of the beam before its weight is acted on, and coordinate $X_1O_1Y_1$ is defined at the center horizontal line of the beam after its weight is acted on. The following discussions are based on coordinate system XOY unless specifically mentioned.

The basic equations for contact portion of the beam can be written as (Timoshenko[1941]):

$$EI\frac{d^4y}{dx^4}+Ky=-q \qquad (-l \le x \le l) \tag{3-1}$$

However, the equation for separated portion of the beam should be:

$$EI\frac{d^4y}{dx^4}=-q \qquad (-l > x \ \ or \ \ x < l) \tag{3-2}$$

In Fig. 3-1 and above equations:

l	is a half of length of contact portion of the beam;
E	is elastic modules of the beam material;
I	is bending inertia moment of the beam section;
g = ΔT/H,	is temperature gradient;
H	is thickness of the beam.
K	is base coefficient of the beam.

The beam responses due to a combination of temperature gradient and loads can be calculated by two steps as shown in Fig. 3-2.

Where:

α is thermal coefficient of the beam material.

The first step is to add two artificial rotation constraints at each end of the beam, and apply a temperature gradient. In this case, the beam ends will be acted by two bending moments ($M = EI\alpha g$) caused by the assumed temperature gradient as shown in Fig. 3-2(b). The second step is to add two moments $M = EI\alpha g$ with directions opposite to the ones in step one and to add other loads as they are, as shown in Fig. 3-2 (c). The total response of displacements and forces in Fig. 3-2(a) is the sum of responses shown in Fig. 3-2(b) and (c).

General solutions

If only a uniformly distributed load to simulate the self-weight of the beam and symmetrically concentrated loads act on the curled area ($-1 > x$ or $x > 1$), the problem can be greatly simplified. The general solution of Eq. (3-1) is:

$$y=e^{\beta x}(A\cos\beta x+B\sin\beta x)+e^{-\beta x}(C\cos\beta x+D\sin\beta x)-\frac{q}{k} \qquad (3\text{-}3)$$

Where:

$$\beta = \left(\frac{k}{4EI}\right)^{0.25} \qquad (3\text{-}4)$$

The following conditions can be used to determine the constants in Eq. (3-3):

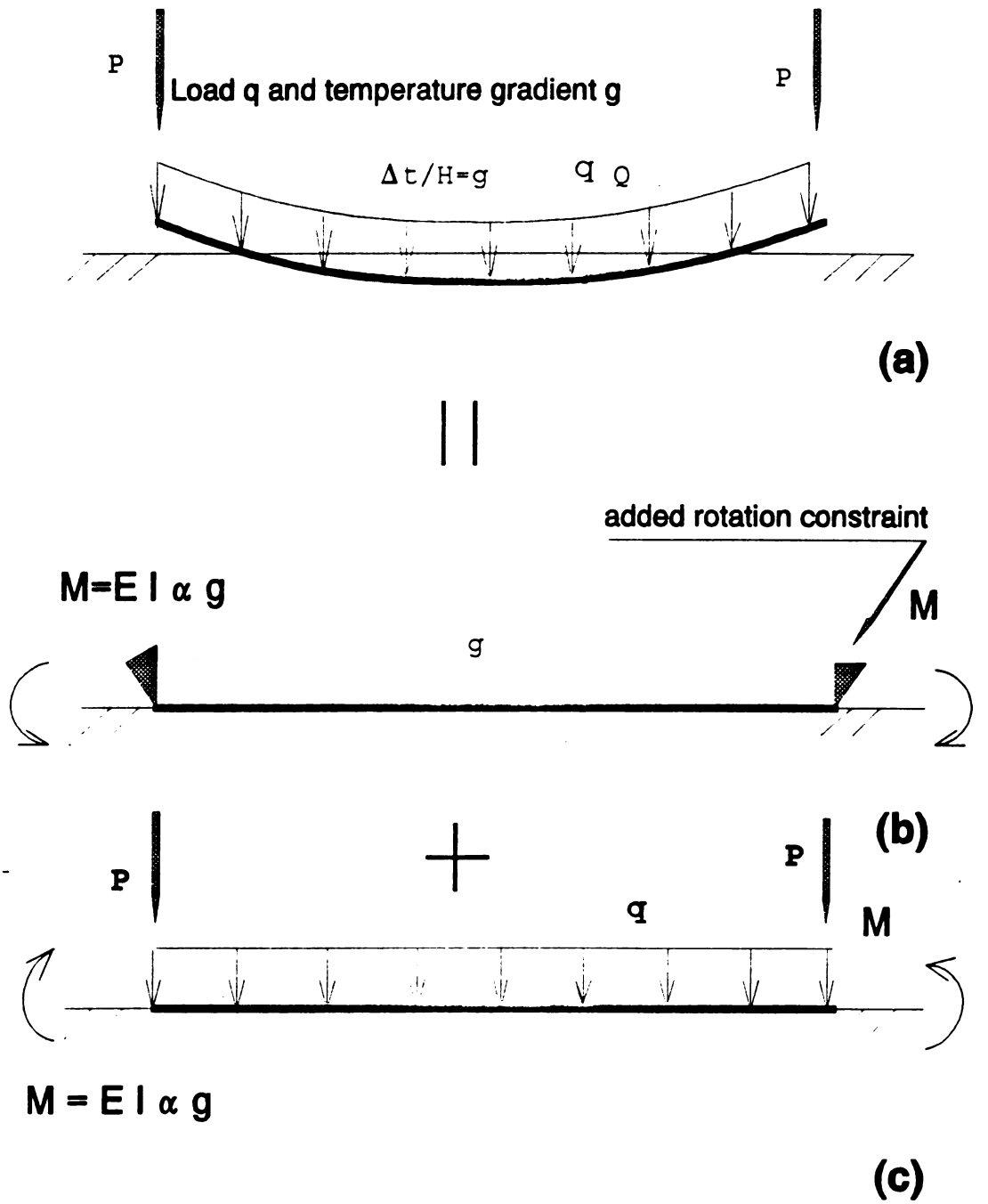

Fig. 3-2 Analysis Procedure

$$y(-x) = y(x) \tag{3-5}$$

$$M(x=l) = EI\frac{d^2y}{dx^2}(x=l) = -\frac{q}{2}(L-l)^2 - \sum_{i=1}^{N} P_i\ (d_i - l) + EI\alpha g \tag{3-6}$$

$$Q(x=l) = EI\frac{d^3y}{dx^3} = q(L-l) + \sum_{i=1}^{N} P_i \tag{3-7}$$

$$\int_0^l ykdx = -qL - \sum_{i=1}^{N} P_i \tag{3-8}$$

$$y(x=l) = 0 \tag{3-9}$$

where N is the total number of concentrated loads acted on the curled portion of half of the beam, and d_i is distance of the ith concentrated load to the center of the beam (origin of the coordinate system, Fig. 3-1(a)).

It can be easily proved that Eq. (3-7) must be satisfied if Eq. (3-8) is satisfied. Therefore, Eq. (3-7) will not be employed in the following discussion. Substituting Eq.(3-3) into Eq. (3-5), we obtain:

$$A = C \tag{3-10}$$

$$B = -D \tag{3-11}$$

Substituting Eq. (3-10) and Eq. (3-11) to Eq. (3-3) to obtain displacement:

$$y = A\,(e^{\beta x} + e^{-\beta x})\cos\beta x + B\,(e^{\beta x} - e^{-\beta x})\sin\beta x - \frac{q}{k} \tag{3-12}$$

Two unknowns (A and B) are included in Eq. (3-12) and they can be solved by substituting Eq. (3-12) into Eq. (3-6) and (3-9). Then A and B can be derived as:

$$\frac{B}{H} = \frac{q^{\circ}a + d[t^{\circ} - q^{\circ}(L^{\circ} - l^{\circ})^2 - \sum_{i=1}^{N} 2P_i^{\circ}(d_i^{\circ} - l^{\circ})]}{a^2 + d^2} \tag{3-13}$$

$$\frac{A}{H} = \frac{1}{d}\left(q^{\circ} - \frac{B}{H}a\right) \tag{3-14}$$

and l° can be obtained by substituting Eq.(3-13) and Eq.(3-14) into Eg.(3-8):

$$F(l^{\circ}) = (b+c)\frac{A}{H} + (b-c)\frac{B}{H} + 2(L^{\circ} - l^{\circ})q^{\circ} + \sum_{i=1}^{N} 2P_i^{\circ} = 0 \tag{3-15}$$

Where:

$$a = \sin l^{\bullet} \left(e^{l^{\bullet}} - e^{-l^{\bullet}}\right)$$

$$b = \sin l^{\bullet} \left(e^{l^{\bullet}} + e^{-l^{\bullet}}\right)$$

$$c^{\bullet} = \cos l^{\bullet} \left(e^{l^{\bullet}} - e^{-l^{\bullet}}\right)$$

$$d = \cos l^{\bullet} \left(e^{l^{\bullet}} + e^{-l^{\bullet}}\right)$$

$$l^{\bullet} = \beta\, l$$

$$L^{\bullet} = \beta\, L$$

$$q^{\bullet} = \frac{q}{kH}$$

$$P_i^{\bullet} = \frac{P_i \beta}{kH}$$

$$d_i^{\bullet} = \beta d_i$$

$$t^{\bullet} = \frac{\alpha g}{2\beta^2 H}$$

Substituting $l^{\bullet} = \beta l$, received from Eq. (3-15), into Eq.(3-12) and dividing by the beam height H obtains the non-dimensional displacement of the

contact portion of the beam as:

$$\frac{y}{H}=\frac{A}{H}\cos\beta x(e^{\beta x}+e^{-\beta x})+\frac{B}{H}\sin\beta x(e^{\beta x}-e^{-\beta x})-q^{*} \qquad \textbf{(3-16)}$$

$$(-1 < x < 1)$$

The curled portion of the beam is statically determinate and the displacement can be derived by fundamental beam theory as:

$$\frac{y}{H}=-\frac{q^{*}L^{*4}}{6}(1-\frac{x}{L})^{4}+\frac{2}{3}(1-\frac{l}{L})^{3}(1-\frac{x}{L})-\frac{1}{2}(1-\frac{l}{L})^{4}-\sum_{i=1}^{N}Y_{P_i}$$
$$+[\frac{A}{H}(c-b)+\frac{B}{H}(c+b)](\beta x-l^{*})+t^{*}L^{*2}(\frac{x}{L}-\frac{l}{L})^{2} \qquad \textbf{(3-17)}$$

$$(-1 > x, \text{ or } x > 1)$$

Where Y_{Pi} is displacement due to the ith concentrated load. If only one concentrated load acts at end of the beam, the following formula can be used:

$$\sum_{i=1}^{N}Y_{P_i}=\frac{2}{3}P^{*}L^{*3}[2(1-\frac{l}{L})^{3}-3(1-\frac{l}{L})^{2}(1-\frac{x}{L})+(1-\frac{x}{L})^{3}] \qquad \textbf{(3-18)}$$

where:

$$P^{*}=\frac{P\beta}{kH} \qquad \textbf{(3-19)}$$

The bending moment of the contact portion of the beam is:

$$M=EI\frac{d^{2}y}{dx^{2}}-EI\alpha g \qquad \textbf{(3-20)}$$

Substituting Eq.(3-16) into Eq. (3-20) obtains the non-dimensional bending moment as:

$$\frac{M}{kH/2\beta^2} = [-\frac{A}{H}\sin\beta x(e^{\beta x}-e^{-\beta x}) + \frac{B}{H}\cos\beta x(e^{\beta x}+e^{-\beta x})] - t^* \qquad \textbf{(3-21)}$$

$$(-1 < x < 1)$$

The curled portion of the beam is statically determinant so its bending moment can be written directly:

$$M = -\frac{q(L-x)^2}{2} - \sum_{i=1}^{N} P_i(d_i-x) \qquad \textbf{(3-22)}$$

$$(-1 > x, \text{ or } x > 1)$$

Its non-dimensional form is:

$$\frac{M}{kH/2\beta^2} = -q^*(L^*-\beta x)^2 - \sum_{i=1}^{N} 2P^*_i(d^*_i-\beta x) \qquad \textbf{(3-23)}$$

3. Accuracy of the Analytical Model

The accuracy of the analytical model can be proved by checking its assumptions and derivation process step by step. An alternative is to compare its results with those obtained by some well known models developed under the same conditions. Fig. 3-3 to Fig. 3-6 present the

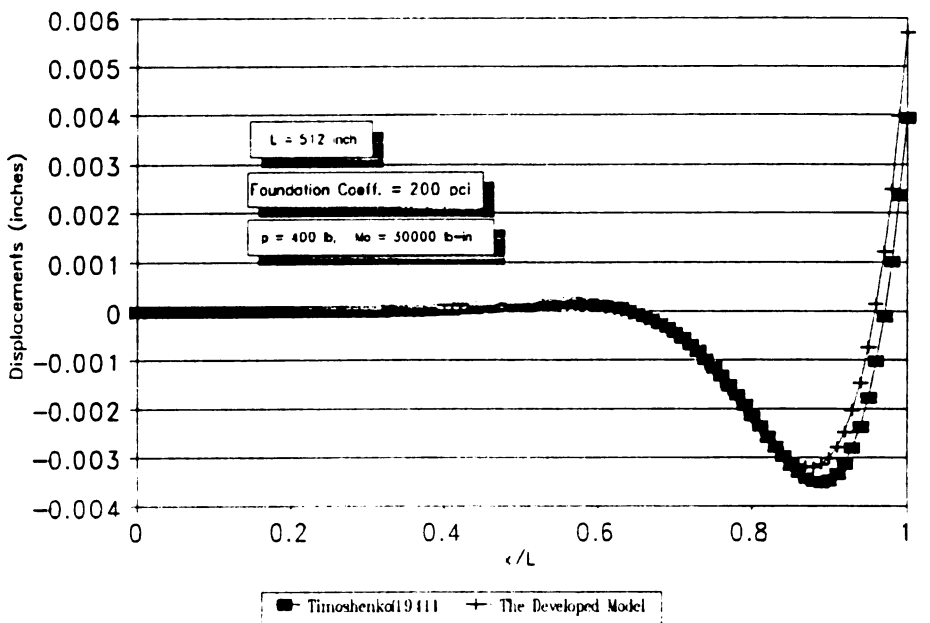

Fig. 3-3 Comparison of Displacements (1)

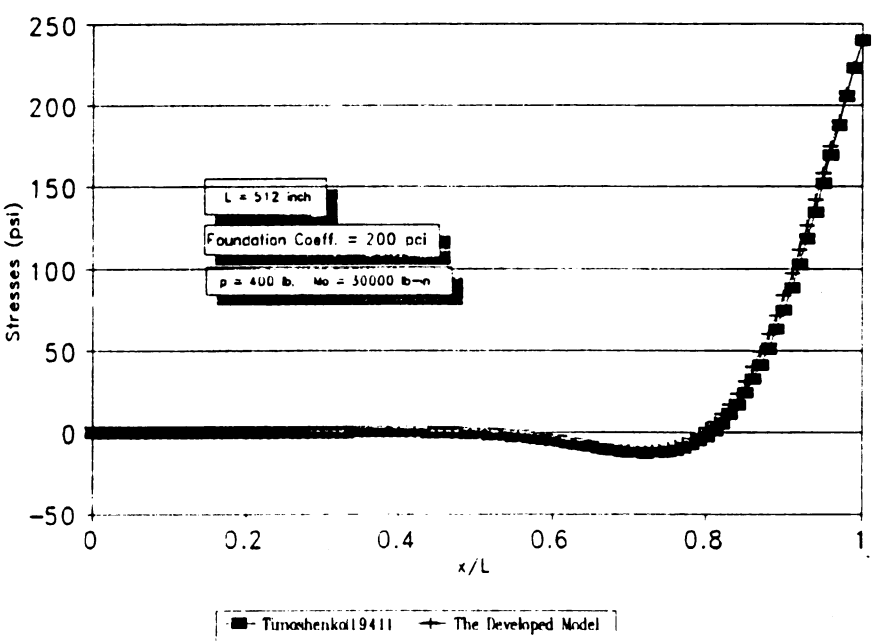

Fig. 3-4 Comparison of Stresses (1)

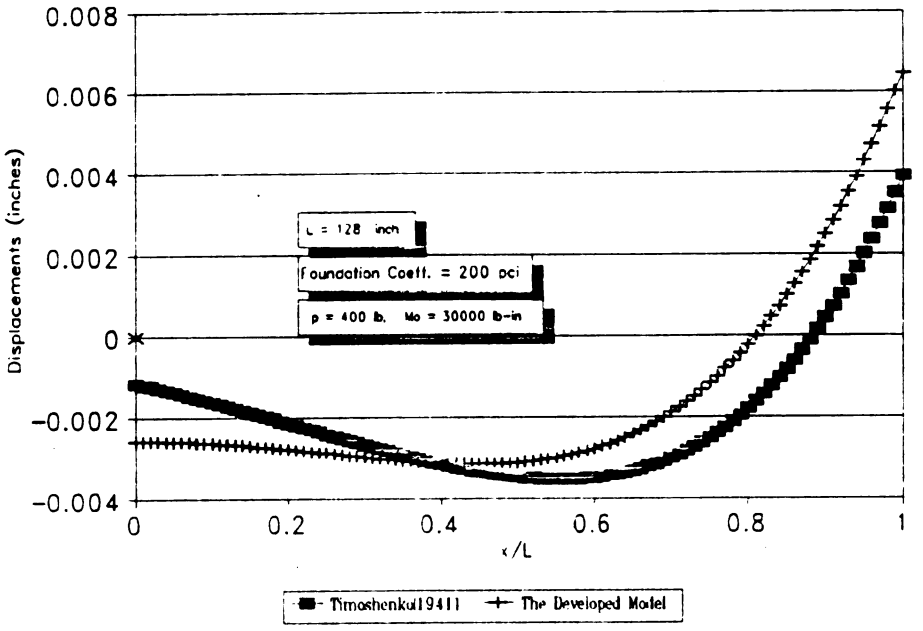

Fig. 3-5 Comparison of Displacements (2)

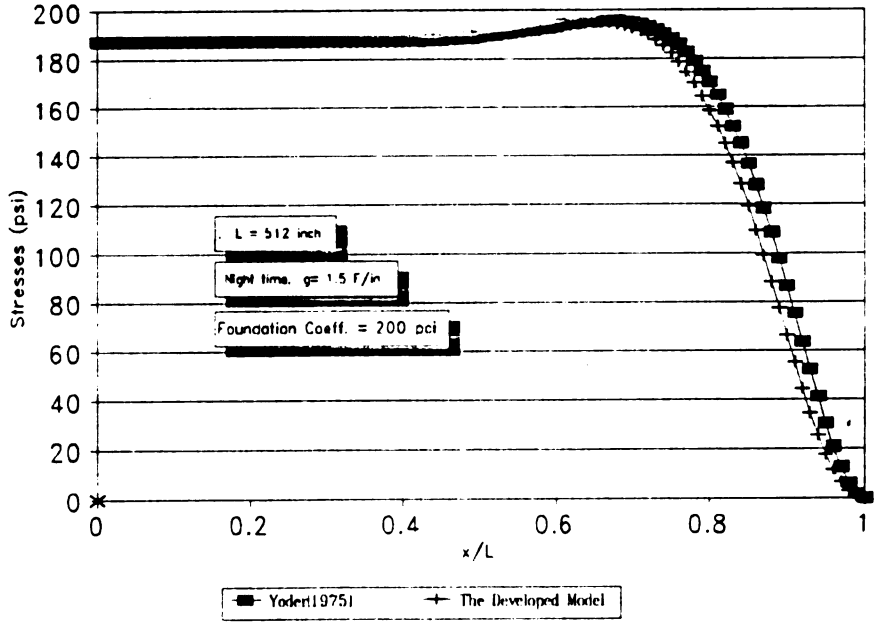

Fig. 3-6 Comparison of Stresses (2)

comparison of displacements and stresses received by the developed procedure and the models given by Timoshenko[1941] and Westergaard (Yoder[1975]). A weightless beam with half length L=512 inches is used, since the models developed by Timoshenko and Westergaard are for infinite beams or slabs. The input data are as follows:

Beam size:	D = 7.5 inch
	H = 10 inch
Material properties:	E = 5000000 psi
	u = 0
	k = 200 pci (K = 1500 psi for beam)
	α = 0.000005 1/°F
Loads:	Mo = 30000 lb-in, same direction to the moment M in Fig. 3-2 (c), acted at the ends
	P = 400 lb, downward, acted at the ends

Fig. 3-3 and Fig. 3-4 show the resulting displacements and stresses. Since the assumption of "extension springs" applies even if a portion of the beam is separated from the base, the results by Timoshenko are smaller than those generated by the developed analytical model. The differences between the displacements near the beam ends are even more significant. Fig. 3-5 also presents the displacements produced by Timoshenko model and the model presented in this chapter, except using a shorter half length, L=128 inch, instead of L=512 inch. As shown in Fig. 3-5, the difference increases as the half length decreases.

Fig. 3-6 shows the comparison of stress predicted by Westergaard formula (Yoder[1975]) and the model in this chapter. A night time temperature gradient g=1.5 °F/in is applied, and the unit weight of the beam is assumed 0.09 pci. No additional loads act on the beam in this case. It can be seen that Westergaard's results overestimate the stress responses since it was also developed based on the assumption that "extension springs" exist, even if a portion of the slab is separated from the base. However, the responses of the location far from the edge, $|x/L| < 0.7$, are identical.

Figs. 3-7 to Fig. 3-10 show the effects on beam length to the thermal response of beam on an elastic base. The night time temperature gradient is 1.5 °F/in, and the unit weight is 0.09 pci. The other parameters are the same as listed above in this section.

Fig. 3-7 presents the deflected shape of the beams with various half beam lengths. When the length of beam is long enough, the displacements of interior portion of the beam approach the average vertical settlement of the beam due to its weight. In this case:

$$d = -\frac{\gamma h}{k} = -\frac{0.09 * 10}{200} = -0.0045 \; inch$$

Thus, the shorter beam would have larger settlement in the middle.

Fig. 3-8 also presents the variation of stress distribution of beams with various half lengths. It can be seen that the effect of beam length is

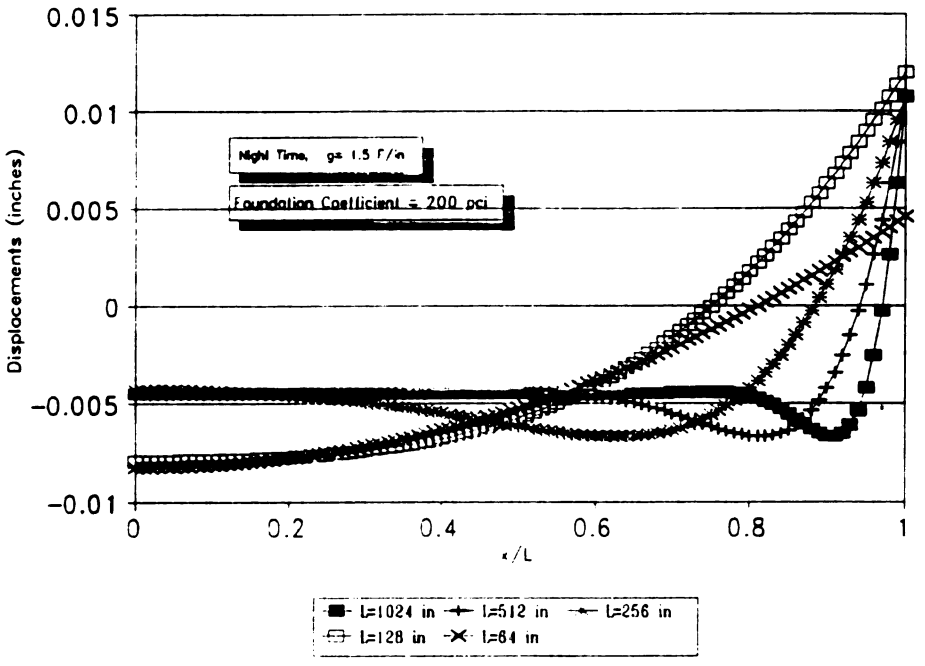

Fig. 3-7 Displacement Distributions for Various Half Beam Lengths (L)

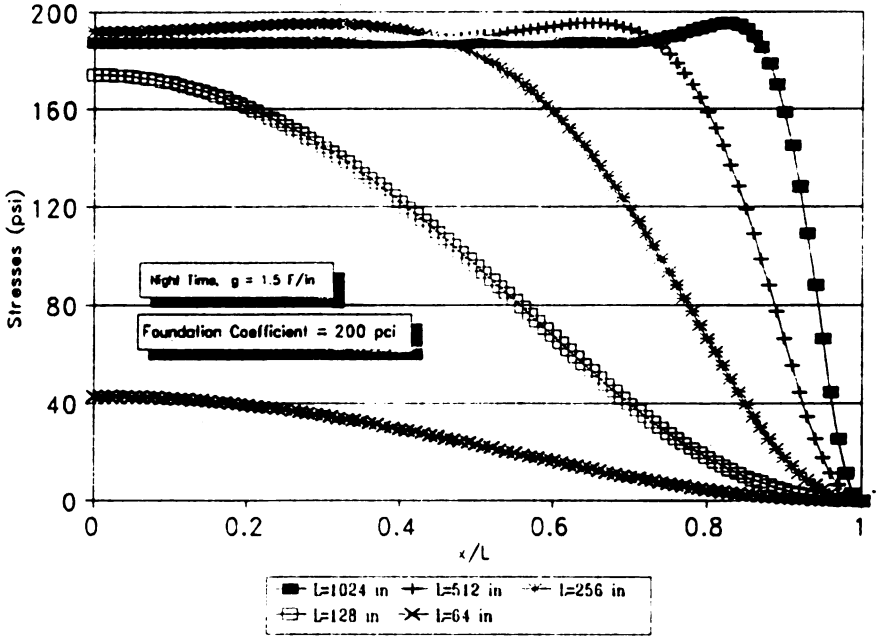

Fig. 3-8 Stress Distributions for Various Half Beam Lengths (L)

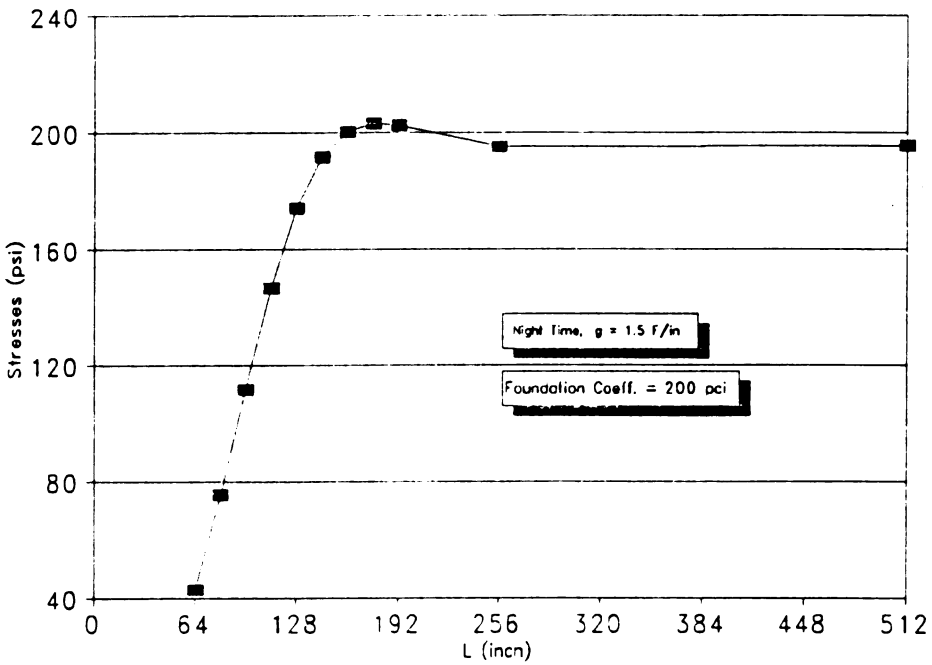

Fig. 3-9 The Maximum Stresses for Various Half Beam Lengths (L)

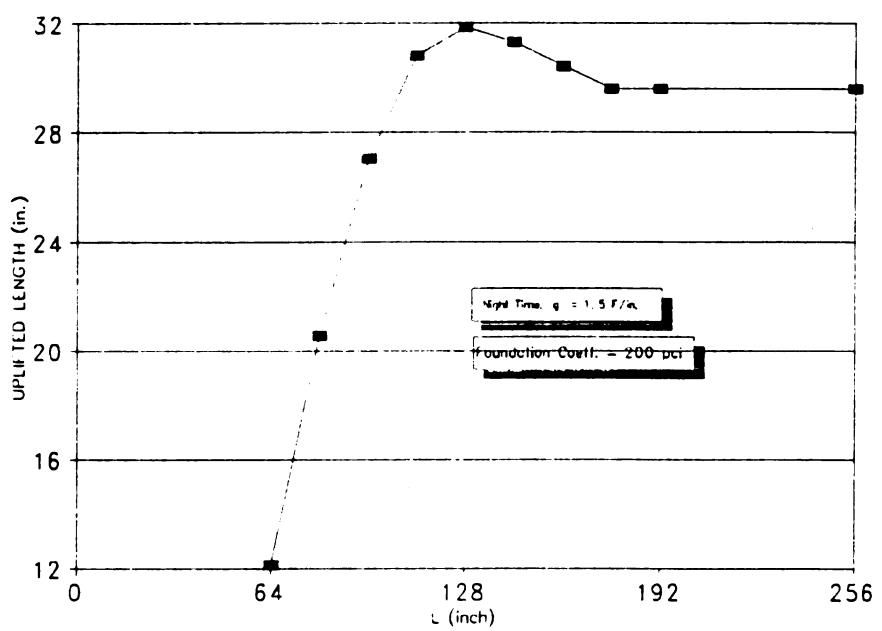

Fig. 3-10 The Uplifted Lengths (L-l) for Various Half Beam Lengths (L)

very significant. The stress at the middle of the beam approaches a constant as the length of the beam increases to infinity. The constant is just the precise interior stress given by Yoder[1975] for infinitely large slab with the assumption of poisson ratio u = 0:

$$\sigma_{interior} = \frac{E\alpha gh}{2(1-\mu)} = \frac{5*10^{6}*5*10^{-6}*1.5*10}{2*(1-0)} = 187.5\ psi$$

Fig. 3-9 presents the maximum bending stresses versus half beam lengths L. The maximum thermal stresses remain constant if the beam's half length is larger than 256 inch (entire length of the beam is longer than 42 feet). When the half length of the beam is approximately 176 inch, the thermal stress of the beam is at a maximum value. It can be seen from Fig. 3-8 that the maximum stresses are not always located at the center of the beam.

Fig. 3-10 shows the length of the uplifted portion versus beam length. It is reasonable that the uplifted lengths will not be changed if the half length of the beam is equal to or longer than 176 inch. The 128 inch long beam would have maximum uplifted length when all beams meet the same temperature gradient.

A group of displacements and stresses for a 144 inch long beam (72 inch half length), subjected to 3°F/in night time temperature gradient and resting on k=300 pci elastic base, are presented in Fig. 3-11 and Fig. 3-12. Load P is acted on two ends of the beam with a unit weight of 0.09 pci. The results reflect the response properties of a beam with finite length and subjected to a combination of uniformly distributed load,

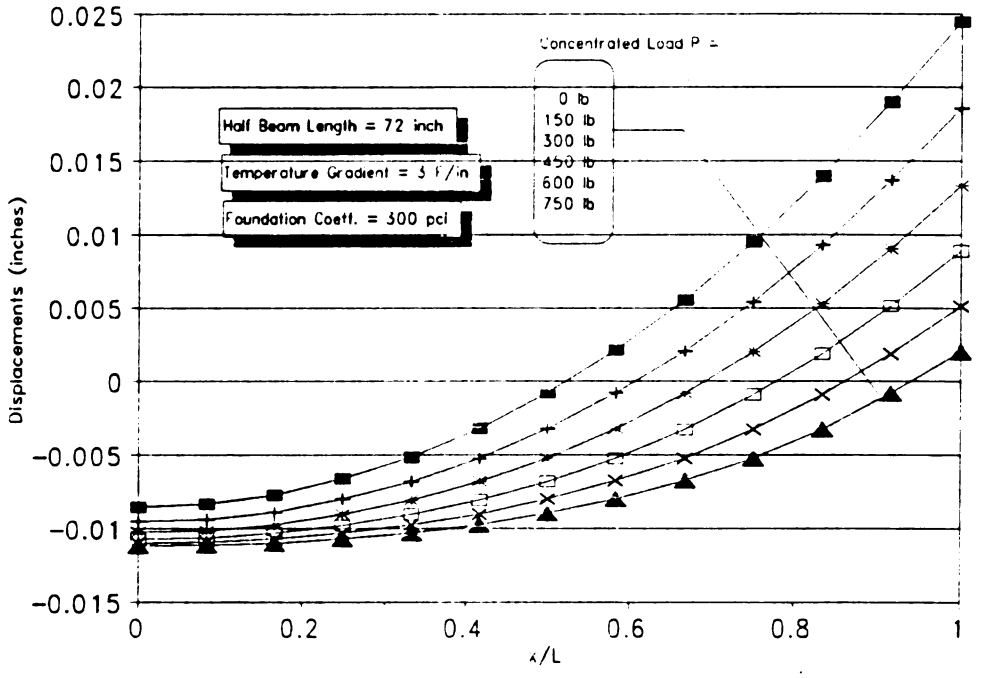

Fig. 3-11 Displacement Distributions for Various Concentrated Loads at Ends

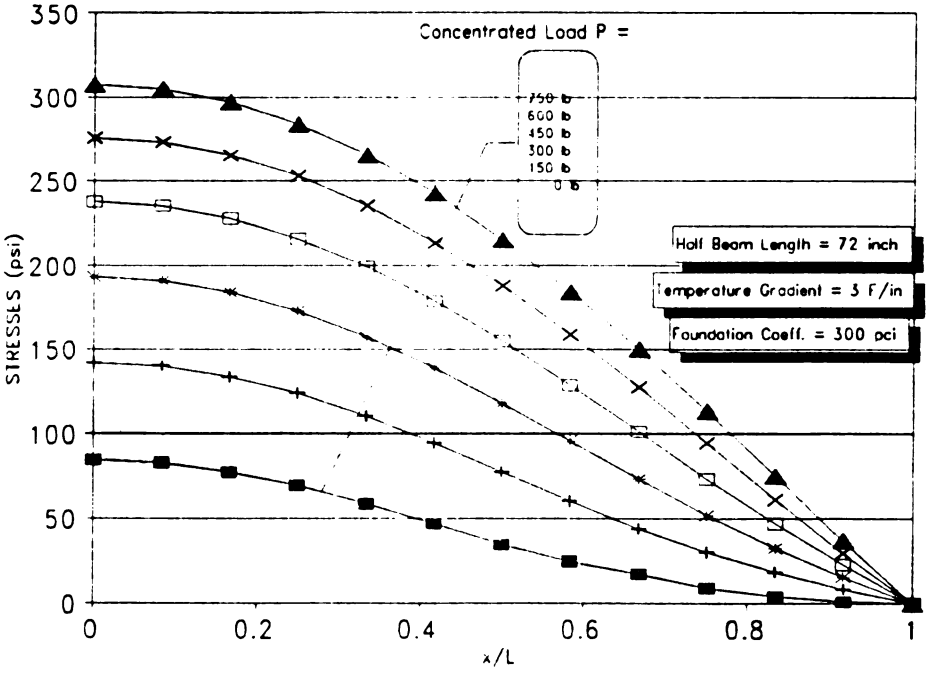

Fig. 3-12 Stresses Distributions for Various Concentrated Loads at Ends

concentrated load, and temperature gradient. The results can be used to check any existing finite element program for analysis of concrete pavements.

4. Problems in JSLAB-86

As mentioned in the introduction, JSLAB has been evaluated by Smith[1990] and Mueller[1990]. JSLAB was selected to conduct the research on dowel bar mathematical modeling because it is a well organized and user friendly software, and is not a copyright reserved program. It will be beneficial for all users of JSLAB if its reliability can be fully studied and improved. Furthermore, there existed disagreements in evaluations of JSLAB. It would be helpful for all to find the appropriate answer.

Stiffness matrices for single slab system in JSLAB-86.

Fig. 3-13 presents the displacements produced by JSLAB-86 and the analytical model. The analytical curve is one of the six shown in Fig. 3-11. The input data used for executing JSLAB-86 are the same as mentioned above, and Poisson's ratio was taken as 0 for the one dimensional problem. The two curves are identical. However, the consistency of displacements does not prove there exist no problems. After carefully checking subroutine ELEM of JSLAB-86, it has been found that S(10,8), S(11,7), S(11,9) and S(12,8) in the subgrade stiffness matrix are the same

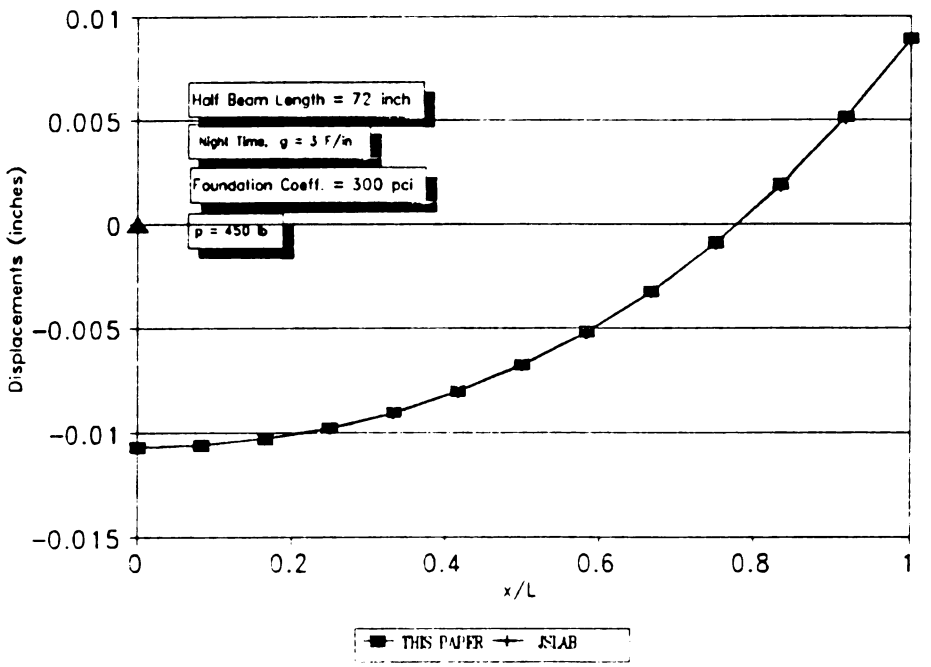

Fig. 3-13 Comparison of Displacement Distributions

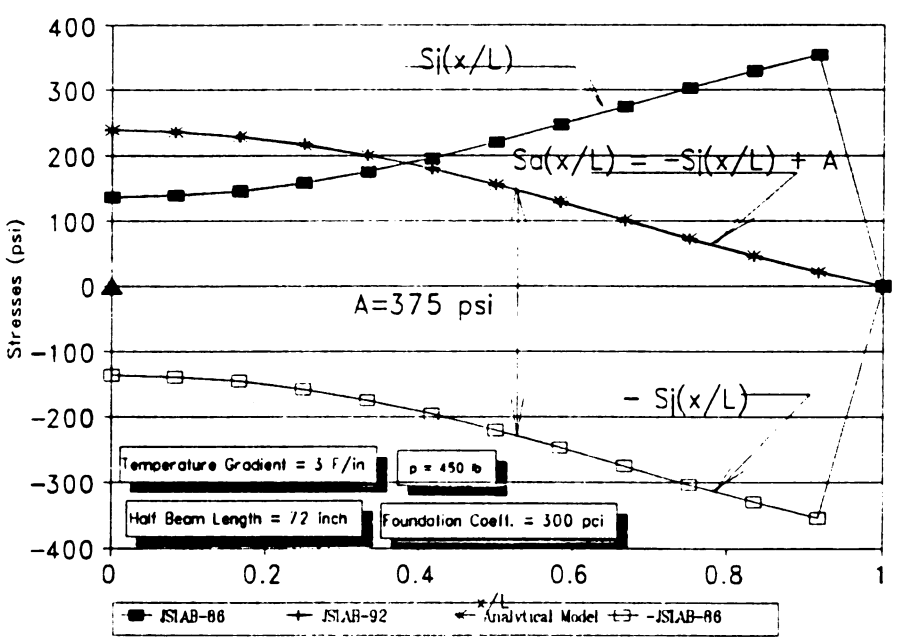

Fig. 3-14 Comparison of Stress Distributions

in magnitude but different in sign to those used by Ioannides[1984]. By using virtual work principle as a check, it has been verified that the results used by Ioannides are correct.

Tables 3-1, 3-2 and 3-3 show the results obtained by JSLAB-86, JSLAB-92 and ILLISLAB for interior, edge and corner loading conditions respectively. The input data and finite element meshes are the same to those used by Ioannides [1984], page 107, 149 and 170 respectively. Although the results of ILLISLAB were obtained by using a mainframe computer with double precision and those of the JSLAB-92 by 486 PC computer with single decision mode, they are nearly identical. Therefore, the following conclusions may be obtained:

(1) The errors in the subgrade stiffness matrix of the original JSLAB causes small differences from the modified JSLAB and ILLISLAB for a single slab system under traffic loads.

(2) The JSLAB-92 program produces the same results as ILLISLAB does, so it is concluded the both are credible to predict the responses of a single slab under traffic loads.

(3) Single precision is applicable in PC computer programs to provide sufficiently accurate responses.

Table 3-1 Interior Loading (Displacements: inches, Stresses: psi, on top)

k(pci)	H(in)	Maximum Displacements			Maximum Stresses		
		J-86	J-92	ILLI	J-86	J-92	ILLI
50	12	.0364	.0358	.0358	553.2*	-562.4	-562.4
200	12	.0169	.0166	.0166	477.7*	-487.2	-487.2
500	12	.0102	.0101	.0101	433.8*	-442.3	-442.3
50	20	.0189	.0188	.0188	222.5*	-226.4	-226.4
200	20	.0085	.0084	.0084	201.7*	-205.3	-205.3
500	20	.0052	.0050	.0050	183.4*	-187.2	-187.1

* The sign of stresses in JSLAB is incorrect, see next section.

Table 3-2 Edge Loading (Displacements: inches, Stresses: psi, on top)

k(pci)	H(in)	Maximum Displacements			Maximum Stresses		
		JSLAB	M-JSLAB	ILLISLAB	JSLAB	M-JSLAB	ILLISLAB
50	12	.1100	.1097	.1097	958.7	-973.8	-974
200	12	.0496	.0492	.0492	802.1	-813.3	-813
500	12	.0296	.0292	.0293	696.6	-704.8	-705
50	16	.0786	.0782	.0785	583.4	-592.9	-593
200	16	.0342	.0341	.0341	507.3	-515.0	-515
500	16	.0203	.0201	.0202	447.7	-453.9	-454
50	20	.0635	.0633	.0633	388.7	-395.2	-395
200	20	.0259	.0258	.0258	350.5	-356.0	-356
500	20	.0152	.0151	.0151	314.5	-319.2	-319

Table 3-3* Corner Loading (Displacements: inches, Stresses: psi, on top)

k(pci)	H(in)	Maximum Displacements		Maximum Stresses	
		M-JSLAB	ILLISLAB	M-JSLAB	ILLISLAB
200	9	.0596	.0595	307.7	307.5
200	9	.0567	.0566	271.3	270.9
200	9	.0539	.0538	242.2	242.7
100	9	.0814	.0814	282.0	282.1
400	9	.0393	.0393	259.8	259.9
200	6	.1003	.1004	563.9	563.6
200	12	.0374	.0375	159.7	159.9

* JSLAB-86 does not have capability to calculate principal stresses.

The sign of stresses and the thermal stress formula

Fig. 3-14 illustrates the stress distributions obtained by JSLAB-86 and the analytical model. The negative values of JSLAB-86 curve plus a constant are close the results prediced by the analytical model. The zero thermal stress at x/L = 1 was predicted by JSLAB-86 since it was determined by boundary conditions directly rather than the thermal stress formula. After comparing the difference, the symmetrical feature can be clearly seen. The following notations are used for convenience.

$S_j(x)$ stress calculated by JSLAB-86

$S_a(x)$ stress calculated by the analytical procedure

The relation between $S_j(x)$ and $S_a(x)$ can be written as:

$$S_a(x) = -S_j(x) + A \qquad (3\text{-}24)$$

Where, A is a constant of 375 psi indicated in Fig. 3-14.

As mentioned in section 2 of this chapter, the total response (including displacements and stresses) should be the sum of responses given in Fig. 3-2(b) and (c). The negative sign in Eq. (3-24) indicates that the sign of stresses calculated by JSLAB-86 was not correct. The constant A indicates that a part of the stress was lost. Carefully checking Fig. 3-2, the stresses due to (c) are not constant, but the stress due to (b) is constant:

$$A=\frac{\frac{EI\alpha g}{DH^2}}{6}=\frac{E\alpha gH}{2}=\frac{5*10^6*5*^{-6}*3*10}{2}=375\ psi$$

Therefore, two problems have been discovered by using the model developed in this chapter: incorrect sign of stress and a term missing in calculating thermal stress. Fig 3-14 shows that the JSLAB-92 provides the same results as the analytical ones.

The JSLAB-92 can calculate correct thermal stresses of slabs

Fig. 3-15 and Fig. 3-16 present the horizontal and vertical stress (σ_x and σ_y) distributions along the symmetrical axis of a slab (2048 in * 2048 in) under a daytime temperature gradient of 3 °F/in by the JSLAB-92 and Westergaard's formula (Yoder[1975]). Fig 3-17 and Fig. 3-18 present the same comparison for nighttime temperature gradient = 1.5 °F/in. As shown in these figures the thermal stresses are practically the same. In all cases, if and only if the slab is large enough, the calculated interior thermal stresses are extremely identical to those obtained by Westergaard

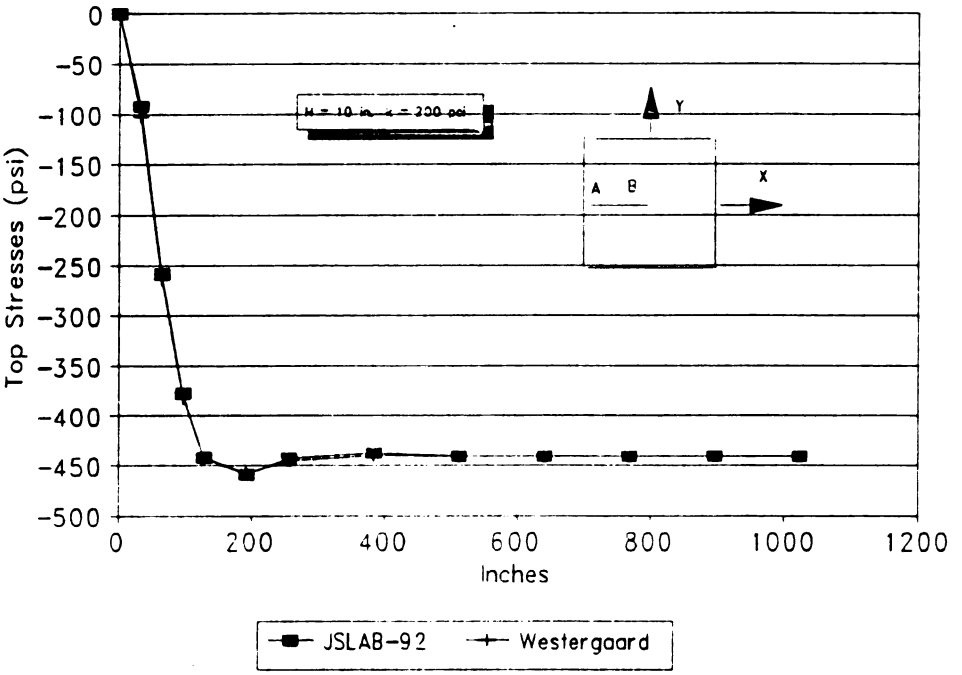

Fig. 3-15 Comparison of σ_x Along AB Line, Day Time, g=3.0 °F/in

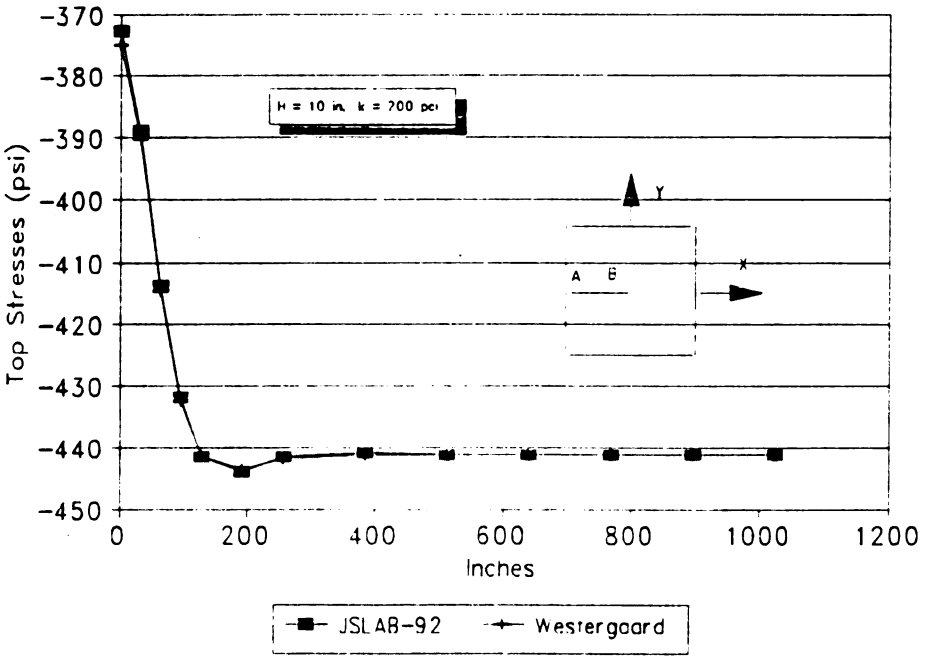

Fig. 3-16 Comparison of σ_y Along AB Line, Day Time, g=3.0 °F/in

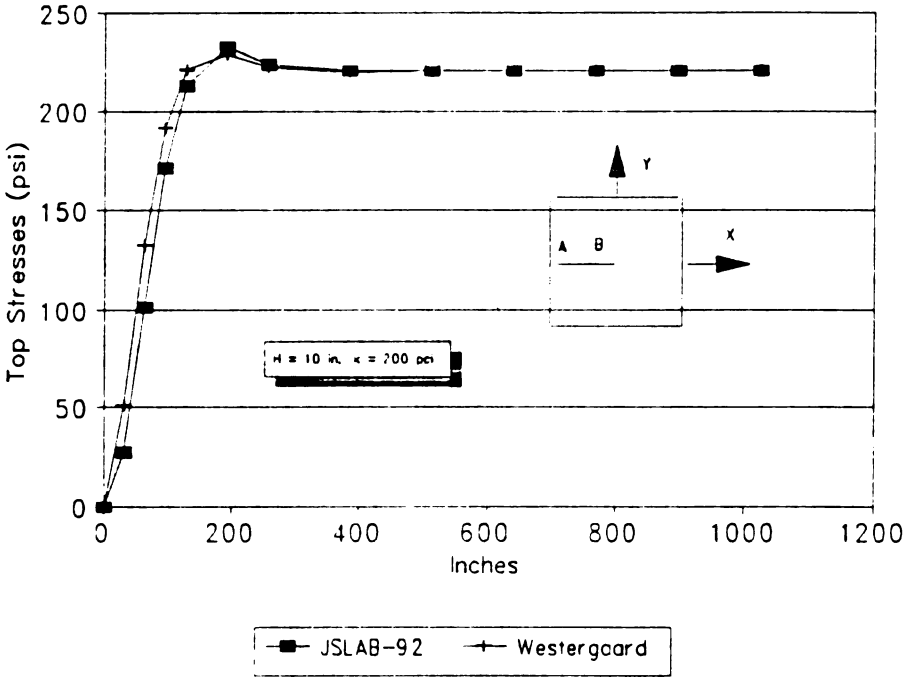

Fig. 3-17 Comparison of σ_x Along AB Line, Night Time, g=1.5 °F/in

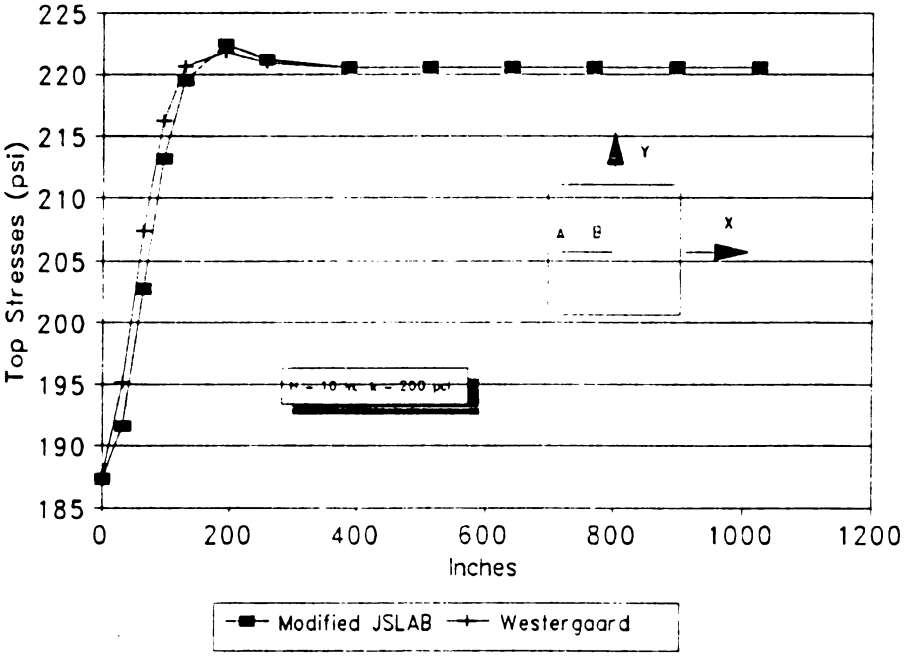

Fig. 3-18 Comparison of σ_y Along AB Line, Night Time, g=1.5 °

close form formula (Yoder[1975]) which is based on elasticity theory. The comparison of stresses near the edge subjected to day time thermal gradient are better than those subjected to the nighttime temperature gradient because the assumed "Extension springs" of Westergaard model in the curled up portion produce greater stresses than actually exist. In case of day time, however, the slab edge remains in contact with the base, the uplifted portion remains a certain distance from the edge and with a smaller amplitude. Thus, the effect of "extension springs" becomes secondary, see Fig. 3-19. The examples are only for checking the accuracy of existing programs.

The incremental responses produced by traffic load and/or temperature gradient

In many cases, engineers need to know the responses of slabs produced by traffic loading and/or temperature gradient only, without consideration of the slab weight. The numerical example given by Tayabji[1986] is given for the mentioned purpose. In this case, the input data of unit weight γ is set equal to zero, and the coordinate $X_1O_1Y_1$ in Fig. 3-1(a) is employed for the analysis.

Using the new coordinate system, Eq. (3-1) and Eq. (3-2) should be replaced by:

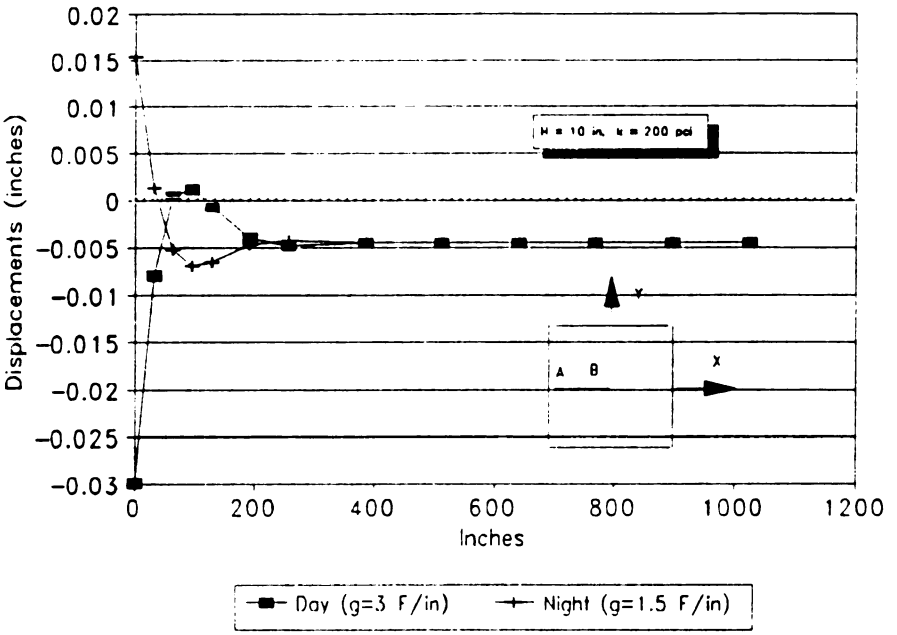

Fig. 3-19 Comparison of Day and Night Displacements Along AB Line

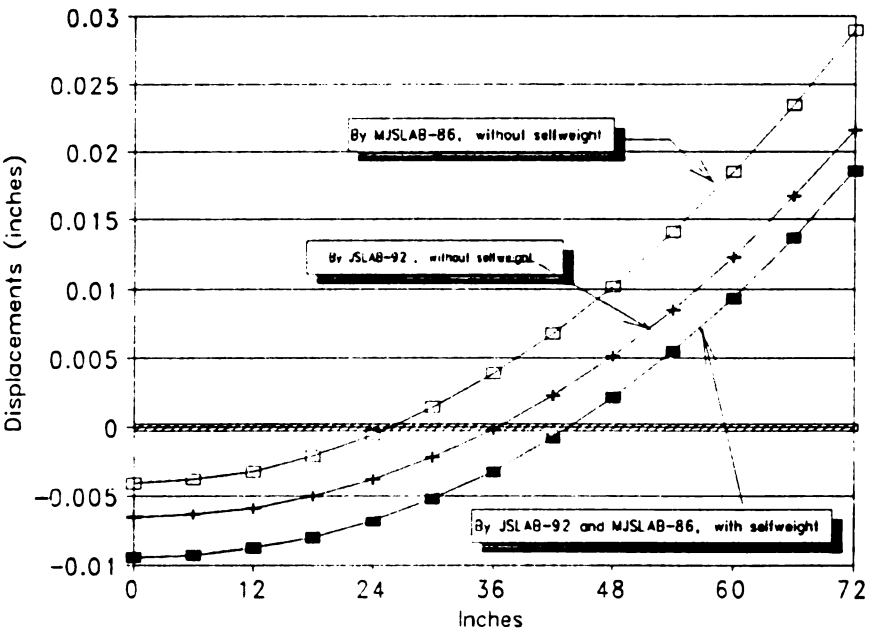

Fig. 3-20 Comparison of Displacements By Different Coordinate Systems

$$EI\frac{d^4Y_1}{dX_1^4} + KY_1 = 0 \qquad (-l \le x \le l) \tag{3-25}$$

$$EI\frac{d^4Y_1}{dX_1^4} = -q \qquad (-l > x \text{ or } x > l) \tag{3-26}$$

The relation between displacement under coordinates XOY and $X_1O_1Y_1$ is:

$$Y_1 = Y + Y_0$$
$$Y_0 = \frac{\gamma H}{k} = \frac{q}{K} \tag{3-27}$$

and the stresses for the two cases are same.

Fig. 3-20 shows that JSLAB-86 with the discovered errors discussed above, and the developed analytical procedure (denoted as JSLAB-92 since their results are very identical) predict the same displacements for the case of unit weight γ = 0.09 pci (under XOY coordinate system). However, the displacements for the weightless case of γ = 0.0 (under $X_1O_1Y_1$ coordinate system) are significantly different. Fig. 3-21 also shows that JSLAB-86 significantly underestimates stresses in case of γ=0 but the developed model has proved that the stresses under two coordinate systems should be same.

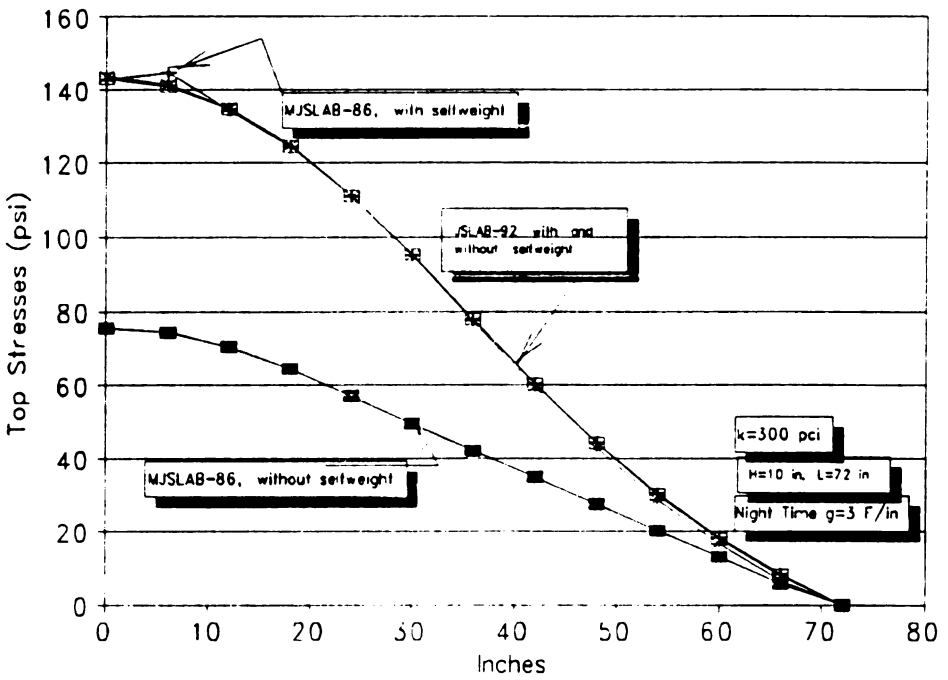

Fig. 3-21 Comparison of Stresses by Different Coordinate Systems

Instead of Eq. (3-26), JSLAB-86 uses the following equation to treat the uplifted portion of the beam:

$$EI\frac{d^4Y_1}{dX_1^4} = 0 \qquad (-l > x \text{ or } l > x) \tag{3-28}$$

In other words, when the uplifted region has been determined by numerical iteration, the weight of the slab is still set equal to zero. It can be found that Eq. (3-25) is correct (q=0) because the weight is balanced by the Winkler forces of the base, whereas Eq. (3-28) is incorrect since no Winkler forces exists for the separated portion. In this case, weight of the beam must be added back to approach the correct results. Fig. 3-20 and Fig. 3-21 also show that the JSLAB-92 produces correct results for both displacement and stress. The mentioned concepts are valid for beams and for slabs.

5. Summary

It would be significant to evaluate a computer program before using its results in engineering design or research. Consistency in displacement does not mean there exist no problems. The developed analytical procedure has been used as a potential tool to find problems in JSLAB-86. All of the discovered problems in JSLAB-86 dealing with single slab responses have been corrected. The modified program is referred to as JSLAB-92. After comparing the results of JSLAB-92 with those of the developed analytical procedure, computer program ILLISLAB, and Westergaard's

equations, it can be concluded that the responses of single slab under different types of loads are correct. The problems related to multiple slab system are presented in Chapter 4.

CHAPTER FOUR
DOWEL MODELS IN FINITE ELEMENT PROGRAMS FOR PCC PAVEMENT ANALYSIS

1. Introduction

Load transfer systems of PCC pavements have been theoretically and experimentally investigated since the 1930's (Teller[1935], Friberg[1938], Keeton[1956][1957] and Teller[1958]). In the application of the finite element method for PCC pavement analysis and design many computer programs (Tabatabaie[1979], Tayabji[1986] and Ioannides[1984]) have modeled dowel bars as beam elements based on classical theory (Timoshenko[1941] and Przemieniecki[1968]).

Some investigators (Tabatabaie[1979], Darter[1977], Ozbeki[1984] and Snyder[1989]) have summarized the behavior of load transfer systems of PCC pavements based on the mentioned classical and finite element models. Results were recently presented by Smith[1990] from many of the currently available models, both mechanistic and empirical, that simulate dowel bar behavior. The finite element approach has been used as an powerful tool to implement the analysis, design and evaluation of load transfer systems. Therefore the reliability of finite element models for PCC pavements becomes very important.

A number of errors were recently discovered in program JSLAB (Tayabli[1986]) and presented in Chapter 3. After the program was

modified, the new version JSLAB-92 produced the same results as the program ILLISLAB, for the responses of a single slab system. As mentioned by Smith[1990], the difference in results from the JSLAB and ILLISLAB for multiple slab systems with dowel bars was even greater than for single slabs. It has been demonstrated in this chapter that part of this difference is caused by the dowel bar stiffness matrices employed in the two programs.

Recently Nishizawa[1989] stated: "Tabatabaie, et. al., used the bar element to present the dowel function. However the bar element can not be used in the case where crack width is so narrow that the length of the bar element becomes too small and thus its rigidity becomes too high. This is caused by the assumption that the displacements at both end nodes of the bar element are the same as those of the slab element." Nishizawa[1989] presented the discrepancies between their experimental results and the predicted results from "the bar element" (Tabatabaie[1979]). However, the actual reason of the discrepancy has never been sufficiently discussed. The "refined model of doweled joint" presented by Nishizawa[1989] contains problems which will be discussed later in this chapter.

The "bar element" used by Tabatabaie[1979] was modified from the standard shear-bending stiffness matrix (Przemieniecki[1968]) for considering the interaction between the dowel and concrete such that the "rigidity" of the element has been greatly reduced. A detailed analysis is presented in this dissertation to discuss the dowel bar models employed by

Tabatabaie[1979] and Ioannides[1984]. The most serious drawback in these two programs is that the dowel bars have been modified into unequilibrium elements. The neglect of equilibrium conditions for the stiffness matrices employed to model dowel bars, is equivalent to the modification of the load vector of the pavement system. Numerical examples show this is very important to the final results for the slab critical stresses. Thus, it is concluded that equilibrium conditions should be considered in developing the stiffness matrix of dowel bars.

Fig. 2-1 depicts a dowel bar system before and after deflection. The dowel bar can be modeled by three segments of a beam: two bending segments embedded in concrete, Ci_b and j_bD in Fig. 2-1(a), and one shear-bending segment in the joint i_bj_b, where subcripts b and s denote the dowel bar and slab respectively. A rigorous model of dowel bar load transfer systems, with minimum modification of classical theory, is briefly introduced. The embedded length of dowel bars and the physical properties of materials have been considered in the model so that it can be employed to investigate optimal design for dowel systems. A 4 x 4 matrix model of a shear-bending beam element and another 2 x 2 matrix model of a shear beam element are also developed. Numerical examples indicate that results produced by the three models are very close to each other for solid dowel bars popularly used in the field. The models developed in this chapter could make a contribution by being able to model different types of load transfer systems.

2. A Direct Finite Element Method Approach

If the displacements of dowel bar at i and j are equal to the displacements of slabs at i and j respectively then the stiffness matrix of beam ij can be written as (Przemieniecki[1968]):

$$S = \frac{EI}{l^3(1+\phi)} \begin{bmatrix} 12 & 6l & -12 & 6l \\ 6l & (4+\phi)l^2 & -6l & (2-\phi)l^2 \\ -12 & -6l & 12 & -6l \\ 6l & (2-\phi)l^2 & -6l & (4+\phi)l^2 \end{bmatrix}$$

$$= \begin{bmatrix} D1x & D2x & -D1x & D2x \\ D2x & D3x & -D2x & D4x \\ -D1x & -D2x & D1x & -D2x \\ D2x & D4x & -D2x & D3x \end{bmatrix} = \begin{bmatrix} S_{11} & S_{12} \\ S_{21} & S_{22} \end{bmatrix} \qquad (4\text{-}1)$$

Where:

E Elastic Modulus of the beam

I Moment of inertia of the cross section

l Length of the beam (or width of the joint)

ϕ $24(1+u)I/A_s l^2$

A_s Cross-sectional area effective in shear (0.9 times the area for circular cross section)

u Poisson ratio

D1X $= 12EI/l^3(1+\phi)$

D2X $= 6EI/l^2(1+\phi)$

D3X $= (4+\phi)EI/l(1+\phi)$

D4X $= (2-\phi)EI/l(1+\phi)$

The force and displacement vectors are defined as:

$$\boldsymbol{P} = [Q_i \;\; M_i \;\; Q_j \;\; M_j]^T \tag{4-2}$$

$$\boldsymbol{V} = [w_i \;\; \theta_i \;\; w_j \;\; \theta_j]^T \tag{4-3}$$

where w and θ are vertical and rotational displacements of, and Q and M are shear force and bending moment of the beam nodes respectively. Their positive directions are defined in Fig. 4-1.

Fig. 2-1(b) is a dowel bar system after deflection and shows the interaction between the steel bar and concrete. The relationship between the two displacement vectors can be written as follows (Timoshenko[1941]):

$$\begin{Bmatrix} P \\ M_0 \end{Bmatrix} = \boldsymbol{k}_T \Delta \boldsymbol{v} = 2\beta^2 EI \begin{bmatrix} 2\beta & 1 \\ 1 & \frac{1}{\beta} \end{bmatrix} \begin{Bmatrix} \delta_0 \\ \theta_0 \end{Bmatrix} \tag{4-4}$$

$$\begin{aligned} \boldsymbol{k}_T &= 2\beta^2 EI \begin{bmatrix} 2\beta & 1 \\ 1 & \frac{1}{\beta} \end{bmatrix} \\ \delta_0 &= W_b - W_s \\ \theta_0 &= \theta_b - \theta_s \\ \beta &= \left(\frac{\Psi D}{4EI}\right)^{\frac{1}{4}} \end{aligned} \tag{4-5}$$

Where the force, moment, displacements and rotations (P, M_0, δ_0 and θ_0) are depicted in Fig. 4-2, Ψ is the interaction coefficient of dowel

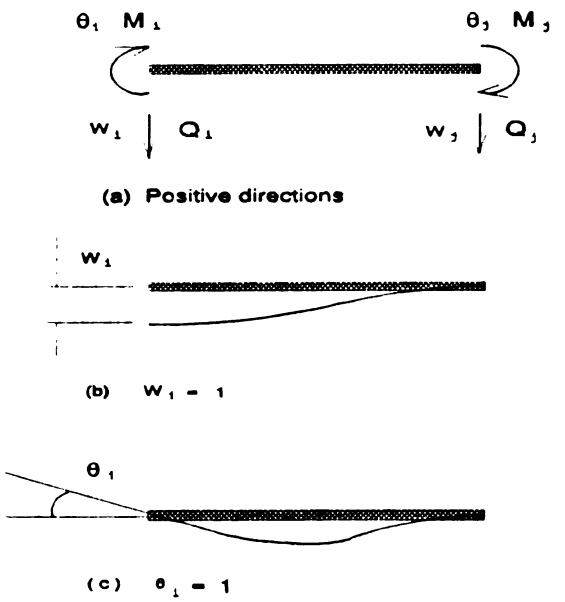

Fig. 4-1 Notations of Displacements and Forces of Dowel Bar Element

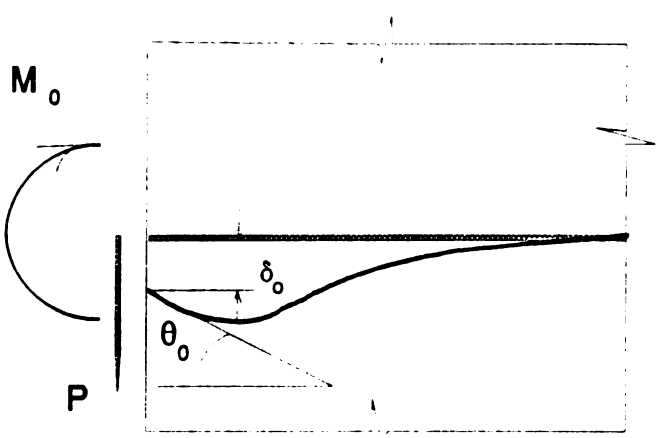

Fig. 4-2 Elastic Beam in Elastic Medium

bar, and D is the dowel bar diameter.

Eq. (4-4) is precise if and only if the beam is assumed to be infinitely long, homogeneous and elastic without consideration of shear deformation, and the concrete is assumed to be a uniform elastic medium. In Eq.(4-5), W_b, θ_b and W_s, θ_s are displacements of dowel bar and slab respectively. If they are defined as independent unknowns for a finite element program, a 4 X 4 stiffness matrix as follows should be added into the global stiffness matrix of the system:

$$S_r = \begin{bmatrix} S_T & -S_T \\ -S_T & S_T \end{bmatrix} \qquad (4\text{-}6)$$

Stoner[1991] uses Eq. (4-6) to model the dowel bars. Although this equation models dowel bar load transfer systems with minimum assumptions (infinitely long beam in pure elastic medium), it also has two significant drawbacks. First the total number of unknowns has to be greatly increased and second the bandwidth of the global stiffness matrix will be larger, which will require much longer computation time and will cause considerable programming difficulties. Therefore, most investigators have established an approximate but direct relation between dowel bar and slab displacements, instead of treating them as independent unknowns.

3. Modified Shear-bending Beam Model

The computer program JSLAB (Tayabli[1986]) employs the following formula to consider the interaction between steel bars and concrete slabs:

$$S_J = \begin{bmatrix} \frac{1}{\frac{1}{D1X}+\frac{1}{DCX}} & D2X & -\frac{1}{\frac{1}{D1X}+\frac{1}{DCX}} & D2X \\ D2X & \frac{1}{\frac{1}{D3X}+\frac{1}{DCXM}} & -D2X & \frac{1}{\frac{1}{D4X}+\frac{1}{DCXM}} \\ -\frac{1}{\frac{1}{D1X}+\frac{1}{DCX}} & -D2X & \frac{1}{\frac{1}{D1X}+\frac{1}{DCX}} & -D2X \\ D2X & \frac{1}{\frac{1}{D4X}+\frac{1}{DCXM}} & -D2X & \frac{1}{\frac{1}{D3X}+\frac{1}{DCXM}} \end{bmatrix} \quad (4\text{-}7)$$

where: $DCX = 2\beta^3 EI$

$DCXM = \beta EI$

Assuming: E = 29,000,000 psi u = 0.30

D = 1.25 inch l = 0.25 in

Ψ = 1500000 pci

then: I = .11984 in^4 β = 0.6060 1/in

ϕ = 54.17

DCX = 1,547,000 lb/in DCXM = 2,106,000 lb-in

D1X = 48,383,000 lb/in D2X = 6,048,000 lb

D3X = 14,658,000 lb-in D4X = -13,146,000 lb-in

In this case, S(1,1) (48,383,000 lb/in, Eq. (4-1)) is replaced by $S_j(1,1)$ (1,499,000 lb/in, Eq. (4-7)) to reduce the stiffness of dowel bar for consideration of the interaction between steel bar and concrete. Similar replacements were employed to modify S(1,3), S(2,2), S(2,4), S(3,1), S(3,3), S(4,2), and S(4,4) in the JSLAB program (Tayabji[1986]). Among the eight elements, S(2,4) and S(4,2) are modified in magnitude as well as in sign. Based on the above data, S(2,4) and S(4,2) are changed from -13,146,000 lb-in to 2,508,000 lb-in.

These assumptions result in two failures to satisfy equilibrium conditions.

First, the force vector (Eq. (4-2)) will usually be a nonequilibrium force system. For example, define a displacement vector Fig. 4-1(b):

$$\boldsymbol{V} = [1 \quad 0 \quad 0 \quad 0]^T \tag{4-8}$$

Premultiplying Eq. (4-8) by stiffness matrix Eq. (4-7), the force vector of the element is obtained:

$$\boldsymbol{P} = \boldsymbol{S_J}\,\boldsymbol{V} = \left[\frac{1}{\frac{1}{D1X}+\frac{1}{DCX}} \quad D2X \quad -\frac{1}{\frac{1}{D1X}+\frac{1}{DCX}} \quad D2X \right]^T \tag{4-9}$$

which fails to satisfy the moment equilibrium condition, $\Sigma M = 0$.

Second, rigid body movement would produce non-zero element forces. For instance, define a rigid body movement vector:

$$V = \left[W_i \quad -\frac{W_i - W_j}{l} \quad W_j \quad -\frac{W_i - W_j}{l} \right]^T \tag{4-10}$$

Premultiplying Eq. (4-10) by Eq. (4-7). a non-zero force vector is obtained. For example, the first element Q_i is:

$$Q_i = \left(\frac{1}{\frac{1}{D1X} + \frac{1}{DCX}} - \frac{2D2X}{l} \right) (W_i - W_j) \neq 0 \quad if \quad W_i \neq W_j \tag{4-11}$$

The ILLISLAB program (Tabatabaie[1979] and Ioannides[1984]) modifies **S(1,1), S(1,3), S(3,1)** and **S(3,3)** the same as JSLAB does while the other matrix elements remain the same as Eq.(4-1). The modification causes similar nonequilibrium problems, as analyzed above.

4. A Component Stiffness Matrix

Nishizawa[1989] developed a "refined model" to simulate dowel bar load transfer systems. The entire dowel bar was divided into three segments as shown in Fig. 4-1. The two segments embedded in concrete were modeled by finitely long bending beams in an elastic medium (Timoshenko[1941]) and the middle segment was modeled by a standard bending beam. The stiffness matrices for each segment were derived and assembled into a 4 x 4 final stiffness matrix for the load transfer system. For cases of a very narrow joint, the contribution of the middle segment was neglected. The major advantages of this model are that:

a. The finite length of the dowel has been considered so that the model is capable of a detailed dowel bar analysis

b. The number of the unknowns remains the same as other simplified models

c. The contributions of the three segments have been involved in the final matrix.

However, the "refined model" also has two potential sources of error in predictions:

a. The equations 18 (a) and (b) of the reference (Nishizawa[1989]) were incorrectly derived, so that the final stiffness matrix expression is different from the one which had been expected by the authors.

b. The middle segment of the dowel bar was inappropriately modeled by a bending beam.

After modifying the derivation given by Nishizawa[1989] and employing the standard shear-bending beam (Eq. (4-1)) to replace the bending beam, the following stiffness matrix is obtained:

$$[K_c]=\begin{bmatrix} T_1 & 0 \\ 0 & T_2 \end{bmatrix}\left(\begin{bmatrix} E & 0 \\ 0 & E \end{bmatrix} - \begin{bmatrix} S_{11}+T_1 & S_{12} \\ S_{21} & S_{22}+T_2 \end{bmatrix}^{-1}\begin{bmatrix} T_1 & 0 \\ 0 & T_2 \end{bmatrix}\right) \qquad (4\text{-}12)$$

Where:

$$[T_1] = \frac{2\beta^2 EI}{C_1^2+C_1^2}\begin{bmatrix} 2\beta(S_1C_1+s_1c_1) & -(S_1^2+s_1^2) \\ -(S_1^2+s_1^2) & \dfrac{(S_1C_1-s_1c_1)}{\beta} \end{bmatrix}$$

$$[T_2] = \frac{2\beta^2 EI}{C_2^2+C_2^2}\begin{bmatrix} 2\beta(S_2C_2+s_2c_2) & (S_2^2+s_2^2) \\ (S_2^2+s_2^2) & \dfrac{(S_2C_2-s_2c_2)}{\beta} \end{bmatrix}$$

$$E = \begin{bmatrix} 1 & 0 \\ 0 & 1 \end{bmatrix}$$

S=shβL, C=chβL, s=sinβL and c=cosβL. Subscripts 1 and 2 indicate the left and right segments respectively. β can be found in Eq. (4-5) and S_{11}, S_{12}, S_{21} and S_{22} can be found in Eq. (4-1). The detailed derivations are given in Appendix D.

5. A Proposed Shear-bending Beam Model (4 x 4 Stiffness Matrix)

Modification of Eq. (4-1)

In all cases where shear deformation is more important than bending deformation, such as a beam with relatively small length compared to width and height, ϕ in Eq. (4-1) is much greater than 1. The dowel bar element typically fits the above condition. In the example given in section three, $\phi = 54.17$. Therefore, the assumption of $1/(\phi+1) \approx 1/\phi$ is substituted into Eq. (4-1) to obtain:

$$S_{MJ1} = \begin{bmatrix} \frac{GA}{l}\xi & \frac{GA}{2}\xi & -\frac{GA}{l}\xi & \frac{GA}{2}\xi \\ \frac{GA}{2}\xi & \frac{GA}{4}l\xi+\frac{EI}{l}\eta & -\frac{GA}{2}\xi & \frac{GA}{4}l\xi-\frac{EI}{l}\eta \\ -\frac{GA}{l}\xi & -\frac{GA}{2}\xi & \frac{GA}{l}\xi & -\frac{GA}{2}\xi \\ \frac{GA}{2}\xi & \frac{GA}{4}l\xi-\frac{EI}{l}\eta & -\frac{GA}{2}\xi & \frac{GA}{4}l\xi+\frac{EI}{l}\eta \end{bmatrix} \qquad (4\text{-}13)$$

Where ξ and η may be defined as two stiffness reduction coefficients for

considering the effects of interaction between dowel bar and concrete, ξ is related to shear stiffness and η is related to bending stiffness. The case of $\xi = 1$ and $\eta = 1$ corresponds to Fig. 1 (a) with the assumption $1/(\phi+1) \approx 1/\phi$.

It can be proved that for any given displacement vector **V** of Eq. (4-3), the corresponding element force vector **F** of Eq. (4-2) can satisfy both vertical force and bending moment equilibrium equations. Premultiplying any rigid body displacement vector of Eq. (4-10) by Eq. (4-13), a force vector **F** is always obtained in which all elements are zero. For example:

$$M_i = \frac{GA}{2}\xi W_i - \left(\frac{GA}{4}l\xi + \frac{EI}{l}\eta\right)\left(\frac{W_i - W_j}{l}\right) - \frac{GA}{2}\xi W_j - \left(\frac{GA}{4}l\xi - \frac{EI}{l}\eta\right)\left(\frac{W_i - W_j}{l}\right) = 0$$

Determination of the shear stiffness reduction coefficient ξ and the bending stiffness reduction coefficient η

If Eq. (4-4) is rewritten to obtain:

$$\delta_0 = \frac{1}{2\beta^3 EI}(P - \beta M_0)$$

$$\theta_0 = -\frac{1}{2\beta^2 EI}(P - 2\beta M_0) \qquad \textbf{(4-14)}$$

Substituting P=1, M_0=0 and P=0, M_0=1 to obtain the vertical displacement δ and rotational angle θ produced by unit load P=1 and M_0=1:

$$\delta = \frac{1}{2\beta^3 EI} = \frac{1}{DCX}$$
$$\theta = \frac{1}{\beta EI} = \frac{1}{DCXM} \qquad (4\text{-}15)$$

Define: ΔW_b as displacement difference between two ends of the dowel bar

ΔW_s as displacement difference between two slab nodes

It can be seen in Fig. 2-1(b) that the displacement of the slab node and the bar end on one side is identical before deflection occurs, and the difference of the two displacements is caused by interaction between steel bar and concrete. Based on above definition and Fig. 2-1(b), the following geometric relation can be obtained:

$$\Delta W_s \approx \Delta W_b + 2\delta Q_b \qquad (4\text{-}16)$$

where, Q_b is shear force of the dowel bar and can be written as:

$$Q_b \approx \frac{GA}{l}\Delta W_b \approx \frac{GA}{l}(\Delta W_s - 2\delta Q_b) \qquad (4\text{-}17)$$

Then the relation between Q_b and ΔW_s can be derived by solving Q_b in Eq.(4-17):

$$Q_b = \frac{GA}{l}\,\frac{1}{1+\frac{2\delta GA}{l}}\,\Delta W_s \qquad (4\text{-}18)$$

Comparing Eq. (4-17) and Eq. (4-18) defines the shear reduction

coefficient as follows:

$$\xi = \frac{1}{1+\frac{2GA\delta}{l}} = \frac{1}{1+\frac{2GA}{l*DCX}} \qquad (4\text{-}19)$$

Introducing a parameter K_1 in Eq. (4-19) to calibrate the model predictions to field data, Eq. (4-19) can be rewritten as:

$$\xi = \frac{1}{1+\frac{2GA}{l*DCX}K_1} \qquad (4\text{-}20)$$

where K_1 may be determined by experimental research and field survey data. If the difference caused by the assumptions employed can be neglected, $K_1 = 1$ may be used.

Similarly the relation between dowel bar bending moment and slab node relative rotational angle, which is different from the rotational angle of the dowel bar ends, can be derived as:

$$M_b = \frac{EI}{l}\frac{1}{1+\frac{2\theta EI}{l}}\theta_s = \frac{EI}{l}\frac{1}{1+\frac{2EI}{l*DCXM}}\theta_s \qquad (4\text{-}21)$$

Then K_2 may be introduced to also consider the effects of these assumptions and to rewrite Eq. (4-21) as:

$$M_b = \frac{EI}{l}\theta_s\eta$$

$$\eta = \frac{1}{1+\frac{2EI}{l*DCXM}K_2} \qquad \textbf{(4-22)}$$

Numerical examples in this chapter show that responses of slabs are relatively insensitive to the values of K_1 and K_2, and that K_2 has much less importance than K_1 so that $K_1=K_2$ is assumed to do numerical analysis to reduce the number of parameters.

6. A Proposed Shear Beam Model (2 x 2 Stiffness Matrix)

It is interesting and significant to investigate whether loads are transfered through dowel bars mostly by shear force and whether the contribution of dowel bar bending stiffness can be neglected in transferring the load. If bending stiffness can be neglected, an alternative 2 x 2 stiffness matrix may be employed:

$$S_{MJ2} = \begin{bmatrix} \frac{GA}{l}\xi & -\frac{GA}{l}\xi \\ -\frac{GA}{l}\xi & \frac{GA}{l}\xi \end{bmatrix} \qquad \textbf{(4-23)}$$

Where, ξ is still defined by Eq. (4-20).

Eq. (4-23) may be derived directly by assuming dowel bars to be modeled by shear beams or obtained by eliminating the second and fourth lines and columns in Eq. (4-13). Eq. (4-17) can still be used and the notation "≈" may be replaced by an "=" in this case.

7. Numerical Examples

Pavement model, finite element mesh and load configuration

The pavement model and finite element mesh are presented in Fig. 1-1. An 18000 lb. single axle load is located at the transverse joint and one tire is at the longitudinal edge as shown in Fig. 1-1. The load configuration is given in Fig. 4-3. The dowel bar system is assumed as the only load transfer system in the pavement and the effects of aggregate interlock are neglected.

The major input data are listed below:

Length of each slab	180 inches
Width of slab	144 inches
Thickness of slab	10 inches
Elastic modulus of concrete	5,000,000 psi
Poisson's ratio of concrete	0.15
Subgrade reaction k-value	200 pci
Unit weight of concrete	0.09 pci
Dowel bar diameter	1.25 inches
Dowel bar spacing	12 inches
Elastic modulus of dowel bar steel	29,000,000 psi
Width of joint	0.25 inch
Poisson's ratio of steel	0.30
Dowel-concrete interaction coefficient	1,500,000 pci

Physical explanation of K_I

As discussed previously, the coefficient K_I can be used to calibrate the model to field or lab. data. The major model assumptions are that:

a. The length of dowel bars is assumed infinite, whereas it is actually finite.

b. The dowel bars are assumed to be perfectly bound by elastic concrete whereas there exists nonlinear behavior of interaction between the concrete and dowel bars which could be caused by construction procedures, dowel bar looseness, installation and other factors.

c. The formula to determine stiffness reduction coefficients ξ and η are approximate, for instance, the effects of dowel bar bending moments are only approximately considered.

d. The dowel-concrete interaction coefficient (Ψ in Eq. (4-7)) is difficult to estimate precisely and the values obtained by different investigators cover a large span (Tabatabaie[1979]).

The first three factors would tend to overestimate the resistance capability of concrete, thus, K_I should be taken greater than 1. The fourth factor could overestimate or underestimate the concrete resistance capability. It is suggested that the fourth factor be neglected in determining K_I. Thus, if the dowel-concrete interaction coefficient Ψ is assumed to be correctly estimated, K_I=1 would be corresponding to the upper bound of the concrete resistance capability. Eq. (4-21) and Eq. (4-23) indicate that the greater the value of K_I the

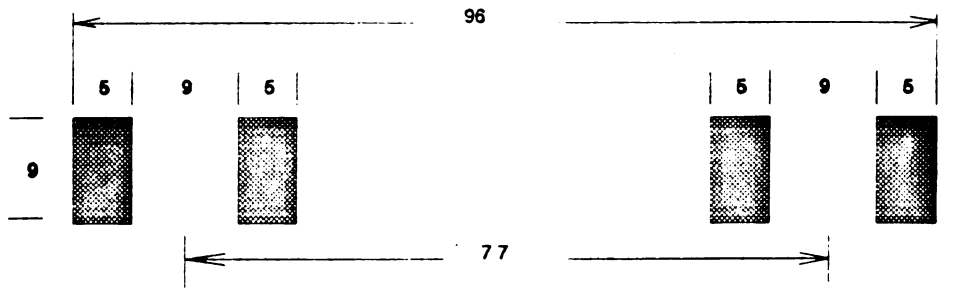

Fig. 4-3 Configuration of Single Axle Load: 18 kips, p=100 psi

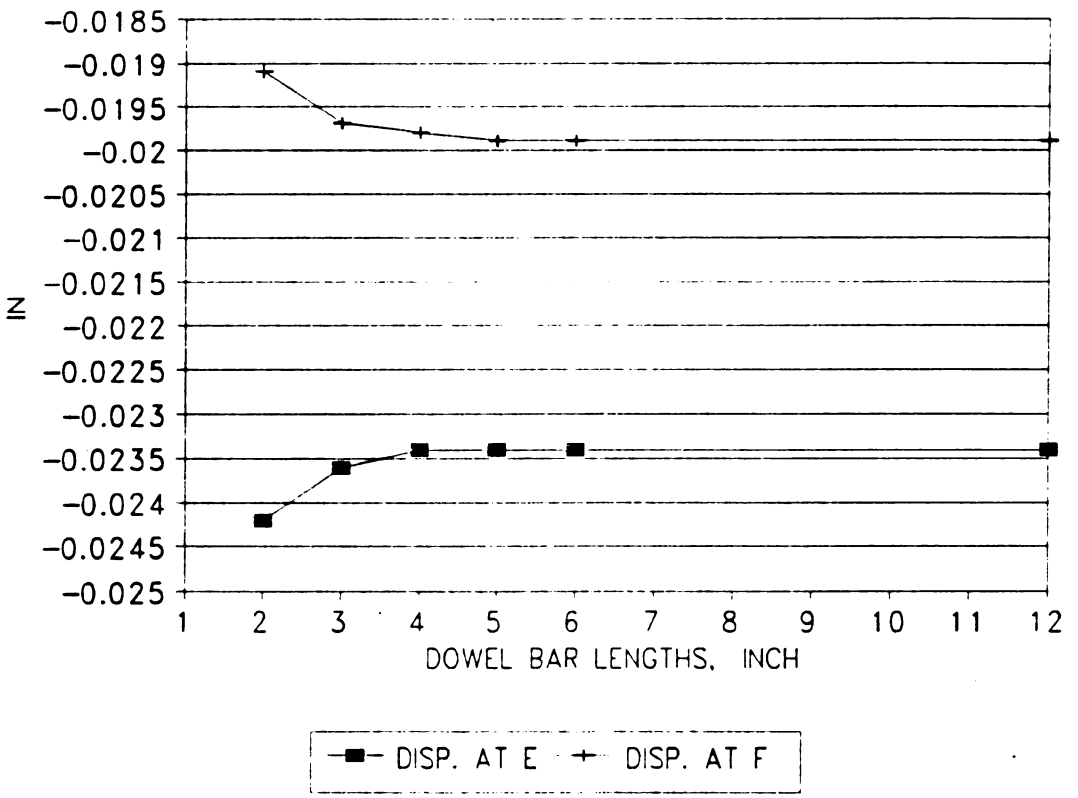

Fig. 4-4 The Maximum Displacements v.s. Dowel Lengths

less the resistance capability of the concrete. So, K_1=1, 2 and 3 are selected in following numerical analysis.

The effects of embedded length of the dowel bars

Fig. 4-4, Fig. 4-5 and Fig. 4-6 present the maximum displacements of the loaded slab at point E and F, total forces transmitted by the load transfer system and the maximum longitudinal stresses of line A-$\bar{A}$, B-$\bar{B}$ (Fig. 1-1) in terms of the embedded length of dowel bars respectively by using the component model. The following conclusions can be obtained:

a. The longer the embedded length the higher the load tranfer capability of the dowel bar system that leads to an increase of maximum displacement and maximum stress in the unloaded slab, the decrease of those in the loaded slab and more total shear force being transmitted from the loaded to the unloaded slabs.

b. Based on the example presented, when the embedded length is longer than five times the diameter of the bar the difference of results between the finitely and infinitely long dowel bar models can be neglected, thus the dowel bars currently used in pavements can be appropriately modeled by assuming the embedded length to be infinitely long.

c. In the example presented, the maximum stresses on line A-E (the loaded side), Fig. 1-1, are always greater than that on line F-$\bar{A}$ (the unloaed side), the comparison of maximum stresses on line B-$\bar{B}$ are likely on the contrary, however, the difference between the maximum stress on the loaded slab and the unloaded slab is less than 1% on line A-$\bar{A}$ and less than 2% on line B-$\bar{B}$.

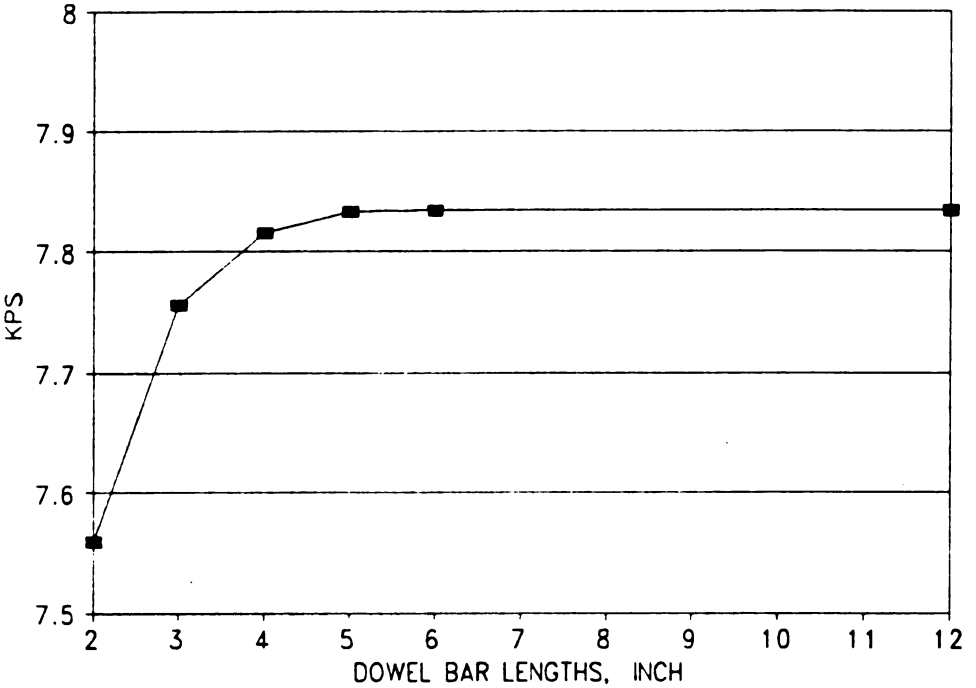

Fig. 4-5 Total Shear Forces Transmitted by the Dowel Bars

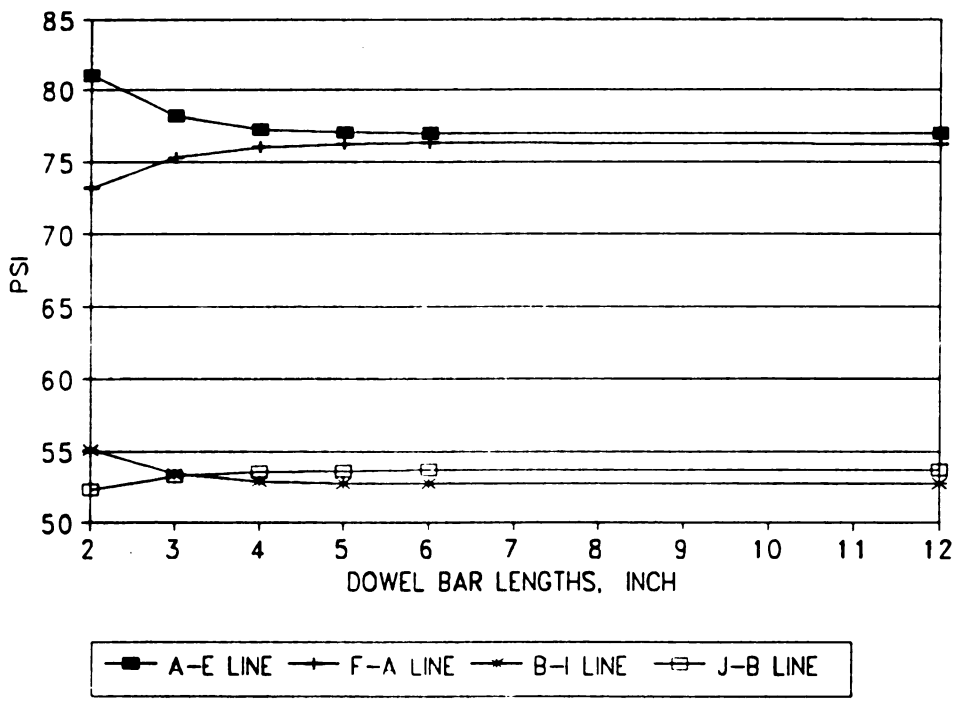

Fig. 4-6 The Maximum Stresses V.S. Dowel Lengths

Comparison of the component model Eq. (4-12), shear-bending beam model Eq. (4-13) and shear beam model Eq. (4-23)

Fig. 4-7 presents the comparison of longitudinal stress distributions of line A-$\bar{A}$, Fig.1-1 predicted by the three models. It can be clearly seen that for the solid dowel bar system, the three models provide very close results. Tables 4-1 to Table 4-3 present a comparison for the maximum stresses, shear forces and bending moments of each dowel bar. The difference of the results predicted by the three models are pratically negligible.

The effects of nonequilibrium stiffness matrix to critical stresses of slab

Fig. (4-7) also shows the stress σ_x distribution produced by program JSLAB-86. As discussed in section three, JSLAB-86 employs a nonequilibrium stiffness matrix Eq. (4-7) which predicts maximum σ_x in the unloaded slab about 30% greater than that of the loaded slab (Table 4-1). Also the JSLAB-86 results in the unloaded slab are greater than all of those by modified JSLAB-86 employing equilibrium stiffness matrix Eq. (4-12), Eq. (4-13) or Eq. (4-23). Whereas the JSLAB-86 results of the loaded slab are smaller than those predicted with the new models.

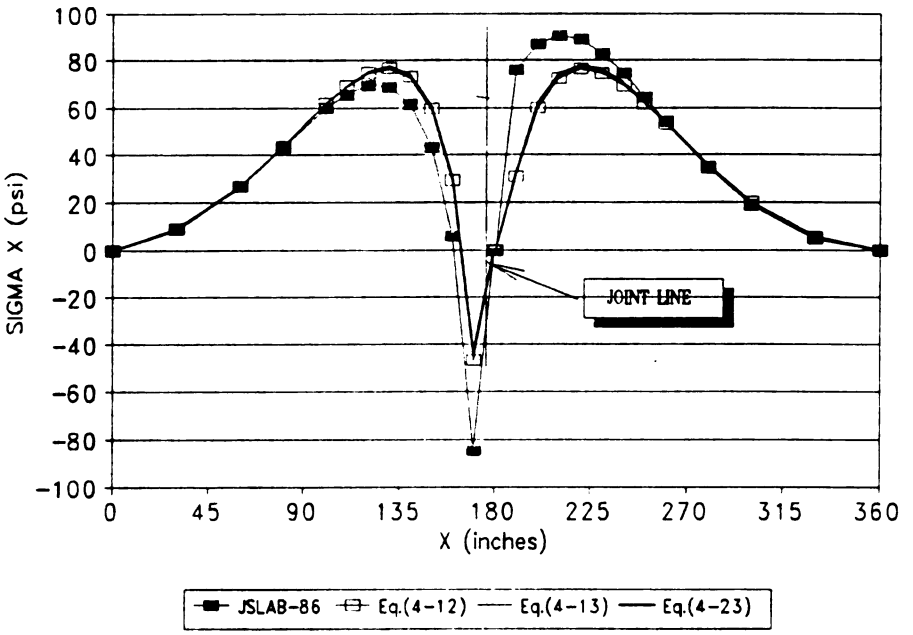

Fig. 4-7 Longitudinal Stresses Along Line A-$\overline{A}$ (in Fig. 1-1)

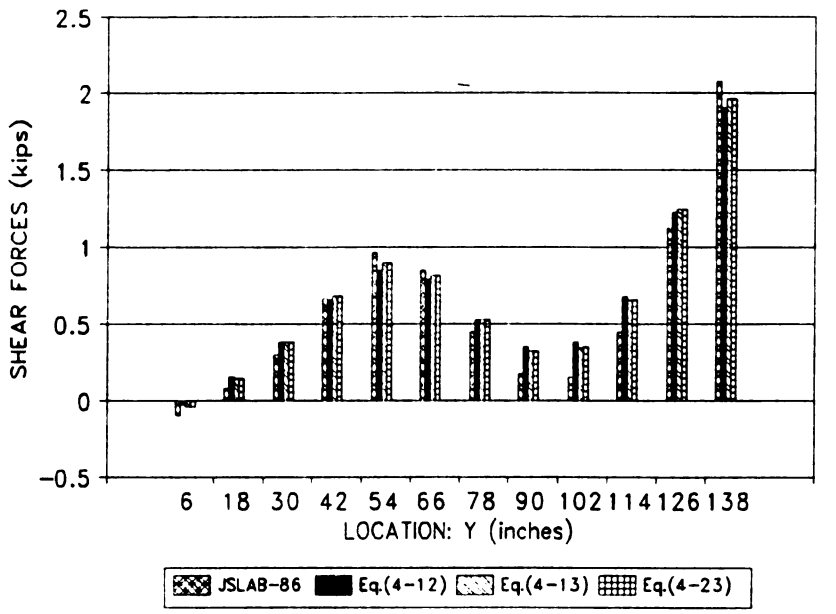

Fig. 4-8 Shear Forces of Dowel Bars

Table 4-1 Comparison of the Maximum Stresses σ_x and σ_y on Top of the Slabs

	σ_{xmax} on AE	σ_{xmax} on $F\bar{A}$	σ_{ymax} on $E\bar{E}$	σ_x at H
JSLAB-86	69.4	90.6	-84.0	-84.8
Eq. (4-13), K=1	76.3	77.1	-92.95	-46.9
Eq. (4-13), K=2	80.9	73.4	-100.9	-43.9
Eq. (4-13), K=3	84.5	70.0	-104.3	-42.0
Eq.(4-23), k=1	77.5	78.2	-92.8	-43.5
Eq. (4-12)	77.0	76.3	-94.88	-46.6

Table 4-1 shows that the maximum σ_x on top of the loaded slab on line AE, Fig. 1-1, predicted with JSLAB is 9.8% smaller than that by the component model Eq. (4-12) and the maximum σ_x on top of the unloaded slab on line FA is 18.7% greater.

Table 4-2 Shear Forces of the Dowel Bars (kps)

Bar No.*	1	2	3	4	5	6	7	8	9	10	11	12	Σ
JSLAB	-.09	0.08	0.30	0.66	0.96	0.85	0.45	0.17	0.15	0.45	1.12	2.07	7.17
A	-.04	0.14	0.38	0.68	0.89	0.81	0.52	0.32	0.34	0.65	1.24	1.96	7.89
B	0.03	0.18	0.37	0.58	0.72	0.69	0.53	0.43	0.49	0.74	1.16	1.66	7.58
C	0.07	0.20	0.35	0.52	0.64	0.63	0.53	0.48	0.55	0.76	1.09	1.48	7.30
D	-.04	0.14	0.38	0.68	0.89	0.81	0.52	0.32	0.34	0.65	1.24	1.96	7.89
E	-.03	0.15	0.38	0.66	0.85	0.78	0.53	0.35	0.38	0.67	1.23	1.89	7.84

* No. 1 bar is located at Y = 6 inch, and No. 12 is at Y = 138 inch in Fig. 1-1. A: Eq. (4-13), K=1. B: Eq. (4-13), K=2. C: Eq. (4-13), K=3. D: Eq. (4-23), K=1. E: Eq. (4-12), component model.

The most significant difference for σ_x occurs at point H by the edge tire, where JSLAB-86's prediction is 81% greater. The critical position of the load stress predicted by JSLAB is point H, only 10 inches away from the joint, however, the critical position predicted by the component model, Eq. (4-13) and Eq. (4-23) is point G which is 50 inches away from the joint.

Fig. 4-9, Fig. 4-10 and Table 4-3 show the comparison of bending moments of the dowel bars predicted with JSLAB-86 and with the JSLAB-92 based on Eg. (4-12), Eq. (4-13) and Eq (4-23). The output of bending moments at two ends of each dowel bar by the JSLAB-92 forms an equilibrium system which satisfy $\Sigma Q_i = 0$ and $\Sigma M_i = 0$, whereas moments output from JSLAB-86 fails to satisfy equilibrium, as discussed in this chapter. The nonequilibrium forces produce significant differences in bending moments. More seriously, it causes an incorrect sign of bending moments on the unloaded slab, which is why JSLAB-86 overestimates the stress responses on the unloaded slab by up to 18.7% and overestimates the stresses on the loaded slab up to 81% in this example.

Different Values of K_i

Table 4-2 also shows comparison of shear forces of each dowel bar calculated by JSLAB-92 based on Eq. (4-13) with K=1, K=2 and K=3. The right hand column in Table 4-2 are total forces transfered by all dowel bars. It can be clearly seen that the larger the value K is used, the less load is transferred from the loaded slab to the unloaded slab, therefore, the greater are the stresses produced on the loaded slab and

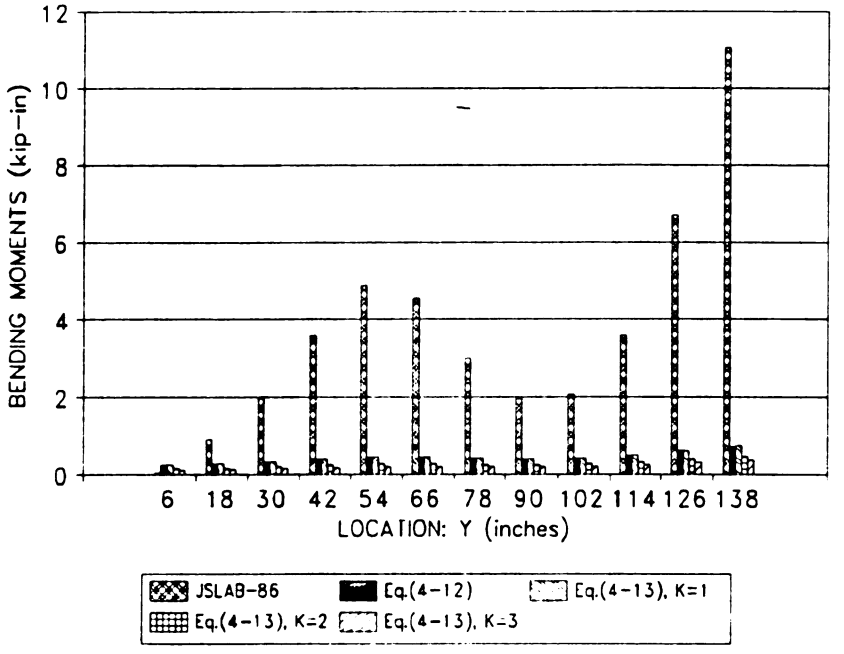

Fig. 4-9 Bending Moments of Dowel Bars on the Loaded Side

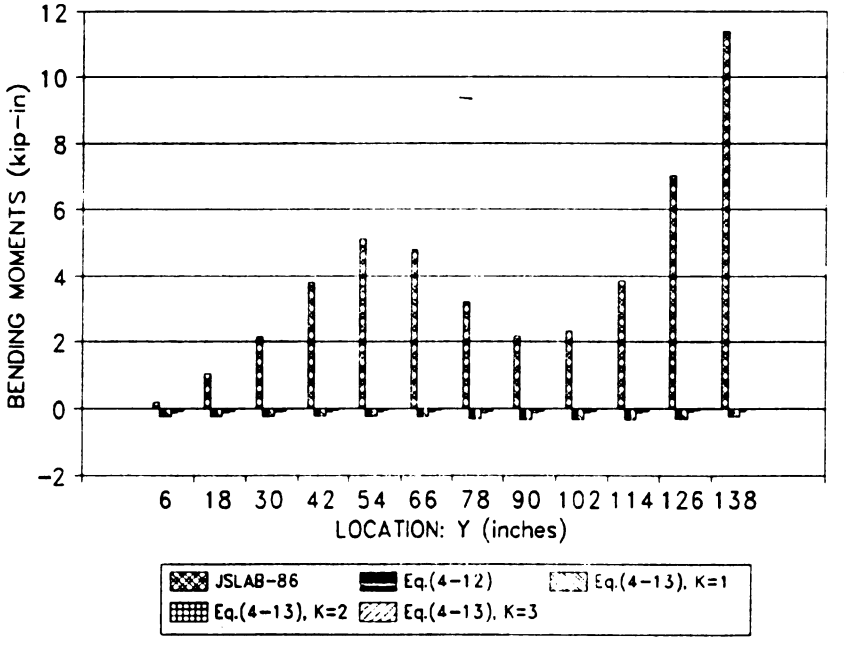

Fig. 4-10 Bending Moments of Dowel Bars on the Unloaded Side

the smaller are produced on the unloaded slab.

Comparison of dowel bar shear forces

Fig. 4-8 presents the shear forces of each dowel bar calculated by JSLAB-86, Eq. (4-12), Eq. (4-13) and Eq. (4-23) with K_l=1. The differences between the shear force results are less significant than the bending moments of the dowel bars and the critical stresses in the slabs.

Table 4-3 Bending Moments of Dowel Bars

		1	2	3	4	5	6	7	8	9	10	11	12
JSLAB	M_i	.04	.88	1.96	3.57	4.87	4.53	2.96	1.95	2.06	3.57	6.70	11.03
-86	M_j	0.20	1.05	2.15	3.78	5.10	4.77	3.21	2.20	2.32	3.86	7.01	11.36
Eq.	M_i	.23	.26	.32	.39	.44	.44	.41	.39	.42	.49	.60	.73
4-13	M_j	-.24	-.23	-.22	-.22	-.22	-.24	-.28	-.31	-.33	-.33	-.30	-.24
Eq.	M_i	.23	.26	.32	.38	.43	.44	.41	.40	.42	.49	.60	.72
4-12	M_j	-.24	-.23	-.22	-.22	-.22	-.24	-.28	-.31	-.33	-.33	-.30	-.25

All figures and tables presented show that the results by using Eq. (4-23) are practically the same as those by Eq. (4-12) and Eq. (4-13) with K=1, including the maximum displacements of the slabs, critical stresses in the slabs, shear forces and bending moments of the dowel bars. The above comparisons lead to a significant conclusion: Eq. (4-12) and Eq. (4-13) with K=1 may be replaced by Eq. (4-23) for simulating the solid dowel bar mechanism in FEM program for concrete pavement analysis. The conclusion implys that the shear beam model is not only a simple but also an applicable model in PCC pavement analysis.

8 Summary

Based on theoretical analysis and numerical examples presented in this chapter, it is concluded that the neglect of equilibrium condition of the dowel bar stiffness matrix causes significant differences in prediction of dowel bar forces and critical slab stresses. The reference (Nishizawa[1989]) was found to provide a good concept to simulate the dowel bar mechanism in detail. The error in derivation should be corrected and the bending beam model to simulate the dowel segment in the joint (between two slabs) should be replaced by a shear-bending beam or a shear beam element. Three new stiffness matrices Eq. (4-12) (component model), a 4x4 matrix Eq. (4-13) and a 2x2 matrix Eq. (4-23) are proposed and investigated in this paper. All of them satisfy the necessary equilibrium conditions. The identical results produced by the three models confirm that the shear resistance capability of the solid steel dowel bars is the dominant parameter of the load transfer system. Furthermore Eq. (4-20) and Eq. (4-22) can be used to determine the stiffness reduction coefficients for simulating the mechanism of interaction between dowel bars and concrete. Numerical examples demonstrate that the shear beam model Eq. (4-23) with K_1=1 is applicable to simulate the solid steel dowel bar in finite element programs for PCC pavement analysis. Eq. (4-12) is developed with minimum assumptions and includes most considerations of dowel bar geometry and physical properties so that it has potential to study dowel behavior for analysis, design and optimization.

CHAPTER FIVE
A NONLINEAR MECHANISTIC MODEL FOR DOWEL BAR LOOSENESS

1 Introduction

Many studies have demonstrated that the capability of load transfer systems significantly affect the service quality and remaining life of the pavement (Hveem[1949], Teller[1958] and Snyder[1989]). Dowel bars are a popularly used system to transfer load from the loaded slab to the unloaded slab. Since the Finite Element Method was introduced into the analysis of rigid pavements, the dowel bar mechanism has been simulated by many models which have been discussed in chapter four. These models are valid for dowels perfectly embedded in concrete, in other words, there exists no gap or void between the dowel and the concrete, or no looseness.

However, some experimental studies (Kushing[1935], Finney[1947], Keeton[1957], Teller[1958], Ball[1975], Snyder[1989] and Reiter[1989]) have shown that dowel bar looseness greatly affects the load transfer efficiency, maximum deflection, critical stresses, pumping, faulting and further the remaining life of the pavement. The maximum stresses of slabs with and without dowel bars under the same traffic loads at the joint, as calculated by the finite element computer program, could have differences of more than 100%. The actual responses of slabs with loose dowel bars should be in between.

Majizadeh[1984] summarized major findings in references published before 1984 and establishes their model to consider the dowel bar looseness through modifying the dowel bar diameter in their computer program RISC. The major assumptions of their model are:

(1) Looseness is uniform for all dowel bars.

(2) The loaded slab has to deflect by the amount of looseness before dowel bars become effective in load transfer, i.e., the loaded slab behaves as a single slab with a free edge until the deflection exceeds the amount of looseness, at which time the free edge is transformed into a joint with fully effective dowel bars and without voids.

(3) A void with depth equal to the amount of looseness forms under the joint of the loaded slab due to the high stress concentration (at the slab-foundation interface) under an undoweled joint.

(4) All dowel bars come into contact at the same time (deflection value) independent of the distance from the applied loads.

Finally, an effective dowel bar diameter $D' = k \times D$, where k is a function of looseness and always smaller or equal to one, is employed in numerical calculation. As explained by the author, the assumptions were made in order to analyze looseness inside a linear elastic model. The model would be improved if:

(1) Looseness was a function of bar location, distribution of the tire load along the transverse joint, and support conditions of the

slab, etc.

(2) Dowel bars came in contact one after another and the contact order depends on the relative location of the loads and each dowel bar

(3) A nonlinear model was used because the second assumption leads to a nonlinear load transfer procedure.

Based on the above discussion, a nonlinear elastic model to simulate the dowel bar looseness mechanism is proposed in this paper. The model can be used to predict responses of doweled rigid pavements with consideration of the effects of the dowel bar looseness. If the looseness of each bar is known, no matter whether they are obtained from field survey or assumed, the developed model can calculate the responses of pavement with any looseness distribution, the order of dowel bars come in contact, and the final critical stresses. Numerical examples are presented in this chapter for demonstrating the validity of the model and for conceptually and quantitatively understanding the nonlinear load transfer mechanism.

Dowel Bar Stiffness Matrix

As discussed in chapter 4, the following equation can be used for dowel bar stiffness matrix for general purpose:

$$S_{MJ1} = \begin{bmatrix} \frac{GA}{l}\xi & \frac{GA}{2}\xi & -\frac{GA}{l}\xi & \frac{GA}{2}\xi \\ \frac{GA}{2}\xi & \frac{GA}{4}l\xi + \frac{EI}{l}\eta & -\frac{GA}{2}\xi & \frac{GA}{4}l\xi - \frac{EI}{l}\eta \\ -\frac{GA}{l}\xi & -\frac{GA}{2}\xi & \frac{GA}{l}\xi & -\frac{GA}{2}\xi \\ \frac{GA}{2}\xi & \frac{GA}{4}l\xi - \frac{EI}{l}\eta & -\frac{GA}{2}\xi & \frac{GA}{4}l\xi + \frac{EI}{l}\eta \end{bmatrix} \qquad (5\text{-}1)$$

where:

E Elastic Modules of the Dowel Bar

I Moment of Inertia of the Cross Section

G Elastic Shear Modules of the Dowel Bar

l Width of the Joint

A Cross Sectional Area Effective in Shear

$$\xi = \frac{1}{1 + \frac{2GA}{l * DCX} K_1} \qquad (5\text{-}2)$$

$$\eta = \frac{1}{1 + \frac{2EI}{l * DCXM} K_2} \qquad (5\text{-}3)$$

where: $DCX = 2\beta^3 EI$

$DCXM = \beta EI$

$\beta = (\Upsilon D/4EI)^{0.25}$

Υ Dowel - Concrete Interaction Coefficient

D Diameter of the Dowel Bar

K_1, K_2 Parameters to be determined for different dowel systems. $K_1 = 1$ and $K_2 = 1$ are suggested in chapter 4 for solid dowel bars.

Due to the fact that load transfer capability is dominated by its capability of shear resistance, Eq. (5-1) can be replaced by a simpler matrix in the computer program:

$$S_{MJ2} = \begin{bmatrix} \frac{GA}{l}\xi & -\frac{GA}{l}\xi \\ -\frac{GA}{l}\xi & \frac{GA}{l}\xi \end{bmatrix} \qquad (5\text{-}4)$$

numerical examples presented in chapter 4 indicate that Eq. (5-1), (5-4) and the component stiffness matrix (Eq. (4-12)) provide very close results for predicting responses of pavements with solid dowel bar system. Among them Eq. (5-4) is the simplest one so that it is employed in this chapter to investigate the effects of dowel bar looseness. Regardless of the application of Eg. (5-4) or (5-1), or another stiffness matrix, the concept and idea to develop a model for dowel bar looseness analysis are same, and suitable for any type of dowel bar stiffness matrix.

2 Load Transfer Procedure of Dowel Bars with Looseness

Fig. 5-1 presents the load transfer procedure of a dowel bar with looseness. Fig. 5-1(a) shows a cross section view of slab with the dowel before any traffic load moves in or after it goes out. Fig. 5-1(b) and (e) show that each slab performs as a single slab with free edge when the relative deflection of the two slabs is smaller than the dowel looseness. Fig. 5-1(c) and (d) show that the dowel bar becomes effective since the relative deflection between the two slabs exceeds the looseness of the dowel bar.

Teller[1958] presented excellent experimental results to study the dowel

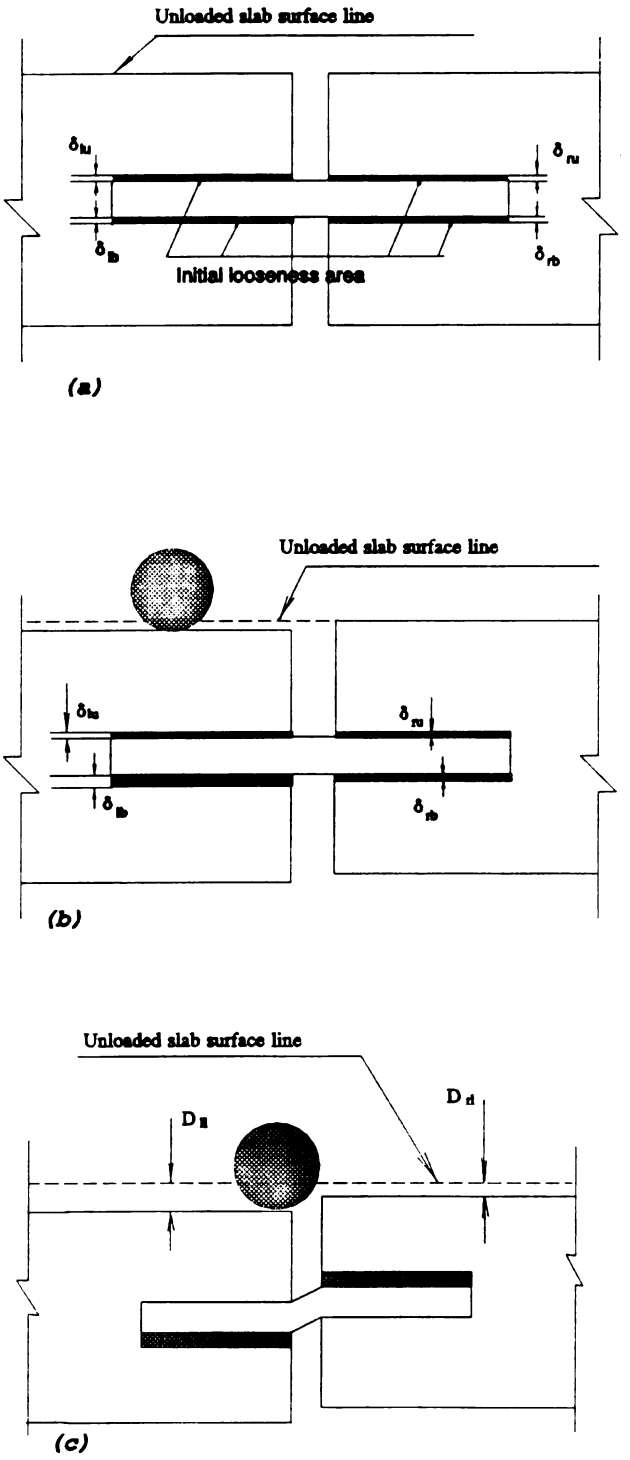

Fig. 5-1 Load Transfer Procedure

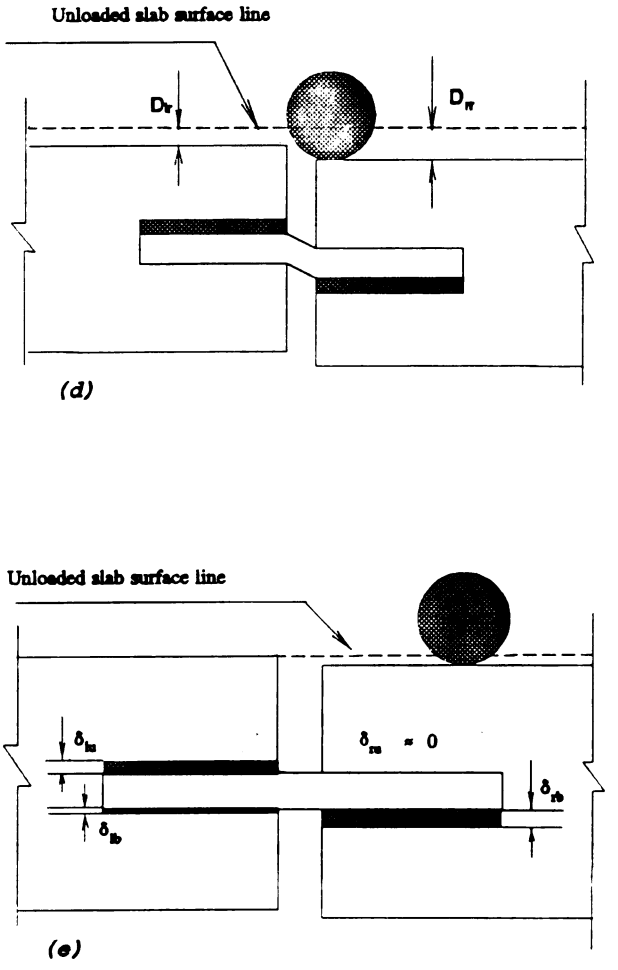

Fig. 5-1 Load Transfer Procedure (continued)

behavior with consideration of the initial looseness and the looseness developed by repetitive loads. Fig. 5-2 shows relation between applied load and relative deflection after various numbers of load cycles and effect of repetitive loading on the development of dowel looseness (Copied from Teller[1958]). The findings can be summarized as follow:

(1) During the first 5000 lb load, the dowels were in a state of adjustment in which existing looseness was being taken up, and a condition of full bearing was being established.
(2) When load was greater than 5000 lb, the relation between increments of load and increments of relative deflection became constant. The slope was independent of the number of load cycles.
(3) Initial looseness may be defined as the vertical coordinate of the intersections between the dashed lines and the y axis, as indicated in Fig. 5-2(a).

Based on the previous research and also because all loads are acted on the approach slab then the leave slab evenly, the following assumptions may be added:

(1) The void, or gap between the dowel bar and concrete is uniformly distributed along the bar. This assumption implies that "The loaded slab has to deflect by the amount of looseness before dowel bars become effective in load transfer."
(2) Before any load moves in, (Fig. 5-1(a)), $\delta_{hu} + \delta_{rb} = \delta_{lb} + \delta_{ru} = L_0$, which is defined as Looseness of the dowel bar (see Fig. 5-2(a)).

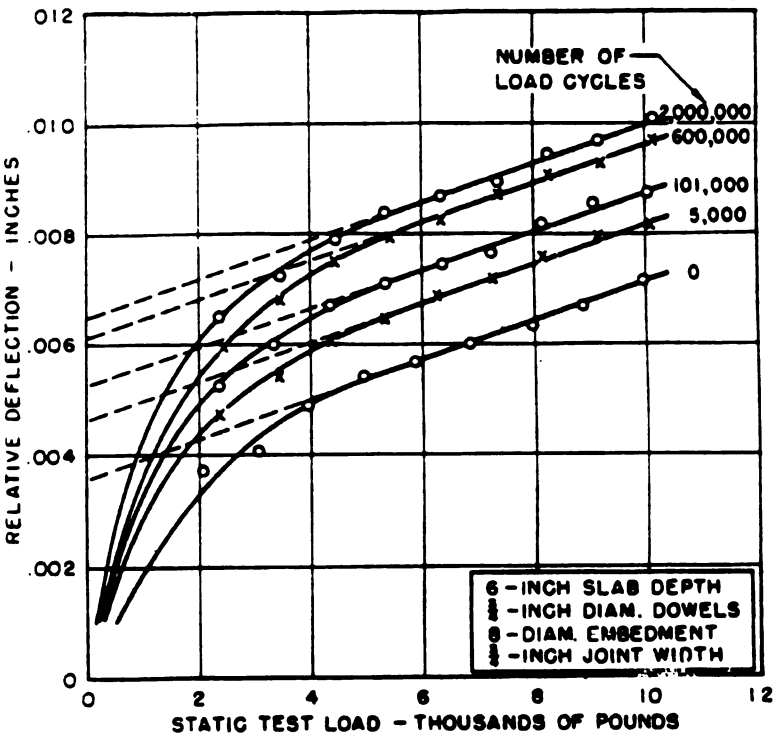

a. Relation Between Applied Load and Relative Deflection, After Various Numbers of Load Cycles. (from Teller, Fig. 5, 1958)

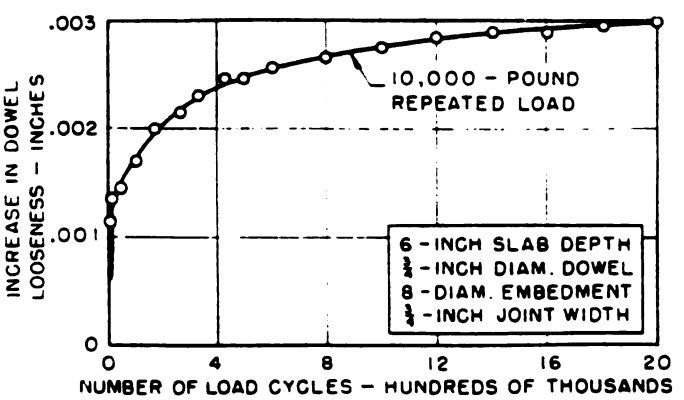

b. Effect of Repetitive Loading on the Development of Dowel Looseness. (from Teller, 1958, Figure. 6)

Fig. 5-2 Dowel Behavior in Experiments

(3) The deformation of dowel bar is assumed inside of elastic range, or the permanent deformation of dowel bar will not be considered in the mean time. So, when the tire moves far away from the joint, the structural cross section view of the slabs will be the same as shown in Fig. 5-1 (a).

(4) The surface of two slabs are in same horizontal line before any load moves in, or, the permanent faulting is not considered in developing dowel bar looseness model. The interactive effects between dowel looseness and faulting will not be considered at this time.

The pavement slabs can still be modeled by elastic plates resting either on an extensionless Winkler base (Tabatabie[1979] and Tayabji[1986]), or on multiple elastic layers (Majidzadeh[1984]), or on stress dependent layers (Ioannides[1984]).

Based on the above assumptions, the behavior of a single dowel bar with looseness can be graphically described in Fig. 5-3(a) and (b), where P is a load acted on a slab node and Δ represents the relative displacement between the loaded and unloaded slabs. S_0 is the stiffness contributed by the loaded slab, base and subgrade under the slab only, and $\Delta_0 = L_0$ is defined by the second assumption. Before the relative displacement between the loaded and unloaded slab nodes exceeds the defined looseness, namely $\Delta < L_0$, the dowel bar is not effective in load transfer. When $\Delta > L_0$, the dowel bar becomes effective and S_1 is contributed by the two slabs and their support system. The Force-Deflection relation is a typical bilinear model.

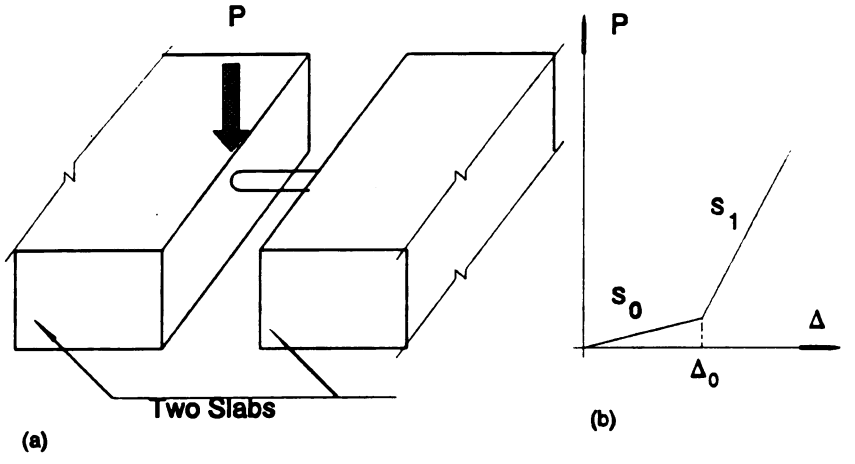

Bilinear Model of Single Dowel Bar with Looseness

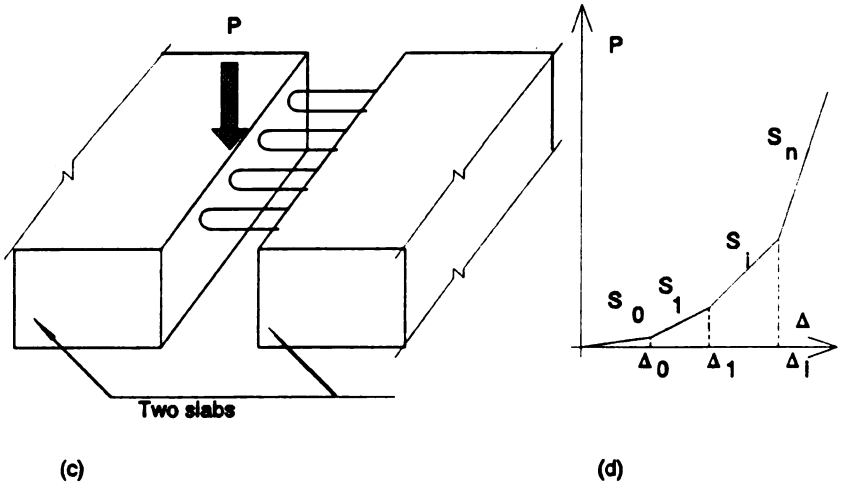

Model for Multiple Dowels

Fig. 5-3 Nonlinear Model of Dowel Bars with Looseness

Similarly, the functional behavior of a multiple dowel bar system can be described in Fig. 5-3(c) and (d). The force-deflection curve of load P and the relative displacement between the loaded and unloaded slabs is given in Fig. 5-3, (d). Δ_0 indicates the first point of changing stiffness of the loosed dowel system. Before the relative displacement exceeds Δ_0, no bar is effective in load transfer, and the loaded slab performs as a single slab without load transfer system. When the displacement is between Δ_0 and Δ_1, only one dowel is in contact and effective in load transfer. The second bar starts in contact when the displacement equal to Δ_1. The stiffness of entire pavement structure becomes greater since a contribution is also provided by the unloaded slab through more effective dowel bars. The curve shown in Fig. 5-3(d) is a multi-linear model which can be coordinated with any available computer program to calculate the responses of pavement system step by step.

3 Looseness Distribution and Input Data

Fig. 5-4(a) indicating effect of increasing the magnitude of the repeated load on the development of dowel looseness was copied from Teller[1958]. Two significant findings can be summarized by analyzing Fig. 5-2(b) and Fig. 5-4(a):

(1) About 40000 load cycles (2% of 2,000,000 total cycles) produced about 50% of looseness by the 2,000,000 cycles. That indicates if magnitude of the repetitive loads remains the same, looseness is developed quickly at the beginning and increases very slowly when

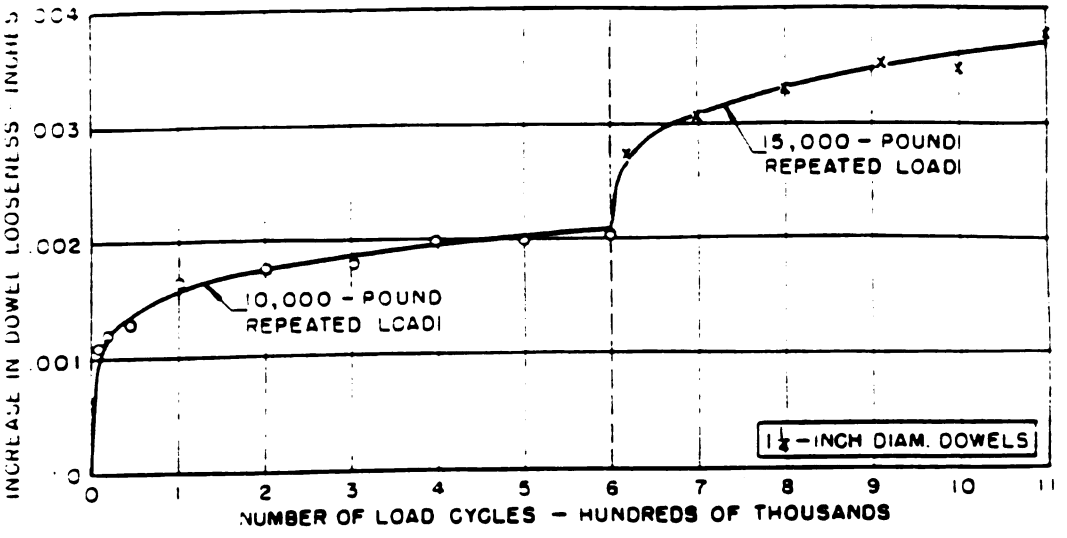

a. Effect of Increasing the Magnitude of the Repeated Load on the Development of Dowel Looseness. (from Teller, Figure. 26, 1958)

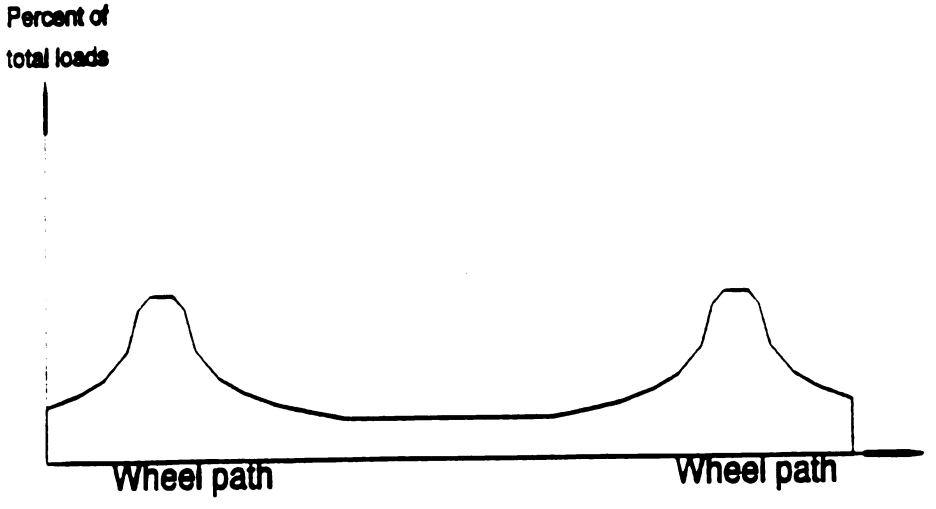

b. Tire Load Distribution

Fig. 5-4 Looseness Distribution Assumption

number of load cycles is large.

(2) When the magnitude of the repetitive loads was replaced by a greater one (Fig. 5-4(a)), new looseness was developed immediately, and the looseness development procedure was still similar to the stage one.

The above findings indicate that most increased looseness of dowel bar is caused by heavy trucks. The percentage of tire loads across a joint can be approximately expressed by Fig. 5-4(b). Although the distribution is not uniform, the percentage of tires passing each dowel spacing could still be more than 2%. If this is true, the experimental findings by Teller[1958] implies that the looseness level of different dowels should not make a significant difference. Therefore, as a first stage of investigating the effects of looseness, a uniform looseness distribution is employed to conduct numerical analysis though the developed model is capable of dealing with any type of looseness distributions.

A finite element mesh (Fig. 1-1) with two load cases is employed in numerical analysis. The pavement analyzed contains two slabs which have equal length and width, so that it is symmetrical in both X and Y directions. The two load cases are:

Load case one: A concentrated 9000 lb load acted at point I in Fig. 1-1, (X=180 inch, on the approach slab and Y=66 inch)

Load case two: An 18000 lb single axle load with four tires which configuration is given in Fig. 4-3.

The major input data are listed as follow:

Elastic Modules of the Concrete	5,000,000 psi
Thickness of the Slab	10 inch
Poison Ratio of the Concrete	0.15
Subgrade Modules	200 pci
Dowel Bar Diameter	1.25 inch
Elastic Modules of Dowel Bar	29,000,000 psi
Width of the Joint	0.25 inch
Poison Ratio of the Steel	0.3
Dowel-Concrete Interaction Coefficient	1,500,000 pci
Dowel Bar Looseness	As indicated

4 Numerical Examples

Displacement shapes

Fig. 5-5(a)-(e) show the displacement shapes in terms of different looseness levels under load case one. The figures indicate that the more serious the looseness, the less percentage of total loads is transmitted from the loaded slab to the unloaded slab. When all dowels are ineffective, the calculated displacements equal to the responses of a single slab without dowels.

Fig. 5-6(a)-(c) present the displacement distributions along Line B-$\bar{B}$, E-$\bar{E}$ and F-$\bar{F}$ (Fig. 1-1) under load case one. Fig. 5-7(a)-(d) present the displacement distributions along Line A-$\bar{A}$, B-$\bar{B}$, E-$\bar{E}$ and F-$\bar{F}$ under load case two (Fig. 4-3). These figures quantitatively show the effects of looseness level to the displacement responses. For instance, Fig. 5-7(b)

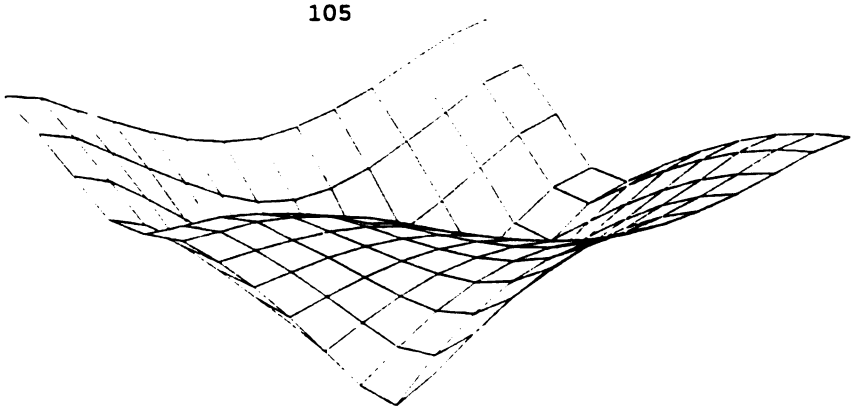

a. Looseness = 0.0, the Maximum Displacement = 0.0086 in

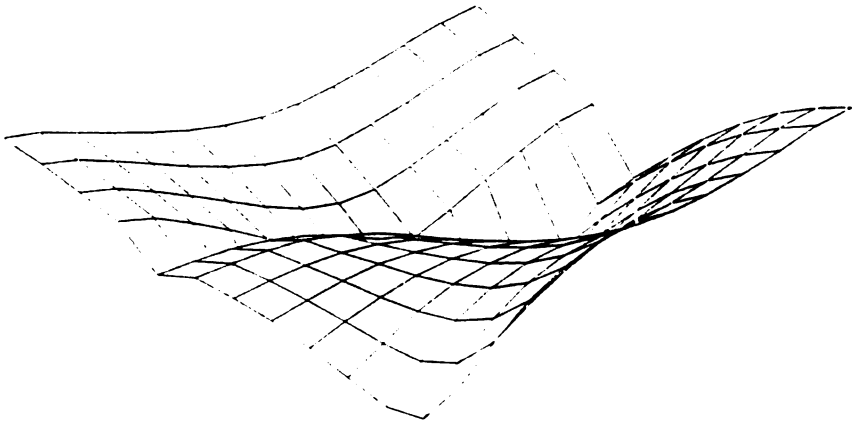

b. Looseness = 0.003 in, the Maximum Displacement = 0.0101 in

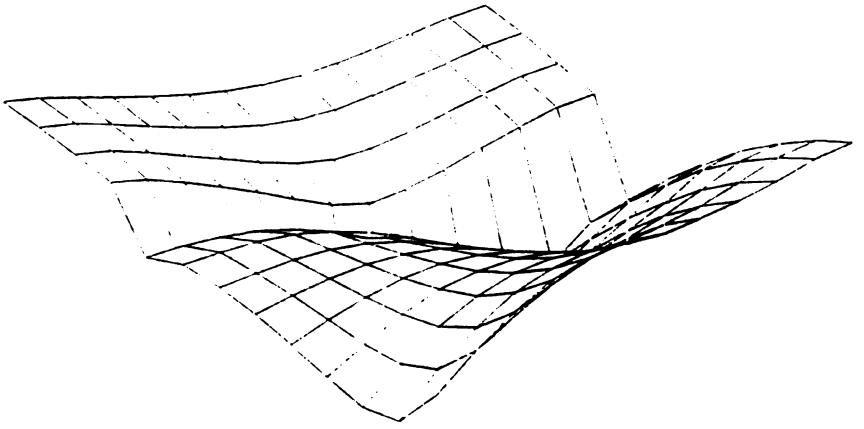

c. Looseness = 0.006 in, the Maximum Displacement = 0.0115 in

Fig. 5-5 Displacement Shapes (load case one)

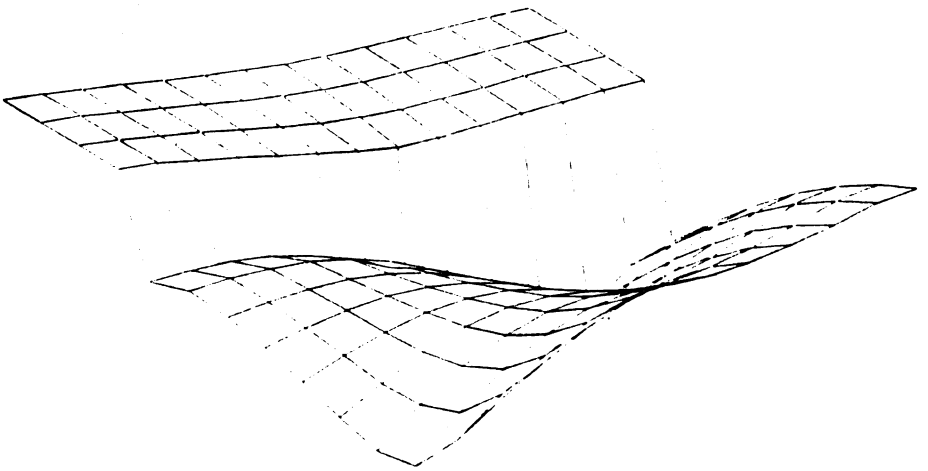

d. Looseness = 0.009 in, the Maximum Displacement = 0.0129 in

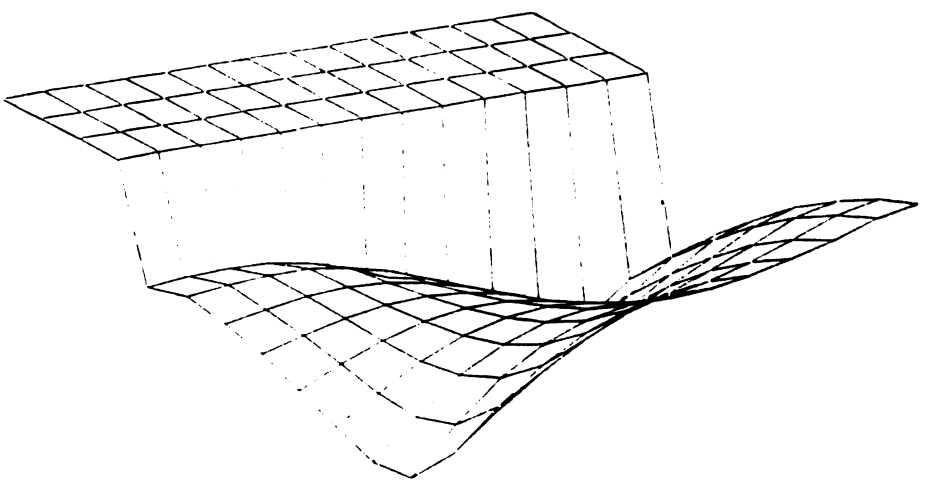

e. Looseness = 0.015 in, the Maximum Displacement = 0.0154 in

Fig. 5-5 Displacement Shapes (continued, load case one)

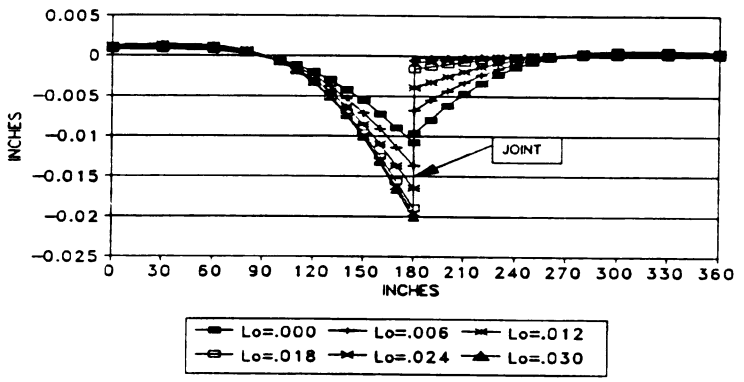

(a) DISPLACEMENTS OF LINE B-B

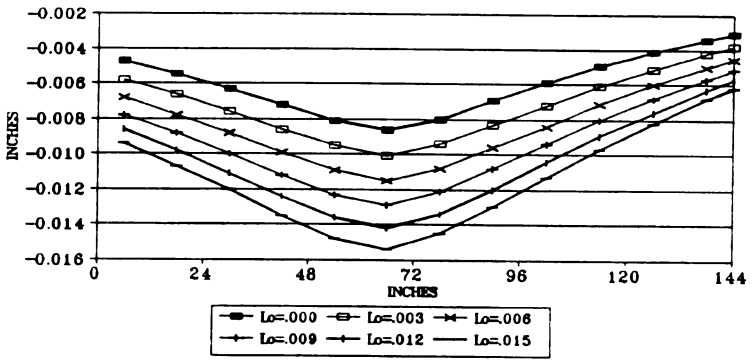

(b) DISPLACEMENT OF LINE E-E

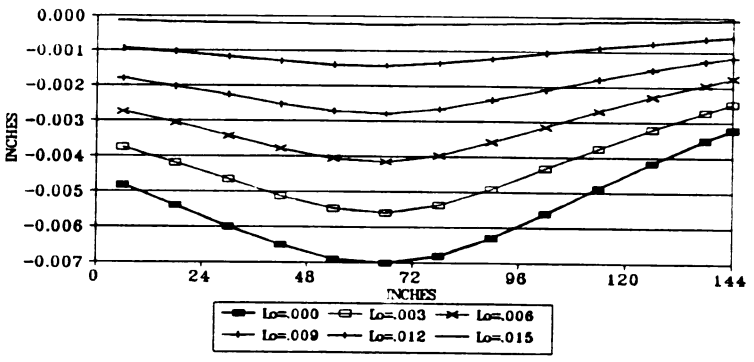

(c) DISPLACEMENT OF LINE F-F

Fig. 5-6 Displacement Distributions (load case one)

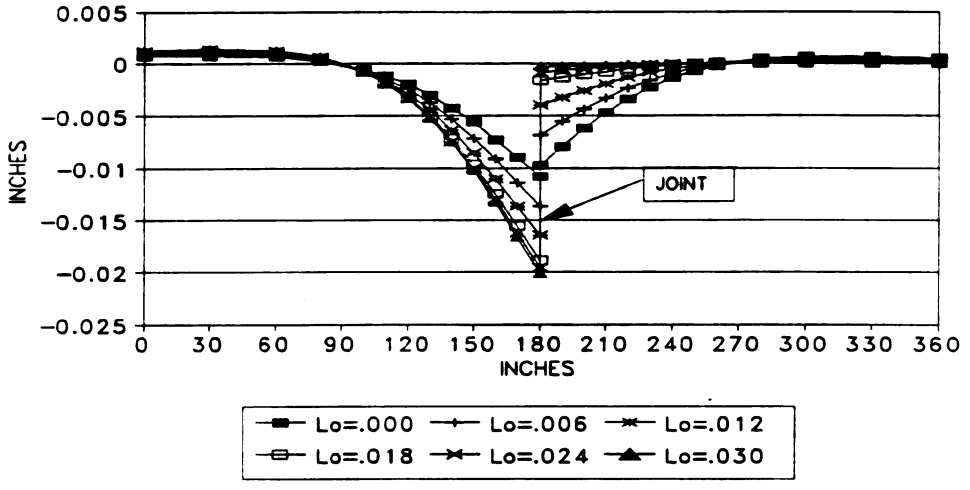

(a) DISPLACEMENTS OF LINE B-B

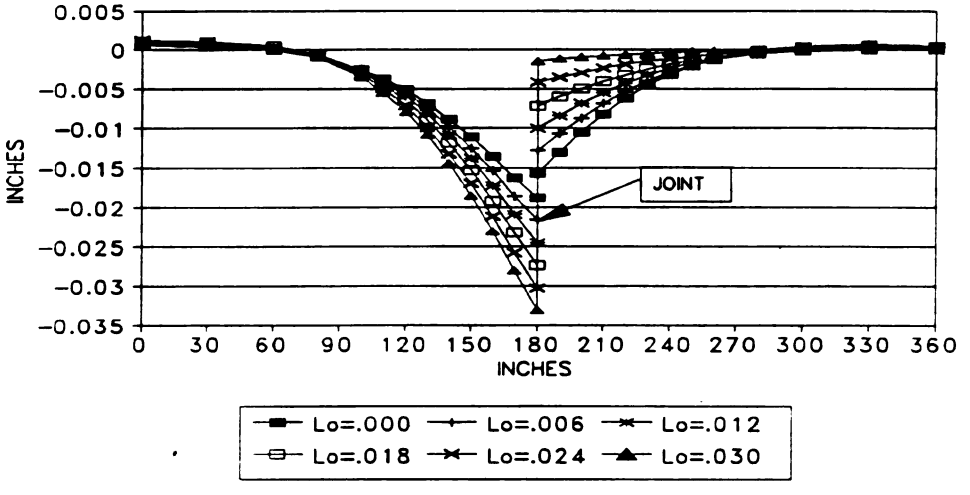

(b) DISPLACEMENTS OF LINE A-A

Fig. 5-7 Displacement Distributions (load case two)

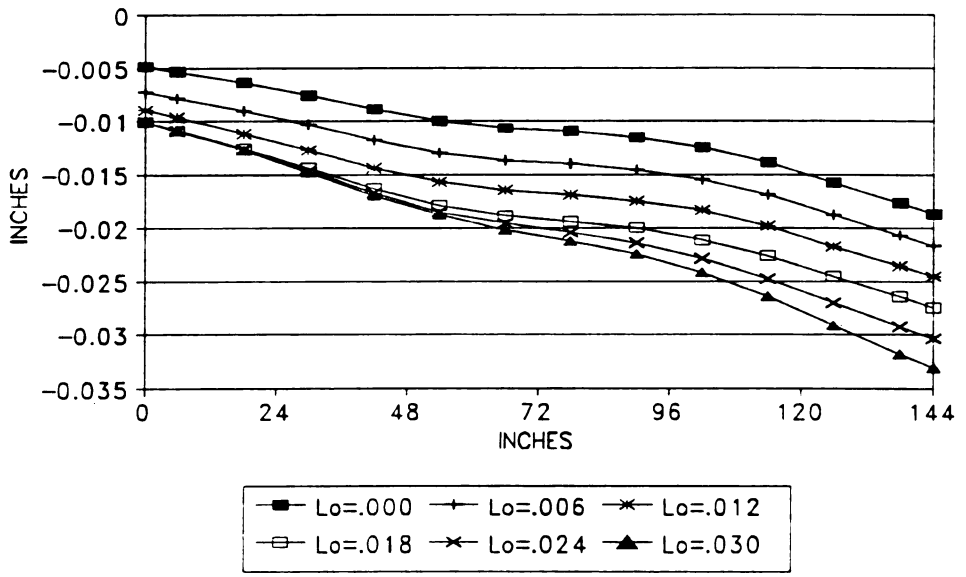

(c) DISPLACEMENTS OF LINE E-E

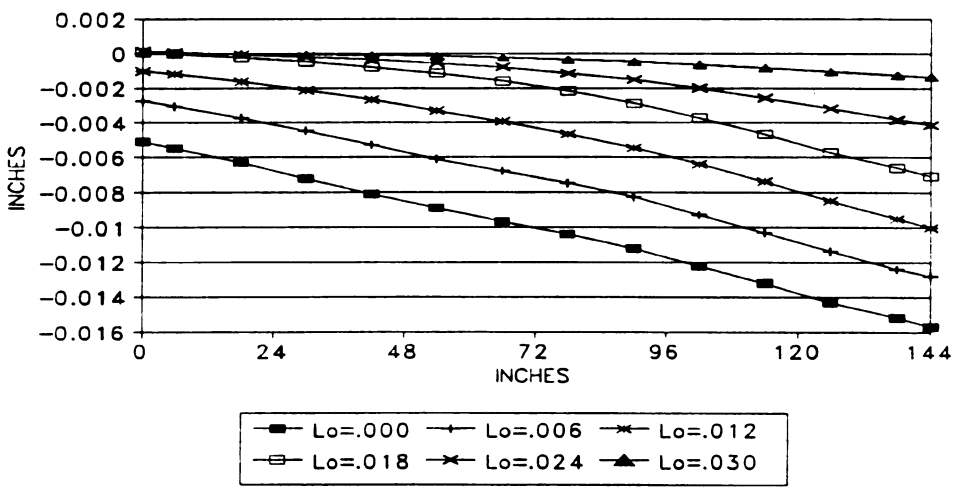

(d) DISPLACEMENTS OF LINE F-F

Fig. 5-7 Displacement Distributions (continued, load case two)

indicates that a 0.006 in looseness increases the displacement at point E from 0.0187 in to 0.0216 in, etc.

Stress distributions

Fig. 5-8(a)-(c) quantitatively present the stress distributions along Line B-$\bar{B}$, E-$\bar{E}$ and F-$\bar{F}$ under load case one and Fig. 5-9(a)-(d) present the similar results along A-$\bar{A}$, B-$\bar{B}$, E-$\bar{E}$ and F-$\bar{F}$ under load case two. For instance, Fig. 5-9(a) and (b) indicate that the full looseness of the dowel bars may cause the maximum longitudinal stress even 100% more than those without looseness, and a 0.006 in looseness may increase the maximum longitudinal stress more than 20%. In load case two, each 0.003 inch looseness could cause approximately 10% in crease in the maximum stress of line A-$\bar{A}$, 14% increase of the maximum stress of line B-$\bar{B}$. When temperature gradient is considered, the mentioned increase of maximum longitudinal stress would become more critical. For PCC pavement thickness design procedures based on fatigue criterion, effect of additional stress due to the dowel bar looseness could be significant.

Where is the most critical point in pavement? Which stress is more critical, corner stress or edge stress? Many investigators have concluded that the edge stress is most critical at the middle between two joints. However, all these research results were obtained based on assumption of no looseness. The serious looseness significantly increases the maximum corner stress whereas the maximum edge stress is not sensitive to the looseness level because the location of the maximum edge stress is far away from the joint. The above analysis plus the consideration of dynamic

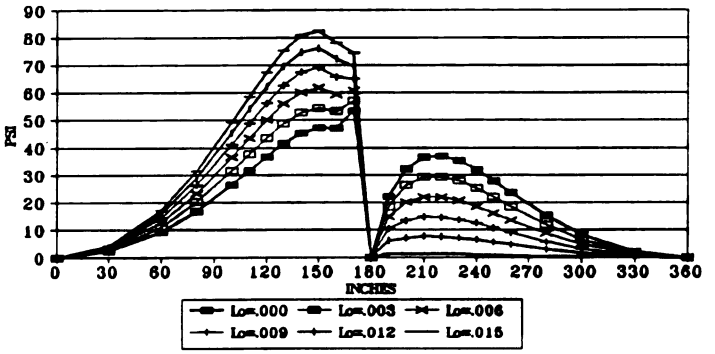

(a) SIGMA-X OF LING B-B

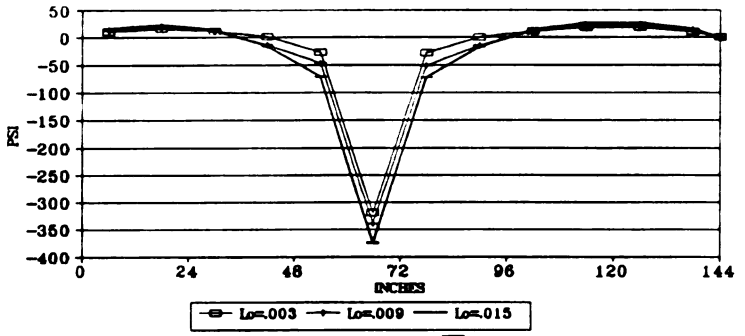

(b) SIGMA-Y OF LINE E-E

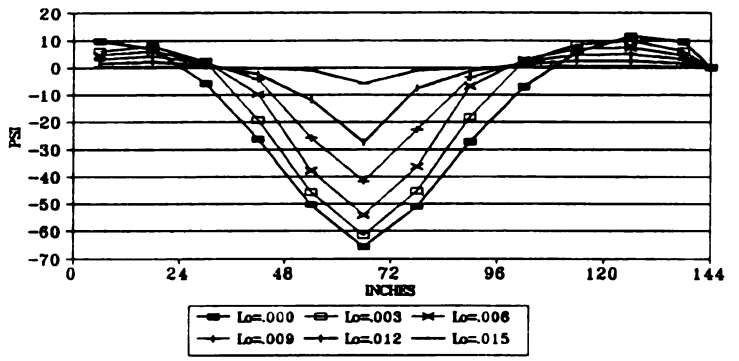

(c) SIGMA-Y OF LINE E-E

Fig. 5-8 Stress Distributions (load case one)

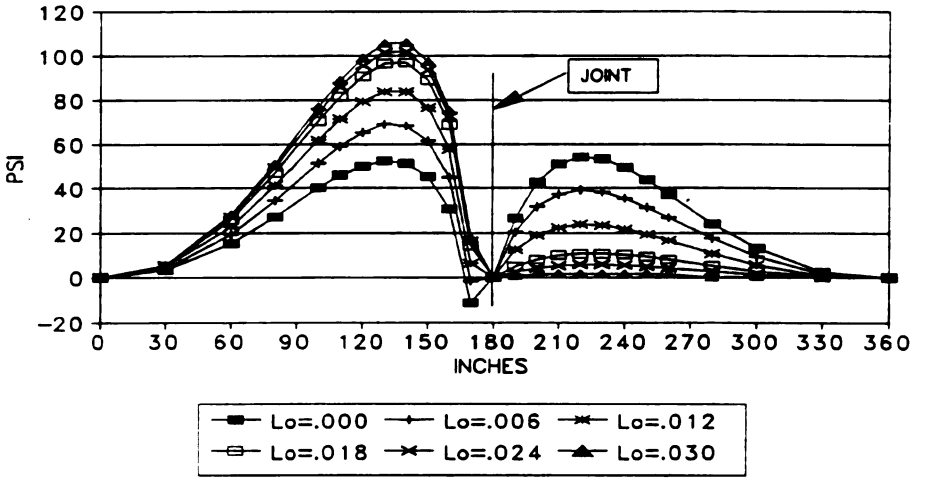

(a) SIGMA-X OF LINE B-B

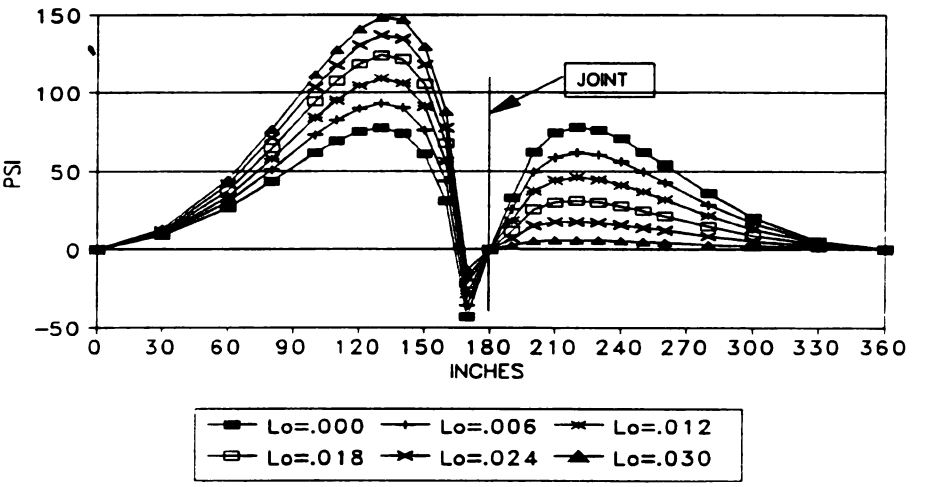

(b) SIGMA-X OF LINE A-A

Fig. 5-9 Stress Distributions (load case two)

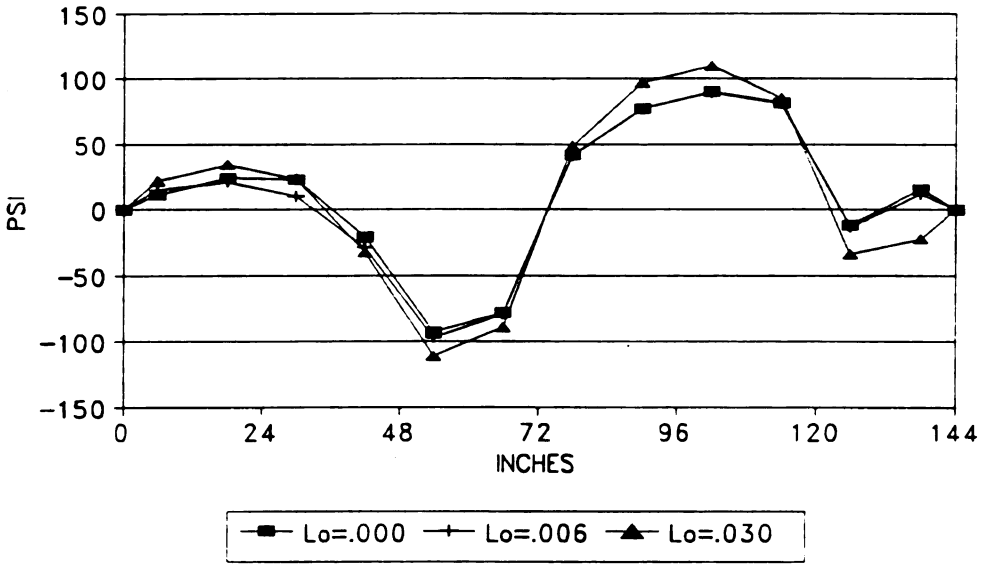

(c) SIGMA-Y OF LINE E-E

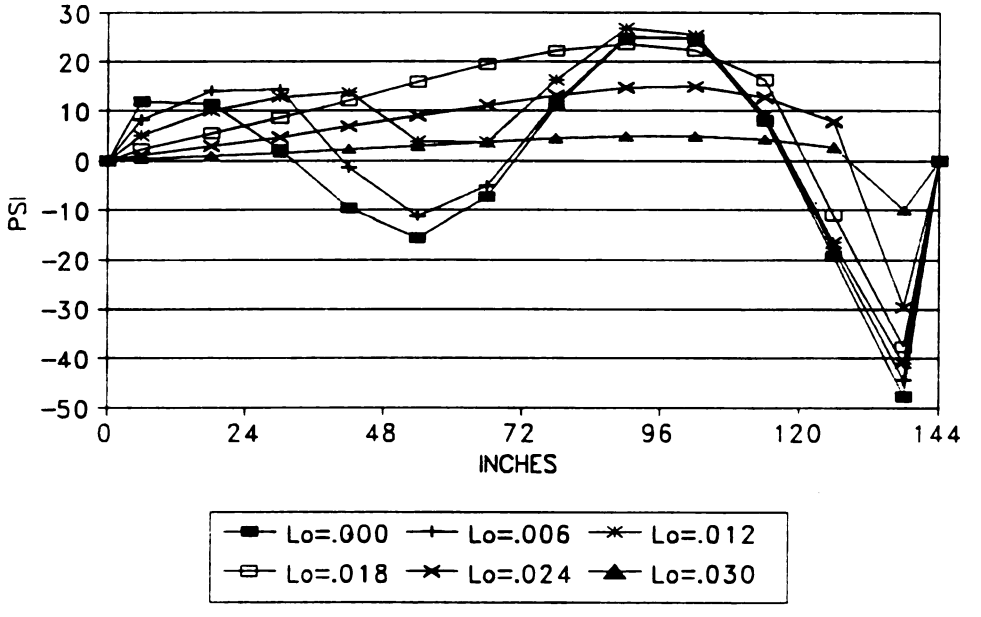

(d) SIGMA-Y OF LINE F-F

Fig. 5-9 Stress Distributions (load case two,continued)

coeeficient due to the interaction between truck and pavement near slab corner being greater than that at slab edge, the critical position needs further study.

Fig.5-8(b) and Fig.5-9(c) demonstrate that the transverse stress distributions of line E-$\bar{E}$ are not sensitive to the dowel bar looseness, and the maximum transverse stress (370 psi) presented in Fig. 5-8(b) does not make sense in rigid pavement design because there exists no concentrated load on the pavement as used in the calculation. Fig. 5-8 presented herein is for numerical comparison only. The results shown in Fig. 5-8(c) and Fig. 5-9(d) look sensitive to the looseness level, however, the effects of looseness are to reduce the maximum stress responses in the unloaded slab. Therefore, the effects are not significant in pavement thickness design.

Load transfer capability

Fig. 5-10(a) and Fig. 5-11(a) present the variation of dowel bar shear forces due to the increase of assumed looseness under load case one and load case two respectively. In load case one, Fig. 5-10(a) indicates that numbers of the effective dowels are reduced from 12 for looseness = 0, to 5 for looseness = 0.003 in and 0.006 in and to 3 for looseness = 0.009 in. The corresponding results in load case two are presented in Fig. 5-11(a): 12 for zero looseness, 9 for looseness = 0.006 in. Fig. 5-10(b) and Fig. 5-11(b) show the decrease of the total forces (the value without looseness is taken as 100%) transmitted from the loaded to unloaded slabs due to the

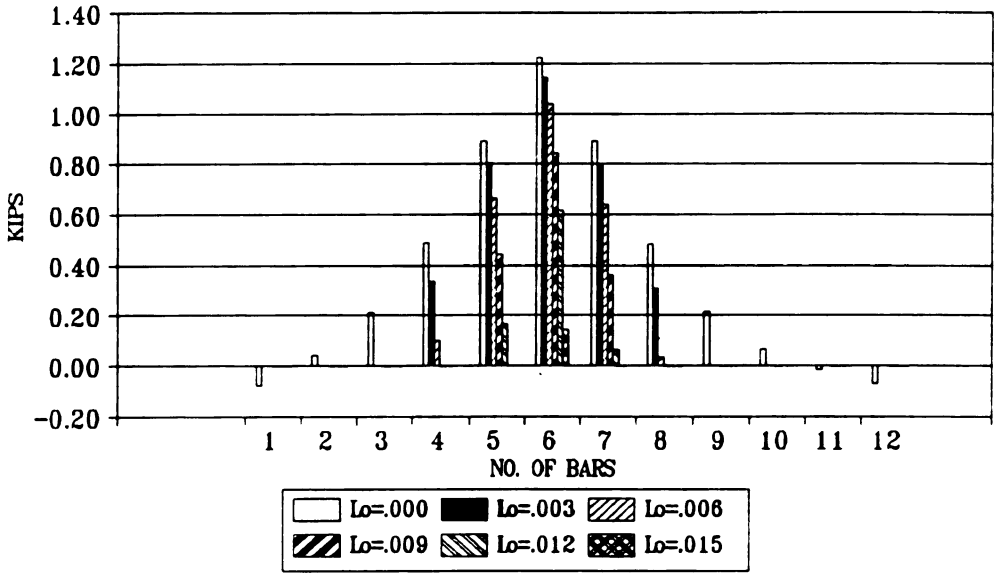

(a) SHEAR FORCES OF DOWEL BARS

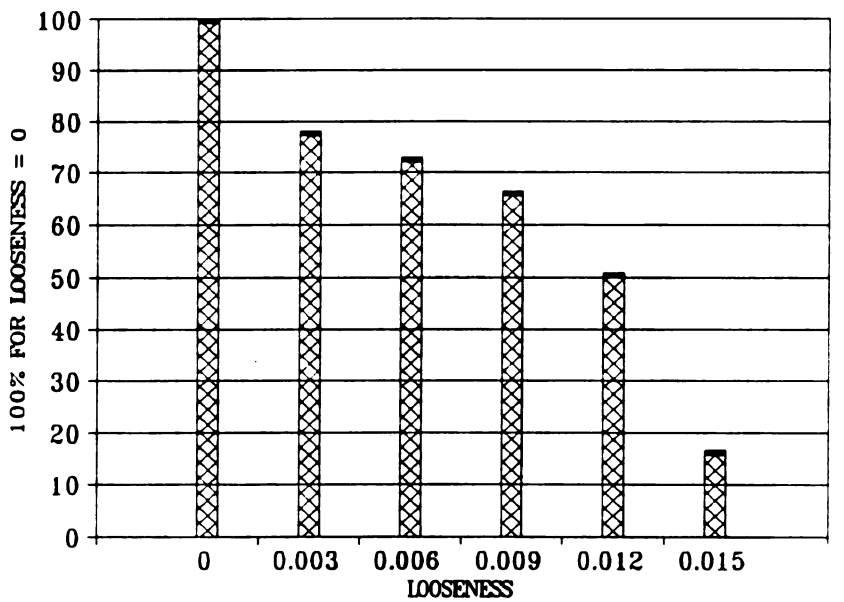

(b) TOTAL SHEAR FORCES TRANSMITTED BY BARS

Fig. 5-10 Load Transfer Properties (load case one)

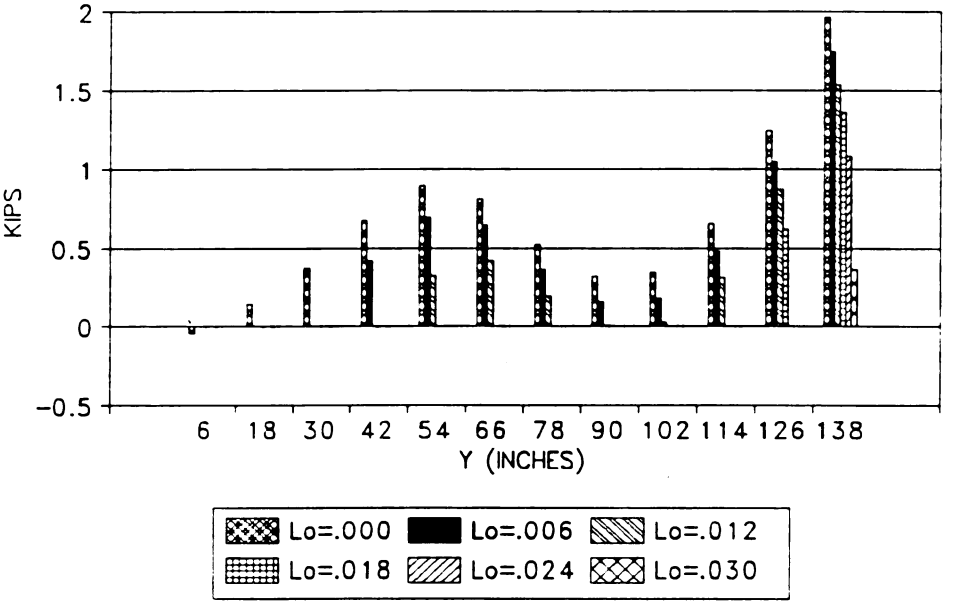

(a) SHEAR FORCES OF THE DOWEL BARS

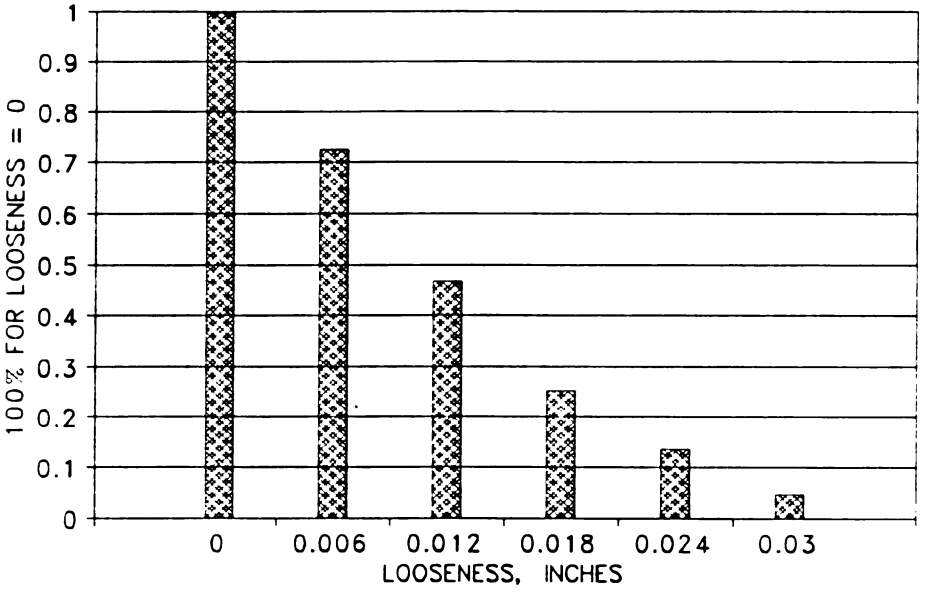

(b) TOTAL FORCES TRANSFERRED BY DOWEL BARS

Fig. 5-11 Load Transfer Properties (load case two)

increase of looseness level. The 0.003 inch looseness causes 22% loss of the load transfer capability for load case one, and approximately 14% loss for load case two. As mentioned by Majidzadeh[1989], .003 - .006 inch looseness is often observed in pavement in service, even the initial dowel bar looseness of new pavement could be greater than .003 inch which still affects load transfer capability significantly.

5 Summary

A nonlinear elastic model to simulate the dowel bar looseness mechanism is proposed in this study. For any given looseness of the dowel bars, the model can predict the responses of the pavement, including the final stress and displacement distributions and load transfer capability. The looseness level depends on the construction quality, pavement service life, accumulate traffic loads, environmental condition of the pavement, etc. Once the looseness level and distribution are measured or estimated by an appropriate model, the responses of pavement at different stages of its service life may be predicted by the developed model. The findings in this chapter are summarized as follow:

(1) Based on the numerical example presented in this paper (load case two), each increase of 0.003 inch looseness could cause a 10% increase in the maximum stress at the edge, 14% increase of the maximum stress in the middle of the slab, and causes 14% loss of the load transfer capability.

(2) The maximum longitudinal stress in pavement is sensitive to the

looseness level. It would become more critical to transverse cracks when temperature gradient is considered. This finding could have a significant effect to any PCC pavement thickness design procedure based on fatigue criterion.

(3) 0.003 inch dowel bar looseness might change the stress distribution quite significantly. That explains why the quality of dowel bar installation is very important to its service quality and life. Further more, any coating material to be used for protecting dowel bars against corrosion should be carefully verified to ensure it is thin and strong enough, and will not produce effect similar to a serious looseness.

(4) The consideration of looseness causes some significant changes in pavement response. More numerical analysis corresponding to pavements with different service periods and under different environmental conditions should be conducted to study the effects of looseness to some existing research conclusions.

CHAPTER SIX
COMPARISON BETWEEN ANALYTICAL AND EXPERIMENTAL RESULTS

1 Research on Load Transfer Characteristics of Dowels by Keeton[1957]

A very significant experimental study on the load transfer characteristics of dowels used in airfield pavement expansion joints was conducted by the U.S. Naval Civil Engineering Research and Evaluation Laboratory in the 1950's. Not only the test results, but also the structural, material and environmental data were presented in the literature, hence, it is possible to use the experimental results to compare the results produced by the analytical models presented in Chapter 4.

The primary objective of the experimental research was the development of a realistic evaluation procedure for load transfer devices. The interrelationships among deflection, moment, shear and bearing pressure during load transfer in an airport pavements, were studied by constructing a full-size concrete slab with instrumented dowels across an expansion joint and imposing upon the slab loads of the magnitude of those resulting from the use of modern aircraft. (Tire load varied from 10,000 lb to 100,000 lb)

The test slab was 10 in. thick, 15 ft. wide and 50 ft. long, consisting of two 25-foot sections jointed by dowels across 0.75 in. expansion joint. A transverse weakened plane joint was provided at the center of

each 25-foot section. Fifteen 1.125 in. diameter steel dowels 20 in. long were placed on 12-inch centers across the joint. The slab was constructed on a prepared subgrade having a modulus of subgrade reaction of about 200 pounds per cubic inch as indicated by bearing tests with a 30-inch diameter plate made just prior to construction of the slab. A complicated slab deflection measuring system covering a large area was embedded under the slabs and fixed on the upper end of steel rods which had been driven 10 feet into the subgrade.

Each dowel was instrumented with 14 strain gages on the upper and lower sides to measure bending moments in the dowel, one gage was placed on each side of the dowel on the neutral axis and was inclined at 45° to measure the shear force in the dowel. Before installation in the field slab, the instrumented dowels were loaded at the center while supported at the ends as simple beams. Moments were calculated for various loads and were used to calibrate each of the gages for the strain readings. Differential transformers with a linear range of 0.15 in. were used to measure slab deflections under loads.

The application of single wheel loads to simulate actual loading of airfield pavements by large bombers, a B-45C tire and wheel were mounted on a specially-designed 50-ton capacity cart which is illustrated in Fig. 6-1. The tire had a diameter of 56 inches, a width of 16 inches, and could be loaded up to 100,000 pounds with tire pressures up to 250 psi. The major test results reported by Keeton[1957] were produced by using a static load of 50,000 pounds and a tire pressure of 200 psi

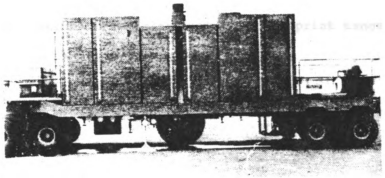

Fig. 6-1 The Cart for Application of Wheel Loads (from Keeton[1957])

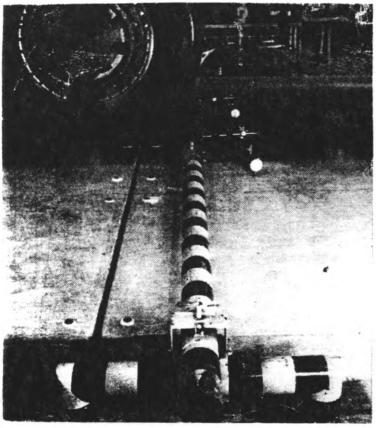

Fig. 6-2 A Static Load Acted at the Joint (from Keeton[1957])

applied at the center of the slab with the tire print tangent to one face of the joint as shown in Fig. 6-2.

2 Formulas of Bending Moment, Shear Force and Bearing Pressure in Dowels Embedded in Concrete

The bending moment and shear forces at two ends of a dowel in the joint (the intersections between the two surfaces of slabs and the center line of the dowel bar) can be calculated using the formulae given in Chapter 4, the detailed derivation can be found in Appendix 4. The reaction moments and shear forces acting on the ends of two segments of the dowel embedded in concrete must be the same as their original moments and forces. Taking the segment embedded in the leave slab as an example and considering Fig. D-1, M_0 and P_0 have been obtained and the following expressions can be written.

Relative displacement of the dowel:

$$\delta(x) = A'ch\beta x\cos\beta x + B'ch\beta x\sin\beta x + C'sh\beta x\cos\beta x + D'sh\beta x\sin\beta x \tag{6-1}$$

bending moment:

$$M(x) = -2\beta^2 EI[D'ch\beta x\cos\beta x - C'ch\beta x\sin\beta x + B'sh\beta x\cos\beta x - A'sh\beta x\sin\beta x] \tag{6-2}$$

Shear force:

$$Q(x) = 2\beta^3 EI[(C'-B')\,ch\beta x\cos\beta x + (A'+D')\,ch\beta x\sin\beta x + (A'-D')\,sh\beta x\cos\beta x + (B'+C')\,sh\beta x\sin\beta x] \quad (6\text{-}3)$$

Bearing pressure:

$$p(x) = \delta(x)\; D\; \Psi \quad (6\text{-}4)$$

Where:

$$A' = \delta_0$$

$$B' = \frac{1}{2}\left(\frac{\varphi_0}{\beta} - \frac{P_0}{2EI\beta^3}\right)$$

$$C' = \frac{1}{2}\left(\frac{\varphi_0}{\beta} + \frac{P_0}{2EI\beta^3}\right) \quad (6\text{-}5)$$

$$D' = \frac{M_0}{2EI\beta^2}$$

Ψ = interaction coefficient between dowel and concrete

D = diameter of the dowel

$\beta = (\psi D/4EI)^{0.25}$

E = Elastic modulus of teh dowel

I = Moment of inertia of the cross section of the beam

δ_0 and ϕ_0 can be solved from the following equation:

$$\begin{pmatrix} P_0 \\ M_0 \end{pmatrix} = -\frac{2EI\beta^2}{C^2+c^2}\begin{pmatrix} 2\beta(SC+sc) & S^2+s^2 \\ S^2+s^2 & \frac{SC-sc}{\beta} \end{pmatrix}\begin{pmatrix} \delta_0 \\ \varphi_0 \end{pmatrix} \quad (6\text{-}6)$$

For convenience of presentation, the positive moment is defined as the bottom surface of the dowel in extension.

3 Some Special Considerations in Input Data Preparation

Modulus of subgrade reaction

Keeton[1957] concluded: "Tests have indicated the presence of an air void at the center of the slab at the joint amounting to about 0.04 in." When responding to the discussion by B. F. Friberg, on the measurement of the modulus of subgrade reaction, Keeton described: "The modulus of subgrade reaction was measured at the joint two days before the construction of the slab and was found to be about 200 psi per in. If the slab were in intimate contact with the subgrade, the measured slab deflections would indicate a maximum subgrade pressure of 17.8 psi based on k=200 pci. This pressure is not likely to cause subgrade failure to the extent of 0.03 in." For verifying the above statement, Keeton also stated: "Over 400 load applications (50,000 lb) were made on the slab. From beginning to end, the test results did not reflect any drastic changes in the subgrade such as would be evident in event of a subgrade failure." From above statement, k = 200 pci is used in most numerical calculations without considering the variation of the modulus of subgrade reaction under the 50,000 lb load or the reduction of the k value due to the air gap. However, it is believed that the complicated slab deflection measuring system embedded under the slabs might have significant effects to the subgrade modulus. A few numerical results are also presented by using k=50 pci for comparison. The presented

results in this chapter are obtained using k=200 pci except those specifically mentioned.

Simulation of the air gap under the slab

Keeton also concluded: "It is most probable that the void beneath the center of the slab at the joint is the result of slab warping during the curing." However, he also described the test environment as: "The slab is inside a building and is therefore subject to minimum ambient temperature changes and is not exposed to the direct rays of the sun." The air void beneath the slab was found by the authors and can also be verified by the presented displacements versus the magnitude of the loads (Table 5 in the reference, Keeton[1957]). Any measured response was the difference of the responses corresponding to the states before and after 50,000 lb load being applied on the slab so that the initial state should be defined as the one before the 50,000 lb load moved on. The determination of the initial state becomes extremely important in comparing the experimental and analytical results. The only significant related information provided by the authors is the existence of air gap beneath the slab. It is assumed here that: the initial shape of the slab was the one with about average 0.04 inch gap at the joint and caused by temperature gradient. By numerical tests, it has been found that 3.2° F/in night-time temperature gradient (g=-3.2) would cause average 0.0405 inch curled-up deflection at the joint. Therefore, the analytical results for comparing the experimental ones are the difference between responses due to 50,000 lb plus g=-3.2° F/in and the responses due to g=-3.2 °F/in temperature gradient only. The assumption

is acceptable because the initial shape of the slab is more important in the analysis than the source which had produced the initial shape.

Simulation of the expansion joint and the weakened plan joints

The 0.75 inch width expansion joint is simulated by using the component model as a dowelled joint and the weakened plan joint at the center of each 25 ft slab is assumed as a 0.1 inch width joint with aggregate interlock only. The existence of the interlocked narrow joint has secondary effects on the response of the dowels and the slab near the expansion joint under the tire load, however, it has significant effects to determine the initial state of the slabs as discussed above.

Determination of elasticity modulus of the concrete

Keeton reported that the concrete had a compressive strength f_c of 6160 psi based on 28-day specimens. The modulus of elasticity E can be predicted with reasonable accuracy from the empirical equation found in ACI Code:

$$E = 33\ \gamma^{1.5}\ \sqrt{f_c} \qquad (6\text{-}7)$$

Carrasquillo[1981] and Martinez[1982] reported that for compressive strength in the range from 6000 to 12000 psi, the ACI Code equation overestimates E for both normal weight and lightweight material by as much as 20%. Based on their research, the following equation is recommended for normal density concretes with f_c in the range from 3000 to 12000 psi:

$$E = (40{,}000\sqrt{f_c} + 1{,}000{,}000)\left(\frac{\gamma}{145}\right)^{1.5} \qquad (6\text{-}8)$$

The units used in the equation are pounds/in^2 for strength and pounds/ft^3 for density γ. Eq. 6-8 was employed to determine the modulus of elasticity of concrete in this analysis.

Input data used in numerical analysis

The major input data used in the analysis are listed below:

Length of each section of the slab	25 ft.
Width of slab	15 ft.
Thickness of slab	10 in.
Elastic modulus of concrete	4,140,000psi
Poisson ratio of concrete	0.15
Subgrade reaction k value	200 pci
Unit weight of concrete	145 pcf
Dowel bar diameter	1.125 in.
Dowel bar spacing	12 in.
Elastic modulus of dowel steel	29000000 psi
Width of joint	0.75 in.
Poisson ratio of steel	0.30
Dowel-concrete interaction coefficient	1,500,000pci
The interlock spring modulus	100,000 psi

The finite element mesh of the slab is given in Fig. 6-3.

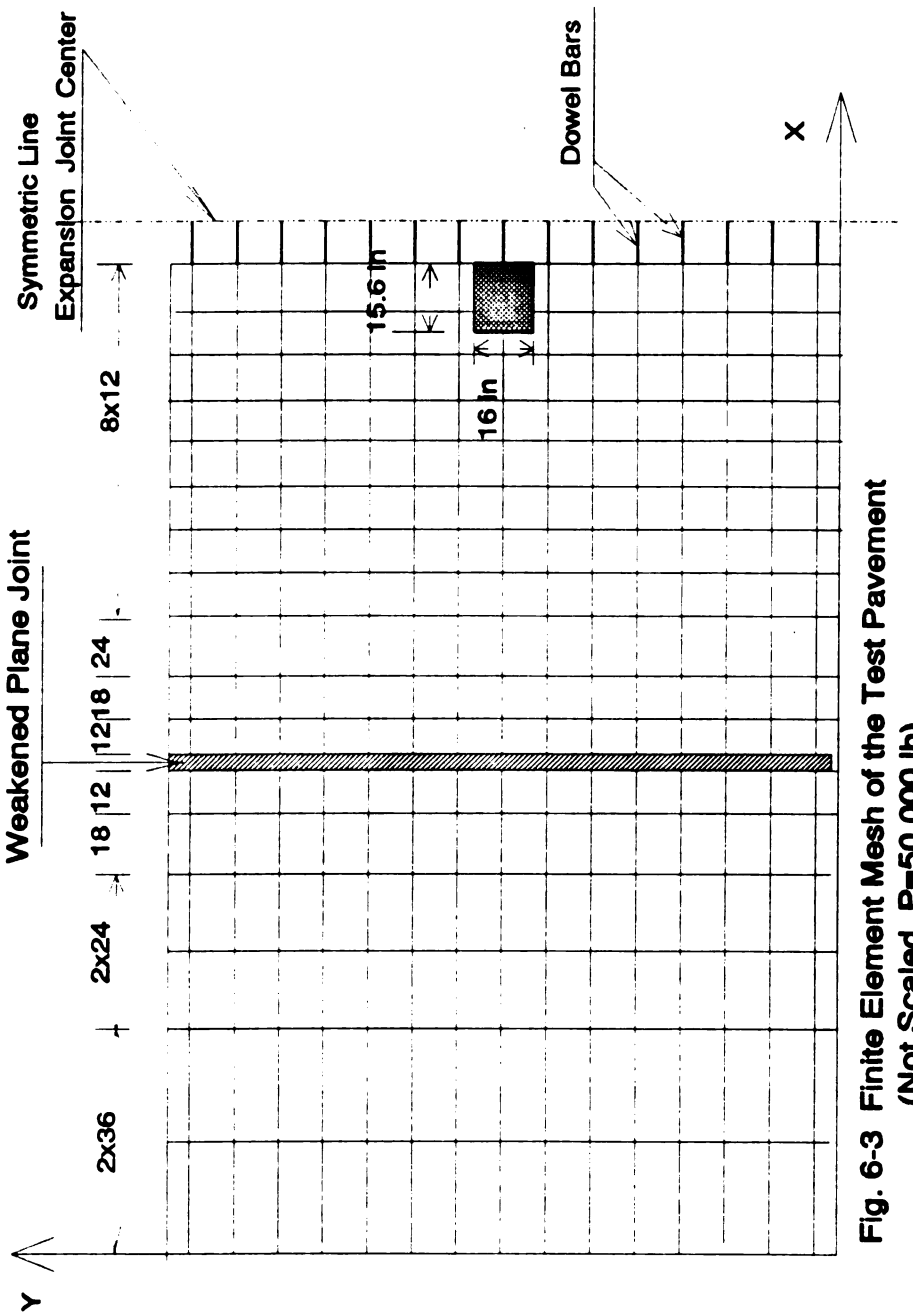

Fig. 6-3 Finite Element Mesh of the Test Pavement
(Not Scaled, P=50,000 lb)

4 Comparison of The Results

The comparison of bending moments of the four dowels just under and with distance 1, 2 and 3 ft from the load center are presented in Figs. 6-4, (a) to (d). The maximum stress of the dowel is 18.1 kpsi (experiment) and 28.0 kpsi (analysis), both are relative high. As discussed in Chapter 4, the critical responses of dowels and slabs affected by the dowel moments usually are not as sensitive as by the shear forces. However, The test slab is only 10 inch thick and the single tire load is very high (50,000 lb), so thatthe maximum bending stress of the dowel under the load becomes relative high. For a 9,000 lb single tire load, the maximum bending stress of the dowel would only be about 5,000 psi. In another word, the 10 inch thickness is not sufficient for airport pavement to withstand very heavy tire load.

The measured shear forces for two symmetrically located dowels on the two sides of the load were different, so Figs. 6-5 (a) to (d) only show the comparison of shear forces of four dowels on the same side of the load. The differences between the measured and the analytical shear forces are no more than 20%. The comparison of bearing pressure on the four dowels are presented in Fig. 6-6. The "measured" maximum bearing pressure (18,100 psi) is much higher than the measured compressive strength of the concrete (6160 psi). It is not clear, however, how and what device was used to measure the bearing pressure in the experiment.

The shear forces of five dowel bars at the joint surface are given in

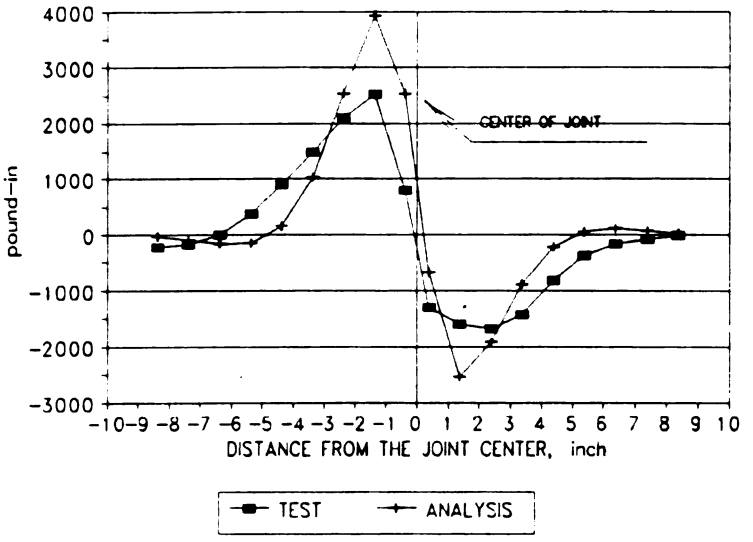

(a) Under the load

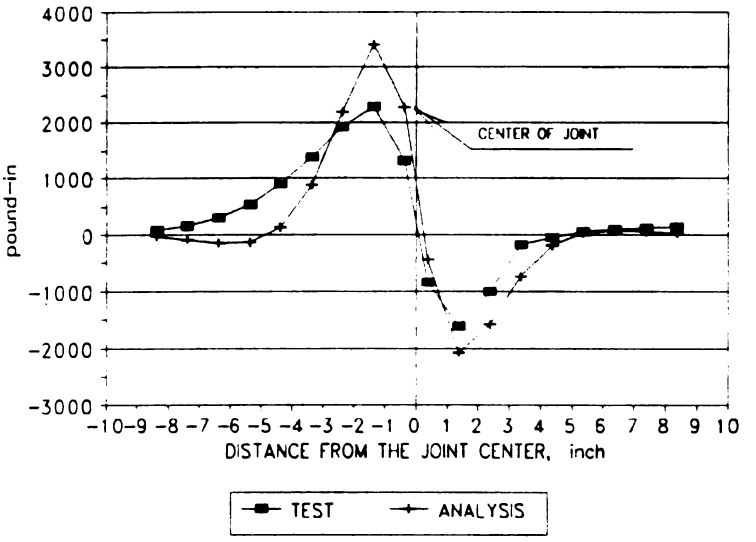

(b) 1 ft. from the load

Fig. 6-4 Bending Moments of the Dowels

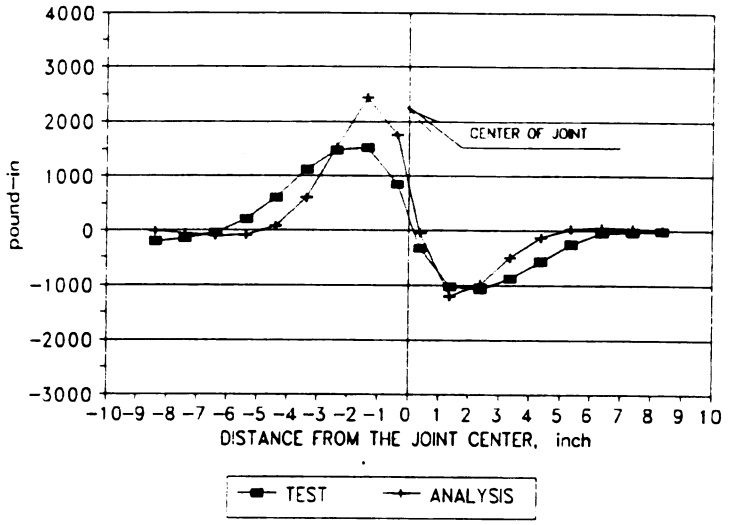

(c) 2 ft. from the load

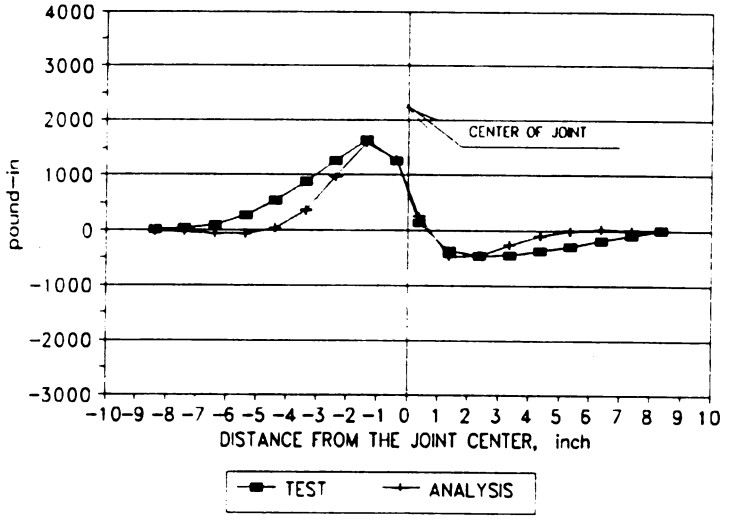

(d) 3 ft. from the load

Fig. 6-4 Bending Moments of the Dowels (continued)

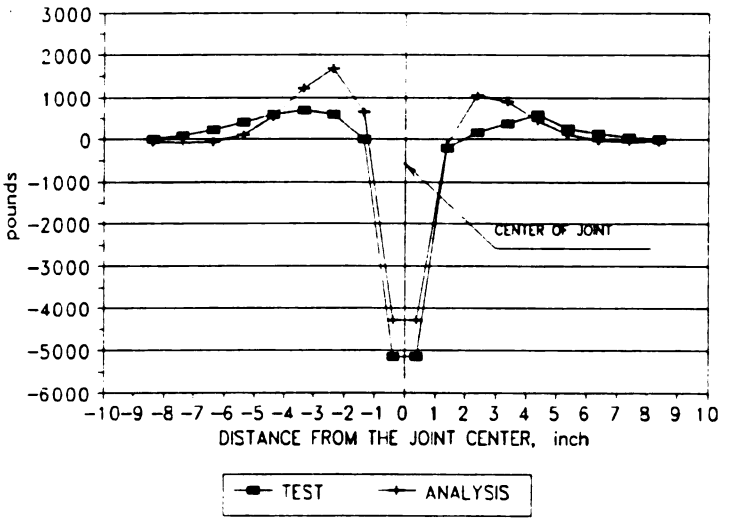

(a) Under the load

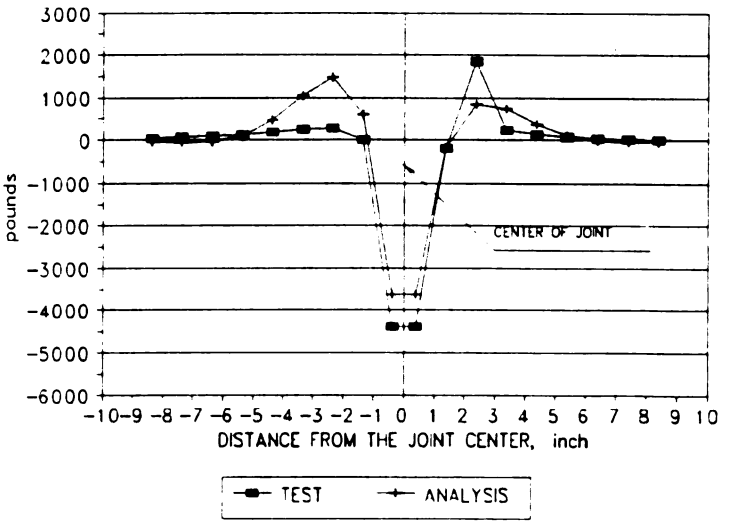

(b) 1 ft. from the load

Fig. 6-5 Shear Forces of the Dowels

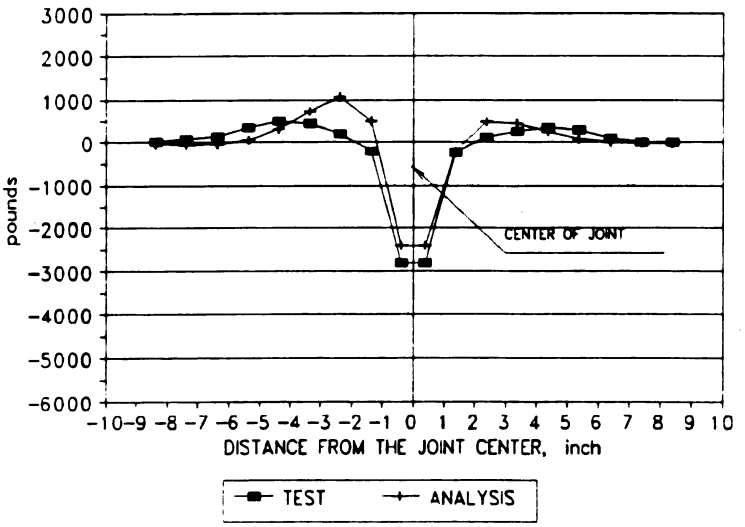

(c) 2 ft. from the joint

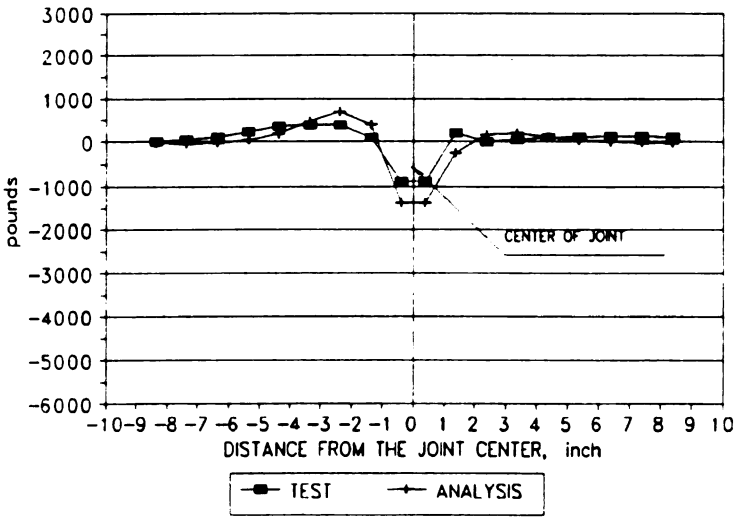

(d) 3 ft. from the joint

Fig. 6-5 Shear Forces of the Dowels (continued)

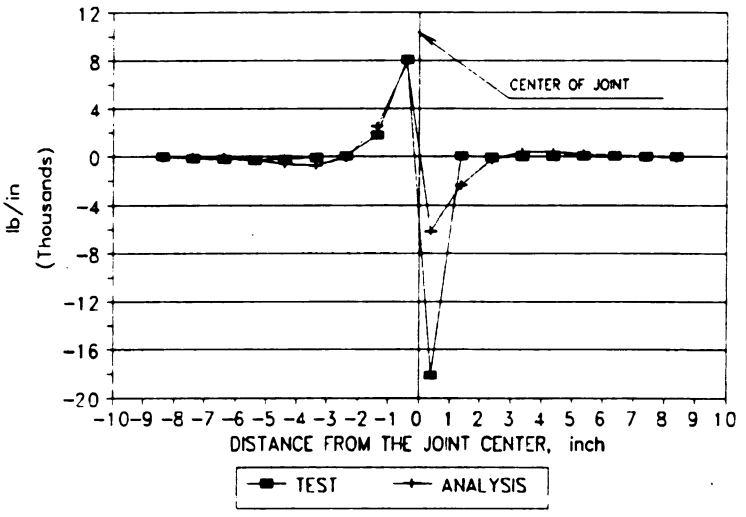

(a) Under the load

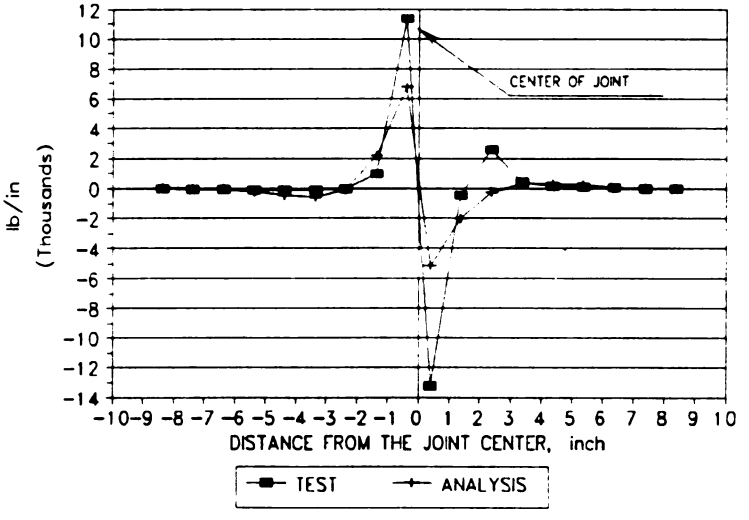

(b) 1 ft. from the load

Fig. 6-6 Bearing Pressure of the Dowels

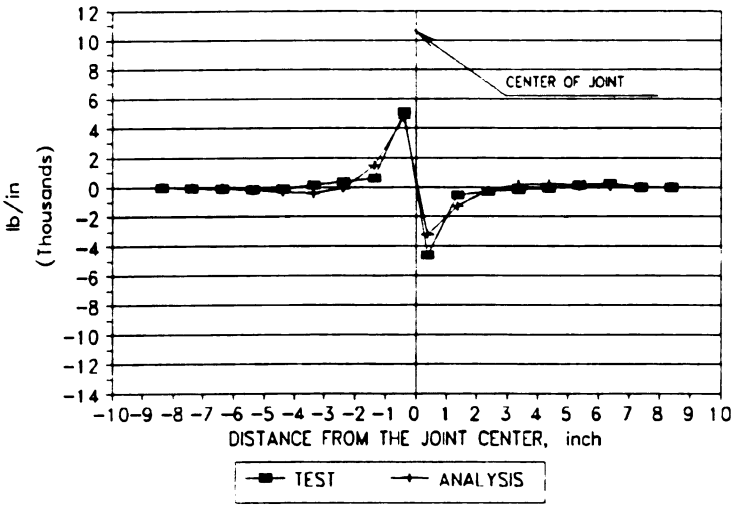

(c) 2 ft. from the load

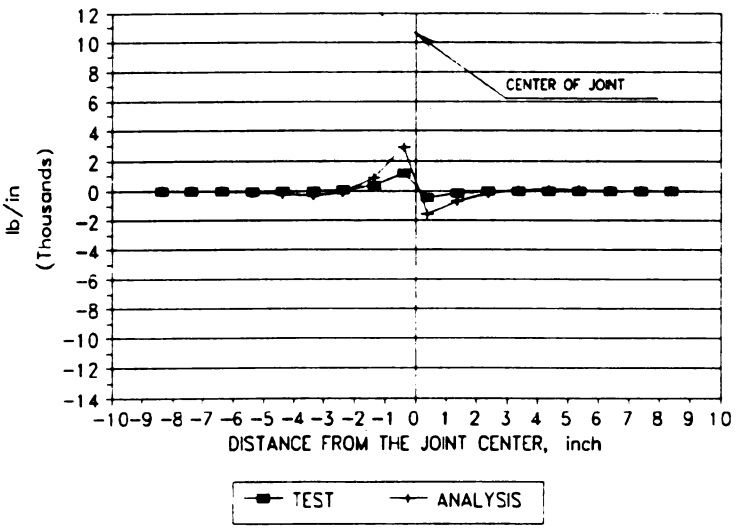

(d) 3 ft. from the load

Fig. 6-6 Bearing Pressure of the Dowels (continued)

Fig. 6-8. The calculated shear forces must be symmetrical to the load center and the same when the load applied at the two sides of the joint if the structural and support conditions of the two slabs were the same. However, the measured ones were not symmetrically distributed when the load was applied on the two sides of the joint. For comparison, the average of the four measured values (shear forces on two symmetrical dowels when the load acted at two sides of the joint) is used. The difference between the maximum experimental and analytical results is less than 10%. Fig. 6-8 suggests that the experimental and analytical shear forces have good agreement.

Fig. 6-7 presents the comparison of longitudinal displacements under and 1, 2 and 3 ft. from the load center. The maximum displacement obtained by using k=200 pci in analysis is 38% lower than the test one. However, if the k value is assumed as 100 pci for considering the effects of the deflection measuring system under the slab, the temperature gradient needed to produce 0.04 inch average joint displacement on the loaded side should be about -3.5 °F/in. The calculated transverse displacements on the two sides of the expansion joint are presented in Fig. 6-9 and Fig. 6-10. The results from using k=200 pci and g=-3.2°F/in are also given in the same figures for comparison. The results with the assumption of k=100 pci are much closer to the test results.

Apart from the responses of the slab and joint under 50,000 pounds at the center of the joint, Keeton also presented shear forces measured at the dowel under the load, 1 and 2 ft from the load and the maximum

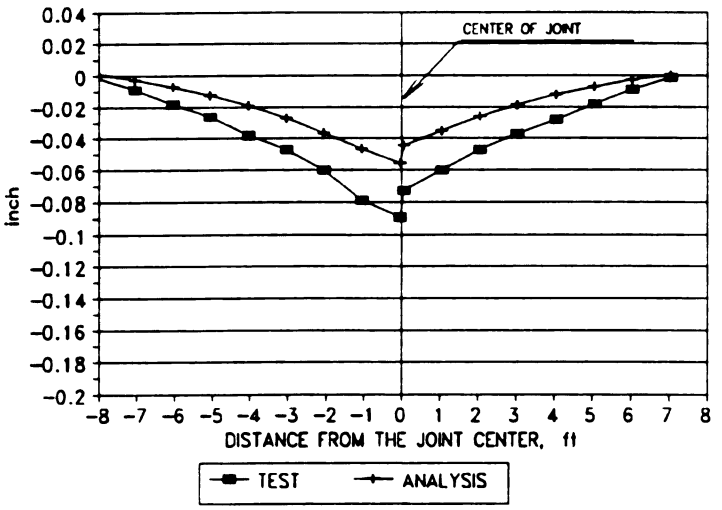

(a) Under the load

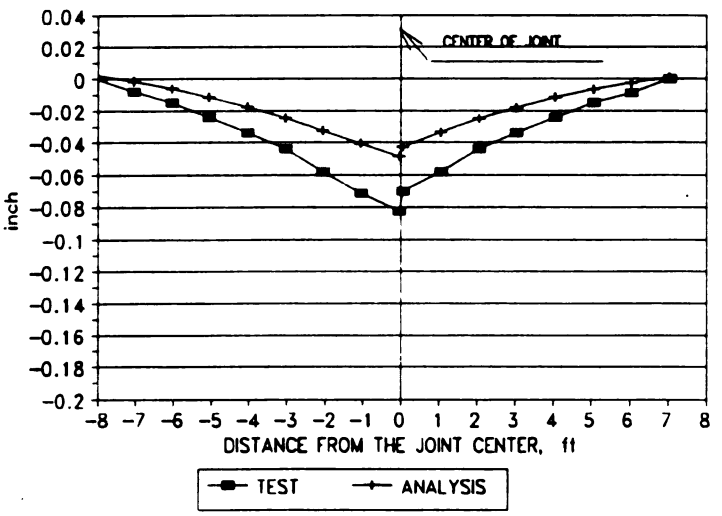

(b) 2 ft. from the load

Fig. 6-7 Longitudinal Displacements

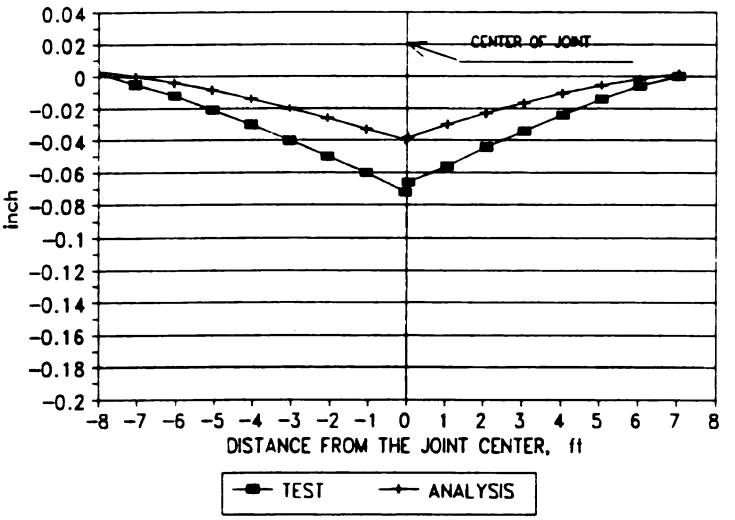

(c) 4 ft. from the load

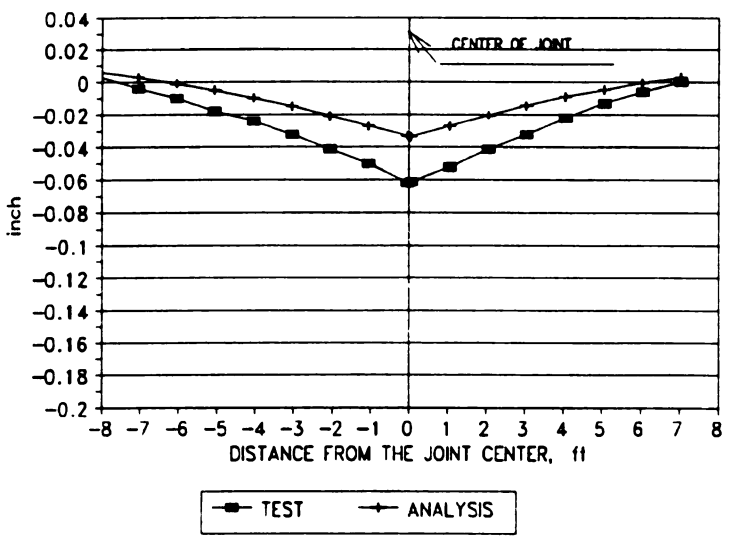

(d) 6 ft. from the load

Fig. 6-7 Longitudinal Displacements(continued)

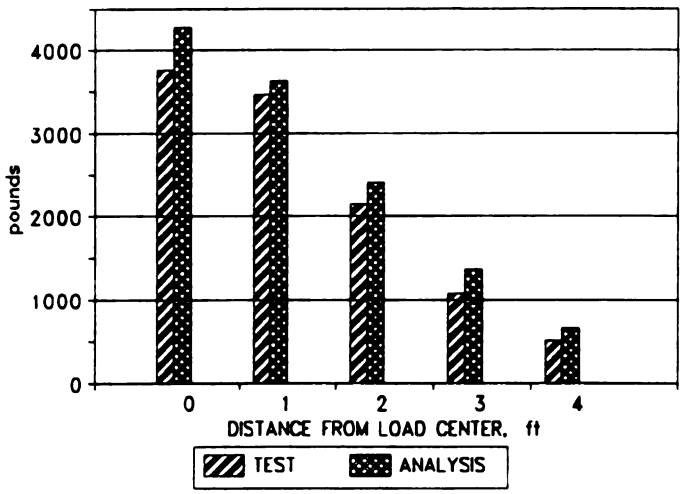

Fig. 6-8 Average Shear Forces in the Joint

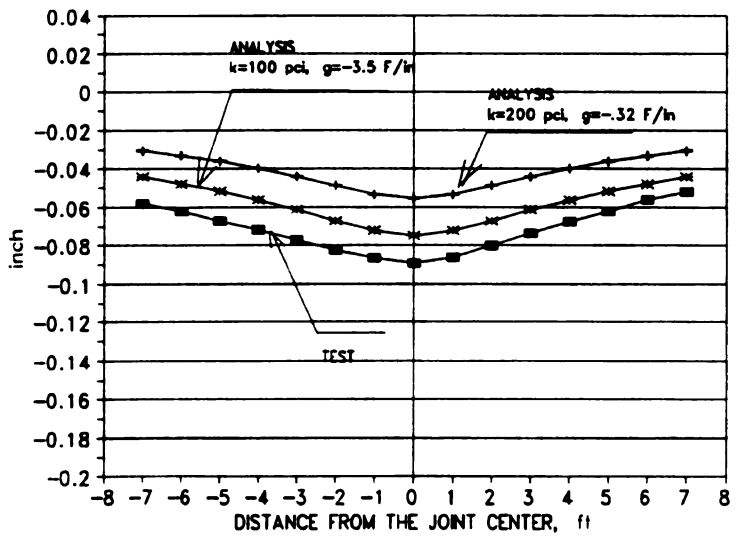

Fig. 6-9 Transverse Displacements of the Joint (on the loaded side)

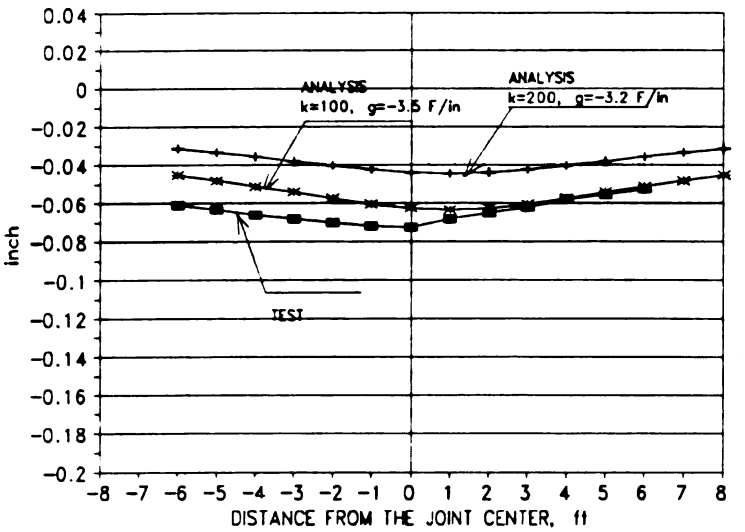

Fig. 6-10 Transverse Displacements of the Joint (on the unloaded side)

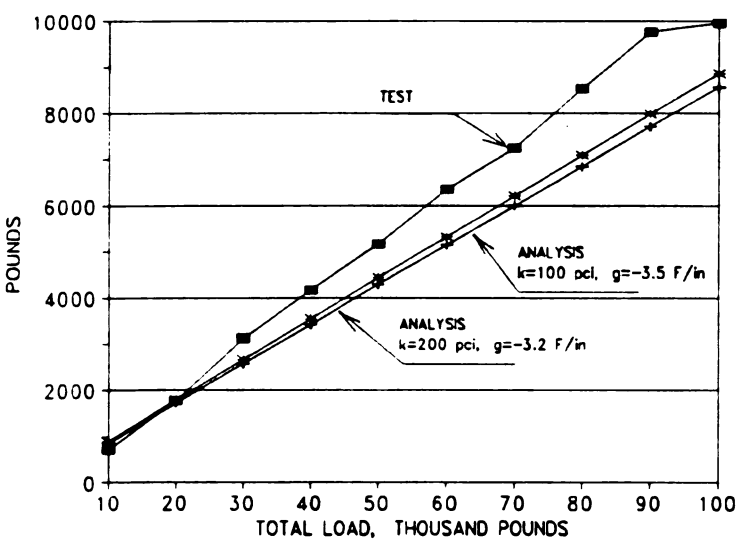

(a) Under the Load Center

Fig. 6-11 Measured and Calculated Dowel's Shear Forces v.s. Load Magnitudes

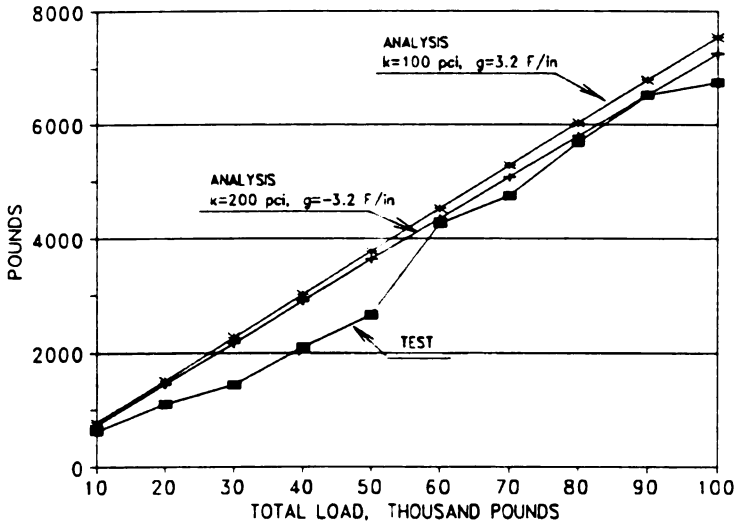

(b) 1 ft from the Load Center

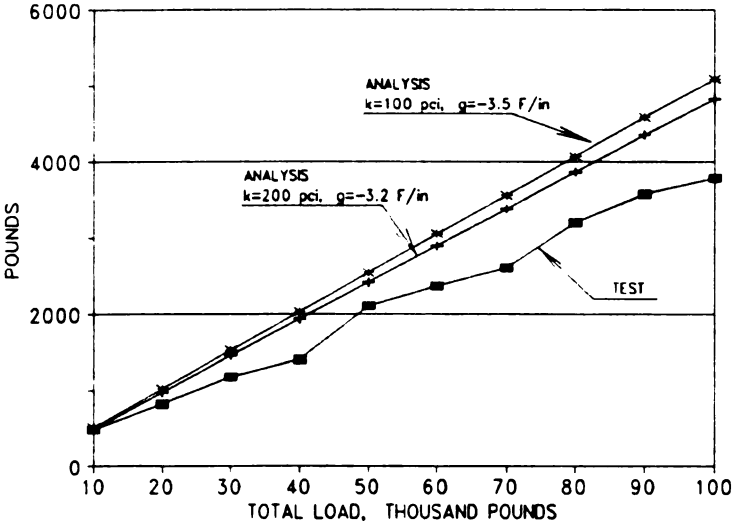

(c) 2 ft from the Load Center

Fig. 6-11 Measured and Calculated Dowel's Shear Forces v.s. Load Magnitudes (continued)

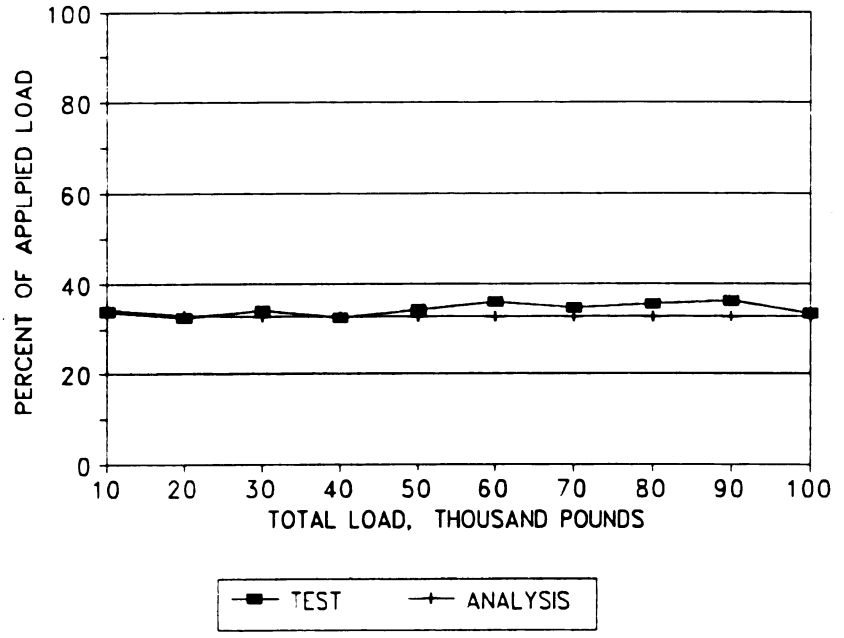

Fig. 6-12 Percentage of Total Load Transferred by Five Dowels

displacement of the slab under the load varying from 10,000 to 100,000 pounds. The comparison between the measured and analyzed shear forces are given in Fig. 6-11. The results by using subgrade modulus k=100 pci and g=-3.5 °F/in are also presented for comparison. It is interesting to point out that the analytical model underestimates almost all shear forces on the dowel just under the load center and overestimates almost all shear forces on the dowel 2 ft away from the load center. The dowel shear forces are not very sensitive to the variation of subgrade modulus k and tempreture gradient g. Fig. 6-12 shows good agreement between the measured and analyzed percentage of total load transferred by the five dowels nearest the load center.

The analytical results under the combination of load and temperature gradient were obtained by using nonlinear iteration procedure, in other words, the nonlinear behavior of the system was considered. The relationship between the shear force and the applied load in Fig. 6-11 indicates that a linear relation exists when temperature gradient remains constant and the magnitudes of load are large enough.

5 Summary

The comparison verifies that the analytical model simulates the load transfer characteristics quite well. All the input data used in the analysis are obtained from the paper published by Keeton[1957]. The only assumption employed in this chapter is the initial state of the slab

shape was produced by temperature gradient.

The shear forces of the dowels obtained by the analysis are in good agreement with those obtained by the experiment. The shapes of all compared responses, including the bending moment, shear force distribution of the dowels, displacement of the slab and the bearing pressure on the concrete, are identical to those of the experiment. The analytical results are closer to the experimental ones, when based on the average values of the measurement. Unfortunately, the distributions of bending moment and shear force on the dowels symmetrical to those with the presented measurement are not available in the reference (Keeton[1957]), hence, the corresponding comparison can only be conducted by using the results on one side of the longitudinal symmetrical line of the slabs.

The modulus of subgrade reaction k and the dowel-concrete interaction coefficient γ can be adjusted to produce analytical results very identical to the measured ones. The essential objective of the comparison is to simulate the load transfer characteristics rather than to simulate the measured results. Therefore, no effort was made to adjust the parameters at this time.

CHAPTER SEVEN
IMPACT TO THE DOWEL DESIGN PROCEDURE

1 Current Design Procedures

Smooth round dowel bars have been employed as a load transfer device in jointed concrete pavements for a long time. Many experimental and analytical researches have been conducted to develop and improve the design procedure of the dowels. Before the 60's, the most influential analytical models were developed by Timoshenko[1925], and Friberg[1938][1940] etc., and some significant experimental research studies for dowelled jointed slabs were conducted by Teller[1936][1958], Kushing[1935] and Keeton[1957] etc. The complete review of these studies and the application in engineering design can be found in Snyder[1989] and Heinrichs[1989].

The conclusion has been obtained that the maximum concrete bearing stress is the most important parameter to be determined in PCC pavement joint design. Currently, the maximum bearing stresses of concrete under dowels are required to be equal to or smaller than the concrete bearing strength. Furthermore, the level of the bearing stress has direct effects on the accumulation of joint faulting which is one of the most important parameter to evaluate the performance of PCC pavements.(Darter[1984] and Heinrichs[1989])

The Friberg procedure can be generally divided into two steps to determine the maximum bearing stress. The first step is to predict the maximum

shear force acting on the critical dowel bar. The second step is to calculate the maximum bearing stress of the concrete under the critical bar by using the maximum shear force obtained in the first step.

The first step is based on three assumptions:

- A certain percentage of the total load is transferred by the dowelled joint. The range of percent varies from 0% to about 50%, depending on the quality of the joint, pavement structural parameters and the load type. 50% would be a conservative estimation, Henrichs[1989] suggests using 45%.
- The dowel shear forces are linearly distributed along the joint, see Fig. 7-1.
- An "Effective Load Transfer Length" L_l was assumed as 1.8 l by Friberg[1940] and all dowels located farther than L_l from the load center are assumed to not contribute in transferring load. Where l is radius of relative stiffness of the slab to be determined by the following formula:

$$l = \left(\frac{Eh^3}{12(1-\mu^2)\,k}\right)^{\frac{1}{4}} \qquad (7\text{-}1)$$

Where E is elasticity modulus of concrete

u is poisson ratio of the concrete

h is thickness of the concrete slab

k is modulus of the subgrade

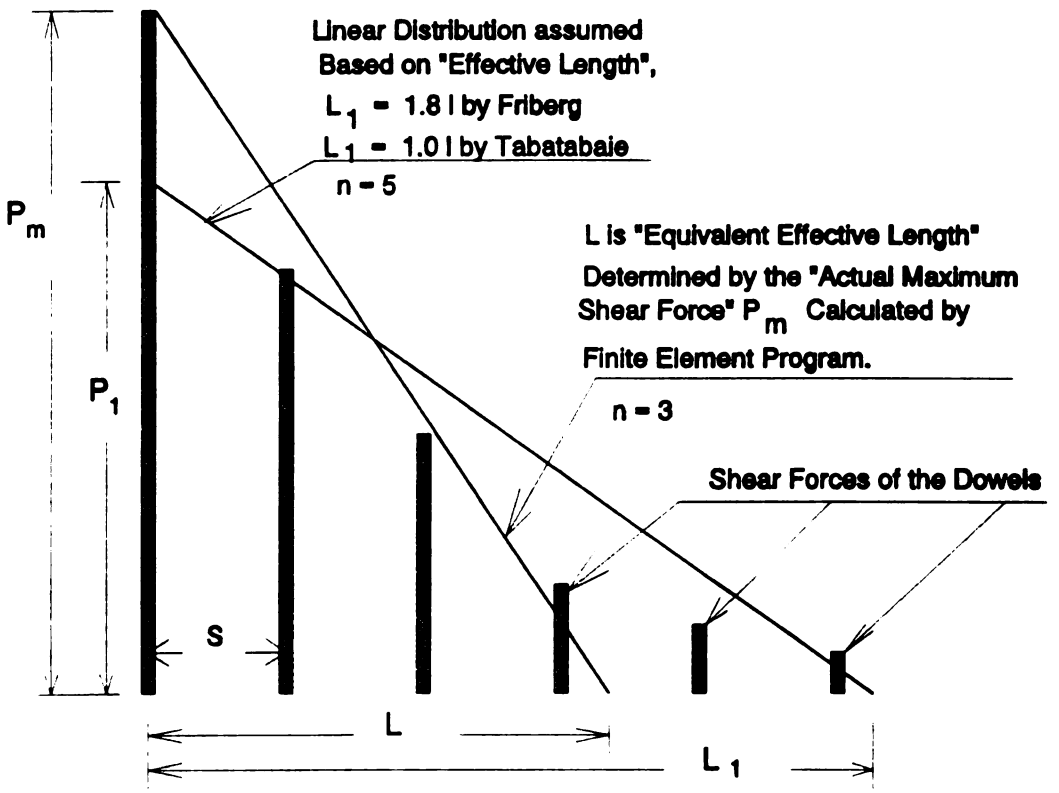

Fig. 7-1 The "Effective Length"(EL) and "Equivalent Effective Length"(EEL)

Using the above assumptions, the maximum shear force acted on the critical dowel bar can be calculated. As mentioned above, $L_1 = 1.8\ l$ was proposed by Friberg based on Westergaard's theory.

In the second step, the shear force of the dowel is assumed known. Timoshenko[1925] model gives a procedure to predict the behavior of a steel bar embedded in "pure elastic" concrete. Based on the Timoshenko theory, Friberg derived the maximum bearing stress formula:

$$\sigma_{max} = \Psi\ \delta_0 \qquad (7\text{-}2)$$

where:

$$\delta_0 = \frac{P_1 (2+\beta\ JO)}{4\beta^3 E_s I} \qquad (7\text{-}3)$$

in which:

P_1	is the maximum shear force acting on the dowel, predicted in the first step
JO	width of the joint opening
E_s	modulus of elasticity of the dowel bar
I	moment of inertia of dowel bar cross-section, $=0.25\ \pi\ (D/2)^4$,
D	Diameter of the dowel bar
β	$(\Psi\ D/4E_sI)^{0.25}$
Ψ(PSI)	Dowel-concrete interaction coefficient

After conducting 3-D finite element analysis for a dowel embedded in elastic concrete space, Tabatabaie[1979] proposed to use the following formula to determine the maximum bearing stress directly:

$$\sigma_{max} = \frac{(800+0.068E)}{D^{\frac{4}{3}}}(1+0.355JO)P_1 \qquad (7\text{-}4)$$

where, P_m is the maximum shear force acting on the critical dowel and was determined by Tabatabaie by using ILLISLAB program as follow:

$$P_1 = \alpha S P_t \qquad (7\text{-}5)$$

in which:

α = 0.0091, for edge load

α = 0.0116, for protected corner load

α = 0.0163, for unprotected corner load

S = dowel spacing

P_t = total load

Based on the results produced by using the finite element program ILLISLAB, Tabatabaie[1979] concluded: "only the dowels within a distance 1.0 l from the center of the load are effective in transferring the major part of the load." It is obvious that the Tabatabaie's assumption is more conservative than the Friberg's. Henrichs[1989] proposed to use the L_l = 1.0 l instead of 1.8 l in the first step to predict the maximum shear force acting on the critical dowel, then to use the Friberg model (Eq. (7-3)) to determine the maximum bearing stress.

2 Some Comments

On the effective length

As summarized above, the determination of the maximum bearing stress can be divided into two steps, the "Effective Length" was introduced to predict the maximum shear force acting on the critical dowel. However, the only purpose of the first step is to determine the maximum shear force on the dowel. If the "Effective Length" assumption is good, the maximum shear force P_l predicted by using the assumed "Effective Length" should be identical or close to the actual maximum shear force P_m. Fig. 7-1 indicates that when the distribution of the dowel shear forces is strongly nonlinear, the mentioned procedure could bring significant error.($P_l < P_m$ in most cases)

Comparison of a few numerical examples

Table 7-1 presents the maximum bearing stresses calculated by using Friberg's model (Eq. 7-2 and Eq. 7-3, with assumption effective length L_l = 1.8 l and L_l = 1.0 l), Tabatabaie's model (Eq. 7-4), and the component dowel bar model developed in Chapter 4.

The parameters are: h = 10 in, Ψ = 1,500,000 pci, E = 4,500,000 psi, J.O. = 0.25 in.

Table 7-1 The Calculated Maximum Bearing Stresses(psi) by Different Models

Friberg's model, L = 1.8 l			
k \ D	0.75 in	1.25 in	1.75 in
50 pci	2387	945	516
200 pci	3208	1270	694
500 pci	3868	1532	837
Friberg's model, L = 1.0 l			
k \ D	0.75 in	1.25 in	1.75 in
50 pci	3907	1547	845
200 pci	5143	2037	1113
500 pci	5962	2361	1290
Component dowel bar model			
k \ D	0.75 in	1.25 in	1.75 in
50 pci	5158	2815	1964
200 pci	4459	2478	1692
500 pci	3846	2229	1524
Tabatabai's model			
D	0.75 in	1.25 in	1.75 in
k=50,200,500pci	3111	1574	1005

Table 7-1 demonstrates that the results received by using different models are very different.

On the effects of the subgrade modulus

Fig. 7-2 was copied from Fig. 44, Henrichs[1989]. It can be seen that the maximum bearing stress increases when the subgrade modulus k increases. the same conclusion can also be obtained by using Eq. (7-2) and (7-3) (see Table 7-1). However, the conclusion is difficult to understand. It seems not logical that the stronger the subgrade support is and the stronger

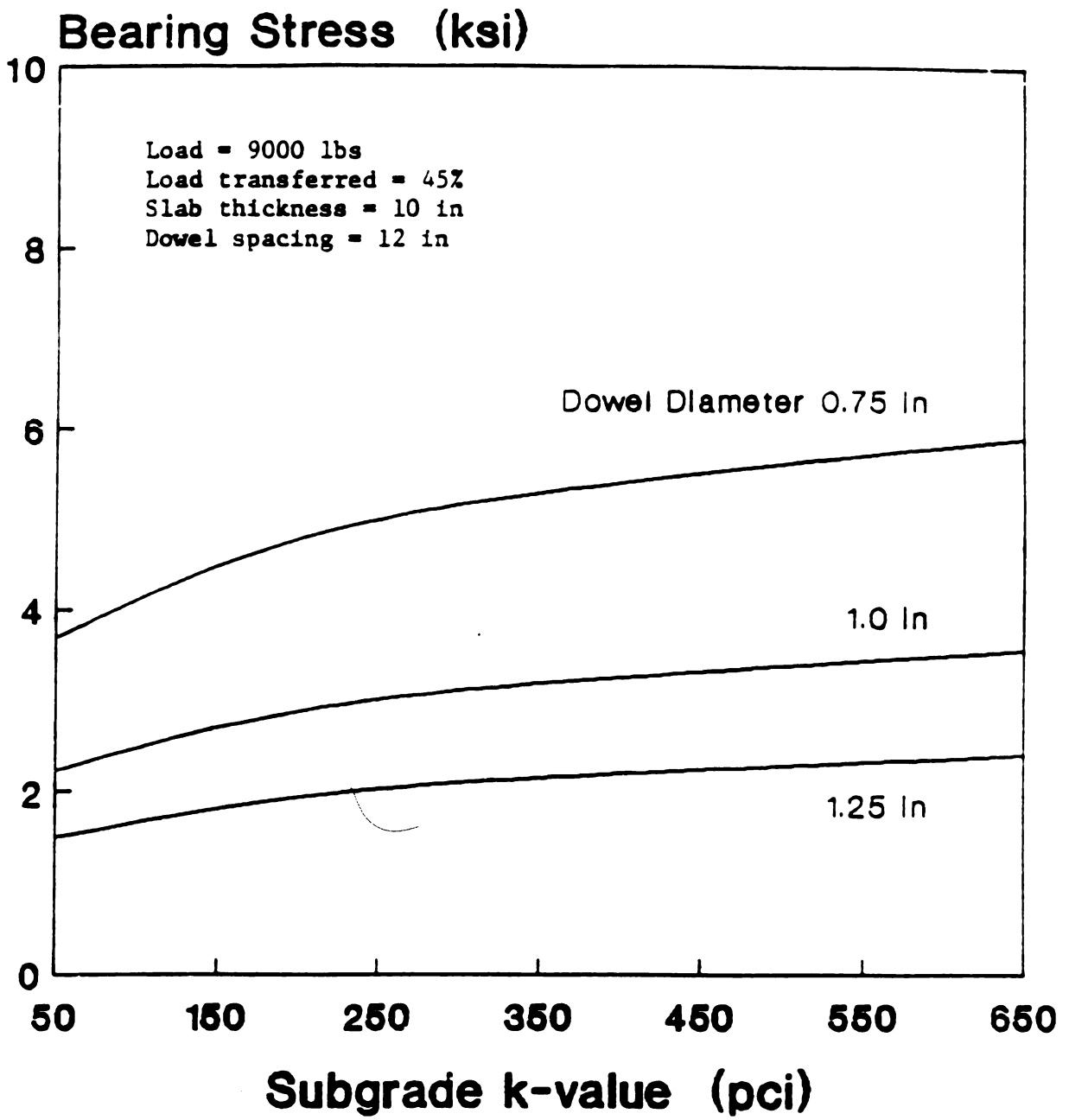

Fig. 7-2 Effects of Subgrade Modulus on the Maximum Bearing Stress (from Henrichs[1989])

capability of withstanding load the loaded side slab has, the greater maximum shear force needs to be transferred across the critical dowel near the load.

On the effects of concrete modulus E

Eq. 7-4 indicates that the maximum bearing stress increases as the concrete modulus increases when the other parameters remains the same. This conclusion does not agree with the results from Friberg's model. As discussed above, the higher concrete modulus means the loaded side has a stronger load resistance capability, so that the total load and the maximum load transferred by the critical dowel should be reduced, but not increased as suggested by Eq. 7-4.

Since developed in 1940's, the "Effective Length" concept has been widely used in PCC pavement design for a half century. It is worth to re-investigate the concept again and improve the design procedure.

3 The Equivalent Effective Length(EEL)

Based on the "Effective Length"(EL) assumption, if the total load is known and the percent of the total load transferred is assumed, the maximum shear force can be calculated by the following formulas:

When the load is located at the edge of the joint:

$$P = \frac{P_t\, C}{2n+1-\frac{Sn(n+1)}{L}} \qquad (7\text{-}6)$$

when the load is located at the unprotected corner of the joint:

$$P = \frac{P_t\, C}{n+1-\frac{n(n+1)S}{2L}} \qquad (7\text{-}7)$$

where, P represents the maximum shear force,

n the number of the effective dowels on one side of the bar under the load,

S the dowel spacing.

C percent of the total load transferred across the joint

l radius of the relative stiffness of the slab

P_t Total load

Some of the above parameters are shown in Fig. 7-1.

Since the most important parameter in the first step of the current design procedure is the Maximum Shear Force, the EEL may be defined as a length L which can be determined by Eq. (7-6) or Eq. (7-7) depending upon the edge or corner loading case. The maximum shear force and the percent of the total load transferred can be calculated by an appropriate finite element program as discussed in Chapter 4. Under the above definition, n is not the total number of the effective dowels on one side of the bar under the load, it is only the number of the dowels which can significantly transfer load. As shown in Fig. 7-1, n is five under the EL definition, but is only 3 under the EEL definition.

The EEL formulas can be obtained by solving L in Eq. (7-6) and Eq. (7-7) as follow:

when the load is located at the edge of the joint:

$$\frac{L}{l} = \frac{P_m\, n\, (n+1)\, S}{l\, [(2n+1)\, P_m - P_t C]} \qquad \textbf{(7-8)}$$

when the load is located at the unprotected corner of the joint:

$$\frac{L}{l} = \frac{P_m\, n\, (n+1)\, S}{2\, l\, [(n+1)\, P_m - P_t C]} \qquad \textbf{(7-9)}$$

In any case the following formula must be satisfied:

$$n \leq \frac{L}{S} \leq (n+1) \qquad \textbf{(7-10)}$$

There exists significant difference between the concept of the EL and of the EEL. The EL is an assumed one to predict the maximum shear force which must different from the actual one more or less, whereas the EEL is the one calculated by using the "actual maximum shear force" predicted by the finite element method so that when it is substituted back to Eq. (7-6) or (7-7), the "predicted" maximum shear force must be equal to the "actual force" calculated by the finite element program.

Friberg proposed $L_1/l = 1.8$ and Tabatabaie suggested $L_1/l = 1.0$, both assumed L/l constant. However, Eq. (7-8) and Eq. (7-9) indicate that L/l, where L is corresponding to the "actual" maximum shear force of the dowels, is a function of n, S, P_m, P_t, C as well as the radius of relative stiffness l.

Some characteristics of the EEL

JSLAB-92 was employed to calculate the maximum shear force of the dowel bar. The finite element mesh is given in Fig. 7-3. The numerical analyses were conducted for two loading cases. The first is a 9000 lb load with tire pressure 50 psi acting at the node I in Fig. 7-3. The loading area is 12 x 15 in^2, and the case is defined as edge loading. The second is the same type of load acting at the node J in Fig. 7-3 and the case is defined as corner loading. Using the calculated maximum shear forces and the percentage of total load transferred across the joint, L/l may be calculated by using Eq.(7-8) to Eq.(7-10).

By using the EL assumption, the higher subgrade modulus always reduces l value (Eq. 7-1), and then reduces L_l (L_l = 1.8 l or L_l = 1.0 l) and the number of effective dowels n (Eq. (7-10). Since the percent of total load transferred is assumed constant, the maximum shear force and bearing stress will be always increased as shown in Table 7-1. However, Fig. 7-4 indicates that L/l increases when the k value increases. Fig. 7-5 shows that the total load transferred decreases as the k value increases. The two figures explain that the increase of subgrade modulus does not have to increase the maximum bearing stress.

Relation between EEL and l

Fig. 7-6 plots the twelve examples with the same dowel-concrete interaction coefficient(1.5 x 10^6 pci), dowel diameter(1.25 in) and joint opening(0.25 in), but with different slab thickness and subgrade modulus

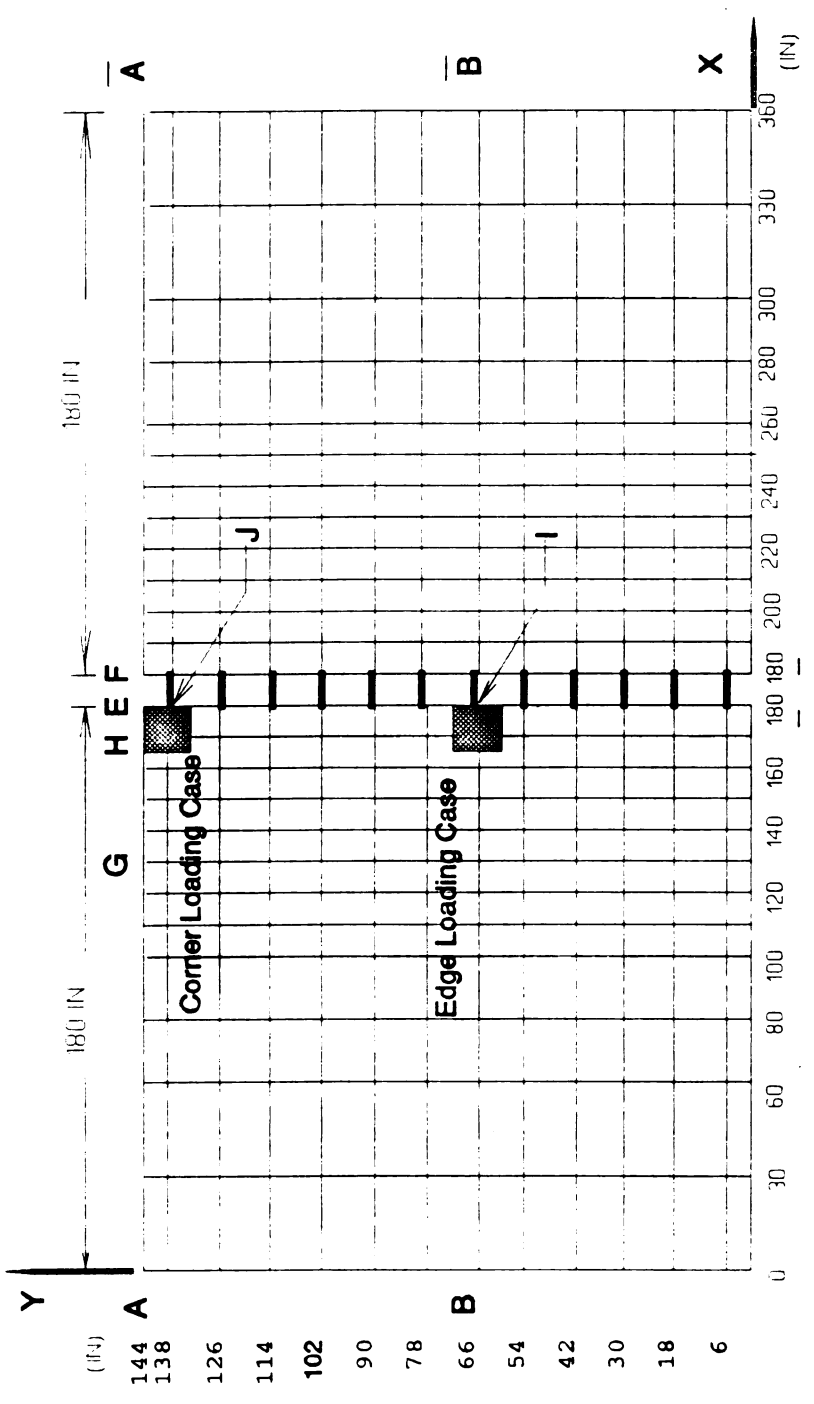

Fig. 7-3 The Finite Element Mesh and Two Load Cases

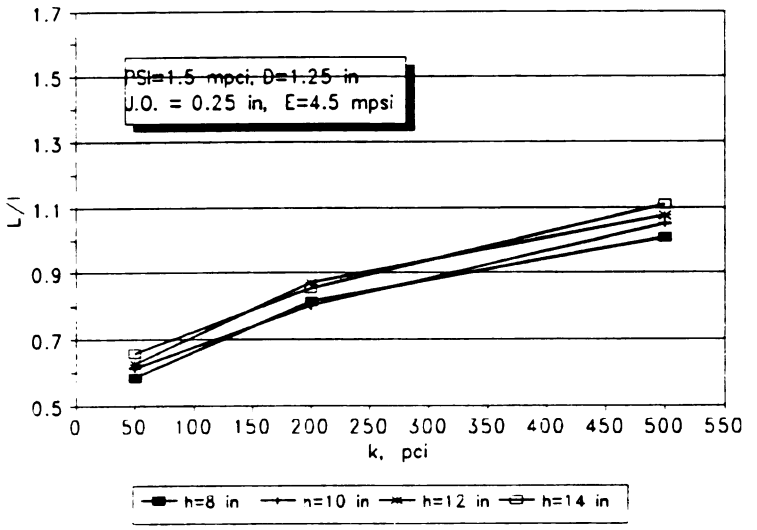

(1) Load at the Corner

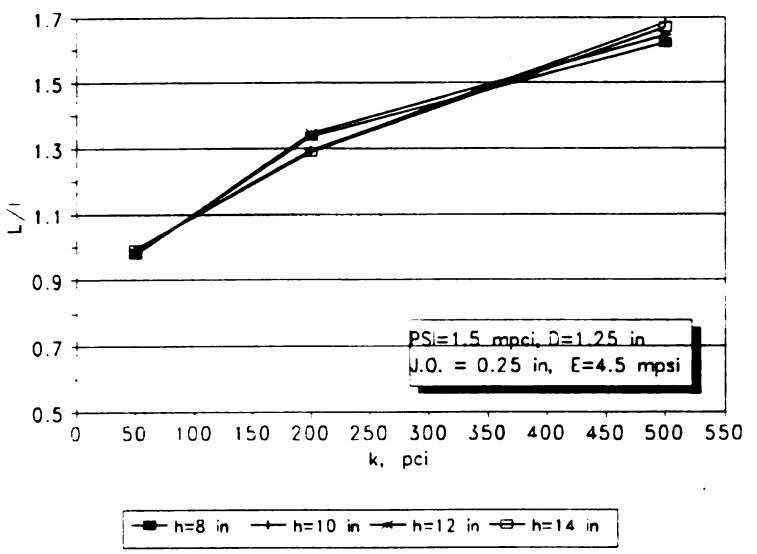

(2) Load at the Edge

Fig. 7-4 Effects of Subgrade Modulus on the EEL

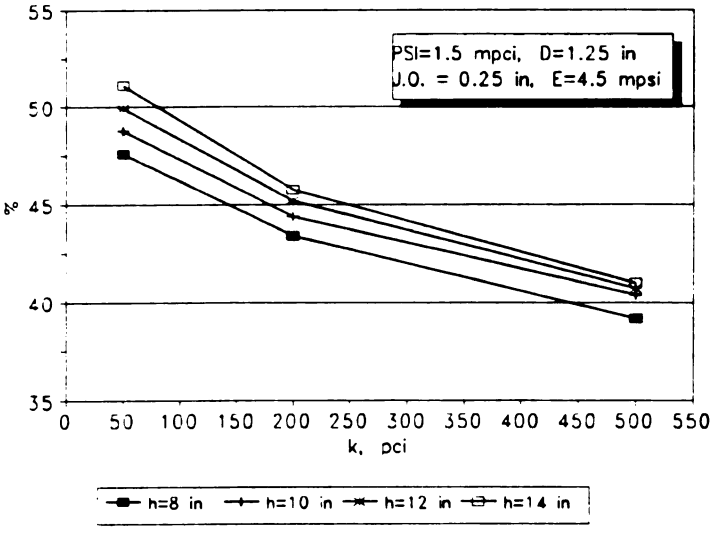

(1) Load at the Corner

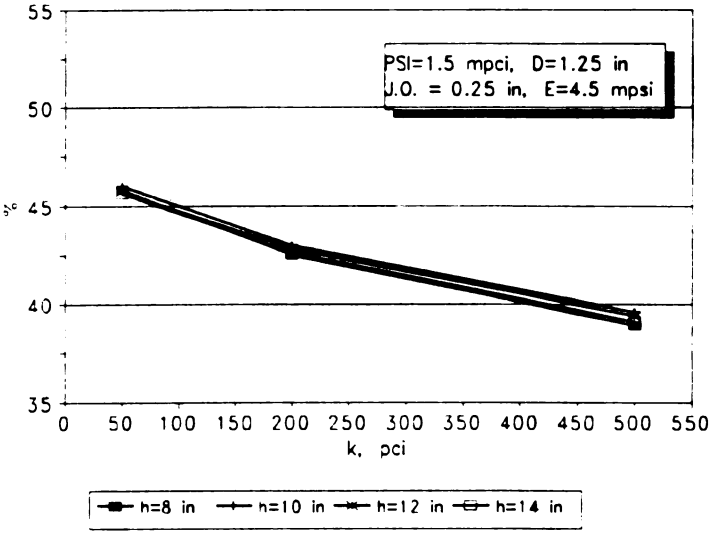

(2) Load at the Edge

Fig. 7-5 Effects of Subgrade Modulus on the Load Transfer Efficiency

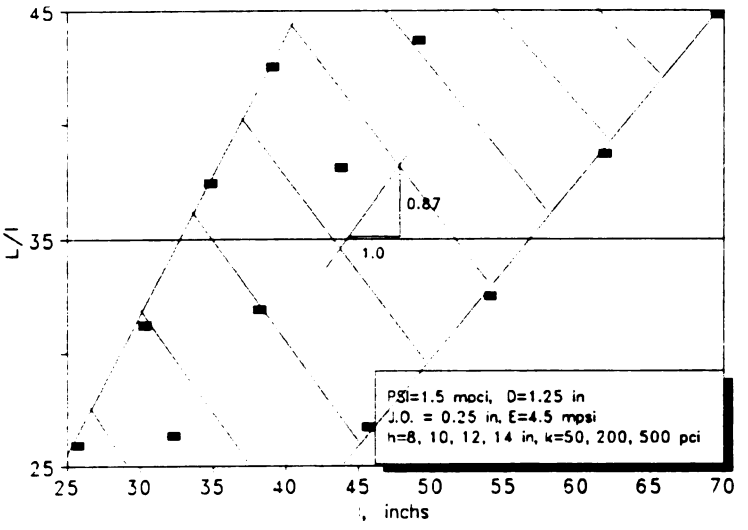

(1) Load at the Corner

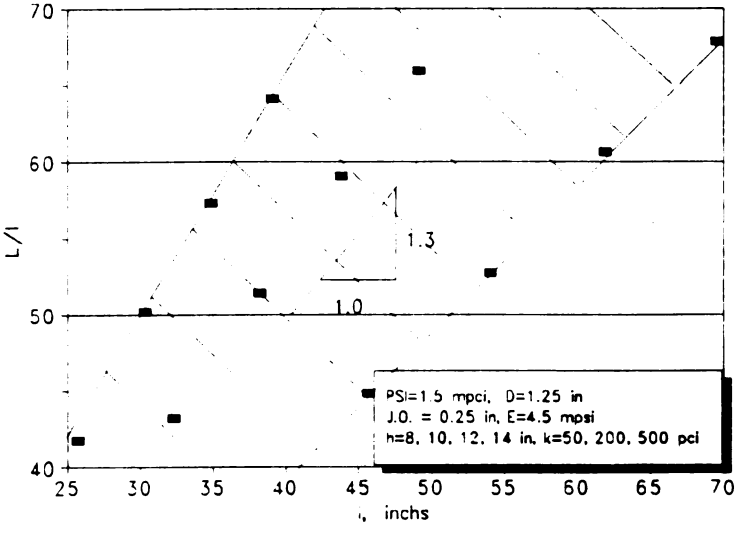

(2) Load at the Edge

Fig. 7-6 Relationship between the EEL and l (the Radius of Relative Stiffness)

for both edge and corner loading cases. For the same radius of the relative stiffness value l, the L values could be very different. The central line of the shaded area indicates that $L/l \approx 1.3$ for the edge loading and $L/l \approx 0.87$ for the corner loading case. Therefore, the rather wide bandwidth suggests that the assumptions of $L/l = 1.8$ or 1.0 might not be an appropriate assumption to accurately predict the maximum shear forces on the critical dowel and the maximum bearing stress of the concrete.

4 Effects on the Maximum Bearing Stress

When Friberg developed the dowel bar analytical model in 1940's, it was impossible to analytically predict the maximum shear force acting on the critical dowel precisely, hence, he proposed the approximate but simple procedure for the dowel bar design. Since the finite element method was developed and the application of high speed computers has been very popular, more options become available in the analysis of load transfer mechanism. For example, it is not necessary to divide the entire analysis procedure into two steps as summarized in section one this chapter. As discussed in Chapter 4, the component model of dowel bar can be installed into a finite element program to calculate the responses of each dowel, including the distribution of bending moments, shear forces, the relative displacements of the beam and the bearing stresses of the concrete. The results are calculated with comprehensive consideration of all inputs simultaneously and without more assumptions such as effective length and percent of total load transferred. In this section, more numerical

examples will be given to analyze the effects of different parameters on the maximum bearing stress of the critical dowel.

Effects of slab thickness and subgrade modulus

Fig. 7-7 shows that the bearing stress decreases when the slab thickness increases. Four curves of the maximum stress v.s. subgrade modulus are presented in Fig. 7-8 which indicates that the maximum stress decreases when the subgrade modulus (k value) increases. This conclusion is different from the results presented by Tabatabaie[1979] and Henrichs[1989], (also see Fig. 7-2 and Table 7-1 in this chapter). It is believed that the discrepancy was caused by using the "Effective Length" assumption which sometime can not accurately describe the maximum bearing stress characteristics.

Effects of dowel diameter and width of the joint opening

Fig. 7-9 indicates that the maximum bearing stress of the concrete is very sensitive to the dowel's diameter D which might be the most sensitive parameter among the all. Smaller diameter can cause dramatic increase of the maximum stress. This finding qualitatively has good agreement with Friberg and Tabatabaie's Formulas. (Eq. (7-2),(7-3) and (7-4)). Both Fig. 7-9 and Fig. 7-10 indicate the insensitivity of the maximum bearing stress due to the variation of width of the joint opening. Using Eq. (7-4) to predict the maximum bearing stress, the increase of joint opening from 0.25 inch to 0.75 inch provides about 16% increase of the maximum bearing

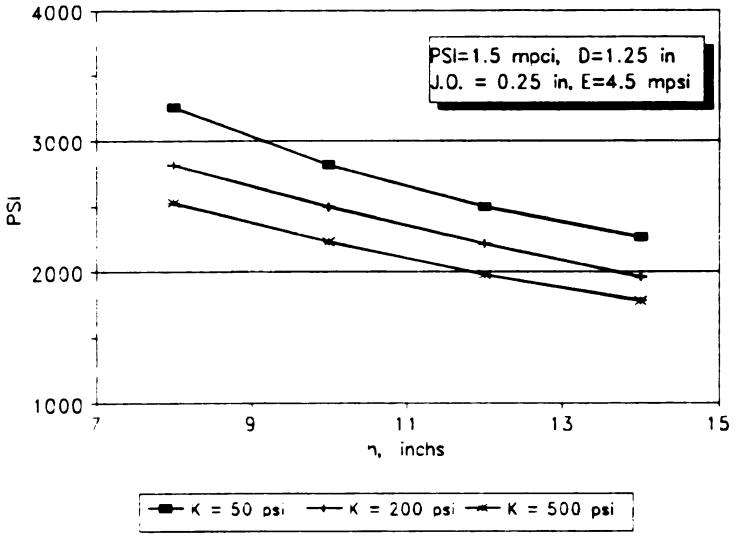

Fig. 7-7 Effects of Slab Thickness on the Maximum Bearing Stress

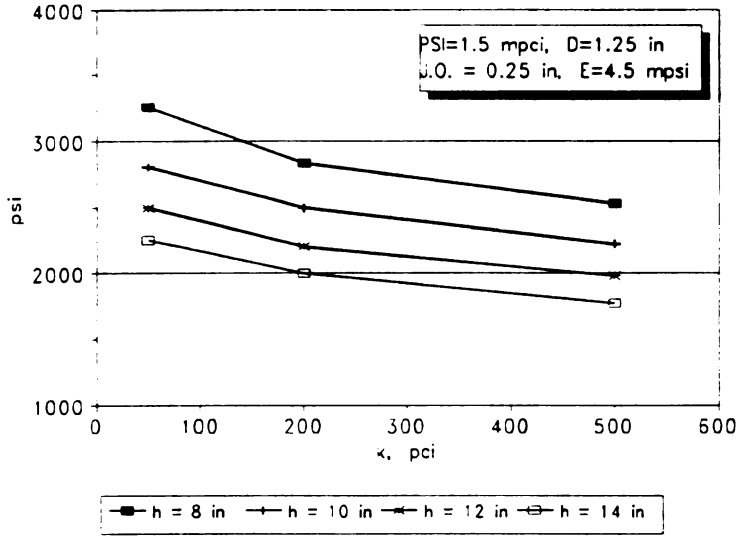

Fig. 7-8 Effects of Subgrade Modulus on the Maximum Bearing Stress

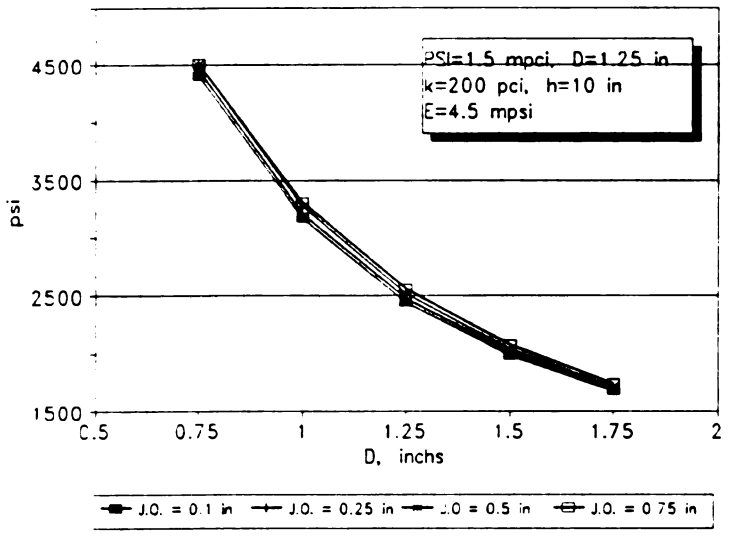

Fig. 7-9 Effects of Dowel Diameter on the Maximum Bearing Stress

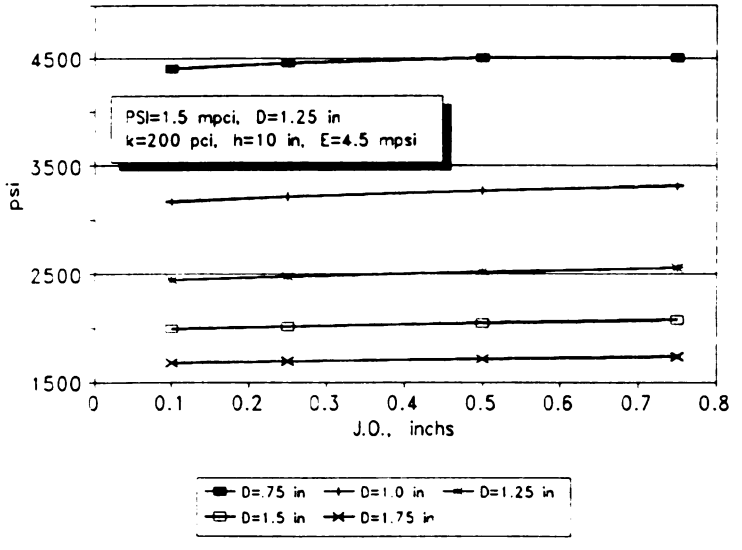

Fig. 7-10 Effects of Width of Joint Opening on the Maximum Bearing Stress

stress (0.355 x (.75-.25)/(1+.355 x .25)) x 100 = 16.3). However, by using the dowel bar component model in JSLAB-92, the increase is only 1.2% for the D = 0.75 inch dowel, 3.3% for the D = 1.25 inch dowel and 2.7% for the D = 1.75 inch dowel.

Effects of concrete elasticity and the dowel-concrete interaction coefficient

Fig. 7-11 presents the maximum stress curves v.s. dowel-concrete interaction coefficient γ. As summarized by Finney[1956], the values of γ measured by different investigators varied from 0.3×10^6 to 8.6×10^6 pci. In practice, 1.5×10^6 pci is often used. However, γ significantly depends on the concrete properties, dowel bar diameter, slab thickness, dowel length, dowel looseness and etc. Fig. 7-11 indicates the sensitivity of γ. The higher γ is corresponding to the higher maximum bearing stress. That means, the dowel in deteriorated joint or with significant looseness would have smaller maximum bearing stress.

Fig. 7-12 shows that the maximum bearing stress decreases when the concrete elasticity modulus increases. As discussed above this is understandable because the higher E value indicates that the stronger loaded slab can withstand heavier load and leave less load transferred across the dowels to the unloaded slab. The role of higher E value is similar to the higher k value of the subgrade, both should reduce the quantity of load transferred across the joint. However, Eq. (7-4) indicates that the higher E value would cause higher maximum bearing

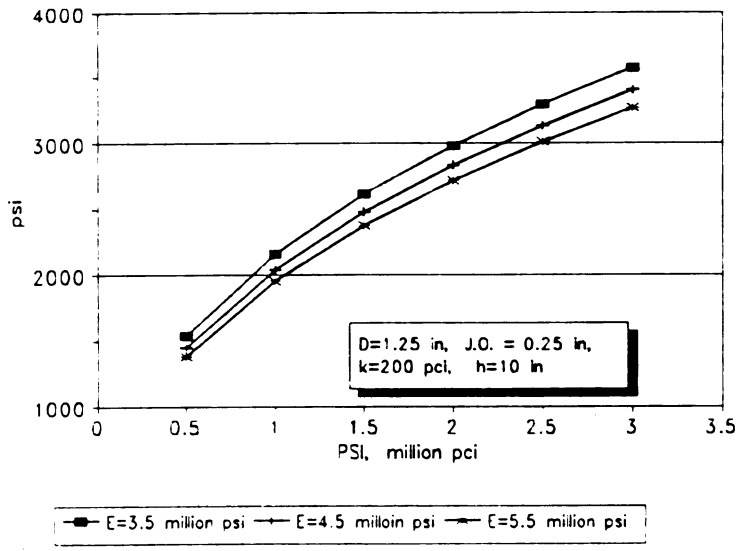

Fig. 7-11 Effects of Dowel-concrete Interaction Coefficient on the Maximum Bearing Stress

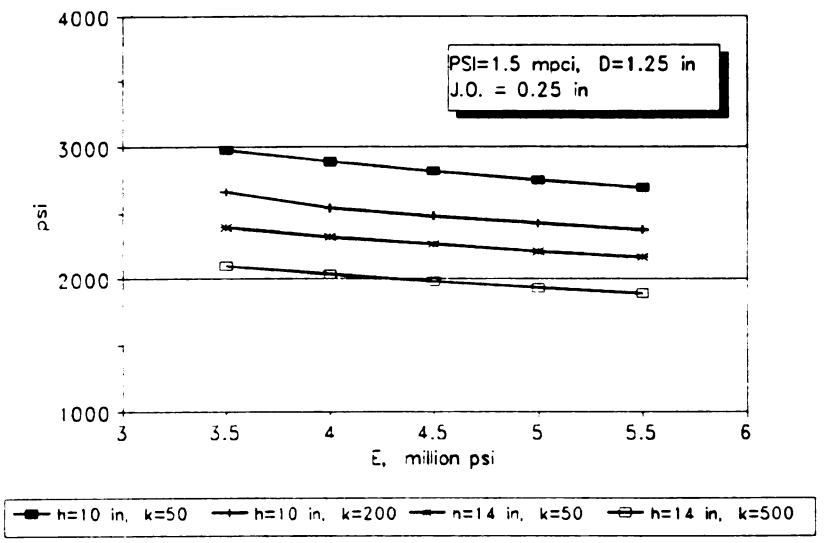

Fig. 7-12 Effects of Concrete Elasticity Modulus on the Maximum Bearing Stress

stress. The discrepancy might be partially caused by the application of Eq. (4-7) in ILLISLAB and Eq. (4-12) in this study. The former one produces nonequilibrium element and might lead to unreasonable results sometime.

For convenience to review, the maximum bearing stress of dowel, for h = 8, 10, 12, 14 inch, k=50, 200, 500 pci, D = 0.75, 1.25 and 1.75 inch, J.O. = 0.25, 0.5, 0.75 inch, E = $3.5x10^6$, $4.5x10^6$, $5.5x^6$ psi are given in Table 7-2, 7-3, and 7-4.

5 Summary

General principle has been found by analyzing the results of hundreds of numerical examples: the higher values of dowel diameter, slab thickness, concrete modulus, and subgrade modulus can reduce the maximum bearing stress of the concrete under the critical dowel. The maximum bearing stress is not sensitive to the width of joint opening but is very sensitive to the dowel-concrete interaction behavior, though which is difficult to control. Three tables are presented for obtaining the maximum bearing stresses of concrete under the critical dowel bar.

The discovery of error in the stiffness matrix of dowel bar used in some finite element programs, and of the inappropriate utilization of the joint effective length made it necessary to re-evaluate some design procedures for the dowel system. The major findings in this chapter are:

- Equation (7-4) could provide some questionable results. The maximum bearing stress does not proportionally increases as the concrete elasticity E increases and it is also not so sensitive to the width of joint opening, as indicated in the equation

- The maximum bearing stress on the critical dowel increases as the subgrade modulus decreases which is different from the conclusion presented in some literatures. This finding indicates that the most critical season in a year for the maximum bearing stress is spring for the thawing reduces the subgrade modulus, rather than winter in the wet-frozen region. And the thawing effect could cause 10 to 20% difference in the maximum bearing stress.

- The utilization of "Effective Length" (EL) assumed in 1940's and modified at end of 1980's underestimates the maximum bearing stress in some cases. The "Equivalent Effective Length" (EEL) concept has been developed to prove that the EL assumption needs more studies.

- The most critical dowel is the one under a tire load nearest to the unprotected corner. The maximum bearing stress could be two times even higher than that of the critical dowel under the tire load at the edge of the joint.

- Due to the significant difference between the existing and the developed models in predicting the maximum bearing stress, it is suggested that all empirical models which use Eq (7-4) to calculate the maximum bearing stress and then to predict the joint faulting should be checked before being employed in engineering projects.

Table 7-2 The Maximum Bearing Stresses (k = 50 pci)

E (10^6psi)	J.O. (in)	D (in)	h (in)			
			8	10	12	14
3.5	0.25	0.75	6271	5446	4833	4390
		0.25	3439	2973	2635	2391
		0.75	2439	2084	1813	1656
	0.5	0.75	6463	5596	4957	4510
		1.25	3507	3134	2687	2438
		1.75	2464	2108	1854	1673
	0.75	0.75	6612	5708	5049	4603
		1.25	3572	3090	2737	2482
		1.75	2488	2131	1876	1693
4.5	0.25	0.75	5948	5158	4584	4176
		1.25	3256	2815	2498	2265
		1.75	2298	1964	1733	1567
	0.5	0.75	6127	5299	4703	4293
		1.25	3323	2872	2548	2311
		1.75	2323	1989	1754	1583
	0.75	0.75	6259	5398	4795	4386
		1.25	3384	2924	2594	2347
		1.75	2347	2012	1775	1601
5.5	0.25	0.75	5707	4937	4395	4018
		1.25	3118	2693	2394	2169
		1.75	2193	1874	1656	1500
	0.5	0.75	5867	5064	4510	4137
		1.25	3181	2748	2440	2217
		1.75	2218	1897	1678	1515
	0.75	0.75	5989	5160	4602	4237
		1.25	3239	2765	2482	2259
		1.75	2242	1918	1695	1534

Table 7-3 The Maximum Bearing Stresses (k = 200 pci)

E (10^6psi)	J.O. (in)	D (in)	h (in)			
			8	10	12	14
3.5	0.25	0.75	5434	4721	4157	3717
		1.25	2973	2611	2324	2097
		1.75	2041	1785	1586	1429
	0.5	0.75	5536	4783	4191	3737
		1.25	3034	2661	2365	2130
		1.75	2069	1810	1608	1450
	0.75	0.75	5587	4799	4187	3722
		1.25	3087	2703	2398	2157
		1.75	2096	1833	1629	1467
4.5	0.25	0.75	5165	4459	3917	3497
		1.25	2836	2478	2201	1980
		1.75	1944	1692	1501	1350
	0.5	0.75	5251	4507	3944	3510
		1.25	2893	2524	2238	2011
		1.75	1971	1716	1522	1369
	0.75	0.75	5289	4513	3932	3492
		1.25	2942	2561	2266	2034
		1.75	1996	1738	1541	1385
5.5	0.25	0.75	4951	4254	3728	3334
		1.25	2728	2374	2102	1893
		1.75	1867	1620	1433	1290
	0.5	0.75	5025	4292	3747	3347
		1.25	2781	2417	2136	1920
		1.75	1893	1643	1453	1308
	0.75	0.75	5052	4291	3732	3325
		1.25	2827	2451	2162	1941
		1.75	1918	1664	1471	1323

Table 7-4 The Maximum Bearing Stresses (k = 500 pci)

E (10^6psi)	J.O. (in)	D (in)	h (in)			
			8	10	12	14
3.5	0.25	0.75	4688	4076	3579	3178
		1.25	2638	2342	2096	1892
		1.75	1796	1599	1436	1302
	0.5	0.75	4705	4061	3544	3132
		1.25	2683	2375	2120	1909
		1.75	1822	1621	1455	1318
	0.75	0.75	4673	4004	3474	3055
		1.25	2717	2399	2135	1918
		1.75	1844	1640	1470	1330
4.5	0.25	0.75	4460	3846	3357	2970
		1.25	2528	2229	1984	1783
		1.75	1723	1524	1362	1231
	0.5	0.75	4464	3821	3316	2920
		1.25	2569	2258	2004	1798
		1.75	1747	1544	1379	1245
	0.75	0.75	4421	3757	3241	2840
		1.25	2599	2277	2016	1803
		1.75	1768	1561	1393	1256
5.5	0.25	0.75	4276	3664	3186	2813
		1.25	2440	2138	1896	1700
		1.75	1664	1464	1305	1176
	0.5	0.75	4271	3633	3140	2760
		1.25	2477	2164	1913	1712
		1.75	1687	1483	1320	1189
	0.75	0.75	4221	3563	3063	2680
		1.25	2504	2181	1922	1716
		1.75	1707	1499	1333	1199

CHAPTER EIGHT
LOOSENESS EFFECTS ON THE PAVEMENT RESPONSES

1 Introduction

A nonlinear elastic model was recently developed to simulate the dowel bar looseness mechanism. For any given dowel bar looseness, this model can predict the pavement responses, including the stress and displacement distributions and load transfer capability. A previous experimental study[Teller, 1958] found that the measured initial looseness was typically about 0.003 inch, and that the looseness was approximately doubled after 2 million load cycles. The numerical results presented in Chapter 5 are limited to the responses of a two-slab system (Fig. 1-1) acted upon by two load cases: a concentrated 9000-lb load acting at the center of the joint and an 18000-lb single axle load with four tires acting at the joint (Fig. 4-3).

Additional numerical results are presented in this chapter to investigate the interactive effects between dowel looseness and several design parameters, such as the subgrade modulus, k, the dowel diameter, D, and the slab thickness, h. The effects of dowel looseness on critical dowel shear forces, maximum principal stress, maximum slab displacements and load transfer efficiency are shown for various looseness levels. Responses of a four-slab system with transverse and longitudinal joints under edge and corner loading cases are also presented in this chapter to further illustrate the effects of dowel bar and tie bar looseness.

2 Major Findings of the Responses of a Two Slab System

A finite element mesh for two-slab system is given in Fig. 1-1. The major example input data are listed as follow:

Elastic Modulus of the Concrete, E_c	4,500,000 psi
Poisson's Ratio of the concrete, u_c	0.15
Elastic Modulus of Dowel Bar, E_s	29,000,000 psi
Width of Joint, JO	0.25 in
Poisson's Ratio of Steel, u_s	0.3
Dowel-concrete Interaction Coefficient,PSI	1,500,000 psi/in
Subgrade Modulus, k	200 psi/in
Slab thickness, h	10 inch
Dowel diameter, D	1.25 inch

The variation of values of k, h, D and looseness are indicated in each figure.

Figures. 8-1 through 8-3 illustrate some responses (the maximum shear force of the top dowel in Fig. 1-1, and the maximum displacement and maximum principal stress of the loaded slab) and the percent of load transferred across the joint versus k, D and h for different dowel bar looseness. The main findings can be summarized as below:

- Increased dowel looseness increases the maximum principal stress of the loaded slab. For k = 50 pci, 0.003 in of looseness can produce a 3.2% stress increase, and 0.006 of looseness can produce a 5.5% increase in the maximum principal stress. For k=500 psi/in,

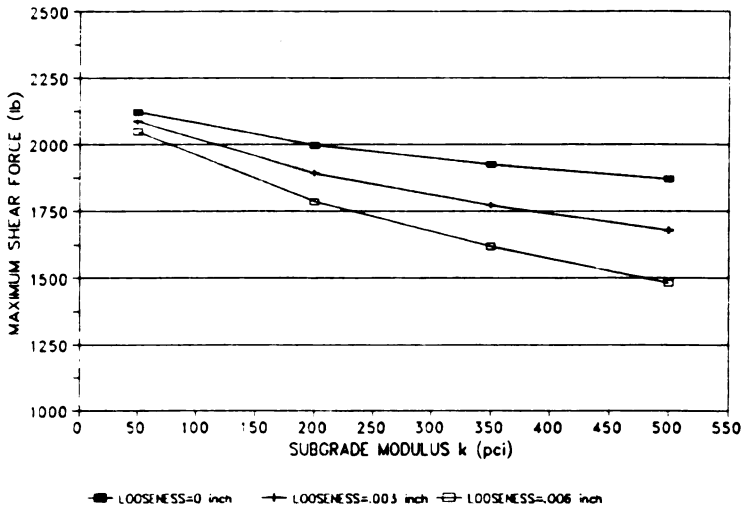

(a) Maximum Shear Forces of the Critical Dowel vs. Subgrade Modulus

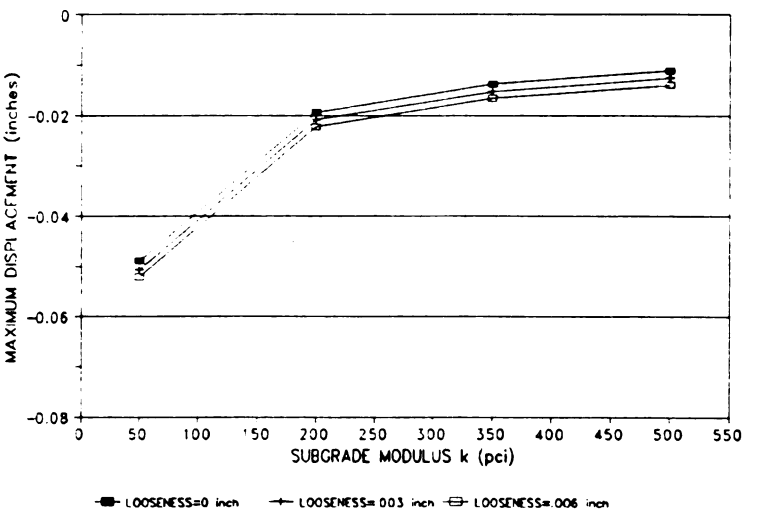

(b) Maximum Displacement vs. Subgrade Modulus

Fig. 8-1 The Effects of k for Varying Dowel Looseness

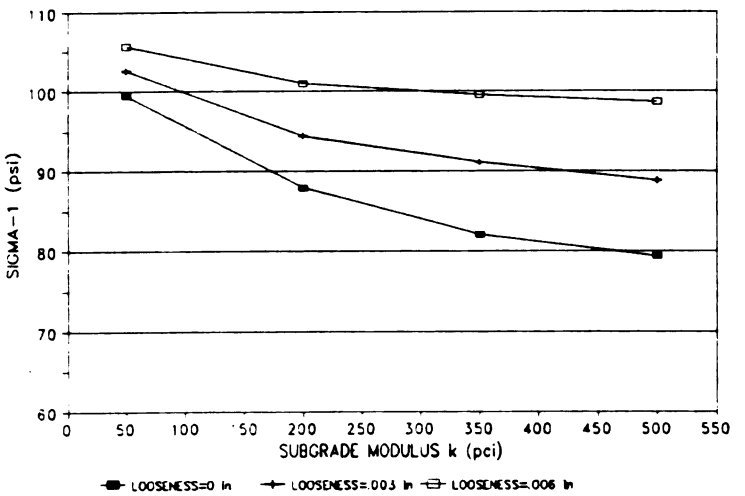

(c) Maximum Principal Stress vs. Subgrade Modulus

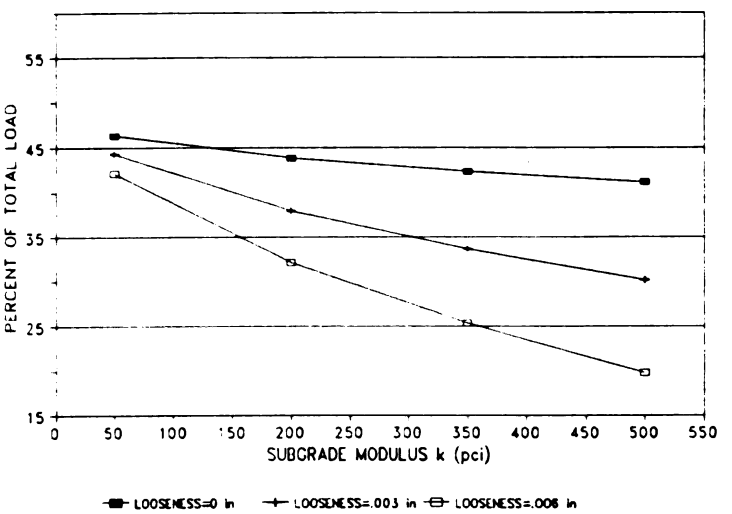

(d) Percent of Total Load Transferred vs. Subgrade Modulus

Fig. 8-1 The Effects of k for Varying Dowel Looseness (continued)

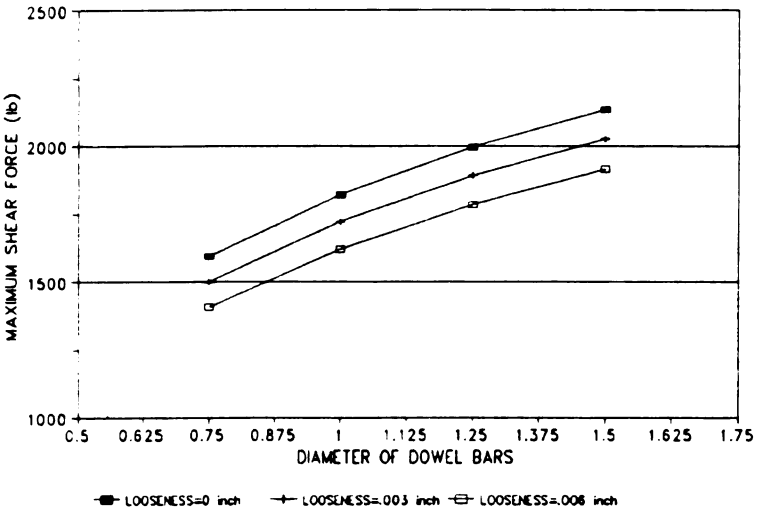

(a) Maximum Shear Forces of the Critical Dowel vs. Dowel Diameter

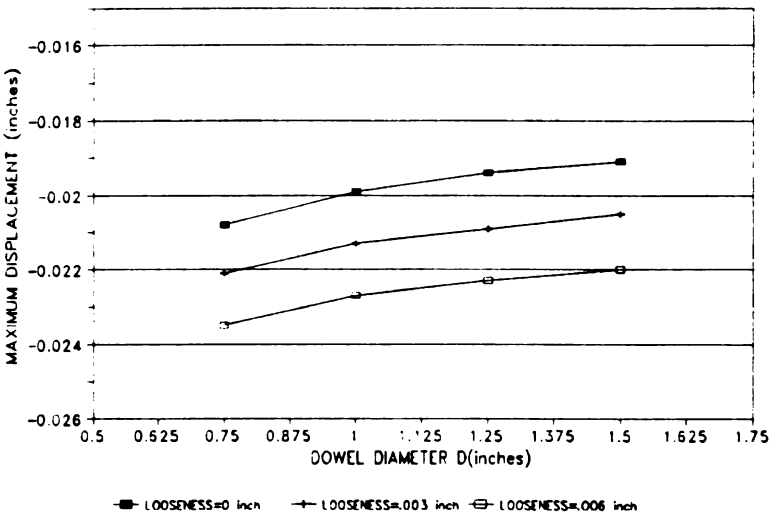

(b) Maximum Displacement vs. Dowel Diameter

Fig. 8-2 The Effects of D for Varying Dowel Looseness

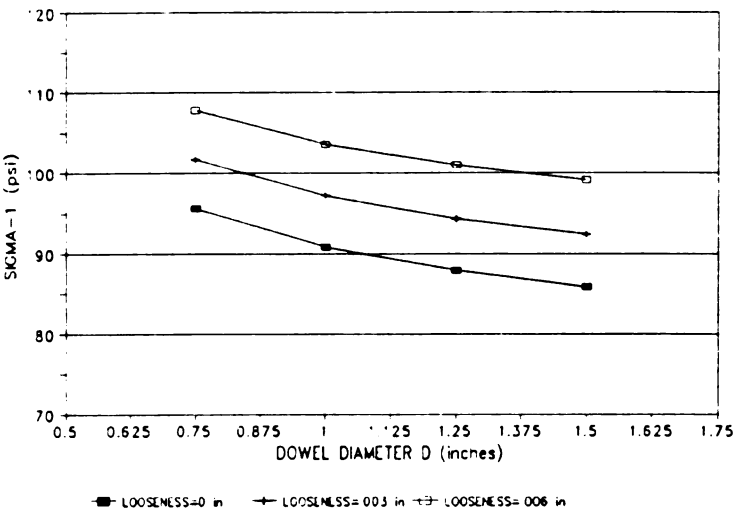

(c) Maximum Principal Stress vs. Dowel Diameter

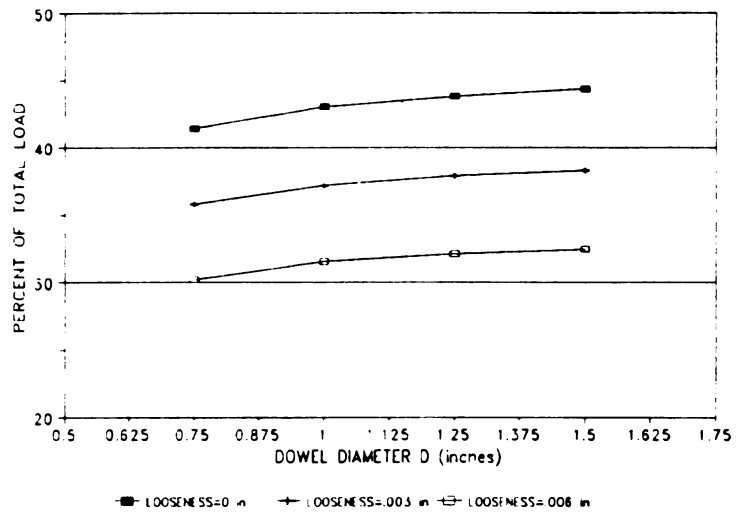

(d) Percent of Total Load Transferred vs. Dowel Diameter

Fig. 8-2 The Effects of D Under for Varying Dowel Looseness(continued)

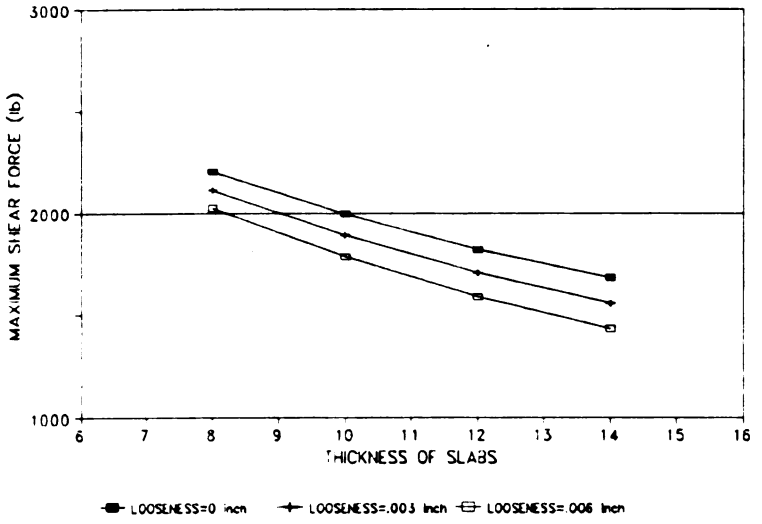

(a) Maximum Shear Forces of the Critical Dowel vs. Slab Thickness

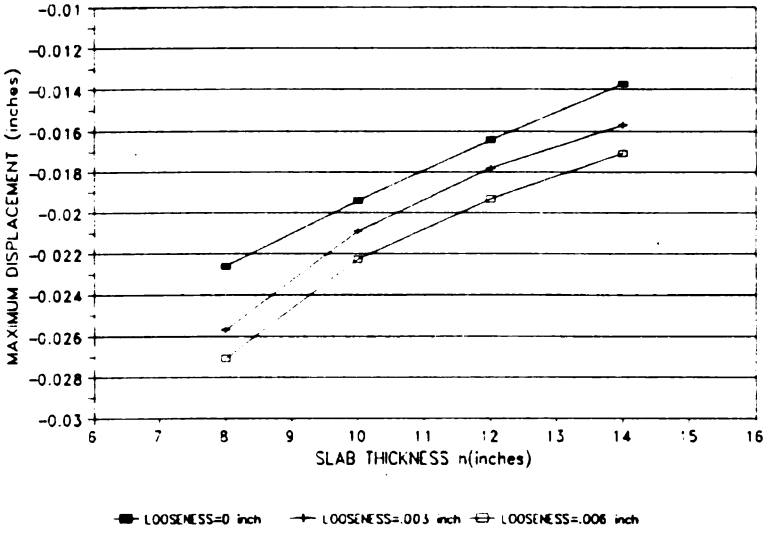

(b) Maximum Displacement vs. Slab Thickness

Fig. 8-3 The Effects of Slab Thickness for Varying Dowel Looseness

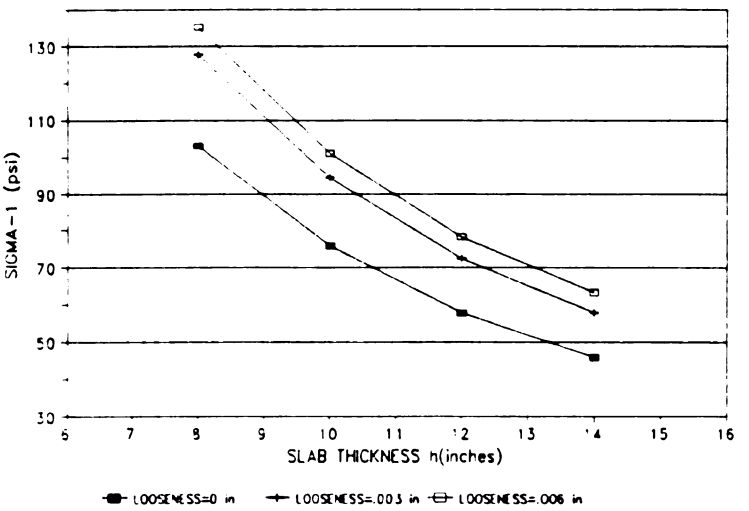

(c) Maximum Principal Stress vs. Slab Thickness

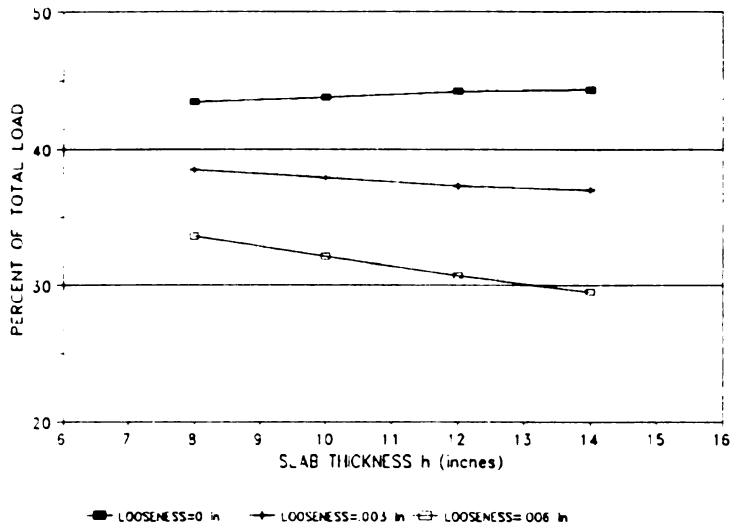

(d) Percent of Total Load Transferred vs. Slab Thickness

Fig. 8-3 The Effects of h for Varying Dowel Looseness(continued)

the corresponding increases are 11.8% and 24.3% respectively. However, the maximum principal stress of the loaded slab resting on a stronger subgrade is always lower than that of the slab resting on a weaker subgrade if all other factors are held constant.

- Increased dowel looseness increases the displacement magnitude of the loaded slab and decreases the displacement magnitude of the unloaded slab. The increases due to 0.006 in looseness for the loaded slab ranged from 6.1% to 25% for k = 50 psi/in to 500 psi/in, from 13% to 15% for D = 0.75 to 1.5 inch, and from 12.0% to 19.6% for h = 8 to 14 inches.

- Increased dowel looseness decreases the amount of load that an be transferred across the joint. Numerical results indicate that the number of dowels which are active in transferring load across the joint decreases when the looseness uniformly increases.

- Increased dowel looseness decreases the maximum shear force on the critical dowel (the top bar in Fig. 1-1). This shear force decrease is caused by the decrease of load transfer efficiency. As discussed in Chapter 7, the maximum bearing stress of concrete is proportional to the shear force. Therefore, dowel looseness does not cause an increase of the maximum bearing stress of concrete.

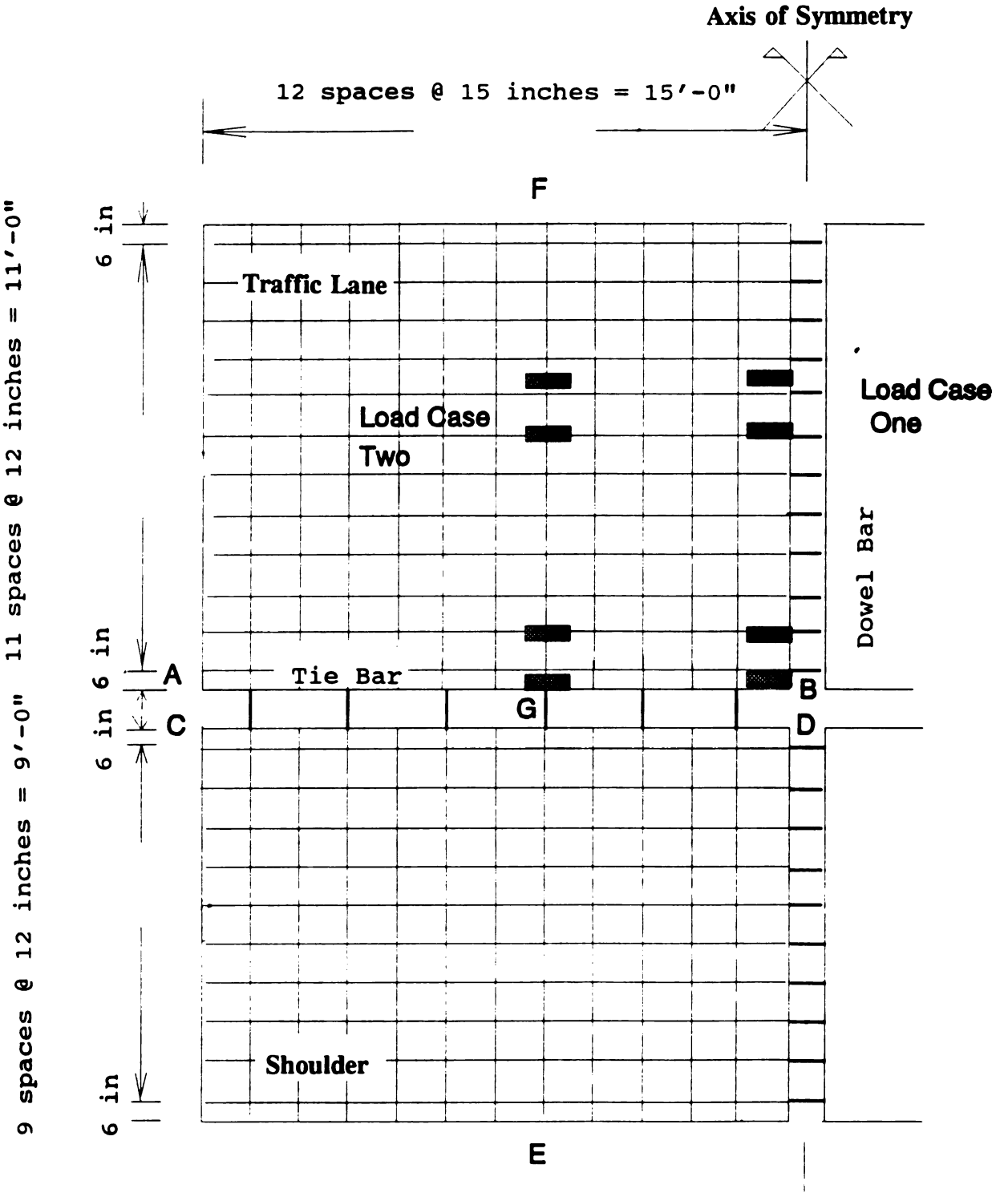

Fig. 8-4 Finite Element Mesh of the Four-Slab System

3 Major Findings from a Four-slab System

A four-slab system with one traffic lane and a shoulder was employed to investigate the effects of looseness of the tie bars which often connect the traffic lane and the shoulder. The system includes 1.25-in diameter dowel spaced 12 inches in the transverse joints, and 0.625-in tie bars on an 30-in centers in the lane-shoulder joint. The plane view of the four-slab system, is shown in Fig. 8-4. Because the system is a symmetric one, only one half of the entire system is given. Two loading cases have been considered: a corner loading case with a single axle load at the transverse joint and a tire at the corner, and an edge loading case with the single axle positioned 75 inch away from the transverse joint and with one tire at the edge of the longitudinal joint. Both loading cases are presented in Fig. 8-4.

Fig. 8-5 shows the shear force distributions of the dowel bars along the transverse joint. A comparison between Fig. 8-5 and Fig. 5-11(a) indicates that the effects of dowel looseness on the two-slab and four-slab systems are similar. Fig. 8-5 shows that the shear force on the critical bar increases slightly when the looseness increases from zero to 0.0015 inch, and then decreases when the looseness continue to increase. The increase due to the 0.0015 inch looseness is 6.2%. Teller[1958] and Snyder[1989] indicated that the initial looseness of dowel could be as much as 0.003 inch. This finding implies that after the dowels are installed in the joint, looseness always decreases the shear forces on the critical dowel bar. Fig. 8-6 shows a similar effect for tie bar looseness.

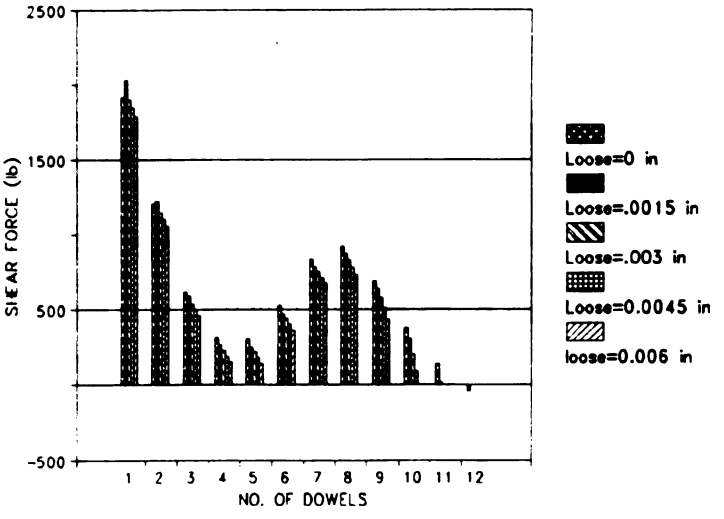

Fig. 8-5 Shear Forces on Dowels in the Transverse Joint (corner loading)

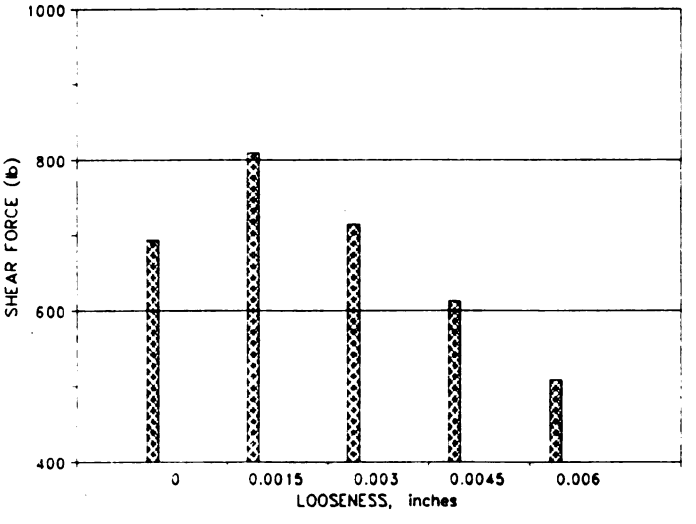

Fig. 8-6 Shear Forces on the Tie Bar Under the Edge Load

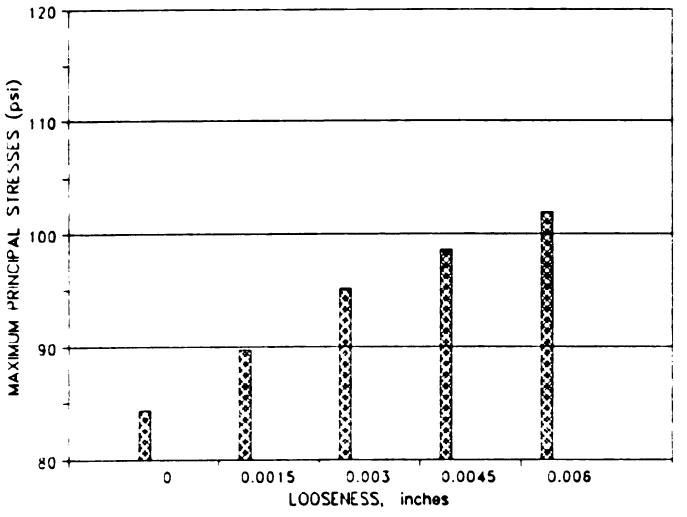

Fig. 8-7 Maximum Principal Stress vs. Looseness (corner loading)

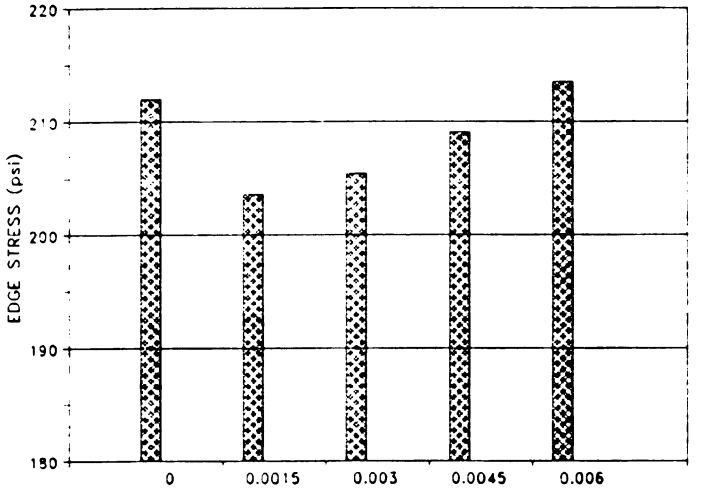

Fig. 8-8 Maximum Edge Stress vs. Looseness (Edge Loading)

Fig. 8-7 shows that increasing the looseness of the dowel bars and tie bars always increases the maximum principal stress for the corner loading case. The 0.003-inch looseness can produce a 13.1% stress increase, and the 0.006-inch looseness can produce a 21.1% stress increase. Fig. 8-8 shows that the maximum edge stress decreases when the looseness increases from zero to 0.0015 inch . When the looseness continues to increase, the maximum edge stress continuously increases. The maximum edge stress for the pavement without tie bars between the traffic lane and shoulder is 234.8 psi, which is 10.7% and 15.3% higher than the results for looseness = 0.0 inch and looseness = 0.0015 inch. As mentioned above, the existence of initial looseness leads to the conclusion that looseness increases the maximum edge stress.

4 Conclusions and Recommendations

The numerical analyses presented in this chapter and in Chapter 5 verify that the effects of dowel bar looseness should be considered in mechanistic design procedures for jointed rigid pavements. The looseness generally increases the pavement responses of the loaded slab, including the maximum displacement, the maximum corner stress and edge stress. Any mechanistic design procedure based on fatigue analysis could be significantly affected if the increases of slab stress due to the looseness of dowels and tie bars are considered.

The numerical results presented in this chapter and Chapter 5 were obtained by static analysis and without consideration of the combination of traffic loads and temperature gradients. If the dynamic effects of traffic loads are considered, the dynamic factor (ratio of the maximum dynamic loading and the static loading) could be between 1.3 to 2.0

(Gillespie[1991], and Stoner[1991]). In this case, the combined effects of dynamic loads and looseness would be even more significant on the maximum stress responses of the slab. When the temperature gradient and moisture variation are considered, the combination of looseness and temperature gradient could produce higher corner stresses during the night and higher edge stresses during the day. The analysis will be more complicated because two types of nonlinear behaviors should be considered: the nonlinear behavior of the loose dowel bars, and the nonlinear support provided to the uplifted slab as it comes in contact with the subgrade gradually under increasing load. The interaction between dowel looseness and dynamic loading, and between dowel looseness and temperature and/or moisture gradients needs further study.

CHAPTER NINE
CONCLUSIONS AND RECOMMENDATIONS

Dowel bars are widely used in rigid concrete pavements to transfer loads across joints and thus prolong the service life of the loaded slabs. It has been shown by many experimental studies that initial looseness exists to some degree in all dowel bars. The looseness is a function of construction quality, accumulation of traffic loads, and exposure to the field environment. In current design procedures dowel bars with small looseness are treated the same as without looseness. Some design procedures consider the effects of looseness by reducing the stiffness of each dowel bar. Both models with or without consideration of the dowel bar looseness are installed in finite element based programs to predict pavement responses.

Recently, some widely used models of dowels without consideration of looseness were checked by basic theory and evaluated by numerical analysis. Some errors in the dowel bar models and in the computer program using the model have been discovered and corrected. A component dowel bar model has been developed to simulate the load transfer mechanism. The impacts of the discovered errors were also discussed. A nonlinear mechanistic model has also been developed to simulate the dowel bar looseness mechanism. The model can be used to predict various pavement responses at different stages of the pavement service life, including stresses, displacement distributions and load transfer capacity.

The major conclusions of this research are summarized below:

- The dowel bar stiffness matrix in some finite element programs for jointed concrete pavements (e.g. JSLAB and ILLISLAB) fails to meet some of the basic requirements of the finite element method. The largest source of error results from this failure to satisfy dowel bar equilibrium conditions. This dissertation presents proof that the stiffness matrices employed by JSLAB and ILLISLAB represent elements that are not in equilibrium. This problem appears to be caused by an inappropriate modification of the shear-bending beam element that is found in many basic structural engineering texts.

- A numerical sensitivity analysis showed that ignoring dowel bar equilibrium requirements can produce significant errors in the predicted responses of concrete slabs and dowel bar load transfer systems. Based on the numerical analysis, it was found that the non-equilibrium stiffness matrix used in JSLAB overestimates the stress responses on the unloaded slab by up to 18.7% and underestimates the stress at edge of the loaded slab by up to 9.8%. The maximum bending moments at two ends of the dowels calculated by the non-equilibrium model was 10 times higher than those calculated by the equilibrium component model.

- A complete comparison between experimental data, published by Keeton[1957], and the analytical results from the component model (including distributions of bending moments and shear forces of the dowels, and bearing stresses of the concrete under the dowels) indicated

that trends of all predicted and measured responses are the same. The comparison verified that the component model can reasonably predict the load transfer characteristics of the dowel bar system and has potential to predict responses of slab and dowel bars by calibrating the subgrade modulus and dowel-concrete interaction coefficient.

- The maximum bearing stress on the concrete under the critical dowel has been found to be one of the most influential parameters in PCC pavement joint design. The magnitude of maximum stresses have direct effects on the accumulation of joint faulting which is a key indicator to evaluate the PCC pavement performance. The sensitivity of the maximum bearing stress has been analyzed using the component model. It was found that higher values of dowel diameter, slab thickness, concrete modulus and subgrade modulus can reduce maximum bearing stress of concrete under the critical dowel. Maximum bearing stress is insensitive to joint opening, but very sensitive to the dowel-concrete interaction coefficient. Unfortunately the interaction coefficient is difficult to estimate. Three tables of the critical maximum bearing stress in terms of slab thickness, subgrade modulus, concrete elasticity modulus, width of joint opening and diameter of dowels are presented in this dissertation as a design reference.

- Existing models for predicting the maximum bearing stress have been compared with the developed component model. Results obtained with these models are different from those obtained by the component model. For example, based on Friberg's[1940] and Tabatabaie's[1979] model the maximum stress

is much more sensitive to the width of joint opening than in the component model. Friberg concluded the higher value of subgrade modulus increases the maximum bearing stress, and Tabatabaie concluded the higher concrete elasticity modulus increases the maximum bearing stress. The source of discrepancy is the effective length assumption developed by Friberg and modified by Tabatabaie. The component model should provide more practical conclusions, since the results are directly obtained using the model installed in a finite element program without additional assumptions.

- Due to the significant difference in bearing stress predictions between existing models and the one developed in this research, pavement performance models which have been developed based on the maximum bearing stress must be evaluated. It is suggested these models be evaluated before being employed in PCC pavement design and rehabilitation.

- A mechanistic nonlinear model to simulate the mechanism of dowel bar looseness was developed. The model estimates pavement responses to load, including stress, displacement distributions and load transfer capability, with consideration of dowel looseness at different stages of the pavement service life.

- Numerical analysis were conducted to investigate the effects of dowel bar looseness on critical pavement responses. Parameters included magnitude of dowel looseness, configuration and location of traffic loads, shoulder edge support effects, variation of subgrade modulus, dowel

diameter and slab thickness. the numerical examples indicate that an increase in dowel looseness of 0.003 inch could produce a corresponding 10% increase in pavement edge stress, a 14% increase in maximum interior stress, and a 14% loss of joint load transfer efficiency. Previous studies have found that this magnitude of looseness exists initially in many doweled full-depth replacement joints. Previous experimental studies have shown that after two million load applications, the amount of looseness had doubled from initial levels, which implies that the resulting critical stress may be 20 to 28% higher than those obtained by if dowel looseness is neglected.

- Numerical examples for a four-slab system using the nonlinear model also show that the looseness of tie bars across the traffic lane-shoulder joint significantly affect the ability of the shoulder to withstand edge loads. The location of critical stresses in the concrete slab depends on the load transfer efficiency of the lane-shoulder ties as well as upon traffic load configuration and location, and transverse joint load transfer efficiency.

- Dowel bar looseness of 0.003 inches can change rigid pavement stress distributions quite significantly. This emphasizes the need for construction quality during dowel bar installation to insure maximum performance life. Furthermore, dowel coatings used for corrosion protection or to prevent bonding to the concrete should be carefully evaluated to insure that they do not allow vertical dowel movement.

- The maximum longitudinal stress and principal stress in rigid pavements are sensitive to dowel looseness. This becomes even more critical to the development of transverse cracks when temperature and moisture gradients (curling and warping stress) are considered. This could significantly affect PCC thickness design procedures that are based on fatigue criteria.

Some recommendations for future research are given below:

- Joints are necessary for PCC pavements, however, they are also the weakest portion in PCC pavements. The joint deterioration is caused by many sources. The understanding of the interactive effects among these source parameters is very important, such as interaction between the loss of subgrade support and dowel bar looseness, dynamic loading, looseness and faulting. The understanding can be reached by experimental studies through field survey and can also be reached by using appropriate mechanistic models. The lack of mechanistic model to simulate the deteriorated pavement suggests that more efforts should be made for developing appropriate mechanistic models to simulate the behavior of deteriorated PCC pavement.

- When more parameters are considered in mechanistic analysis, optimal design of PCC pavement will become a desired goal. Objective function should be determined based on long term benifit, constrain conditions might be selected based on Federal and State requirements and local needs.

The incorporation of mechanistic and empirical models may simplify the mathematical problem and make it possible to select the design parameters to minimize the objective function.

- Efforts should be made to develop a technique to measure the looseness of dowel bars by non-destructive test. The information is needed not only for pavement response prediction, but also for the pavement performance prediction.

REFERENCES

AASHTO, 1986.
"AASHTO Guide for Design of Pavement Structures," American Association of State, Highway, and Transportation Officials, Washington, D. C., 1986.

ACI Committee 325, 1956.
"Structural Design Considerations foe Pavement Joints," Journal of the American Concrete Institute, July, 1956.

Ball,C.G., et al., 1975.
"Test of Joints for Concrete Pavements," Portland Cement Association, 1975.

Bathe, K J., 1982.
"Finite Element Method," Englewood Cliffs, N.J., 1982.

Beeson, M G., et al., 1981.
"A Comparative Analysis of Dowel Placement in Portland Cement Concrete Pavements," A Report for American Concrete Paving Association, Dec., 1981.

Bradrury, R.D., 1932.
"Design of Joints in Concrete Pavements." Proceedings of the Hiway Research Board, 12th Annual Meeting, 1932.

Chou, Y T., 1981.
"Structural Analysis Computer Programs for Rigid Multicomponent Pavement Structures with Discontinuities - WESLIQID and WESLAYER," Report I, II and III, Technical Report GL-81-6 (U.S. Army Engineer Waterway Experiment Station, May,1981.)

Ciolko, A.T., et al., 1979.
"Load Transfer of Dowel Bars and Starlugs," Final Report, FHWA-LA-79-210P, March, 1979.

Colley, B E., et al., 1978.
"Evaluation of Concrete Pavements with Tied Shoulders or Widened Lanes," TRR, No. 666, 1978.

Darter, M I., 1977.
"Design of Zero-Maintenance Plain Jointed Concrete Pavement, Vol. I - Development of Design Procedures," Report No. FHWA-RD-77-111, June, 1977.

Darter, M I., et al., 1984.
"Development of a Concrete Pavement Evaluation System (COPES)", Vol. I, NCHPR Report 277, 1984.

Dempsey, B J., et al., 1986.
"Environmental Effect on Pavements - Vol. III: Theory Manual," FHWA Report, FHWA -RD-84-115, 1986.

FAA, 1978.
"Airport Pavement Design and Evaluation," Advisory Circular No. 150/5320-6C, Federal Aviation Administration, Dec., 1978.

FHWA, 1980.
"Rigid Pavement Joints," FHWA Technical Advisory No. T140.18, Dec. 1980.

Finney, E.A., et al., 1947.
"Progress Report on Load Deflection Tests Dealing with Length and Size of Dowels," Proceedings, HRB, Vol. 27, 1947.

Friberg, B.F., 1938.
"Load and Deflection Characteristics of Dowels in Transverse Joints of Concrete Pavements," Proceeding of HRB, Vol. 18, 1938.

Friberg, B.F., 1940
"Design of Dowels in Transverse Joints of Concrete Pavements," Transactions of the American Society of Civil Engineers, Vol. 105, 1940.

Gillespie, T D., et al., 1991.
"Effects of Heavy Vehicle Characteristics on Pavement Response and Performance," Report No. UMTRI 92-2, The University of Michigan Transportation Research Institute, Dec., 1991.

Gulden, W., et al., 1983.
"Improving Load Transfer in Existing Jointed Concrete Pavements," Final Report, FHWA, Georgia DOT, Nov., 1983.

Guo, H., et al., 1992.
"An analytical Model for Evaluating Computer Programs for Structural Analysis of Jointed Concrete Pavements," presented in the Workshop on Load Equivalency, Mathematical Modeling of PCC Pavements, Feb., 1992.

Guo, H., et al., 1992.
"Dowel Bar Modeling of Finite Element Program for PCC Pavement Analysis,"presented in the Workshop on Load Equivalency, Mathematical Modeling of PCC Pavements, Feb., 1992.

Heinrichs, K W., 1988.
"Rigid Pavement Analysis and Design," FHWA Report, FHWA-RD-88-068, 1988.

Hoit, M I., et al., 1988
"Enhanced Techniques for Understanding Portland Cement Cincrete Pavement Behahior," Report No. FL-DOT-MO-0401.

Huang, Y.H., et al., 1973.
"Finite-Element Analysis of Concrete Slabs and Its Implications for Rigid Pavement Design," HRR 466, 1973.

Hveem, F.N., 1949.
"An Investigation to Determine Causes for Displacement and Faulting at the Joints in Portland Cement Concrete Pavements on California Highways," a report for Division of Highway, State of California, May, 1949.

Ioannides, A.M. et al., 1984.
"Analysis of Slabs-on-grade for a Variety of Loading and Support Conditions," AFOSR-83-0143, Dec., 1984.

Keeton, J.R., 1956.
"Investigation of Load Transfer Characteristics of Dowels." Proceedings of the Highway Research Board, 35th Annual Meeting, 1956.

Keeton, J.R., et al., 1957.
"Load Transfer Characteristics of a Doweled Joint Subjected to Aircraft Wheel Loads," HRB Proceeding, Vol. 36, 1957.

Kushing, J.W., et al., 1935.
"Joint Testing Experiments with a Theory of Load Transfer Distribution Along the Length of Joint," Proceedings, HRB Vol. 15, 1935.

Kusing, J.W., et al., 1940.
Design of Load Transfer Loints in Concrete Pavements." Proceedings of the Highway Research Board, 20th Annual Meeting, 1940.

Larralde, J., 1985.
"Structural Analysis of Rigid Pavement with Pumping," Final Report, FHWA Report, FHWA-RD-85?

Larrasquillo, R.L., et al., 1981
"Properties of High Strength Concrete Subject to Short Term Loads," J. ACI, Vol 78, No 3, May/June 1981.

Majidzadeh, K., et al.; 1984.
"Mechanistic Design of Rigid Pavements," Vol I & II, DT-FH-11-9568, June, 1984.

Majidzadeh, K., et al., 1986.
"Structural Design of Roadway shoulders" - Final Report, FHWA-RD-86-089.

Marcus, Henri., 1952.
"Load Carrying Capacity of Dowels at Transverse Pavement Joints," Proceedings of the American Concrete Institute, Vol. 48, 1952.

Martinez, A.H., et al., 1982.
"Short-Term Mechanical Properties of High Strength Lightweight Concrete," Research Report No. 82-9, Dept. of Structural Engineering, Cornell University, August 1982.

Mueller, A L., et al., 1990
"Performance of Jointed Concrete Pavements," Vol. VI, FHWA-RD-89-141, July, 1990.

Nashizawa,T., et al., 1989.
"A Refined Model of Doweled Joint for Concrete Pavement Using FEM Analysis," Proceedings of the 4th International Conference on Concrete Pavement Design and Rehabilitation," Apr., 1989.

Nasim, M A., et al., 1991
"The Behavior of a Rigid Pavement Under Moving Dynamic Loads," Presented at 1991 TRB Annual Meeting, Jan, 1991.

Ortiz, D., et al., 1986.
"Effectiveness of Existing Rehabilitation Techniques for Jointed Concrete Pavements," FHWA report, FHWA/IL/UI-215, 1986.

PCA, 1984
"Thickness Design for Concrete Highway and Street Pavements," Portland Cement Association, 1984.

Przemieniecki, J.S., 1968.
"Theory of Matrix Structural Analysis," 1968.

Parmenter, B S., 1973.
"The Design and Construction of Joints in Concrete Pavements," TRRL Report 512, 1973.

Reiter, M.J., et al., 1989.
"Rehabilitation of Concrete Pavements," Vol. IV, FHWA RD-88-071,074, July, 1989.

Sawan, J S., et al., 1982.
"Structural Analysis an Design of PCC Shoulders," Report No. FHWA-RD-81-122, Apr., 1982.

Smith, K D., et al., 1990.
"Performance of Jointed Concrete Pavements," Vol II, FHWA reports, FHWA-RD-89-137, Nov., 1990.

Snyder, M.B., 1989.
"Dowel Load Transfer Systems for Full-Depth Repairs of Jointed Portland Cement Concrete Pavements," Thesis for the Degree of Ph.D., University of Illinois, 1989.

Stone, J.W., et al., 1990.
"Dynamic Simulation Methods for Evaluating Motor Vehicle and Roadway Design and Resolving Policy Issues," Report of the Midwest Transportation Center and University of Iowa, Jan, 1990.

Stone, J W., et al., 1991
"Dynamic Simulation Methods for Evaluating Vehicle Configuration and Roadway Design," Report of the Midwest Transportation Center and the University of Iowa, July, 1991.

Tabatabaie, A.M., et al., 1979.
"Analysis of Load Transfer System for Concrete Pavements," FAA-RD-79-4, 1979.

Tabatabaie, A M., 1991.
"Dynamic Analysis of Pavement Systems, Model Evaluations," Presented at the 1991 TRB Annual Meeting, Jan., 1991.

Tajabji, S.D., et.al., 1986.
"Analysis of Jointed Concrete Pavements," FHWA-RD-86-041, Feb., 1986.

Teller, L W., et al., 1936.
"A Study of Structural Action of Several Types of Transverse and Longitudinal Joint Designs," Public Roads, Vol. 17, No. 7-8, Oct., 1936.

Teller,L.W., et al., 1958.
"Performance of Dowels Under Repetitive Loading," Public Roads, Vol. 30, No. 1, April 1958.

Timoshenko, S., et al., 1925.
"Applied Elasticity,"Westing House Technical Night School Press, 1925.

Timoshenko, S., "Strength of Materials, Part II, Advanced Theory and Problems," Second Edition, D. Van Nostrand Company, Inc., 1941.

Timoshenko, S., et al., 1959
"Theory of Plates and Shells," McGraw-Hill, New York, N.Y., 1959.

Van Ness, N J., 1987.
"Summary of State Highway Practices on Rigid Pavement Joints and Their Performance," Memorandum, Federal Highway Administration, May 1987.

Vyce, J M., 1987.
"Performance of Load-Transfer Devices," Research Report 140, FHWA/NY/RR-87/140.

Westergaard, J M., 1926.
"Stresses in Concrete Pavements Computed by Theoretical Analysis," Public Roads, Vol. 7, 1926.

Westergaard, H M., 1928.
"Spacing of Dowels," Proceedings, Vol. 8, Transportation Research Board, 1928.

Yoder, E J., et al., 1975.
"Principles of Pavement Design," John Wiley & Sons, Inc., 1975.

Zienkiewicz, O C., 1977.
"The Finite Element Method," McGraw-Hill Book Company Limited, London, England, 1977.

APPENDIX A
SHAPE FUNCTIONS, STRAIN AND STRESS MATRICES OF A PLATE ELEMENT

1. Notations

The jth nodal displacement vector is:

$$\Delta_j = \begin{pmatrix} w \\ \theta_x \\ \theta_y \end{pmatrix}_j$$

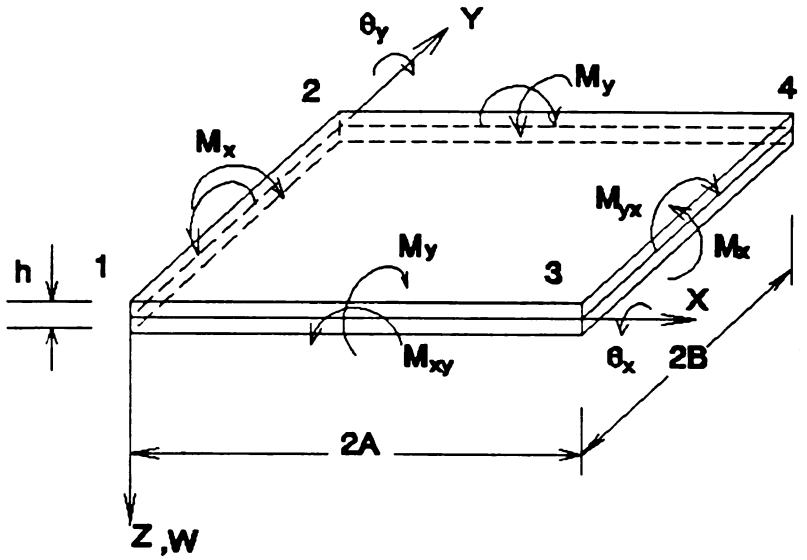

Fig. A-1 The Positive Direction of Forces and Displacements

2 Assumed Displacement Function

$$W(x,y) = a_1 + a_2x + a_3y + a_4x^2 + a_5xy + a_6y^2 + a_7x^3 + a_8x^2y + a_9xy^2 + a_{10}y^3 + a_{11}x^3y + a_{12}xy^3$$

3 Shape Functions

$$N_1 = 1 - \frac{3x^2}{4A^2} - \frac{xy}{4AB} - \frac{3y^2}{4B^2} + \frac{x^3}{4A^3} + \frac{3x^2y}{8A^2B} + \frac{3xy^2}{8AB^2} + \frac{y^3}{4B^3} - \frac{x^3y}{8A^3B} - \frac{xy^3}{8AB^3}$$

$$N_2 = -y + \frac{xy}{2A} + \frac{y^2}{B} - \frac{xy^2}{2AB} - \frac{y^3}{4B^2} + \frac{xy^3}{8AB^2}$$

$$N_3 = x - \frac{x^2}{A} - \frac{xy}{2B} + \frac{x^3}{4A^2} + \frac{x^2y}{2AB} - \frac{x^3y}{8A^2B}$$

$$N_5 = \frac{y^2}{2B} - \frac{xy^2}{4AB} - \frac{y^3}{4B^2} + \frac{xy^3}{8AB^2}$$

$$N_6 = \frac{xy}{2B} - \frac{x^2y}{2AB} + \frac{x^3y}{8A^2B}$$

$$N_7 = \frac{3x^2}{4A^2} + \frac{xy}{4AB} - \frac{x^3}{4A^3} - \frac{3x^2y}{8A^2B} - \frac{3xy^2}{8AB^2} + \frac{x^3y}{8A^3B} + \frac{xy^3}{8AB^3}$$

$$N_8 = -\frac{xy}{2A} + \frac{xy^2}{2AB} - \frac{xy^3}{8AB^2}$$

$$N_9 = -\frac{x^2}{2A} + \frac{x^3}{4A^2} + \frac{x^2y}{4AB} - \frac{x^3y}{8A^2B}$$

$$N_{10} = -\frac{xy}{4AB} + \frac{3x^2y}{8A^2B} + \frac{3xy^2}{8AB^2} - \frac{x^3y}{8A^3B} - \frac{xy^3}{8AB^3}$$

$$N_{11} = \frac{xy^2}{4AB} - \frac{xy^3}{8AB^2}$$

$$N_{12} = -\frac{x^2y}{4AB} + \frac{x^3y}{8A^2B}$$

4 Elements of Strain Matrix

$$B(1,1) = \frac{3}{2A^2} - \frac{3x}{2A^3} - \frac{3y}{4A^2B} + \frac{3xy}{4A^3B}$$

$$B(2,1) = \frac{3}{2B^2} - \frac{3x}{4AB^2} - \frac{3y}{2B^3} + \frac{3xy}{4AB^3}$$

$$B(3,1) = -\frac{1}{2AB} + \frac{3x}{2A^2B} + \frac{3y}{2AB^2} - \frac{3x^2}{4A^3B} - \frac{3y^2}{4AB^3}$$

$$B(1,2) = 0$$

$$B(2,2) = -\frac{2}{B} + \frac{x}{AB} + \frac{3y}{2B^2} - \frac{3xy}{4AB^2}$$

$$B(3,2) = \frac{1}{A} - \frac{2y}{AB} + \frac{3y^2}{4AB^2}$$

$$B(1,3) = \frac{2}{A} - \frac{3x}{2A^2} - \frac{y}{AB} + \frac{3xy}{4A^2B}$$

$$B(2,3) = 0$$

$$B(3,3) = -\frac{1}{B} + \frac{2x}{AB} - \frac{3x^2}{4A^2B}$$

$$B(1,4) = \frac{3y}{4A^2B} - \frac{3xy}{4A^3B}$$

$$B(2,4) = -\frac{3}{2B^2} + \frac{3x}{4AB^2} + \frac{3y}{2B^3} - \frac{3xy}{4AB^3}$$

$$B(3,4) = \frac{1}{2AB} - \frac{3x}{2A^2B} - \frac{3y}{2AB^2} + \frac{3x^2}{4A^3B} + \frac{3y^2}{4AB^3}$$

$$B(1,5) = 0$$

$$B(2,5) = -\frac{1}{B} + \frac{x}{2AB} + \frac{3y}{2B^2} - \frac{3xy}{4AB^2}$$

$$B(3,5) = -\frac{y}{AB} + \frac{3y^2}{4AB^2}$$

$$B(1,6) = \frac{y}{AB} - \frac{3xy}{4A^2B}$$

$$B(2,6) = 0$$

$$B(3,6) = \frac{1}{B} - \frac{2x}{AB} + \frac{3x^2}{4A^2B}$$

$$B(1,7) = -\frac{3}{2A^2} + \frac{3x}{2A^3} + \frac{3y}{4A^2B} - \frac{3xy}{4A^3B}$$

$$B(2,7) = \frac{3x}{2AB^2} - \frac{3xy}{4AB^3}$$

$$B(3,7) = \frac{1}{2AB} - \frac{3x}{2A^2B} - \frac{3y}{2AB^2} + \frac{3x^2}{4A^3B} + \frac{3y^2}{4AB^3}$$

$$B(1,8) = 0$$

$$B(2,8) = -\frac{x}{AB} + \frac{3xy}{4AB^2}$$

$$B(3,8) = -\frac{1}{A} + \frac{2y}{AB} - \frac{3y^2}{4AB^2}$$

$$B(1,9) = \frac{1}{A} - \frac{3x}{2A^2} - \frac{y}{2AB} + \frac{3xy}{4A^2B}$$

$$B(2,9) = 0$$

$$B(3,9) = \frac{x}{AB} - \frac{3x^2}{4A^2B}$$

$$B(2,5) = -\frac{1}{B} + \frac{x}{2AB} + \frac{3y}{2B^2} - \frac{3xy}{4AB^2}$$

$$B(3,5) = -\frac{y}{AB} + \frac{3y^2}{4AB^2}$$

$$B(1,6) = \frac{y}{AB} - \frac{3xy}{4A^2B}$$

$$B(2,6) = 0$$

$$B(3,6) = \frac{1}{B} - \frac{2x}{AB} + \frac{3x^2}{4A^2B}$$

$$B(1,7) = -\frac{3}{2A^2} + \frac{3x}{2A^3} + \frac{3y}{4A^2B} - \frac{3xy}{4A^3B}$$

$$B(2,7) = \frac{3x}{2AB^2} - \frac{3xy}{4AB^3}$$

$$B(3,7) = \frac{1}{2AB} - \frac{3x}{2A^2B} - \frac{3y}{2AB^2} + \frac{3x^2}{4A^3B} + \frac{3y^2}{4AB^3}$$

$$B(1,8) = 0$$

$$B(2,8) = -\frac{x}{AB} + \frac{3xy}{4AB^2}$$

$$B(3,8) = -\frac{1}{A} + \frac{2y}{AB} - \frac{3y^2}{4AB^2}$$

$$B(1,9) = \frac{1}{A} - \frac{3x}{2A^2} - \frac{y}{2AB} + \frac{3xy}{4A^2B}$$

$$B(2,9) = 0$$

$$B(3,9) = \frac{x}{AB} - \frac{3x^2}{4A^2B}$$

$$B(1,10) = -\frac{3y}{4A^2B} + \frac{3xy}{4A^3B}$$

$$B(2,10) = -\frac{3x}{4AB^2} + \frac{3xy}{4AB^3}$$

$$B(3,10) = -\frac{1}{2AB} + \frac{3x}{2A^2B} + \frac{3y}{2AB^2} - \frac{3x^2}{4A^3B} - \frac{3y^2}{4AB^3}$$

$$B(1,11) = 0$$

$$B(2,11) = -\frac{x}{2AB} + \frac{3xy}{4AB^2}$$

$$B(3,11) = \frac{y}{AB} - \frac{3y^2}{4AB^2}$$

$$B(1,12) = \frac{y}{2AB} - \frac{3xy}{4A^2B}$$

$$B(2,12) = 0$$

$$B(3,12) = -\frac{x}{AB} + \frac{3x^2}{4A^2B}$$

Substituting x=y=0 (defined as node 1) into above element formulae, the strain matrix for node 1 can be obtained:

$$\boldsymbol{B}_1 = \begin{pmatrix} \frac{3}{2A^2} & 0 & \frac{2}{A} & 0 & 0 & 0 & -\frac{3}{2A^2} & 0 & \frac{1}{A} & 0 & 0 & 0 \\ \frac{3}{2B^2} & -\frac{2}{B} & 0 & -\frac{3}{2B^2} & -\frac{1}{B} & 0 & 0 & 0 & 0 & 0 & 0 & 0 \\ -\frac{1}{2AB} & \frac{1}{A} & -\frac{1}{B} & \frac{1}{2AB} & 0 & \frac{1}{B} & \frac{1}{2AB} & -\frac{1}{A} & 0 & -\frac{1}{2AB} & 0 & 0 \end{pmatrix}$$

Similarly, for the other three nodes:

$$\boldsymbol{B}_2 = \begin{pmatrix} 0 & 0 & 0 & \frac{3}{2A^2} & 0 & \frac{2}{A} & 0 & 0 & 0 & -\frac{3}{2A^2} & 0 & \frac{1}{A} \\ -\frac{3}{2B^2} & \frac{1}{B} & 0 & \frac{3}{2B^2} & \frac{2}{B} & 0 & 0 & 0 & 0 & 0 & 0 & 0 \\ -\frac{1}{2AB} & 0 & -\frac{1}{B} & \frac{1}{2AB} & \frac{1}{A} & \frac{1}{B} & \frac{1}{2AB} & 0 & 0 & -\frac{1}{2AB} & -\frac{1}{2A} & 0 \end{pmatrix}$$

$$\boldsymbol{B}_3 = \begin{pmatrix} -\frac{3}{2A^2} & 0 & -\frac{1}{A} & 0 & 0 & 0 & \frac{3}{2A^2} & 0 & -\frac{2}{A} & 0 & 0 & 0 \\ 0 & 0 & 0 & 0 & 0 & 0 & \frac{3}{2B^2} & -\frac{2}{B} & 0 & -\frac{3}{2B^2} & -\frac{1}{B} & 0 \\ -\frac{1}{2AB} & \frac{1}{A} & 0 & \frac{1}{2AB} & 0 & 0 & \frac{1}{2AB} & -\frac{1}{A} & -\frac{1}{B} & -\frac{1}{2AB} & 0 & \frac{1}{B} \end{pmatrix}$$

$$\boldsymbol{B}_4 = \begin{pmatrix} 0 & 0 & 0 & -\frac{3}{2A^2} & 0 & -\frac{1}{A} & 0 & 0 & 0 & \frac{3}{2A^2} & 0 & -\frac{2}{A} \\ 0 & 0 & 0 & 0 & 0 & 0 & -\frac{3}{2B^2} & \frac{1}{B} & 0 & \frac{3}{2B^2} & \frac{2}{B} & 0 \\ -\frac{1}{2AB} & 0 & 0 & \frac{1}{2AB} & \frac{1}{A} & 0 & \frac{1}{2AB} & 0 & -\frac{1}{B} & -\frac{1}{2AB} & -\frac{1}{A} & \frac{1}{B} \end{pmatrix}$$

5 Stress Matrix

Let:

$$p = \frac{A}{B}$$

$$\boldsymbol{D} = \begin{pmatrix} D_x & D_1 & 0 \\ D_1 & D_y & 0 \\ 0 & 0 & D_{xy} \end{pmatrix}$$

The partitioned stress matrices can be written as:

$$\boldsymbol{R}_j = [\boldsymbol{R}_{j1}\ \boldsymbol{R}_{j2}] = \boldsymbol{D}\,\boldsymbol{B}_j \qquad (j = 1,2,3,4)$$

where:

$$\boldsymbol{R}_{11}=\frac{1}{4AB}\begin{pmatrix} 6P^{-1}D_x+6pD_1 & -8AD_1 & 8BD_x & -6pD_1 & -4AD_1 & 0 \\ 6p^{-1}D_1+6pD_y & -8AD_y & 8BD_1 & -6pD_y & -4AD_y & 0 \\ -2D_{xy} & 4BD_{xy} & -4AD_{xy} & 2D_{xy} & 0 & 4AD_{xy} \end{pmatrix}$$

$$\boldsymbol{R}_{12}=\frac{1}{4AB}\begin{pmatrix} -6p^{-1}D_x & 0 & 4BD_x & 0 & 0 & 0 \\ -6p^{-1}D_1 & 0 & 4BD_1 & 0 & 0 & 0 \\ 2D_{xy} & -4BD_{xy} & 0 & -2D_{xy} & 0 & 0 \end{pmatrix}$$

$$\boldsymbol{R}_{21}=\frac{1}{4AB}\begin{pmatrix} -6pD_1 & 4AD_1 & 0 & 6p^{-1}D_x+6pD_1 & 8AD_1 & 8BD_x \\ -6pD_y & 4AD_y & 0 & 6p^{-1}D_1+6pD_y & 8AD_y & 8BD_1 \\ -2D_{xy} & 0 & -4AD_{xy} & 2D_{xy} & 4BD_{xy} & 4AD_{xy} \end{pmatrix}$$

$$\boldsymbol{R}_{22}=\frac{1}{4AB}\begin{pmatrix} 0 & 0 & 0 & -6p^{-1}D_x & 0 & 4BD_x \\ 0 & 0 & 0 & -6p^{-1}D_1 & 0 & 4BD_1 \\ 2D_{xy} & 0 & 0 & -2D_{xy} & -4BD_{xy} & 0 \end{pmatrix}$$

$$\boldsymbol{R}_{31}=\frac{1}{4AB}\begin{pmatrix} -6p^{-1}D_x & 0 & -4BD_x & 0 & 0 & 0 \\ -6p^{-1}D_1 & 0 & -4BD_1 & 0 & 0 & 0 \\ -2D_{xy} & 4BD_{xy} & 0 & 2D_{xy} & 0 & 0 \end{pmatrix}$$

$$\boldsymbol{R}_{32}=\frac{1}{4AB}\begin{pmatrix} 6P^{-1}D_x+6pD_1 & -8AD_1 & -8BD_x & -6pD_1 & -4AD_1 & 0 \\ 6p^{-1}D_1+6pD_y & -8AD_y & -8BD_1 & -6pD_y & -4AD_y & 0 \\ 2D_{xy} & -4BD_{xy} & -4AD_{xy} & -2D_{xy} & 0 & 4AD_{xy} \end{pmatrix}$$

$$\boldsymbol{R}_{41}=\frac{1}{4AB}\begin{pmatrix} 0 & 0 & 0 & -6p^{-1}D_x & 0 & -4BD_x \\ 0 & 0 & 0 & -6p^{-1}D_1 & 0 & -4BD_1 \\ -2D_{xy} & 0 & 0 & 2D_{xy} & 4BD_{xy} & 0 \end{pmatrix}$$

$$\boldsymbol{R}_{42}=\frac{1}{4AB}\begin{pmatrix} -6pD_1 & 4AD_1 & 0 & 6P^{-1}D_x+6pD_1 & 8AD_1 & -8BD_x \\ -6pD_y & 4AD_y & 0 & 6p^{-1}D_1+6pD_y & 8AD_y & -8BD_1 \\ 2D_{xy} & 0 & -4AD_{xy} & -2D_{xy} & -4BD_{xy} & 4AD_{xy} \end{pmatrix}$$

APPENDIX B
BENDING MOMENTS OF UNBONDED AND BONDED TWO-LAYER ELEMENTS

The general form of bending moment of unit length is:

$$M = \int_h z\,\sigma\,dz$$

where σ is the bending stress, z is the distance between the stress point and the neutral axis of the cross section area, h is thickness of the cross section.

1. Unbonded case

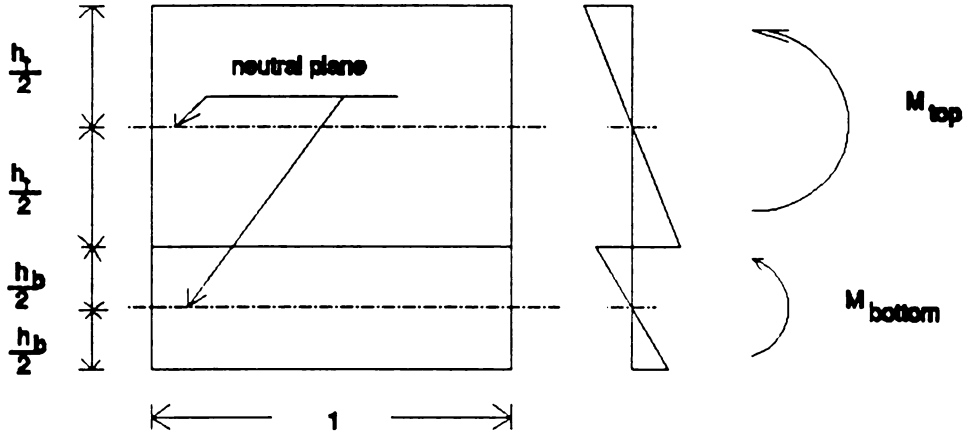

Fig. B-1 Unbonded Case

$$M = M_{top} + M_{bottom} = D\,K_c + M_t \qquad \text{(B-1)}$$

Where

$$M_{top} = \left(\int_{-\frac{h_t}{2}}^{\frac{h_t}{2}} z^2 C_{top}\, dz \right) K_c + M_t = \frac{h_t^3}{12} C_{top} K_c + M_t \qquad \text{(B-2)}$$

Similarly

$$M_{bottom} = \frac{h_b^3}{12} C_{bottom} K_c \qquad \text{(B-3)}$$

So

$$D = \frac{h_t^3}{12} C_{top} + \frac{h_b^3}{12} C_{bottom}$$

$$= D_{top} + D_{bottom}$$

$$= \sum_{layer} \frac{E\,h^3}{12(1-\mu^2)} \begin{pmatrix} 1 & \mu & 0 \\ \mu & 1 & 0 \\ 0 & 0 & \frac{1-\mu}{2} \end{pmatrix} \qquad \text{(B-4)}$$

2. Bonded case

(1) An Equivalent Layer

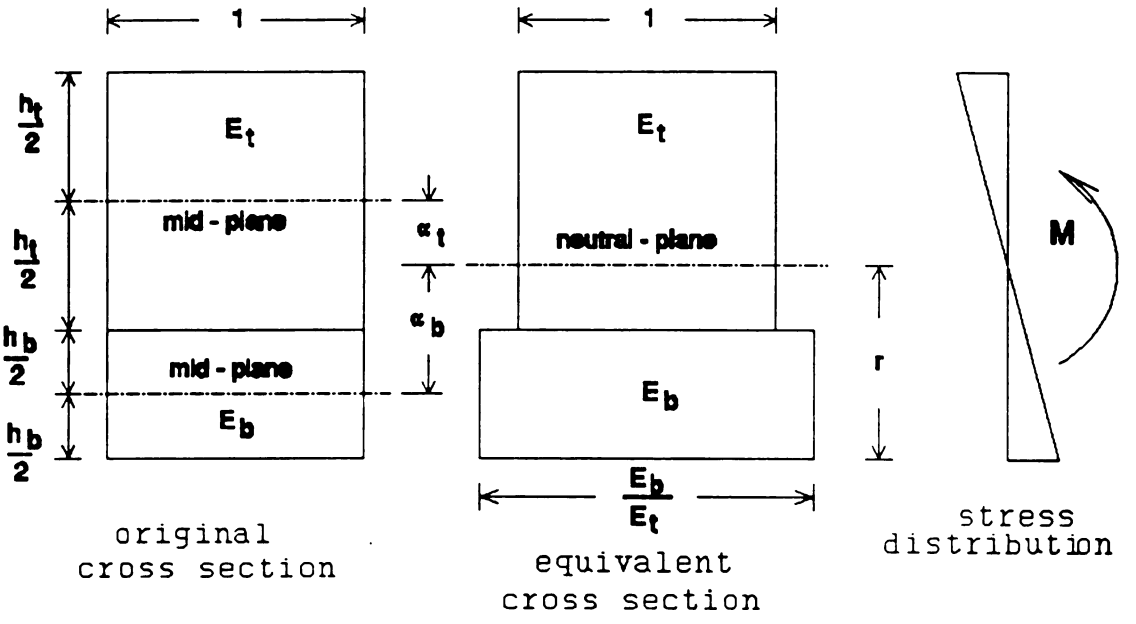

Fig B-2 Equivalent Layer

$$r\left(h_t+\frac{E_b}{E_{th_b}}\right)=h_t\left(h_b+\frac{h_t}{2}\right)+\frac{E_b}{E_t}\ \frac{h_b^2}{2}$$

(B-5)

$$r=\frac{\frac{h_t^2}{2}+h_t\,h_b+\frac{h_b^2}{2}\ \frac{E_b}{E_t}}{h_t+\frac{E_b}{E_t}\,h_b}$$

$$\alpha_b = r - \frac{h_b}{2} = \frac{\frac{1}{2} h_t (h_t + h_b)}{h_t + \frac{E_b}{E_t} h_b} \qquad \text{(B-6)}$$

$$\alpha_t = \frac{1}{2} (h_t + h_b) - \alpha_b \qquad \text{(B-7)}$$

(2) Bending Moment for Two-Layer Element

$$\boldsymbol{M} = \left(\int_{-(\alpha_t + \frac{h_t}{2})}^{-(\alpha_t - \frac{h_t}{2})} z^2 \boldsymbol{C}_{top} \, dz + \int_{\alpha_b - \frac{h_b}{2}}^{\alpha_b + \frac{h_b}{2}} z^2 \boldsymbol{C}_{bottom} \, dz \right) \boldsymbol{K}_c + \boldsymbol{M}_t$$

$$= (\boldsymbol{D}_{top} + \boldsymbol{D}_{bottom}) \boldsymbol{K}_c + \boldsymbol{M}_t$$

$$= \sum_{layer} \frac{E(12\alpha^2 h + h^3)}{12(1-\mu^2)} \begin{pmatrix} 1 & \mu & 0 \\ \mu & 1 & 0 \\ 0 & 0 & \frac{1-\mu}{2} \end{pmatrix} \boldsymbol{K}_c + \boldsymbol{M}_t \qquad \text{(B-8)}$$

$$= \boldsymbol{D} \boldsymbol{K}_c + \boldsymbol{M}_t$$

APPENDIX C
STIFFNESS MATRICX OF A PLATE ELEMENT

1 The Virtual Work Principle

The internal virtual work of layered pavement can be written as:

$$\delta W_{int} = \iint_{area} \delta \boldsymbol{K}_c^{\mathsf{T}} \boldsymbol{M}\, dxdy \qquad \text{(C-1)}$$

where δK_c is virtual curvature vector corresponding to the virtual displacement vector δV^e, and

$$\delta K_c = B\ \delta V^e$$

$$\delta K_c^{\mathsf{T}} = (\delta V^e)^{\mathsf{T}}\ B^{\mathsf{T}}$$

$$M = D\ K_c + M_t = D\ B\ V^e + M_t$$

Substituting the above expressions into Eq. (C-1) to obtain:

$$\delta W_{int} = \delta \boldsymbol{V}^{e\mathsf{T}} \left(\iint \boldsymbol{B}^{\mathsf{T}}\, \boldsymbol{D}\, \boldsymbol{B}\, dxdy \right) \boldsymbol{V}^e + \delta \boldsymbol{V}^{e\mathsf{T}} \iint \boldsymbol{B}^{\mathsf{T}}\, \boldsymbol{M}_t\, dxdy$$

Employing:

$$\boldsymbol{D} = \boldsymbol{D}_{top} + \boldsymbol{D}_{bottom}$$

to obtain:

$$\begin{aligned} \delta W_{int} &= \delta \boldsymbol{V}^{e\mathsf{T}} \left(\iint (\boldsymbol{B}^{\mathsf{T}}\, \boldsymbol{D}_{top}\, \boldsymbol{B} + \boldsymbol{B}^{\mathsf{T}}\, \boldsymbol{D}_{bottom}\, \boldsymbol{B})\, dxdy \right) \boldsymbol{V}^e \\ &\quad + \delta \boldsymbol{V}^{e\mathsf{T}} \iint \boldsymbol{B}^{\mathsf{T}}\, \boldsymbol{M}_t\, dxdy \qquad \text{(C-2)} \\ &= \delta \boldsymbol{V}^{e\mathsf{T}} (\boldsymbol{S}_{top} + \boldsymbol{S}_{bottom}) \boldsymbol{V}^e - \delta \boldsymbol{V}^{e\mathsf{T}}\, \boldsymbol{P}_t \end{aligned}$$

S_{top} and S_{bottom} in Eq. (C-2) are the stiffness matrices of the top and bottom layers of the pavement respectively. P_t is an equivalent nodal force

vector due to temperature variation. The expressions are given in Eq. (C-6).

The external virtual work consists two portions, one is contributed by load p(x,y), the other is contributed by the subgrade reaction forces. Winkler model is employed in the study, so that:

$$q(x,y) = -k(x,y)\,W(x,y) \tag{C-3}$$

where k(x,y) is the modules of subgrade reaction. The external virtual work can be written as:

$$\delta W_{ext} = \iint_{area} \delta W\,[p(x,y) + q(x,y)]\,dxdy$$

By using Eq. (2-8), the virtual displacement vector can be written as:

$$\delta W = \boldsymbol{N}\,\delta \boldsymbol{V}^{e} = \delta \boldsymbol{V}^{e\mathrm{T}}\,\boldsymbol{N}^{\mathrm{T}}$$

Thus:

$$\begin{aligned}\delta W_{ext} &= \delta \boldsymbol{V}^{e\mathrm{T}} \iint_{area} p(x,y)\;\boldsymbol{N}^{\mathrm{T}}\,dxdy \\ &\quad - \delta \boldsymbol{V}^{e\mathrm{T}} \iint_{area} k\,\boldsymbol{N}^{\mathrm{T}}\,\boldsymbol{N}\,dxdy\;\boldsymbol{V}^{e} \\ &= \delta \boldsymbol{V}^{e\mathrm{T}}\left[\boldsymbol{P}_{d} - \boldsymbol{S}_{sub}\,\boldsymbol{V}^{e}\right]\end{aligned} \tag{C-4}$$

Where, $\mathbf{P}_d$ is equivalent nodal force vector due to applied loads and $\mathbf{S}_{sub}$ is

the stiffness matrix of the subgrade. They are given in Eq. (C-6). Equating the internal and external virtual works of each element to lead:

$$(\mathcal{S}_{top} + \mathcal{S}_{bottom} + \mathcal{S}_{sub})\ V^e = P_d + P_t \qquad \text{(C-5)}$$

where:

$$\mathcal{S}_{top} = \iint_{area} B^T D_{top} B\ dxdy$$

$$\mathcal{S}_{bottom} = \iint_{area} B^T D_{bottom} B\ dxdy$$

$$\mathcal{S}_{sub} = \iint_{area} k\ N^T N\ dxdy$$

$$P_d = \iint_{area} p(x,y)\ N^T\ dxdy \qquad \text{(C-6)}$$

$$P_t = -\iint_{area} B^T M_t\ dxdy$$

So:

$$\mathcal{S}^e = \mathcal{S}_{top} + \mathcal{S}_{bottom} + \mathcal{S}_{sub} \qquad \text{(C-7)}$$

2 Stiffness Matrix of Top Layer S_{top} and Bottom Layer S_{bottom}

The following notations are used in computer program:

S(i,j) The element of stiffness matrix at the ith row and the jth column.

2A Length of the element in x direction

2B Length of the element in y direction

E Modules of elasticity

u Poisson's ratio

h Thickness of each layer

R $=Eh^3 / [60AB \times 12(1-u^2)]$ for unbounded case

$=E(12\alpha^2h+h^3) / [60AB \times 12(1-u^2)]$ for bonded case

α Distance between the mid-plane of each layer and the neutral axis of the equivalent cross section

U $=(1-u) / 2$

AB $= A \times B$

BS $= (B / A)^2$

AS $= (A / B)^2$

AS4 $= 4 \times A^2$

BS4 $= 4 \times B^2$

The elements of stiffness matrix are listed as follow:

S(1,1) = R x (60 x BS + 60 x AS + 30 x u + 84 x U)

S(2,1) = R x (-30 x AS - 15 x u - 6 x U) x 2B

S(2,2) = R x (20 x AS + 8 x U) x BS4

S(3,1) = R x (30 x BS + 15 x u + 6 x U) x 2A

S(3,2) = R x (-15 x u) x 4AB

S(3,3) = R x (20 x BS + 8 x U) x AS4

S(4,1) = R x (30 x BS - 60 x AS - 30 x u - 84 x U)

S(4,2) = R x (30 x AS + 6 x U) x 2B

S(4,3) = R x (15 x BS - 15 x u - 6 x U) x 2A

S(4,4) = S(1,1)

S(5,1) = -S(4,2)

S(5,2) = R x (10 x AS - 2 x U) x BS4

S(5,3) = 0

```
S(5,4) = -S(2,1)

S(5,5) = S(2,2)

S(6,1) = S(4,3)

S(6,2) = 0

S(6,3) = R x (10 x BS - 8 x U) x AS4

S(6,4) = S(3,1)

S(6,5) = -S(3,2)

S(6,6) = S(3,3)

S(7,1) = R x (-60 x BS + 30 x AS - 30 x u - 84 x U)

S(7,2) = R x (-15 x AS + 15 x u + 6 x U) x 2B

S(7,3) = R x (-30 x BS - 6 x u) x 2A

S(7,4) = R x (-30 x BS - 30 x AS + 30 x u + 84 x U)

S(7,5) = R x (-15 x AS + 6 x U) x 2B

S(7,6) = R x (-15 x BS + 6 x U) x 2A

S(7,7) = S(1,1)

S(8,1) = S(7,2)

S(8,2) = R x (10 x AS - 8 x U) x BS4

S(8,3) = 0

S(8,4) = -S(7,5)

S(8,5) = R x (5 x AS + 2 x U) x BS4

S(8,6) = 0

S(8,7) = S(2,1)

S(8,8) = S(2,2)

S(9,1) = -S(7,3)

S(9,2) = 0

S(9,3) = R x (10 x BS - 2 x U) x AS4
```

S(9,4) = -S(7,6)

S(9,5) = 0

S(9,6) = R x (5 x BS + 2 x U) x AS4

S(9,7) = -S(3,1)

S(9,8) = -S(3,2)

S(9,9) = S(3,3)

S(10,1) = S(7,4)

S(10,2) = -S(7,5)

S(10,3) = S(7,6)

S(10,4) = S(7,1)

S(10,5) = -S(7,2)

S(10,6) = S(7,3)

S(10,7) = S(4,1)

S(10,8) = S(4,2)

S(10,9) = -S(4,3)

S(10,10) = S(1,1)

S(11,1) = S(7,5)

S(11,2) = S(8,5)

S(11,3) = 0

S(11,4) = -S(7,2)

S(11,5) = S(8,2)

S(11,6) = 0

S(11,7) = S(5,1)

S(11,8) = S(5,2)

S(11,9) = 0

S(11,10) = -S(2,1)

S(11,11) = S(9,4)

S(12,1) = S(9,9)

S(12,2) = 0

S(12,3) = S(9,6)

S(12,4) = -S(7,3)

S(12,5) = 0

S(12,6) = S(9,3)

S(12,7) = -S(6,1)

S(12,8) = 0

S(12,9) = S(6,3)

S(12,10) = -S(3,1)

S(12,11) = S(3,2)

S(12,12)= S(3,3)

Since the stiffness matrix is symmetric, only the lower triangular portion is given. S(i,j) = S(j,i) can be used to evaluate the upper triangular portion of the matrix.

3 S_{sub}, Stiffness Matrix of Subgrade

If the modules of subgrade is uniform, k(x,y) = k = constant, the following formulae can be derived:

Q = (k x A x B) / 44100

Q1 = A x Q

Q2 = B x Q

Q3 = A x A x Q

Q4 = B x B x Q

```
Q5 = A x B x Q


S(1,1) = 24178 x Q
S(2,1) = -6454 x Q2
S(2,2) = 2240 x Q4
S(3,1) = 6454 x Q1
S(3,2) = -1764 x Q5
S(3,3) = 2240 x Q3
S(4,1) = 8582 x Q
S(4,2) = -3836 x Q2
S(4,3) = 2786 x Q1
S(4,4) = S(1,1)
S(5,1) = -S(4,2)
S(5,2) = -1680 x Q4
S(5,3) = 1176 x Q5
S(5,4) = -S(2,1)
S(5,5) = S(2,2)
S(6,1) = S(4,3)
S(6,2) = -S(5,3)
S(6,3) = 1120 x Q3
S(6,4) = S(3,1)
S(6,5) = -S(3,2)
S(6,6) = S(3,3)
S(7,1) = S(4,1)
S(7,2) = -2786 x Q2
S(7,3) = 3836 x Q1
```

```
S(7,4) = 2758 x Q
S(7,5) = 1624 x Q2
S(7,6) = 1624 x Q1
S(7,7) = S(1,1)
S(8,1) = S(7,2)
S(8,2) = 1120 x Q4
S(8,3) = -S(5,3)
S(8,4) = -S(7,5)
S(8,5) = -840 x Q4
S(8,6) = -784 x Q5
S(8,7) = S(2,1)
S(8,8) = S(2,2)
S(9,1) = -S(7,3)
S(9,2) = S(5,3)
S(9,3) = -1680 x Q3
S(9,4) = -S(7,6)
S(9,5) = S(8,6)
S(9,6) = -840 x Q3
S(9,7) = -S(3,1)
S(9,8) = -S(3,2)
S(9,9) = S(3,3)
S(10,1) = S(7,4)
S(10,2) = -S(7,5)
S(10,3) = S(7,6)
S(10,4) = S(7,1)
S(10,5) = -S(7,2)
```

```
S(10,6) = S(7,3)
S(10,7) = S(4,1)
S(10,8) = S(4,2)
S(10,9) = -S(4,3)
S(10,10) = S(1,1)
S(11,1) = S(7,5)
S(11,2) = S(8,5)
S(11,3) = -S(9,5)
S(11,4) = -S(7,2)
S(11,5) = S(8,2)
S(11,6) = S(9,2)
S(11,7) = S(5,1)
S(11,8) = S(5,2)
S(11,9) = -S(5,3)
S(11,10) = -S(2,1)
S(11,11) = S(2,2)
S(12,1) = S(9,4)
S(12,2) = -S(9,5)
S(12,3) = S(9,6)
S(12,4) = -S(7,3)
S(12,5) = S(8,3)
S(12,6) = S(9,3)
S(12,7) = -S(6,1)
S(12,8) = -S(6,2)
S(12,9) = S(6,3)
S(12,10) = -S(3,1)
```

S(12,11) = S(3,2)

S(12,12) = S(3,3)

4 P_d, The Equivalent Nodal Force Vector Due to Loads

Fig. C-1 presents a distributed load acted on a part of element. The following formulae are valid only for the constant load intensity p.

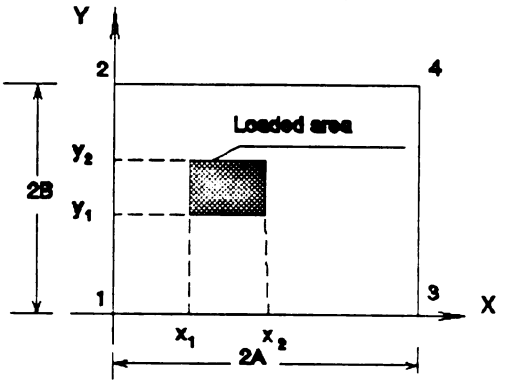

Fig. C-1 A Element partially acted by load

Using following notations:

$F1 = p \times (X_2 - X_1) \times (Y_2 - Y_1)$

$F2 = p \times (X_2 \times X_2 - X_1 \times X_1) / 2$

$F3 = p \times (X_2 - X_1) \times (Y_2 \times Y_2 - Y_1 \times Y_1) / 2$

$F4 = p \times (X_2^3 - X_1^3) \times (Y_2 - Y_1) / 3$

$F5 = p \times (X_2^2 - X_1^2) \times (Y_2^2 - Y_1^2) /4$

$F6 = p \times (X_2 - X_1) \times (Y_2^3 - Y_1^3) / 3$

$F7 = p \times (X_2^4 - X_1^4) \times (Y_2 - Y_1) / 4$

$F8 = p \times (X_2^3 - X_1^3) \times (Y_2^2 - Y_1^2) / 6$

$F9 = p \times (X_2^2 - X_1^2) \times (Y_2^3 - Y_1^3) / 6$

$F10 = p \times (X_2 - X_1) \times (Y_2^4 - Y_1^4) / 4$

$F11 = p \times (X_2^4 - X_1^4) \times (Y_2^2 - Y_1^2) / 8$

$F12 = p \times (X_2^2 - X_1^2) \times (Y_2^4 - Y_1^4) / 8$

$A2 = A^2$

$B2 = B^2$

$AB = A \times B$

$A3 = A^3$

$B3 = B^3$

$AB2 = A \times B^2$

$A2B = A^2 \times B$

$AB3 = A \times B^3$

$A3B = A^3 \times B$

The elements of the equivalent force vector are listed as follow:

$P_d(1) = F1 - 0.75 \times F4 / A2 - 0.25 \times F5 / AB - 0.75 \times F6 / B2$
$+ 0.25 \times F7 / A3 + 0.375 \times F8 / A2B + 0.375 \times F9 / AB2$
$+ 0.25 \times F10 / B3 - 0.125 \times F11 / A3B - 0.125 \times F12 / AB3$

$P_d(2) = -F3 + 0.5 \times F5 / A + F6 / B - 0.5 \times F9/AB - 0.25 \times F10 / B2$
$+ 0.125 \times F12 / AB2$

$P_d(3) = F2 - F4 / A - 0.5 \times F5 / B + 0.25 \times F7 / A2 + 0.5 \times F8 / AB$
$- 0.125 \times F11 / A2B$

$P_d(4) = 0.25 \times F5 / AB + 0.75 \times F6 / B2 - 0.375 \times F8 / A2B$
$-0.375 \times F9 / AB2 - 0.25 \times F10 / B3 + 0.125 \times F11 / A3B$
$+ 0.125 \times F12 / AB3$

$P_d(5) = 0.5 \times F6 / B - 0.25 \times F9 / AB - 0.25 \times F10 / B2$
$+ 0.125 \times F12 / AB2$

$P_d(6) = 0.5 \times F5 / B - 0.5 \times F8 / AB + 0.125 \times F11 / A2B$

$P_d(7) = 0.75 \times F4 / A2 + 0.25 \times F5 / AB - 0.25 \times F7 / A3$
$-0.375 \times F8 / A2B - 0.375 \times F9 / AB2 + 0.125 \times F11 / A3B$
$+ 0.125 \times F12 / AB3$

$P_d(8) = -0.5 \times F5 / A + 0.5 \times F9 / AB - 0.125 \times F12 / AB2$

$P_d(9) = -0.5 \times F4 / A + 0.25 \times F7 /A2 + 0.25 \times F8 / AB$
$- 0.125 \times F11 / A2B$

$P_d(10) = -0.25 \times F5 / AB + 0.375 \times F8 / A2B + 0.375 \times F9 / AB2$
$- 0.125 \times F11 /A3B - 0.125 \times F12 / AB3$

$P_d(11) = 0.25 \times F9 /AB - 0.125 \times F12 / AB2$

$P_d(12) = -0.25 \times F8 /AB + 0.125 \times F11 / A2B$

5 P_t, The Equivalent Nodal Force Vector Due to Temperature Gradient

If the temperature variation along slab thickness is linear, M_t is a constant vector as shown in Eq. (2-18), the equivalent thermal nodal force vector can be written as:

$$\boldsymbol{P}_t=[0 \;\; aM_0 \;\; -bM_0 \;\; 0 \;\; -aM_0 \;\; -bM_0 \;\; 0 \;\; aM_0 \;\; bM_0 \;\; 0 \;\; -aM_0 \;\; bM_0]^T$$

where:

$$M_0=\frac{E\alpha h^3}{12(1-\mu)}g$$

APPENDIX D
COMPONENT MODEL FOR DOWEL BAR SYSTEM

1 The Nodes of Slabs and Dowel Bars

A dowel bar can be divided into three segments as shown in Fig. 2-1(a). Segment Ci and jD are embedded in concrete and the segment ij is in between the two slabs. i_s and j_s are denoted the slab nodes and i_b and j_b the dowel bar nodes. Before any load being acted on the system, i_s, i_b and j_s, j_b are assumed to be identical respectively. However, after the loads being moved on, the slabs are deflected and i_b and j_b are separated from i_s and j_s respectively. δ_i and δ_j are defined as the relative deflection between the dowel bar nodes i_b, j_b and the slab nodes i_s and j_s respectively. Similarly, θ_i and θ_j are defined as the relative rotation angles between the slabs and the dowel bar. The relative deformation, including deflection and rotation angle, can be analyzed by a beam resting on elastic foundation.

2 The Stiffness Matrix of Dowel Bar

For segment ij (Fig. 2-1)

The stiffness equation of segment ij is:

$$\begin{pmatrix} f_i \\ f_j \end{pmatrix}_b = g_b \begin{pmatrix} d_i \\ d_j \end{pmatrix}_b \qquad \text{(D-1)}$$

where:

$$S_b=\begin{pmatrix} S_{11} & S_{12} \\ S_{21} & S_{22} \end{pmatrix}=\frac{EI}{l^3(1+\phi)}\begin{pmatrix} 12 & 6l & -12l & 6l \\ 6l & (4+\phi)l^2 & -6l & (2-\phi)l^2 \\ -12 & -6l & 12 & -6l \\ 6l & (2-\phi)l^2 & -6l & (4+\phi)l^2 \end{pmatrix} \quad \text{(D-2)}$$

E Elastic modules of the dowel bar

I Moment of the cross-sectional inertia of the bar

l Width of the joint opening, length of the element

ϕ $24(1+\ )I/A_e l^2$, shear deformation factor

u Poisson's ratio of the dowel bar

A_e Cross-sectional area effective in shear of the bar

f $= [Q\ M]^T$ Force vector of the bar's node

d $= [w\ \theta]^T$ Displacement vector of the bar's node

Their positive direction are shown in Fig. 2-2.

For segment Ci and jD (Fig. 2-1)

The positive notations of relative deflections, rotation angles and forces are shown in Fig. D-1.

Where:

$\delta = w_s - w_b$

$\phi = \theta_s - \theta_b$

w_s and w_b are displacements at the nodes of the slab

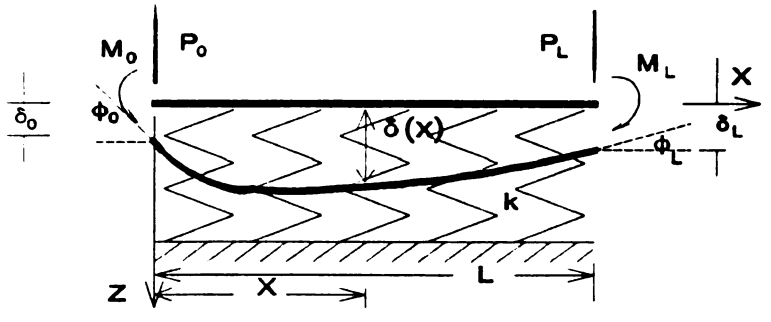

Fig. D-1 A Beam on Elastic Base

and dowel bars. The beam element equilibrium equation can be written as(Timoshenko[1941]):

$$EI\frac{d^4\delta(x)}{dx^4} + k\delta(x) = 0 \qquad (0 \le x \le L) \tag{D-3}$$

where k is base coefficient of the beam, i.e. the product of interaction coefficient of bar and concrete and the diameter of the bar. The general solution of Eq. (D-3) is:

$$\begin{aligned}\delta(x) = {} & A' ch\beta x \cos\beta x + B' ch\beta x \sin\beta x \\ & + C' sh\beta x \cos\beta x + D' sh\beta x \sin\beta x\end{aligned} \tag{D-4}$$

where $\beta = (k/4EI)^{0.25}$

A,B,C and D can be determined by the boundary conditions at x = 0:

$$\begin{aligned}\delta(0) &= \delta_0 \\ \phi(0) &= \frac{d\delta(x)}{dx}\Big|_{x=0} = \phi_0 \\ M(0) &= EI\frac{d^2\delta(x)}{dx^2}\Big|_{x=0} = M_0 \\ Q(0) &= -EI\frac{d^3\delta(x)}{dx^3}\Big|_{x=0} = P_0\end{aligned} \tag{D-5}$$

The solutions are:

$$A' = \delta_0$$

$$B' = \frac{1}{2}\left(\frac{\phi_0}{\beta} - \frac{P_0}{2EI\beta^3}\right)$$

$$C' = \frac{1}{2}\left(\frac{\phi_0}{\beta} + \frac{P_0}{2EI\beta^3}\right) \qquad \text{(D-6)}$$

$$D' = \frac{M_0}{2EI\beta^2}$$

Substituting Eq. (D-6) into Eq. (D-4) and using the boundary conditions:

$$M(x=L) = 0 \text{ and } Q(x=L) = 0 \qquad \text{(D-7)}$$

δ_0 and ϕ_0 can be expressed by M_0 and Q_0 as fol:

$$\begin{pmatrix}\delta_0\\ \phi_0\end{pmatrix} = \frac{1}{2EI\beta^2(S^2-s^2)}\begin{pmatrix}\frac{sc-SC}{\beta} & S^2+s^2\\ S^2+s^2 & -2\beta(SC+sc)\end{pmatrix}\begin{pmatrix}P_0\\ M_0\end{pmatrix} \qquad \text{(D-8)}$$

In which:

$$S=sh\beta L,\ C=ch\beta L,\ s=\sin\beta L \text{ and } c=\cos\beta L \qquad \text{(D-9)}$$

Similarly, let:

$$M(x=0) = 0 \text{ and } Q(x=0) = 0 \qquad \text{(D-10)}$$

δ_L and ϕ_L can be obtained:

$$\begin{pmatrix}\delta_L\\ \phi_L\end{pmatrix} = \frac{1}{2EI\beta^2(S^2-s^2)}\begin{pmatrix}\frac{SC-sc}{\beta} & S^2+s^2\\ S^2+s^2 & 2\beta(SC+sc)\end{pmatrix}\begin{pmatrix}P_L\\ M_L\end{pmatrix} \qquad \text{(D-11)}$$

Comparing the positive directions of the nodal forces and displacements in Fig. 2-2 and Fig. D-1, it is obvious that Eq. (D-11) can be directly used for segment Ci in Fig. 2-1. After P_0 and M_0 replaced by $-P_0$ and $-M_0$, Eq. (D-8) can be used for segment jD in Fig. 2-1.

Notice: $\Delta w = \delta$, $\Delta\theta = \phi$, $\Delta P = P$ and $\Delta M = M$, the following eqations at node i of the segment Ci can be written:

$$\begin{pmatrix}\Delta w\\ \Delta\theta\end{pmatrix} = \frac{1}{2EI\beta^2(S_1^2-s_1^2)}\begin{pmatrix}\frac{S_1C_1-s_1c_1}{\beta} & S_1^2+s_1^2\\ S_1^2+s_1^2 & 2\beta(S_1C_1+s_1c_1)\end{pmatrix}\begin{pmatrix}\Delta P\\ \Delta M\end{pmatrix} \qquad \textbf{(D-12)}$$

where S_1, s_1, C_1 and c_1 are obtained by substituting $L=l_1$ in Eq. (D-9).

At node j of the segment jD in Fig. 2-1:

$$\begin{pmatrix}\Delta w\\ \Delta\theta\end{pmatrix} = \frac{1}{2EI\beta^2(S_2^2-s_2^2)}\begin{pmatrix}\frac{S_2C_2-s_2c_2}{\beta} & -(S_2^2+s_2^2)\\ -(S_2^2+s_2^2) & 2\beta(S_2C_2+s_2c_2)\end{pmatrix}\begin{pmatrix}\Delta P\\ \Delta M\end{pmatrix} \qquad \textbf{(D-13)}$$

where S_2, s_2, C_2 and c_2 are obtained by substituting $L=l_2$ in EQ. (D-9).

ΔP and ΔM can be solved, for node i of the segment Ci in Fig.2-1:

$$\begin{pmatrix}\Delta P\\ \Delta M\end{pmatrix} = T_1\begin{pmatrix}\Delta w\\ \Delta\theta\end{pmatrix} \qquad \textbf{(D-14)}$$

for node j of the segment jD in Fig. 2-1:

$$\begin{pmatrix}\Delta P\\ \Delta M\end{pmatrix} = \boldsymbol{T}_2\begin{pmatrix}\Delta w\\ \Delta\theta\end{pmatrix} \tag{D-15}$$

where:

$$\boldsymbol{T}_1 = \frac{2\beta^2 EI}{C_1^2+C_1^2}\begin{pmatrix}2\beta\,(S_1C_1+S_1C_1) & -(S_1^2+S_1^2)\\ -(S_1^2+S_1^2) & \dfrac{(S_1C_1-S_1C_1)}{\beta}\end{pmatrix} \tag{D-16}$$

$$\boldsymbol{T}_2 = \frac{2\beta^2 EI}{C_2^2+C_2^2}\begin{pmatrix}2\beta\,(S_2C_2+S_2C_2) & (S_2^2+S_2^2)\\ (S_2^2+S_2^2) & \dfrac{(S_2C_2-S_2C_2)}{\beta}\end{pmatrix} \tag{D-17}$$

Using the following notations for any node n:

$$\boldsymbol{F}_n = \begin{pmatrix}Q_n\\ M_n\end{pmatrix} \tag{D-18}$$

$$\boldsymbol{d}_n = \begin{pmatrix}w_n\\ \theta_n\end{pmatrix} \tag{D-19}$$

and notice the geometric relations between relative displacements and global displacements, Eq. (D-14) and Eq. (D-15) can be rewritten as:

for nodes i_s and i_b:

$$\begin{pmatrix}\boldsymbol{F}_{i_s}\\ \boldsymbol{F}_{i_b}\end{pmatrix} = \begin{pmatrix}\boldsymbol{T}_1 & -\boldsymbol{T}_1\\ -\boldsymbol{T}_1 & \boldsymbol{T}_1\end{pmatrix}\begin{pmatrix}\boldsymbol{d}_{i_s}\\ \boldsymbol{d}_{i_b}\end{pmatrix} \tag{D-20}$$

for nodes j_s and j_b:

$$\begin{pmatrix}\boldsymbol{F}_{j_s}\\ \boldsymbol{F}_{j_b}\end{pmatrix} = \begin{pmatrix}\boldsymbol{T}_2 & -\boldsymbol{T}_2\\ -\boldsymbol{T}_2 & \boldsymbol{T}_2\end{pmatrix}\begin{pmatrix}\boldsymbol{d}_{j_s}\\ \boldsymbol{d}_{j_b}\end{pmatrix} \tag{D-21}$$

Component Stiffness Matrix for the Entire Dowel Bar

Indeed, a dowel bar is the assemblege of three segments. The assembled stiffness matrix of the dowel bar can be obtained by taking summation of the three stiffness matrices as follow:

$$\begin{pmatrix} F_{i_a} \\ F_{i_b} \\ F_{j_b} \\ F_{j_a} \end{pmatrix} = \begin{pmatrix} T_1 & -T_1 & 0 & 0 \\ -T_1 & S_{11}+T_1 & S_{12} & 0 \\ 0 & S_{21} & S_{22}+T_2 & -T_2 \\ 0 & 0 & -T_2 & T_2 \end{pmatrix} \begin{pmatrix} d_{i_a} \\ d_{i_b} \\ d_{j_b} \\ d_{j_a} \end{pmatrix} \qquad \text{(D-22)}$$

Since there are not nodal forces acted at the bar's nodes, the following equations can be written:

$$F_{i_b} = F_{j_b} = o \qquad \text{(D-23)}$$

Thus:

$$\begin{pmatrix} d_{i_b} \\ d_{j_b} \end{pmatrix} = \begin{pmatrix} S_{11}+T_1 & S_{12} \\ S_{21} & S_{22}+T_2 \end{pmatrix}^{-1} \begin{pmatrix} T_1 & 0 \\ 0 & T_2 \end{pmatrix} \begin{pmatrix} d_{i_a} \\ d_{j_a} \end{pmatrix} \qquad \text{(D-24)}$$

Substituting Eq. (D-24) into the first and the fourth equations in Eq. (D-22), the stiffness equation for the dowel bar can be written in terms of the nodal forces and displacements of the slabs:

$$\begin{pmatrix} F_{i_a} \\ F_{j_a} \end{pmatrix} = S_c \begin{pmatrix} d_{i_a} \\ d_{j_a} \end{pmatrix} \qquad \text{(D-25)}$$

thus, the component stiffness matrix S_c becomes:

$$S_c = \begin{pmatrix} T_1 & 0 \\ 0 & T_2 \end{pmatrix} \left(\begin{pmatrix} E & 0 \\ 0 & E \end{pmatrix} - \begin{pmatrix} S_{11}+T_1 & S_{12} \\ S_{21} & S_{22}+T_2 \end{pmatrix}^{-1} \begin{pmatrix} T_1 & 0 \\ 0 & T_2 \end{pmatrix} \right) \qquad \text{(D-26)}$$

where, **E** is a 2 x 2 unit matrix.